TECHNICAL REPORT
66-3-CM

THERMAL-PHYSICAL PARAMETERS OF MATERIALS

by
R. E. Larson and A. R. Kydd

Applied Science Division
Litton Systems, Inc.
St. Paul, Minnesota

Contract No. DA19-129-QM-1998 (OI 6082)

January 1966

UNITED STATES ARMY
NATICK LABORATORIES
Natick, Massachusetts 01760

Clothing & Organic
Materials Division
C&OM-16

Distribution of this
document is unlimited

AD_____

TECHNICAL REPORT

66-3-CM

THERMAL-PHYSICAL PARAMETERS OF MATERIALS

by

R. E. Larson and A. R. Kydd
Applied Science Division
Litton Systems, Inc.
St. Paul, Minnesota

Contract No. DA 19-129-QM-1998(OI 6082)

Project reference:
1K0-24401-A113

Series: C&OM-16

January 1966

Clothing and Organic Materials Division
U. S. ARMY NATICK LABORATORIES
Natick, Massachusetts

FOREWORD

This is a final report covering three years of research on the thermal-physical parameters of materials. The purpose of the research was to establish, on the basis of theoretical studies, a simplified mathematical model of the fabric-skin system using heat flow equations and to solve these equations by means of programming on a Control Data G-15D digital computer. The results of the calculations, when compared with literature values and with measurements made in the laboratory on fabric systems as to surface temperature and heat transfer, will provide better insight into the chemical degradation processes taking place in materials exposed to high intensity thermal energy pulses. This will lead eventually to new materials affording higher thermal protection than that provided by present conventional materials.

The work was begun by the Aerospace Research Department of General Mills' Electronics Division under Contract No. DA-19-129-QM-1998. On 11 September 1963, the Aerospace Engineering and Research Departments of General Mills' Electronics Division were purchased by Litton Industries and are now known as the Applied Science Division (ASD), Litton Systems, Inc. Since the sale transferred all facilities, personnel and capabilities involved in this program, the research continued without interruption under the same contract. The first annual report was issued by General Mills; the second annual report and this final report by the Applied Science Division, Litton Systems, Inc. The work was directed during the first year by Mr. Sheldon Steinberg, and in the second and third years by Mr. R. E. Larson with Mr. A. R. Kydd assisting.

The contract was initiated under Project No. 1KO-24401-A113 and was administered under the Materials Research Branch of the Clothing and Organic Materials Division of the U. S. Army Natick Laboratories, with Mr. David Feldman acting as Project Officer and Dr. William E. C. Yelland as Alternate Project Officer.

The authors wish to express their appreciation to Dr. George R. Thomas, U. S. Army Natick Laboratories, for helpful advice and supporting efforts during the entire program. They also wish to thank ASD personnel for consultation and direct participating contributions to this study, especially Mr. Sheldon Steinberg, who was the original project scientist, and also Messrs. A. Anderson, G. Gauvin, N. Konopliv, R. Kuehrl, P. Preese, G. Rhodes and J. Schmoker.

S. J. KENNEDY
Director
Clothing & Organic Materials Division

APPROVED:

DALE H. SIELING Ph.D.
Scientific Director

W. W. VAUGHAN
Brigadier General, USA
Commanding

CONTENTS

LIST OF FIGURES

LIST OF FIGURES (continued)

LIST OF FIGURES (continued)

LIST OF FIGURES (continued)

LIST OF FIGURES (continued)

LIST OF FIGURES (continued)

SYMBOLS AND ABBREVIATIONS

Symbol	
c	specific heat
D	diathermancy factor
F_{f-s}	radiation interchange factor between fabric and skin
g	acceleration of gravity
Gr	Grashof number
H	plate length, or dimensionless heat transfer coefficient
h	heat transfer coefficient
i	radiant heat flux
k	heat conductivity
L	fabric or air gap thickness or characteristic length
Nu	Nusselt Number
Pr	Prandtl number
q	heat flux
t	temperature
x, y	distance
α	absorptivity or diffusivity
β	expansion coefficient
γ	extinction coefficient
δ	thermal layer thickness
Δ	difference

ϵ	emissivity
μ	viscosity
ν	kinematic viscosity
ρ	density or reflectivity
σ	Stefan-Boltzmann constant
τ	time or transmissivity

Subscript

a	air gap or air
c	convection or conduction
e	environment
eff	effective
f	fabric or field
i	inner surface of fabric or initial value
o	outer surface or impinging radiation
p	constant pressure
s	skin
w	wall
x	wetted distance

ABSTRACT

This is the final report of a three-year program of research on the thermal-physical parameters of materials necessary for protection against intense thermal radiation. It briefly summarizes the theoretical and experimental studies of the first two years, and includes a more comprehensive discussion of the work performed during the final year of the contract.

In the theoretical studies, a simplified model of the fabric-skin system was chosen and the heat flow equations were solved using an explicit finite difference calculation procedure programmed for solution on a Control Data G-15D digital computer. Several sample calculations were compared with results existing in the literature and a limited parameter study was performed with variation of the fabric surface heat transfer coefficients.

Fabric test samples were irradiated in an arc image furnace test facility and the heating and degradation processes were qualitatively and quantitatively studied with a Mach-Zehnder interferometer. This instrument provided fabric surface temperature data, heat transfer coefficient information, and a better insight into the chemical processes taking place.

THERMAL-PHYSICAL PARAMETERS OF MATERIALS

1. INTRODUCTION

During recent years, considerable research effort has been expended on studying the effects of intense thermal radiation, such as that from released nuclear energy, on military clothing fabrics. A variety of experimental techniques and procedures have been used; screening tests on all types of fabrics have been carried out for various thermal radiation exposures. Several theoretical models have been postulated and studied. The influence of such effects as fabric diathermancy, moisture content, surface heat losses, and time dependent heat inputs have been investigated. But at the present time, a basic insight into the detailed processes involved in protection against intense thermal radiation has not been obtained.

The general scope of the study reported herein is to determine the physical properties required in a new material that could be used as a clothing fabric for protection against intense thermal radiation. Optimum values are to be determined for these properties on the basis of a theoretical analysis and parameter study. To complement the theoretical study, an experimental investigation is required to perfect procedures and techniques to measure thermal, physical, and optical properties of existing fabric materials.

To accomplish these objectives a five-year program of research was originally outlined - three years of which have been completed. Reductions in DASA funds curtailed the completion of the entire five-year research program. This final report summarizes our accomplishments of the above specific objectives to the extent possible.

During the first year (as reported in Reference 1), a simplified mathematical model was chosen, and the heat-flow equation was solved

using an explicit finite difference technique. Considered in the analysis were a time-dependent heat input, fabric diathermancy, and nonlinear radiation and convection boundary conditions.

Not included in this theoretical model are various physicochemical effects which occur in a real fabric as the temperature increases. These can include thermal property variations and changes in the fabric optical properties. In addition, heat liberation or absorption processes which accompany some chemical reactions effectively create heat sources or sinks in the fabric which must be accounted for.

Several sample calculations were performed for comparison with existing theories. A concurrent experimental investigation was initiated to provide much needed information pertaining to the fabric heat-flow problem. A major purpose of this investigation was to provide information pertaining to the heat-flow processes at the front surface of the fabric and in the air-gap region. In addition, further information pertaining to the thermal, optical, and physical properties of various fabrics were also needed.

Theoretical considerations were given to the flash discharge method for determining thermal diffusivity of diathermanous materials. An equation describing the temperature time variation of a specimen rear surface for energy absorption in depth, as opposed to absorption at the front surface, was derived. An extension of this developed equation was derived to consider front surface heat losses.

Laboratory test experiments with the flash tube apparatus were conducted and thermal property data were obtained for several opaque conductors (metals) and for opaque and diathermanous non-conductors (plastics). The temperature time histories compared favorably with theoretical predicted values.

During the second year of this program theoretical procedures were extended and a computational study was performed to better understand the relative significance of various parameters isolated during the first year's

efforts. Explicit finite difference calculations were performed on a Control Data G-15D digital computer. (Refer to Reference 2).

Emphasis on experimental efforts was increased during the second year. An arc image furnace, thermal test chamber, and optical visualization equipment were set up to study heating effects of fabrics exposed to square wave radiant energy heat pulses. Techniques utilizing a Mach-Zehnder Interferometer were developed to measure fabric surface temperature. The interference events were recorded with motion picture cameras allowing accurate descriptions of temperature-time variations for the transient heating phenomena. A 6-ounce cotton poplin, an 8.8-ounce cotton sateen and an 8-ounce wool (OG107) were selected for considerable experimental testing.

Complete description of equipment and experimental procedures, with major emphasis given the interferometer, and results of calibration tests and preliminary temperature time variation recordings are included in the Second Annual Report.[2]

During the third and final year major emphasis was given experimental investigations using interferometer techniques. Experiments were conducted on fabric-airspace-skin models and temperature-time variations compared with the theoretical non-dimensional heat transfer response characteristics for the model developed during the first year. Results from interference temperature recordings are presented in terms of various heat transfer parameters.

Further interferometer techniques were developed to enable determination of degradation gases and concentrations as a function of temperature and time. The necessity for considering chemical properties evolved from requirements for obtaining accurate interferometer temperature-heat transfer data. Refractive index variations due to the presence of unknown degradation gases were studied. To analyze these variations a multi-wavelength technique and a multi-environmental test technique were considered in detail. Expressions for interference

fringe shift displacements in terms of temperature, gas molecular refractivity, and gas concentration were developed for both techniques and programmed for solution on a Control Data 1604 Digital Computer. Comprehensive tests were made on fabric systems in separate environments of air, helium, nitrogen, argon, and CO_2. For water saturated fabrics under heat loads of approximately 6 cal/cm^2-sec concentrations of vapor at the fabric surface were determined as a function of temperature and time.

Fabric front and rear surface heat transfer coefficients were measured both for steady state and transient heat flow conditions. These tests showed that extreme caution must be shown in properly evaluating heat transfer coefficients for conditions of rapidly changing surface temperatures.

2. THEORETICAL STUDIES

2.1 Previous Theoretical Studies

Solutions to problems involving the conduction of heat in solids can be found in such textbooks as Carslaw and Jaeger.[3] They present several solutions for semi-infinite slabs in which the use of the Laplace transform makes the solution relatively simple. Boundary conditions involving radiation (convection and linearized thermal radiation) into a medium with temperature varying with time are reduced to the case of constant environment conditions by Duhamel's theorem. Exact solutions for nonlinear boundary conditions or when properties are a function of temperature are not presented.

The fabric-skin heat transfer problem was studied by Chen and Jensen,[4] who emphasized a numerical graphical technique patterned after Schmidt's[5] original method (with modifications of initial conditions and method of boundary subdivision), linearized radiation and convection losses at the fabric surfaces and combined them into single heat-loss terms. Their method was developed for square-wave radiation heat input, although they showed how it could be applied to a time-dependent heat pulse. Fabric diathermancy was considered, and optical and physical properties were assumed constant. The results were presented in a general nondimensional form for the case of fabric opacity, and a "three-curve" method was presented which provided fairly accurate results for various fabric diathermancies.

In another report, Hottel, et al.,[6] extended the work of Reference 4 to include the case of a moist cloth-skin system and discussed the computational methods in great detail. A method was developed for square-wave radiation impinging on opaque fabric, but the possibilities of extending the calculations to include diathermanous fabric and a time-variant heat input were mentioned. Experiments were carried

out to substantiate both the dry- and moist-cloth models, and results agreed fairly well with the calculations. The authors reported that the greatest uncertainties existed in the evaluation of heat and mass transfer coefficients and water vapor diffusivity.

In a research program at Armour,[7] an analytical study of single and composite slab systems irradiated by square-wave and variable intensity radiation was reported. Working charts to allow prediction of the degree of burn were presented for a composite slab exposed to variable intensity radiation, neglecting the effects of surface re-radiation.

Calculations that included the re-radiation term were made for a protecting material of finite thickness in perfect thermal contact with an infinite slab (the skin). This nonlinear boundary condition was handled by formulating a function which described the temperature-time variation at the outer surface. Two parameters in the function were evaluated by trial and error.

The A. D. Little Company[8] has also completed a theoretical and experimental investigation of heat transfer to skin through a cloth layer. One of the models they considered was multilayered with the inner layer having a low thermal conductivity (air), overlayed first by a low emissivity layer, and finally an outer layer which evaporates, and in so doing, absorbs heat. A constant property solution was obtained and square wave and triangular approximations of the thermal pulse were assumed. Their first model assumed no temperature gradients normal to the outer two layers and a constant temperature at the bottom of the air space. They also linearized the radiation boundary condition term for one calculation and retained it for another. An improved model made it possible to vary the temperature both in the air space and in the skin at the bottom of the air space. Their final model allowed the temperature to vary with depth in the outer clothing layer. They retained the nonlinear radiation boundary condition and used a finite difference method of solution. They did not consider any diathermancy

effects through the cloth. Their final model considered the effectiveness of smoke generation in reducing heat transfer to the skin.

The heat conduction equation has been solved for many configurations using both analytical and numerical methods. However, the boundary conditions used were not general enough to apply to our problem.

Additional theoretical studies pertaining to the present problem are included in Reference 1. In addition, new results have since been reported in the literature. The new studies will not be discussed, however, as they do not appreciably advance the present state of the knowledge. The greatest improvment in the fabric-skin theory now available will come when chemical effects can be included in the mathematical analysis.

2.2 Development of Theoretical Model

The studies discussed in 2.1, above, and in the First Annual Report[1] have contributed in varying degrees toward the attainment of a basic understanding of the fabric-skin heat transfer problem. Various assumptions have been made regarding the proper heat transfer mechanisms to insert into the surface boundary conditions. Factors such as fabric diathermancy, moisture content, and time-dependent heat inputs have been considered. But further work, both analytical and experimental, is needed to better define the heat flow processes within the fabric and at the surfaces. Very little information is available regarding actual temperature distributions through the fabric during a heat pulse because of the experimental difficulties involved. Usually the effectiveness of a protective fabric layer is judged by the heating effects experienced by a skin simulant or calorimeter placed behind the fabric.

Under conditions of high radiant loading and associated fabric temperatures, chemical reactions influence the heat flow process to a considerable extent. The intimate interrelationship between heat transfer

and chemical reactions (such as ablation, sublimation, oxidation and reduction, and degradation) have long been recognized and studied in great detail in nose cone re-entry problems. To our knowledge, the effects of chemical reactions in the fabric-skin heat transfer problem have not been included in any analysis. These reactions complicate any mathematical or experimental studies because they can give rise to heat absorption or generation, physical and optical property variation and surface degradation that greatly influences both absorbed and re-radiated energy.

Fabric moisture content is important (as shown in Reference 6), and additional analytical and experimental efforts are needed to understand the transfer processes involved. Heat transfer processes between the fabric rear surface and skin, and convection and reradiation at the front surface should be investigated further. Additional information is needed regarding the temperature dependence of a fabric's physical and optical properties.

The model initially chosen for the present investigation is fairly simple; it does not allow inclusion of all the basic mechanisms and processes mentioned above. It will, however, be improved as further insight is obtained from our experiments and parameter studies. More of the fabric's physical and optical properties will appear during the formulation of the heat flow equations. A meaningful insight into the problem can only be obtained if the relative importance of parameters formulated from these properties is determined. Initial emphasis will be placed on the fabric itself, rather than on the heat transfer and degree of burn experienced by the skin.

For our problem, two one-dimensional models are postulated (see Figure 1). Both involve infinite flat surfaces of finite thickness. In the first, the flat plate is separated from another structure, the skin, by an air space; in the second model, the fabric is in intimate contact with the skin. In the actual case, combinations of these two limiting conditions would probably be obtained.

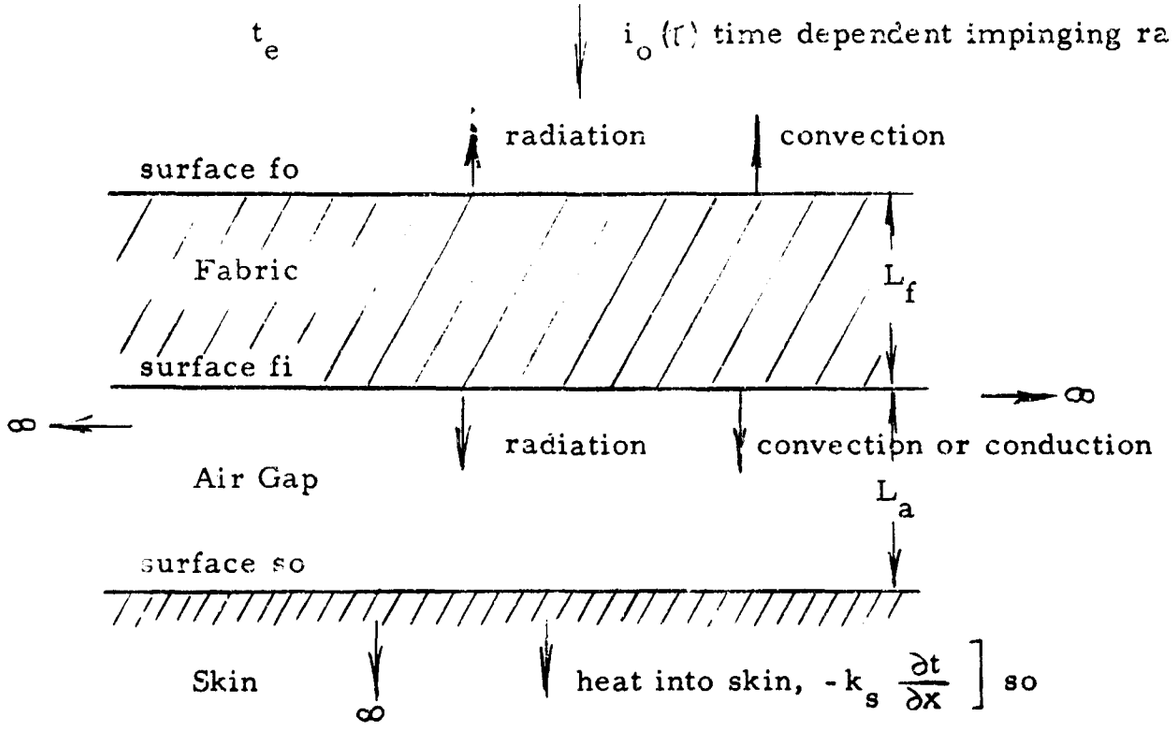

Model No. 1

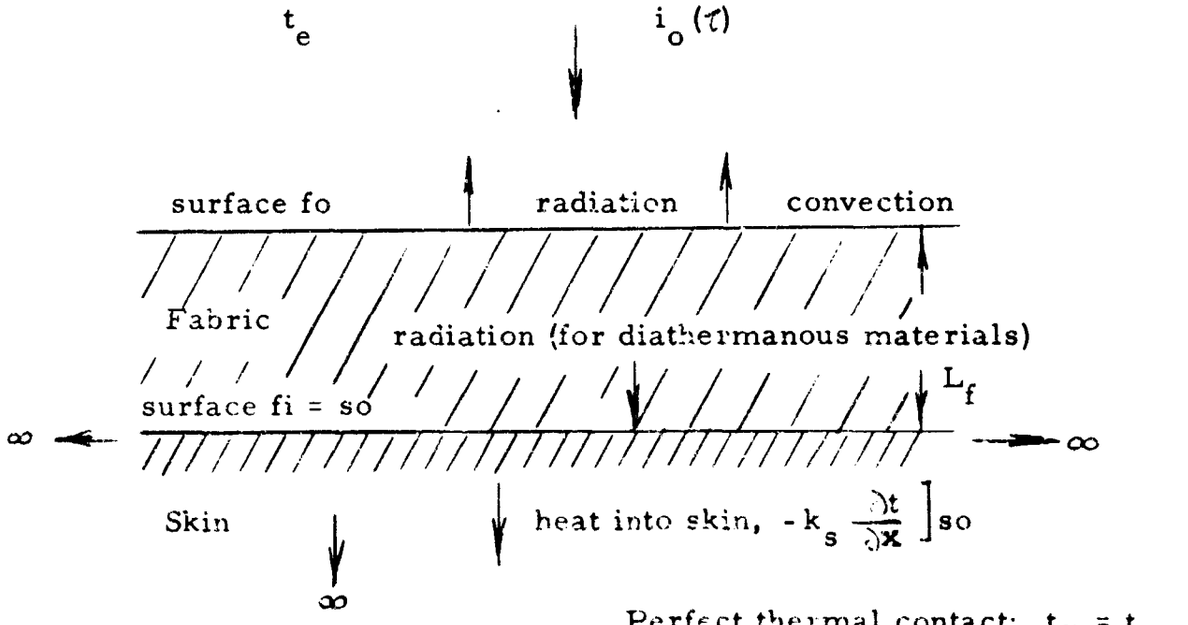

Model No. 2

Figure 1. Heat Transfer Models

The first model actually involves solution of a three-layer problem, the fabric and air space of finite thickness and the skin layer extending to infinity. We have assumed that a heat input varying with time is impinging on the fabric outer surface. A certain portion will be reflected and the rest absorbed and diffused into the fabric. Chemical reactions will not be considered, so no exothermic or endothermic heat processes will take place and the surface properties will remain constant.

Of the energy absorbed, a portion will be reradiated and convected from the outer surface. The rest will diffuse into the fabric and make its presence felt by raising the back surface temperature. Depending on the configuration, heat transfer will then take place to the skin by processes of conduction, convection and radiation. The degree of burn experienced by the cutaneous skin layer will be a function of this heat flux.

2.3 Heat Flow Equations and Boundary Conditions

The problem of a time-dependent radiant-heat input into a fabric-skin system is extremely complex and practically unsolvable if rigid adherence to the true physical situation is shown. To simplify the problem, the following assumptions have been made for the first model:

1) The fabric-airspace-skin system is assumed to be one dimensional.

2) Physical and optical properties of the system remain constant during the radiant exposure.

3) No chemical reactions are taking place.

4) The fabric is only slightly diathermanous to thermal radiation, and the skin is completely opaque.

5) The fabric has no moisture content.

6) The fabric is treated as a homogenous solid.

Heat losses from the front surface of the fabric consist of free convection and reradiation. Both terms appear in the front surface boundary condition, and no attempt is made to linearize them or to group them into a single linearized heat-loss term. Similarly, at the back surface of the fabric, radiation interchange is allowed to take place between the fabric and the skin, and heat transfer by conduction or free convection through the air space is also assumed. This allows explicit inclusion of fabric emissivity and absorptivity in the equations, and the heat-transfer processes and coefficients can be studied separately. If a diathermanous material is assumed, impinging short-wave radiation is absorbed in depth across the fabric, and the one-dimensional, heat-flow equation must include a heat source term. Assuming absorption according to the Beer-Lambert law, the equation is

$$(\rho c)_f \frac{\partial t}{\partial \tau} = k_f \frac{\partial^2 t}{\partial x^2} - i \frac{\partial}{\partial x} \left[\exp(-\gamma x)\right] \tag{1}$$

where $i = i_o (1 - \rho_{fo})$. In the skin, which is assumed to be completely opaque to thermal radiation, the equation without the heat source term is

$$(\rho c)_s \frac{\partial t}{\partial \tau} = k_s \frac{\partial^2 t}{\partial x^2} \tag{2}$$

with the assumption of constant properties in both equations.

The boundary conditions are as follows:

1) At the outer surface of the fabric

$$k_f \frac{\partial t}{\partial x}\Bigg]_{x_f = 0} - h_{fo}(t_{fo} - t_e) - \epsilon_{fo}\,\sigma(t_{fo}^4 - t_e^4) + iD = 0 \tag{3}$$

where the first three terms are the conduction, convection, and reradiation at the surface, and the last is the radiation input term. From a strictly mathematical viewpoint, the diathermancy factor D is either

0 or 1. Inclusion of the diathermancy term in Equation (1) with a defined value of the extinction coefficient requires selection of the former. If the material is completely opaque, the diathermancy term vanishes as in Equation (2), and D becomes 1 as is usually assumed for electrically conductive materials. When the equations are cast into a finite-difference form, it will be shown that selection of a D other than 0 or 1 is physically realistic, even though doing so is mathematically improper when a differential representation is used.

2) At the inner surface of the fabric

$$k_f \frac{\partial t}{\partial x}\Bigg]_{x_f = L_f} + h_{a_{eff}} (t_{fi} - t_{so}) + F_{f-s}\,\sigma(t_{fi}^4 - t_{so}^4) = 0 \qquad (4)$$

where the second term represents heat transfer by conduction or free convection through the air gap, and the last term is the radiation interchange between fabric and skin. Further discussion of the effective air-gap, heat-transfer coefficient $h_{a_{eff}}$ is included in Section 3.4.

3) And at the skin layer

$$k_s \frac{\partial t}{\partial x}\Bigg]_{x_s = 0} + h_{a_{eff}} (t_{fi} - t_{so}) + F_{f-s}\,\sigma(t_{fi}^4 - t_{so}^4) + i\alpha_{so} \exp(-\gamma L_f) = 0 \qquad (5)$$

with the last term representing the radiation directly transmitted through the fabric and absorbed by the skin. The factor α_{so} is the absorptivity of the skin for short-wavelength radiation. Values of α_{so} less than unity give rise to reflected short-wavelength radiation which is absorbed in depth in the fabric. This effect is neglected in the present development.

A detailed discussion of the above equations, sample calculations, and a parameter study are presented in Appendix A.

3. EXPERIMENTAL STUDIES

3.1 General

An important finding of the theoretical and experimental studies reported in References 1 and 2 is the lack of information pertaining to heat transfer processes at the fabric front surface and in the air space between the fabric and skin. Because of the difficulties associated with the measurement of fabric temperatures under transient conditions, experimental data are not available to compare with theoretically predicted variations. Thus new techniques such as utilization of the Mach-Zehnder interferometer become essential.

The interferometer provides an insight into the conduction and convection heat transfer processes occurring at both surfaces of the fabric and in the air spaces between layer systems. This instrument also permits study of the various degradation processes and eventual combustion of fabrics.

The interferometer as well as the schlieren and shadowgraph, operates on the characteristic phenomenon that density and pressure changes in a gas produce changes in the refractive index of that gas. Whereas the schlieren apparatus is sensitive to density gradients and the shadowgraph to changes in the density gradients, the interferometer indicates a direct change in density itself. In a constant pressure environment a direct measure of temperature changes may be obtained.

The Mach Zehnder interferometer has been used to great extent in aerodynamic studies. It has been used less extensively in heat transfer work. Eckert and Soehngen[9] and Kennard[10] were among the first to use the Mach Zehnder interferometer to investigate heat transfer phenomena. Other more recent studies include that of Carlson,[11] Goldstein[12] Novotny[13] Bevens,[14] Azzam[15] McLean[16] and Schneider.[17] A brief review of some of these works is included in Reference 2 and in Section 3.4 of this report.

In our review of the literature we found no studies where the interferometer was used to record phenomena surrounding a body heated by an intense radiant source such as the arc image furnace. Furthermore we have found no investigations that concern interferometric heat transfer studies involving fabrics. In general, little attention has been given to transient problems in various heat flow processes and the use of the interferometer for recording heat transfer or mass diffusion about a fabric-airspace-skin system under high thermal loadings represents a new area of investigation.

As described herein the combustion processes of materials under exposure to high intensity radiation can be examined with the interference technique. The possibility of using the interferometer to arrive at gas composition and concentrations during the heating stages and eventual combustion and buring of an exposed fabric is an important consideration in this program.

3.2 Experimental Equipment and Techniques

3.2.1 Thermal Radiation Test Facility

The basic component of this facility is the carbon arc-image furnace. The furnace is used as a high temperature radiation source to simulate solar energy and thermal radiation from nuclear energy release; it has a heat flux capability of 75 cal/sec (11 cal/cm^2-sec). A U. S. Navy 24-inch carbon arc searchlight was acquired and modified for use as the furnace. The parabolic mirror was replaced by an elliptical mirror to permit focal imaging of the arc. Power for the furnace is supplied by a 15-kw motor-generator set. Figure 2 shows an overall view of the facility.

Flux intensities are measured with various standard and miniature slug calorimeters developed by ASD. Heat pulse initiation and duration are automatically controlled and measured by a glow-tube counter (adjusted to 0.01 sec) and by timing systems (0.001 sec timing increments) coupled to the furnace signal key and motor gear assembly.

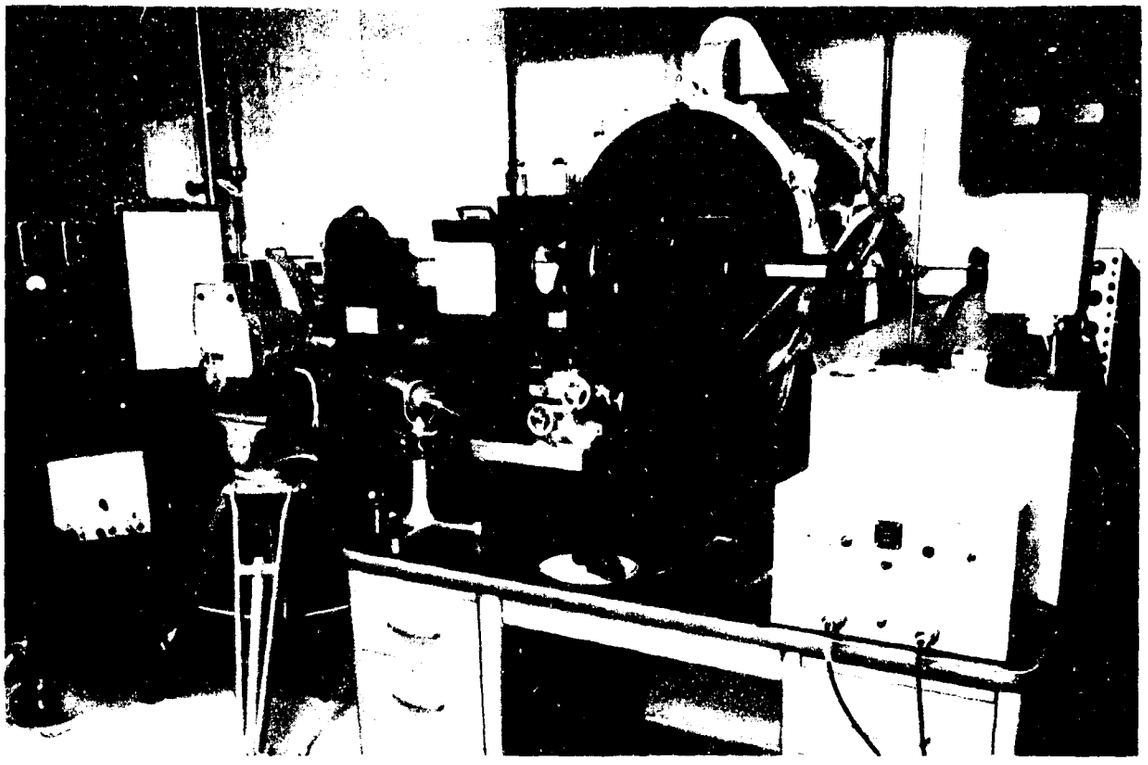

Figure 2. Overall View of Thermal Radiation Test Facility

Figure 3. Fabric Holder and Flux Redistributor

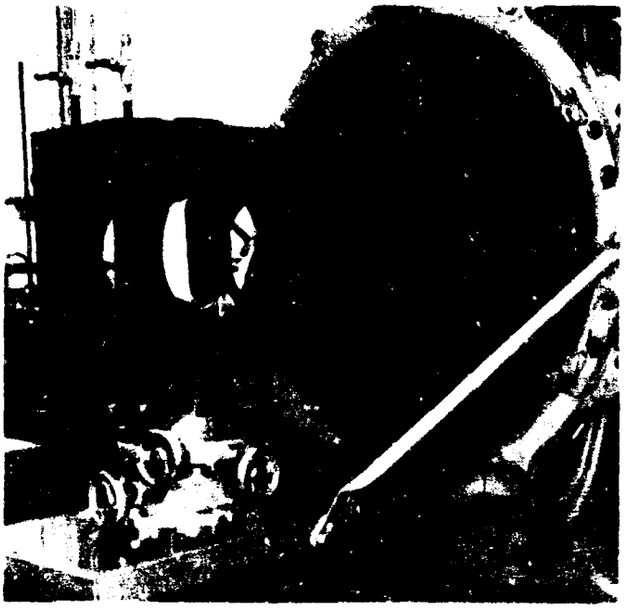

Figure 4. Thermal Test Chamber

Flux intensity and uniformity are controlled with various flux redistributor systems that transform the circular focal image of the arc into a rectangular pattern on the test specimen. This permits closer approximation of one-dimensional heating processes and easier correlation with theory. (Refer to Figure 3.)

An integral part of this facility is a special test chamber which can enclose in a controlled environment samples, sample holders, slug calorimeters, flux distributors, and other associated instrumentation. A quartz window at the front of the chamber transmits the arc beam onto the test specimen, and two optical quality viewing windows allow observation of the heating effects. The chamber is shown in Figure 4.

3.2.2 Mach-Zehnder Interferometer and Associated Equipment

The Mach-Zehnder interferometer and associated optical equipment are used to obtain qualitative and quantitative measurements of the heating effects on fabrics. Included are an optical bench, Fastax and still cameras, various light sources, and other optical and electronic instruments.

The interferometer used in the present investigations was originally developed for wind tunnel flow visualization studies. Without modification, this instrument was used to study the heat transfer processes at fabric surfaces and between fabric and skin surfaces for this present study. The optical elements of the interferometer which are mounted on a 2-1/2-centimeter thick aluminum plate, are 5 cm in diameter and provide an elliptical viewing area with dimensions of approximately 3 cm x 5 cm.

A schematic diagram of the interferometer is shown in Figure 5 and Figure 2 also shows the interferometer and some of the photographic equipment.

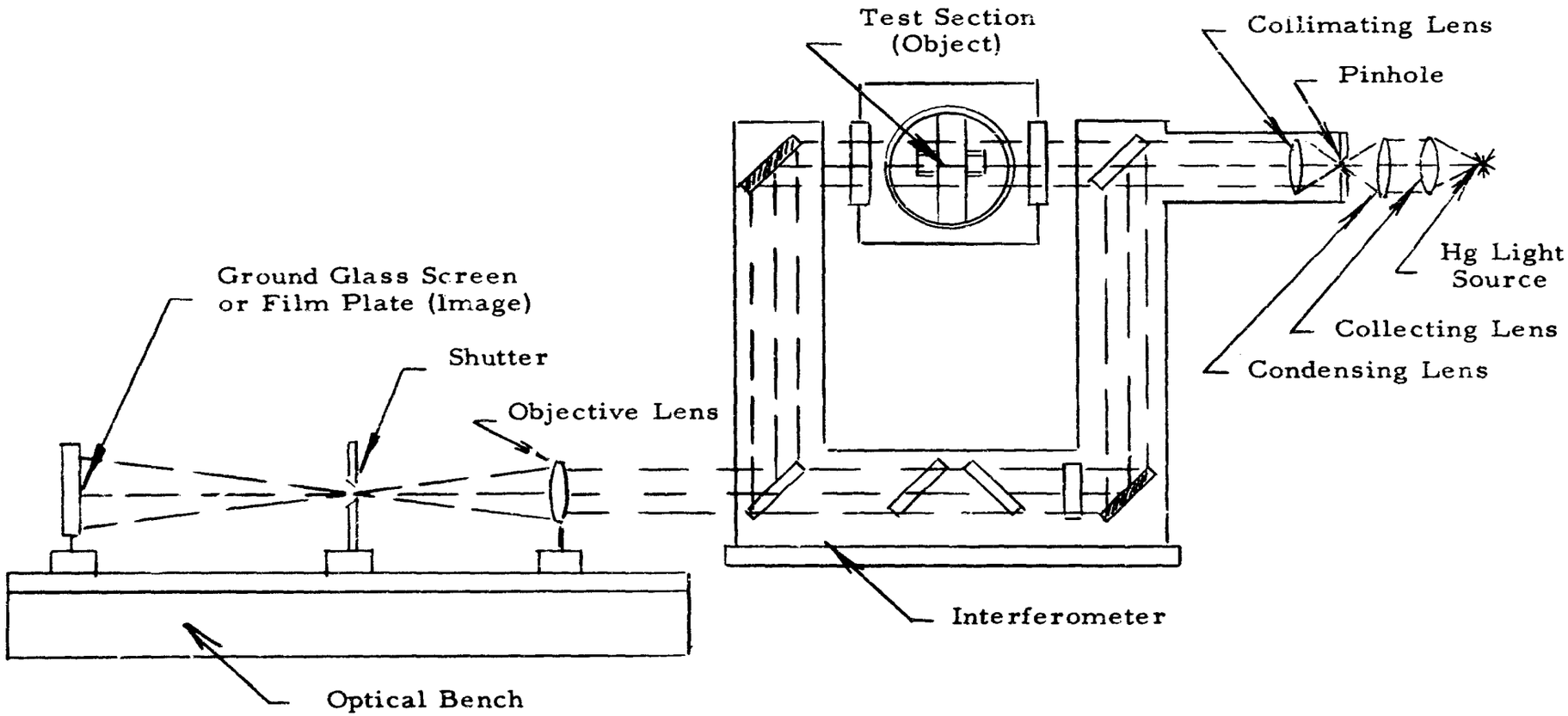

Figure 5. Schematic of Interferometer and Optical Bench Setup

3.3 Interferometric Photographic Studies

3.3.1 Single Environment Tests

3.3.1.1 Still Photographic Measurements

A series of heating tests on various fabrics exposed to approximately 5 cal/cm^2-sec radiant heating loads of various pulse duration were performed using still photographic techniques. The arc shutter timing mechanism was set for a given pulse duration and immediately following the close of the arc shutters interferograms were taken at 1/400th of a second using plus X film (ASA 160). Figure 6 shows interference fringe patterns for undisturbed heated and burning conditions of a white cotton twill weave suede cloth. When burning occurs the combustion enhances the free convection boundary layer thickness considerably as shown by the fringe bulging in Figure 6(c). The flame front extends well into the exit opening of the flux redistributor and distortion of the burning patterns are clearly shown.

From Figure 6(b), the temperature field distributions on both sides of the fabric have been determined and plotted in Figure 7. The constant temperature bands are conveniently measured fringe shift divisions and account for the particular temperature readings shown. The boundary thickness temperature distribution for the center of heated area is shown in the scaled insert to the right, evidencing the higher temperature of the front surface. In subsequent motion picture sequences from which interference temperature data were extracted, the differences from the front to rear surfaces were found to be considerably greater for 8.9 oz cotton sateen than that indicated in Figure 7.

Interferometric recordings were made at different instances in the heating phase in the manner described above for a variety of fabric materials. For cottons, although the combustion temperature depends on moisture content, rate of heating, fabric purity, etc., the ignition

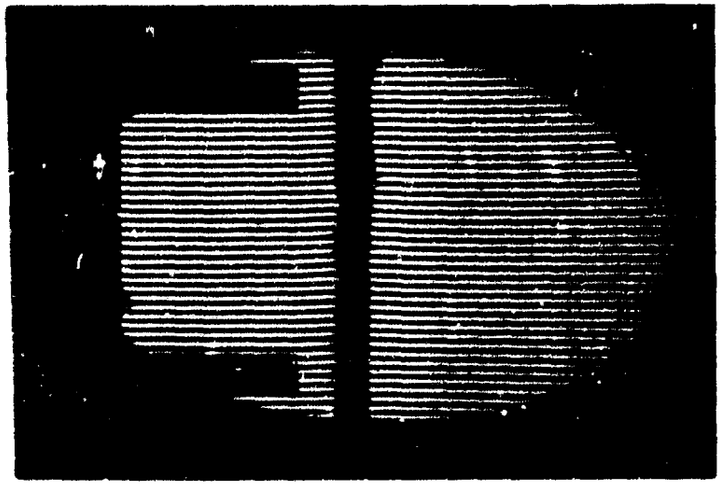

a. Undisturbed Fringe Pattern

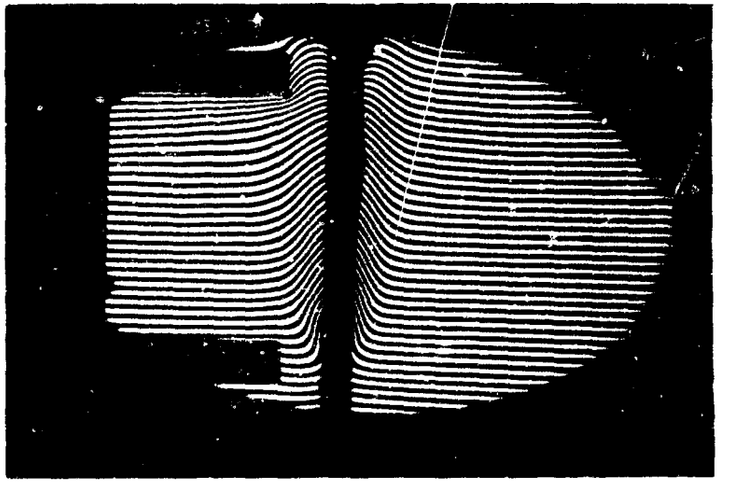

b. After 1.95 Second Arc Exposure

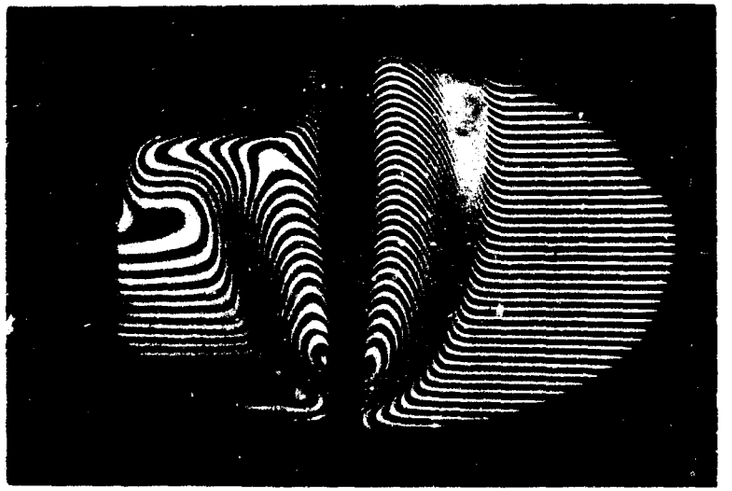

c. Burning Occurring (3.85 Second Arc Exposure)

Figure 6. Interference Fringe Displacement Effects for Vertically Heated White Cotton Twill-Weave Suede Cloth

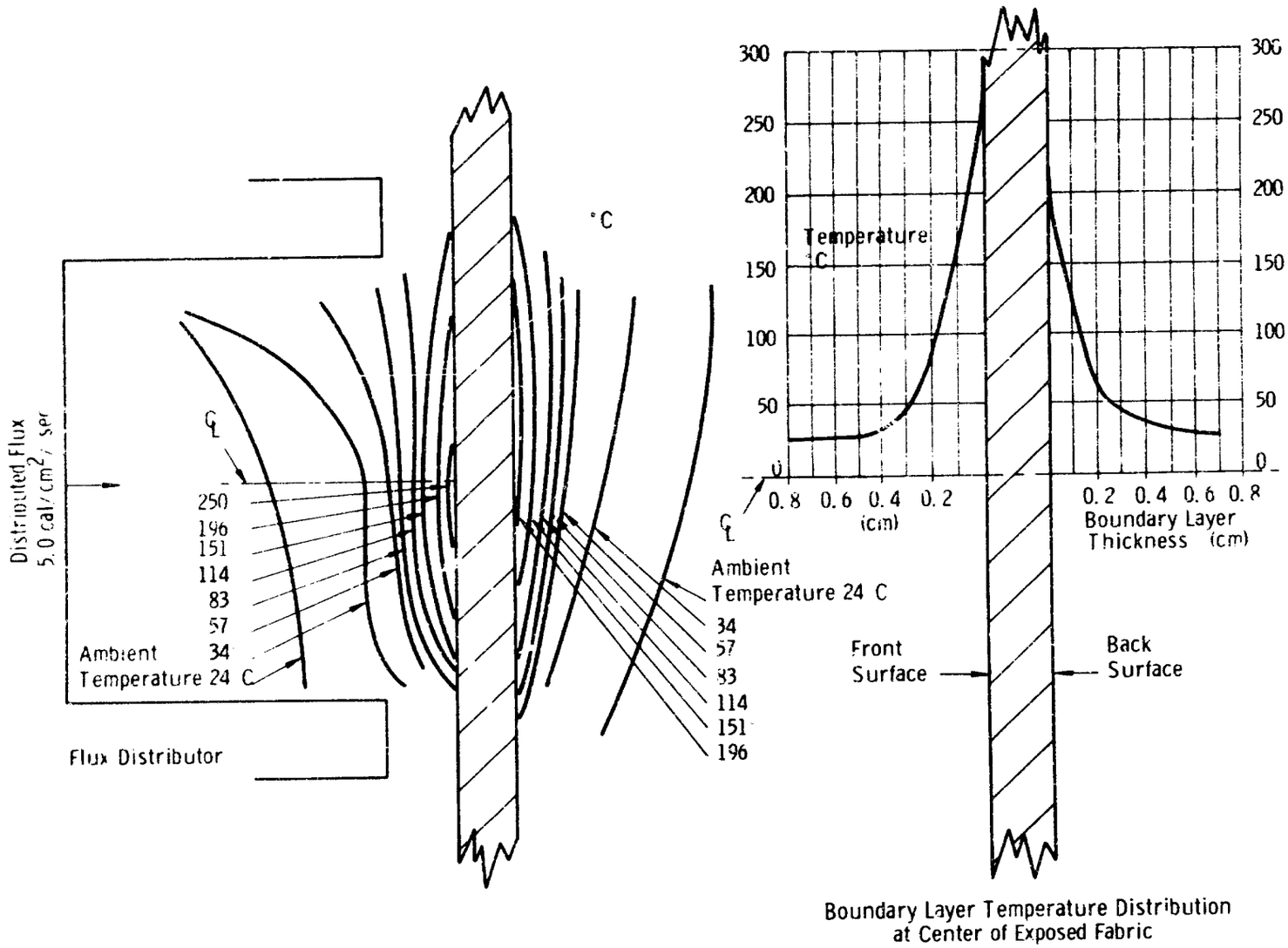

Figure 7. Temperature Gradients in Thermal Boundary Layer for Heated White Cotton Twill-Weave Suede Cloth (1.95 second arc exposure)

temperature as indicated from these interferograms corresponds quite well with values presented by MacHattie[18] in his measurements of fabric rear surface temperature using a radiometric method. In Figure 8 a two-layer cotton system (spacing 0.6 cm) is shown before heating (a), after heating for 1 second (b), and after burning occurs (c). It is interesting to observe the effects heating or burning of a front layer has on a second layer. When the first fabric layer ignites, the flame front, shown qualitatively in the interference fringe pattern, appears squeezed between the fabrics prior to ignition of the second layer. As the spacing decreases the flame front appears further contained and does not develop fully as at a free surface. Finally, for close spacing, to the point of contact, burning envelops both layers with combustion of these layers occurring after a greater heat input than required for combustion of a single test layer or for two test layers of greater spacing.

It must be realized that the laboratory results of a multi-layer diathermanous fabric system cannot be directly related to field conditions. Due to scattering, and since the incident energy impinges on a relatively small area, the direct energy received by the second layer is spread over a larger area with a resultant decrease in flux density. Under field conditions the incident flux is distributed over a large area and localized effects do not occur.

3.3.1.2 Motion Picture Measurements

Interferometric temperature time data were taken from motion picture recordings of the arc heated fabrics. Sequences were filmed at speeds of 64 frames per second to 9000 frames per second. For sequences of several seconds duration recordings at 64 frames per second were adequate for data analysis purposes. During the final heating stages and combustion instances recordings were made at 1000 to 9000 frames per second using the 400-foot, 16-mm film capacity of the Fastax camera. Timing marks at 0.001-second intervals permitted

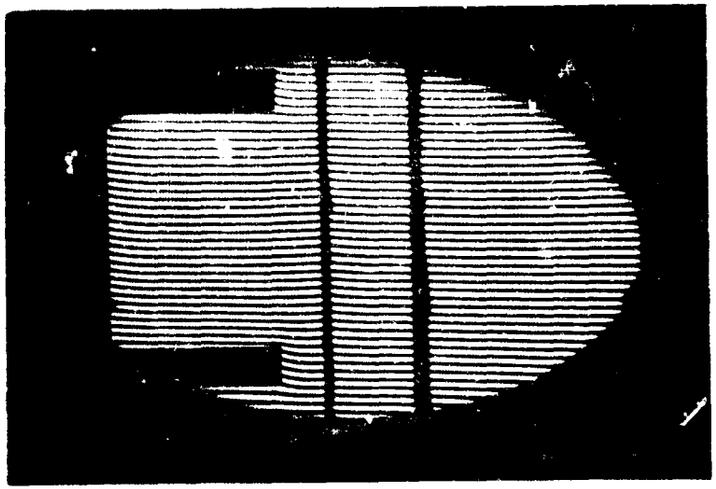

a. Undisturbed Fringe Pattern

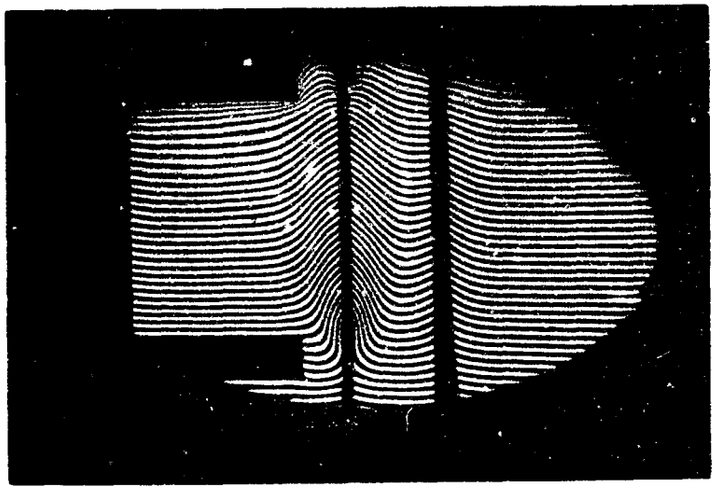

b. After 1.00 Second Arc Exposure

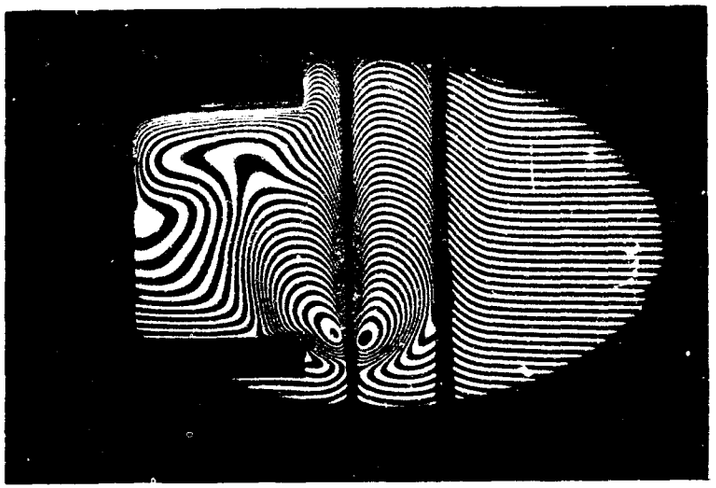

c. Burning Occurring - 1.05 Second Arc Exposure

Figure 8. Fringe Displacement Effects for Two Layer, Light Green Cotton System (Spacing 0.6 cm)

accurate time measurements through the event. Selected frames for the heating and combustion sequences for a heated cotton specimen are included as Figure 9. Because of the rapid sequence of events during the intermediate phases of combustion, photographs at 0.001-second increments are shown starting at 1.705 to 1.710 seconds. The remainder of the photographs are presented at 0.005 – second increments.

The indicated fabric surface temperature for a 6-oz OG-107 cotton fabric, as a function of time after heat pulse initiation, is shown in Figure 10. The dashed curve is a correction for errors in the measurements attributed to end effects. These errors, associated with boundary layer growth at the edges of the fabric (increasing refractive path length) was determined from the calibration curve (Figure B-14 of Appendix B) for a metal disc 0.3 cm thick. Since the fabric thickness varies it was determined that the correction does not truly apply (see Reference 11).

These tests in general were carried out until severe fabric damage is visually discerned. Test conditions were taken at ambient air and room humidity (approximately 28 percent relative humidity). In other experiments, oven-dried fabric heating response characteristics were compared with room humidity tests.

Indicated temperature values were found true during the early and intermediate heating stages; thereafter errors due to the presence of degradation gases and combustion produces were too great and analysis was not made.

In Figures 11 through 14, front and rear surface indicated temperature values are plotted for representative military style fabrics. The heavier cotton (8.8-oz sateen) demonstrates a greater temperature difference from front to rear for a given heat load over that shown for the 6-oz cotton poplin variety as would be expected. The temperature difference indications for these fabrics are considerably greater than that noted in earlier still-photo recordings where interferograms were taken upon close of the arc-furnace shutter. No corrections for end effect were made.

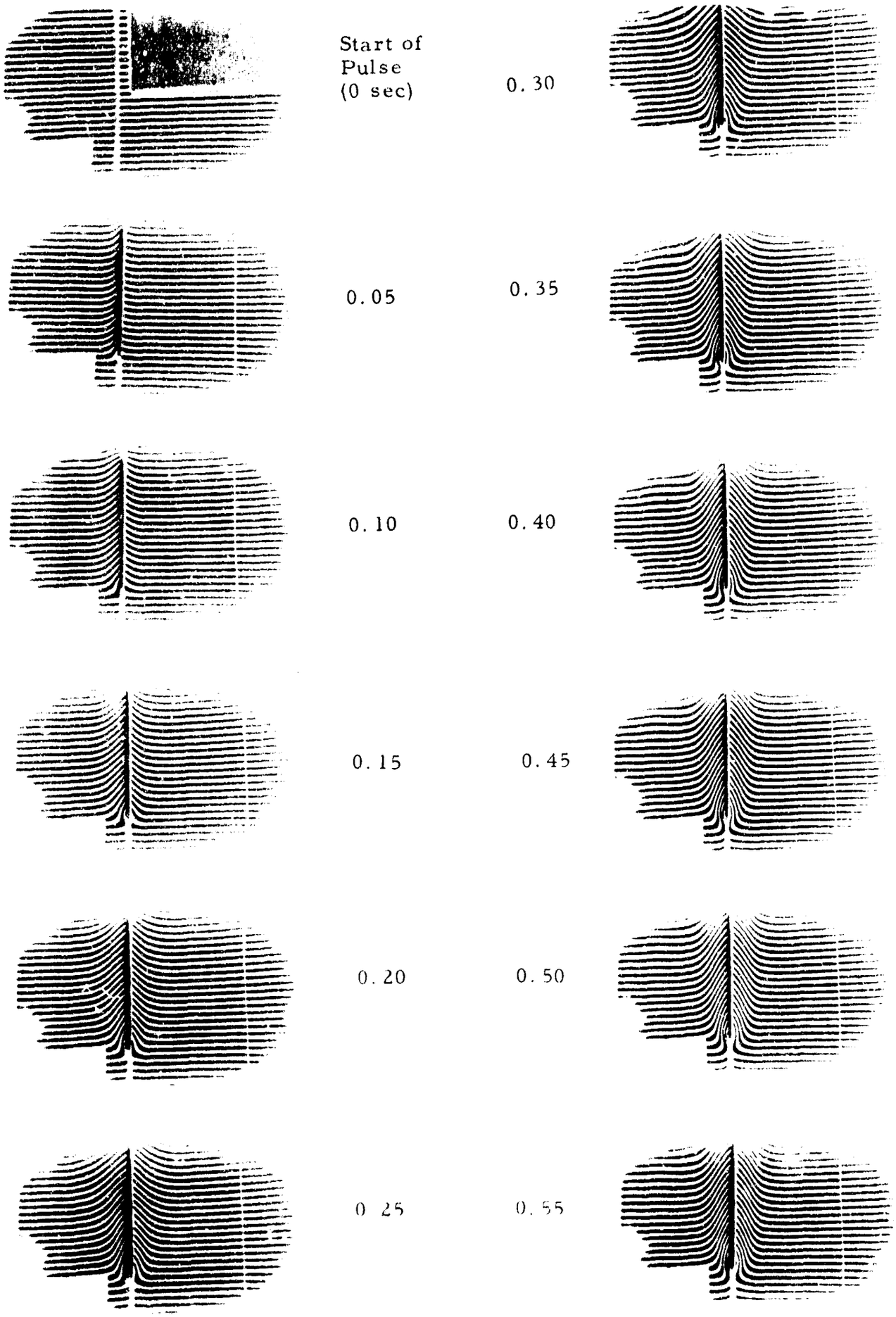

Figure 9. Fastax Photographs Showing Heating and Combustion of a Dry Cotton Fabric (9000 Frames/Sec: Time Increments Shown in Sec)

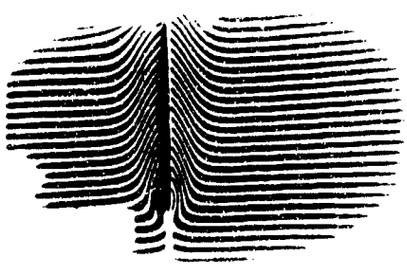

0.60

0.90

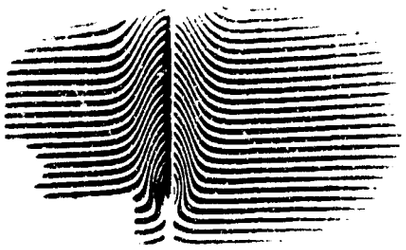

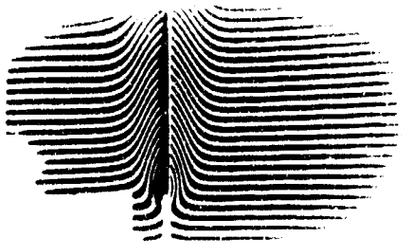

0.65

0.95

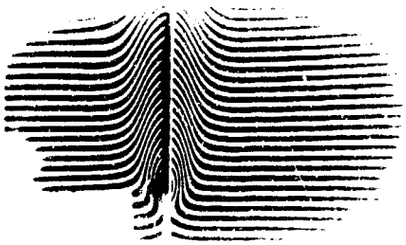

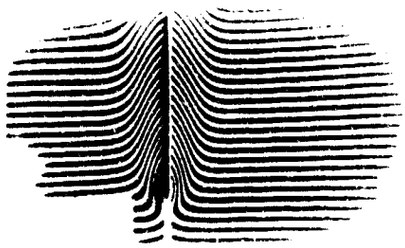

0.70

1.00

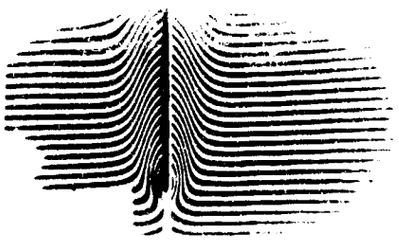

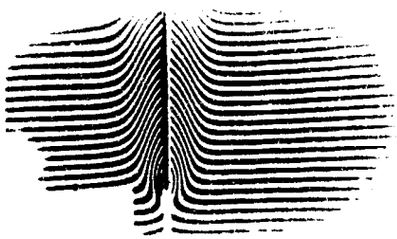

0.75

1.05

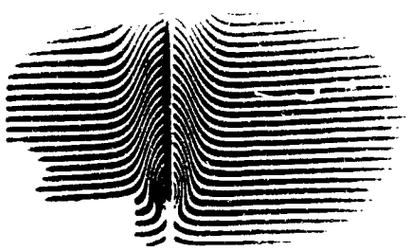

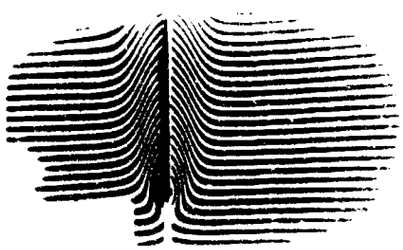

0.80

1.10

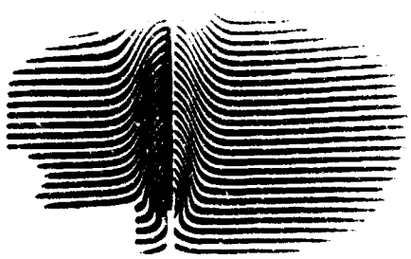

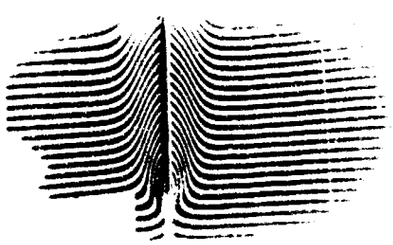

0.85

1.15

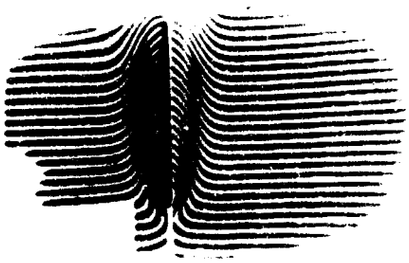

Figure 9. (Continued)

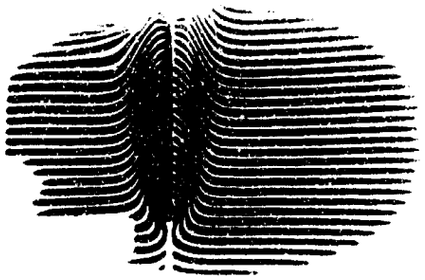

1.20

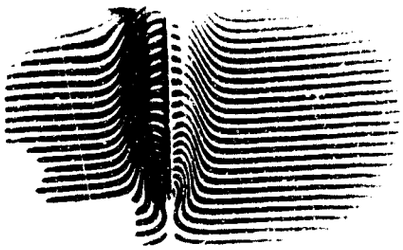

1.50

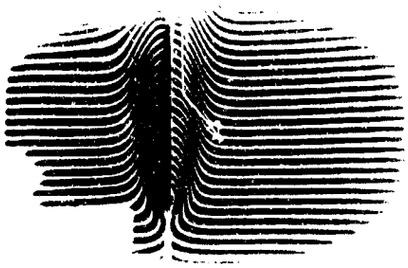

1.25

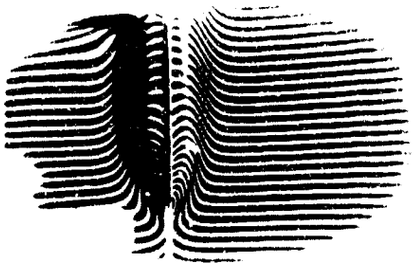

1.55

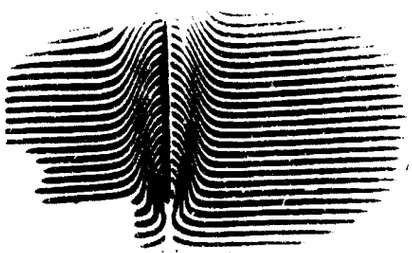

1.30

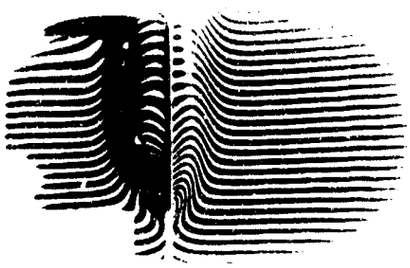

1.60

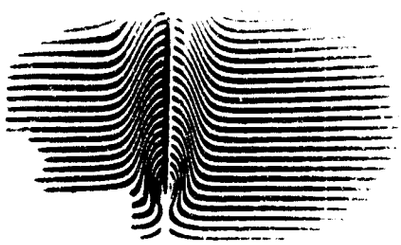

1.35

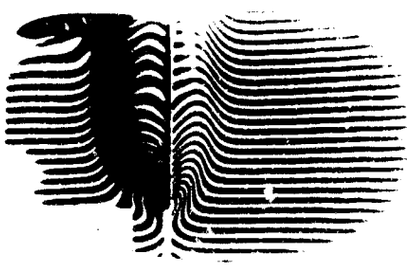

1.65

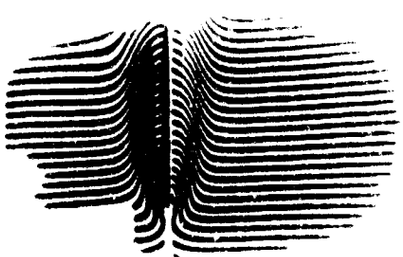

1.40

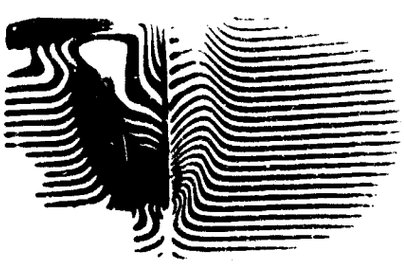

1.70

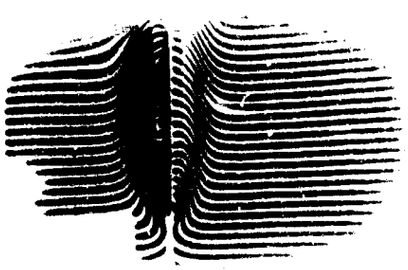

1.45

Figure 9. (Continued)

1.705

1.708

1.706

1.709

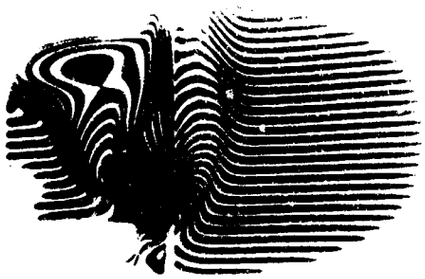

1.707

1.710

Figure 9 (Continued)

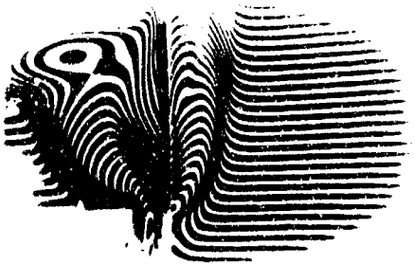
1.715
1.740
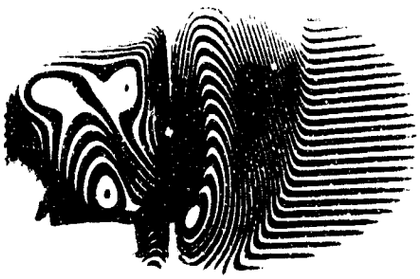

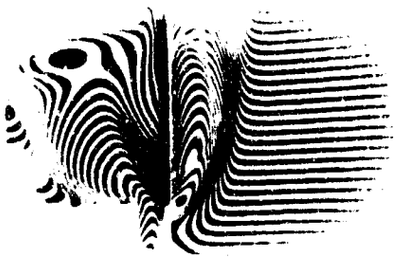
1.720
1.745
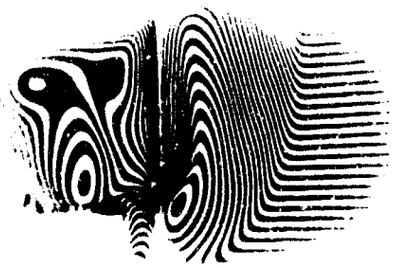

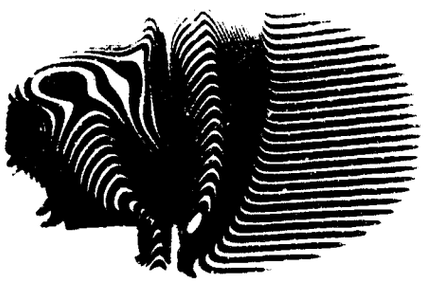
1.725
1.750
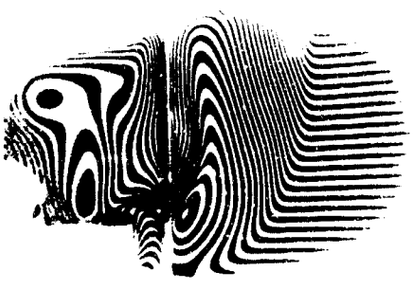

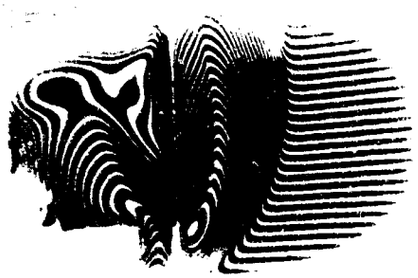
1.730
1.755
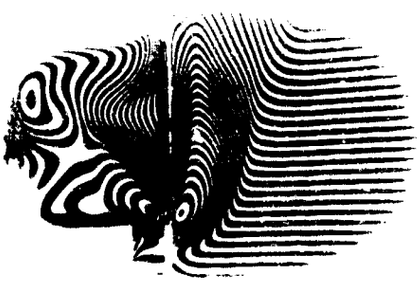

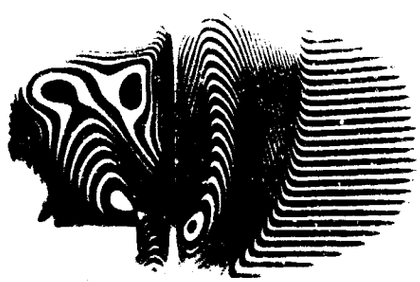
1.735
1.760


Figure 9. (Continued)

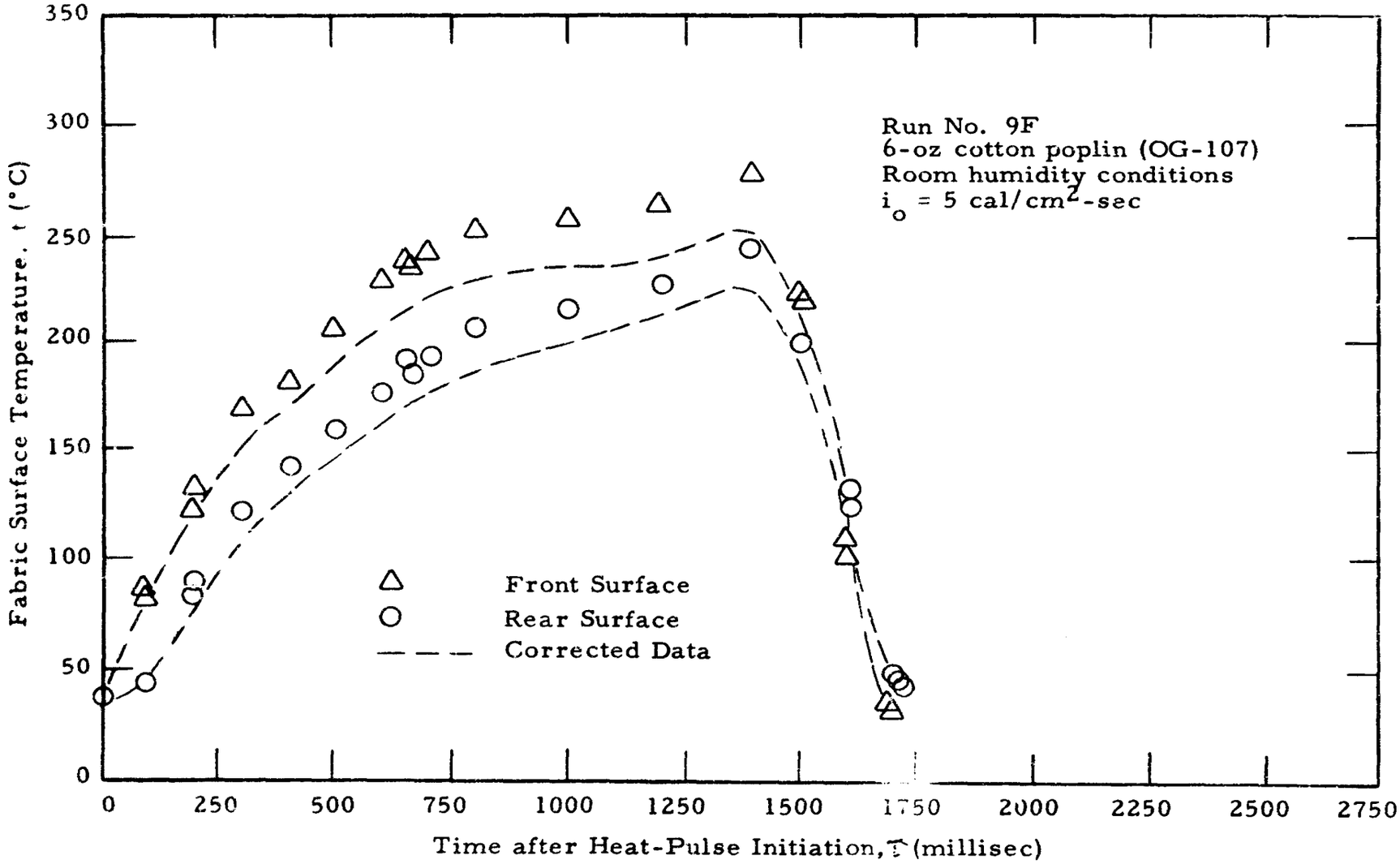

Figure 10. Temperature-Time Variation of Cotton Poplin Fabric Surfaces

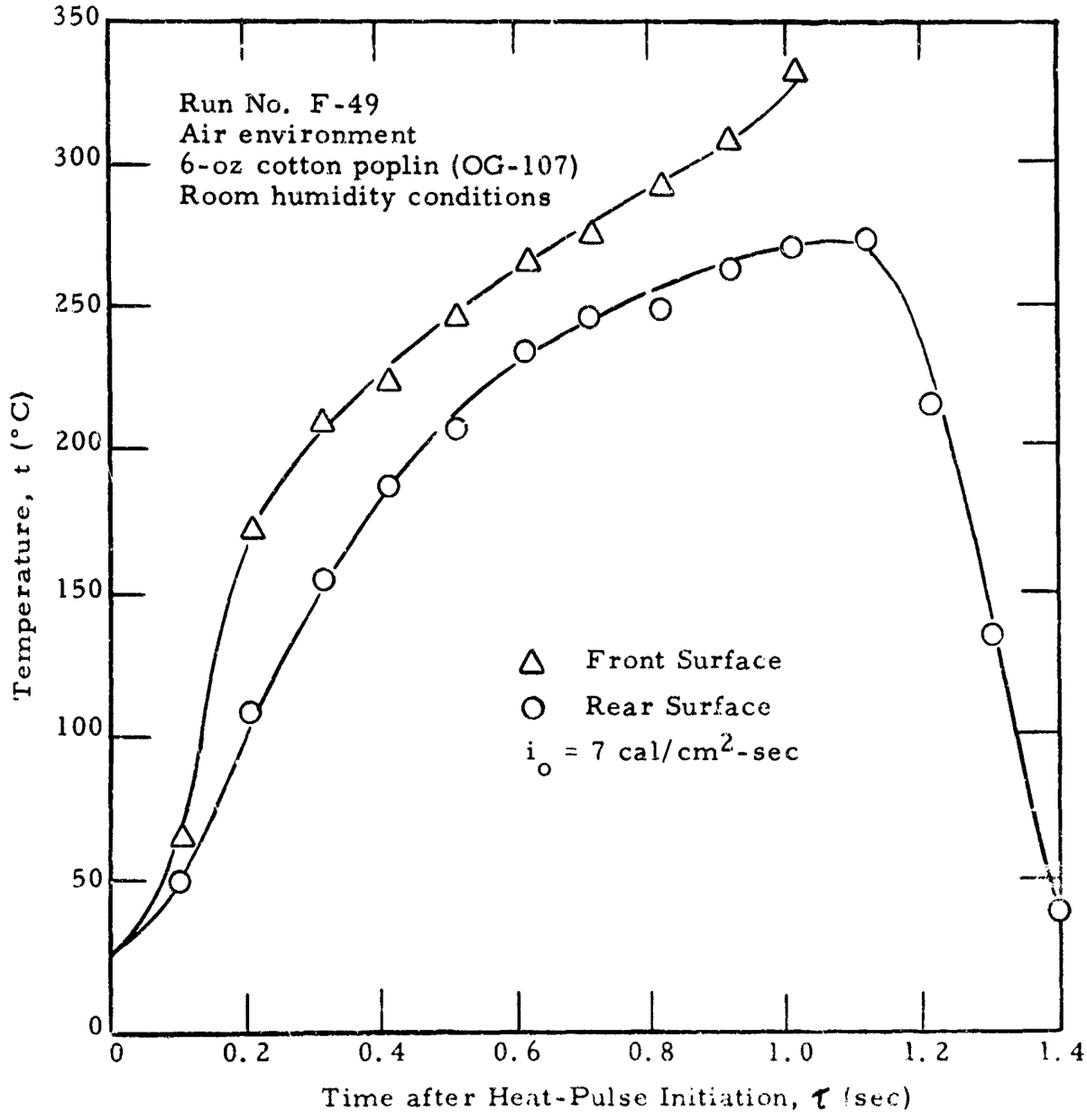

Figure 11. Temperature-Time Variation of 6-oz Cotton Fabric Surfaces

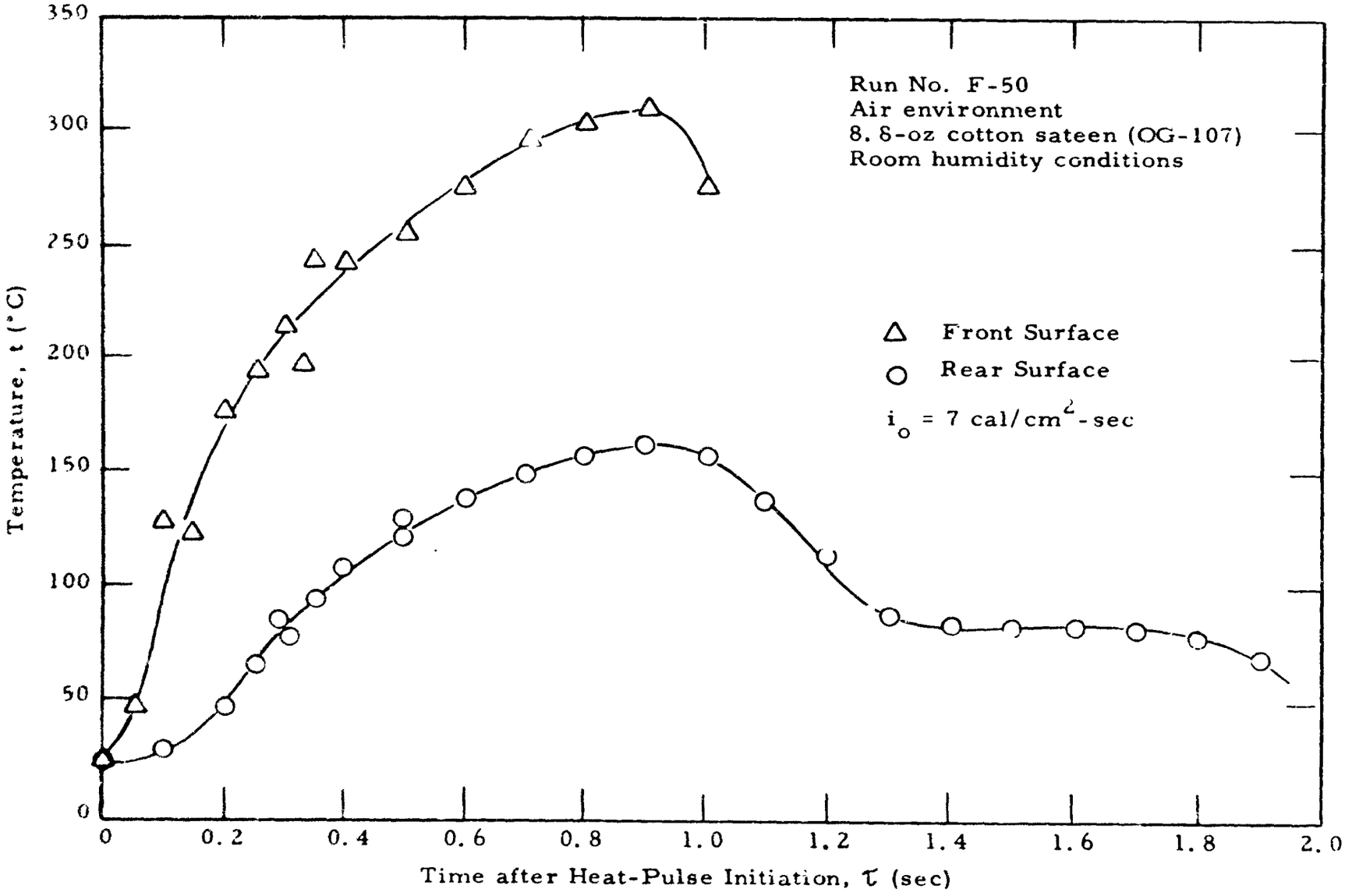

Figure 12. Temperature-Time Variations of 8.8-oz Cotton Fabric Surfaces

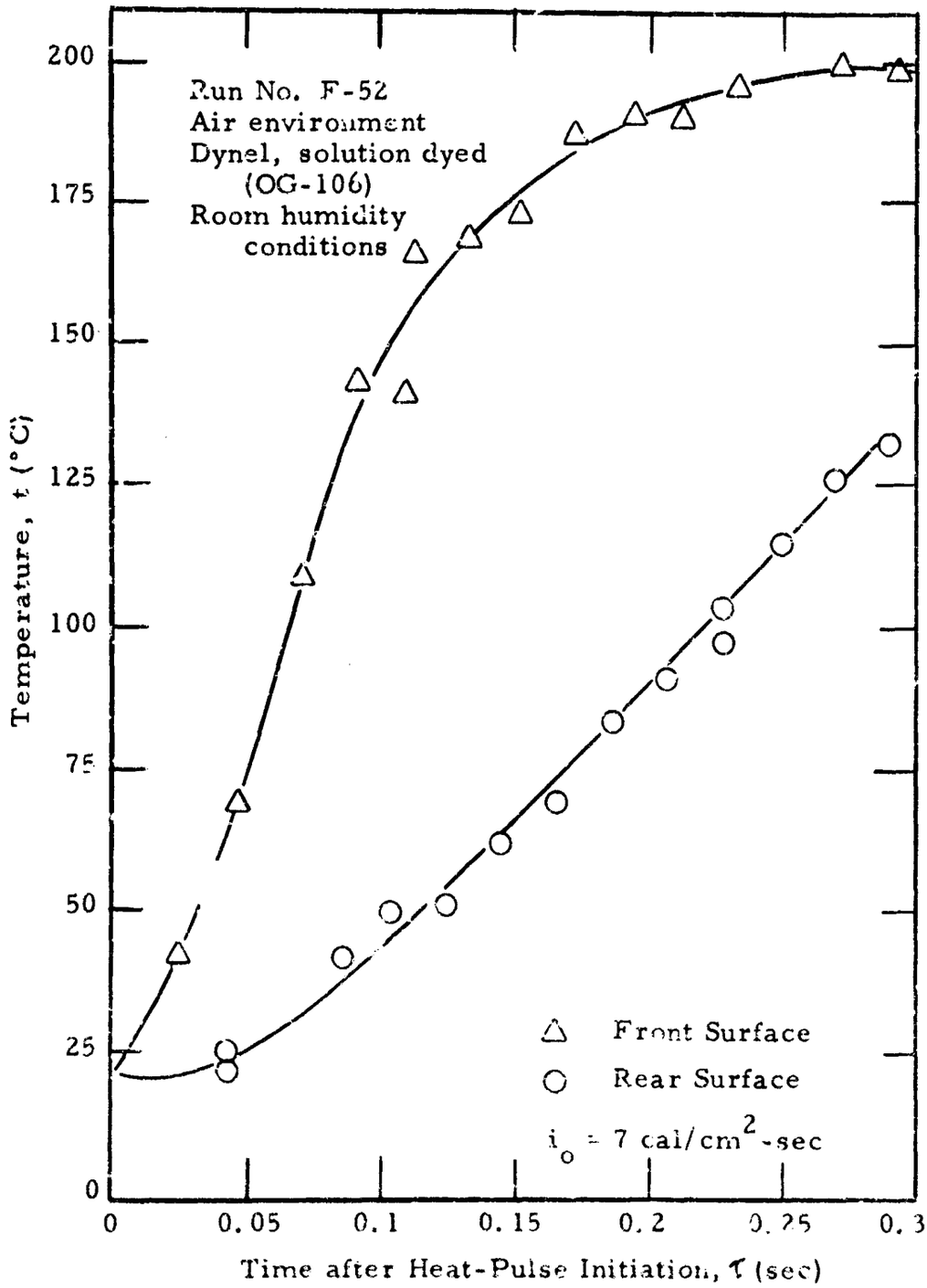

Figure 13. Temperature-Time Variation of Dynel Fabric Surfaces

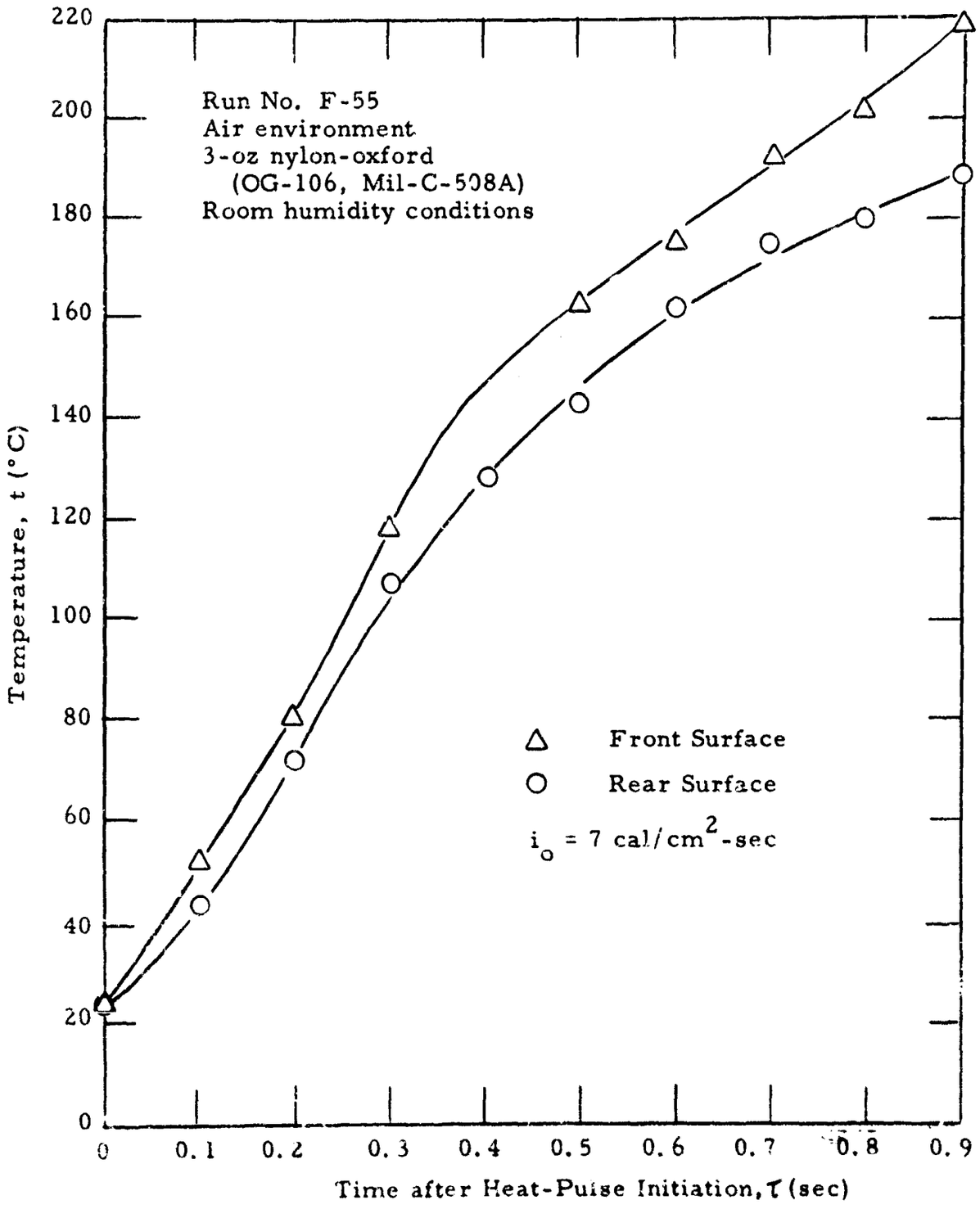

Figure 14. Temperature-Time Variation of Nylon Fabric Surfaces

3.3.2 Multi-Environment Tests

3.3.2.1 General Test Conditions

Interferometric recordings of the fabric heating degradation processes were made with the motion picture camera at 64 frames per second. High-speed motion picture sequences at 1000 frames per second or more were not needed because the heating rate in current tests only required data analysis at approximately 0.10-second intervals for sufficient resolution.

3.3.2.2 Fabric Tests - Ambient Humidity

The test procedure involved evacuation of the thermal test chamber and introduction of a particular environment. To speed the test processes and the number of tests per given time, a vacuum of 5 mm Hg was obtained and the new gas flushed into the chamber while the vacuum pump was still pumping. It was anticipated that purging was not complete and the environment conceivably contaminated with up to 1/2 percent air. This would result in a small, but undetermined error in the assumed molecular refractivity of the environmental gas.

The first series of tests in the different environments were conducted on cottons and wool at room humidity conditions. Figure 15 is a plot of the interference fringe shift variations with time (raw data form) for a heated 6-oz cotton poplin specimen in a helium environment. Included in this plot are rear boundary layer fringe values during degradation. The depression in the fringe shift values for helium prior to complete degradation (from 0.2 to 0.7 second) suggests that some small degradation reactions are occurring. It was determined that mainly water vapor (residual moisture content) and air (entrapped in the fabric during evacuation procedures) were evidenced during the heating cycle.

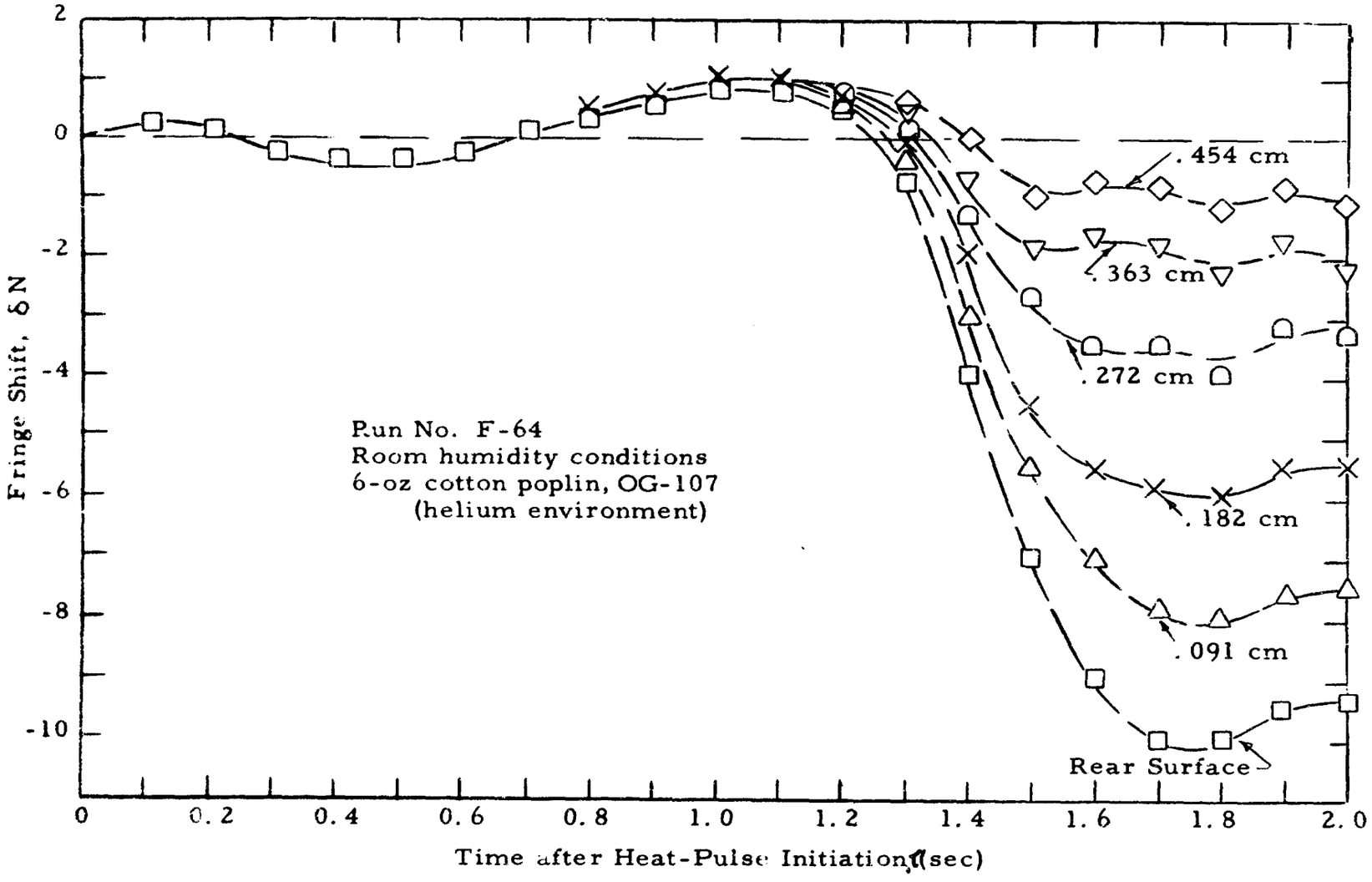

Figure 15. Fringe Shift Variations of Rear Fabric Surface and Rear Boundary Layer in a Helium Environment

The presence of both water vapor and air were noted also in the helium environment tests on 6-oz cotton poplin, 8.8-oz cotton sateen, and on 8-oz wool specimens. See Figures 16 through 18. The fringe shift variations in other environments do not readily indicate the presence of these gases (representative curves presented in Figures 19 and 20). Argon and nitrogen have molecular refractivities close to that of air and thus display quite similar fringe shift curves for some tests even during the degradation reactions where it would be expected that combustion (in air) should differ substantially from the processes encountered in an inert environment. From tests in CO_2 and with identical tests in helium and in nitrogen, an indication of the composite foreign gas molecular refractivity is obtained.

One would imagine a greater moisture content or more air entrapped in the heavier 8.8-oz cotton sateen over that of the light 6-oz cotton and possibly an even greater amount of both constituents in wool over that of the cottons. To some extent the fringe values observed at the rear facing surface for the three materials substantiate this, wool having a negative fringe value of approximately 1.9 before rising positively, the 8.8-oz cotton sateen fringe value of approximately -1.0 and the 6-oz cotton poplin a value of -0.6. The rear surface variations in helium are compared to a nearly identical test in air (Figure 21).

In the air environment during the initial and intermediate stages of heating the small amount of water present having a molecular refractivity not greatly different than air did not adversely affect the interference fringe number or the determined temperature values for the 6-oz cotton specimen. As calculated in Appendix B for a 100 percent saturation of water vapor in air at 100°C (water vapor effectively constituting the entire gaseous phase) the indicated temperature would be too high by 70°C. For this test with the 6-oz cotton (room humidity), water vapor did not exceed a fractional concentration of 10 percent as compared with the completely saturated test. With an indeterminate percentage concentration of entrapped air which would not affect the

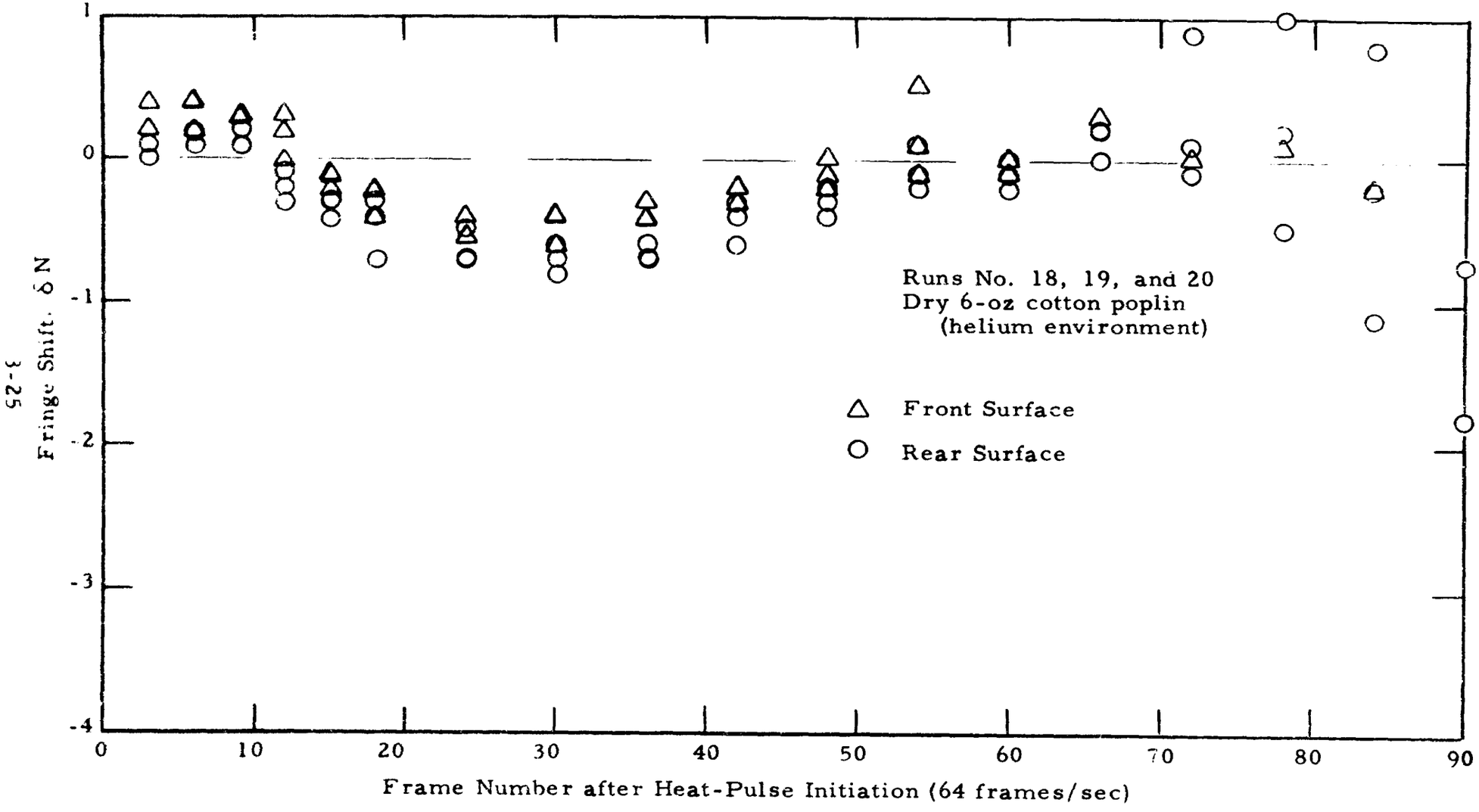

Figure 16. Fringe Shift Variations for Dry o-oz Cotton Poplin in Helium Environment

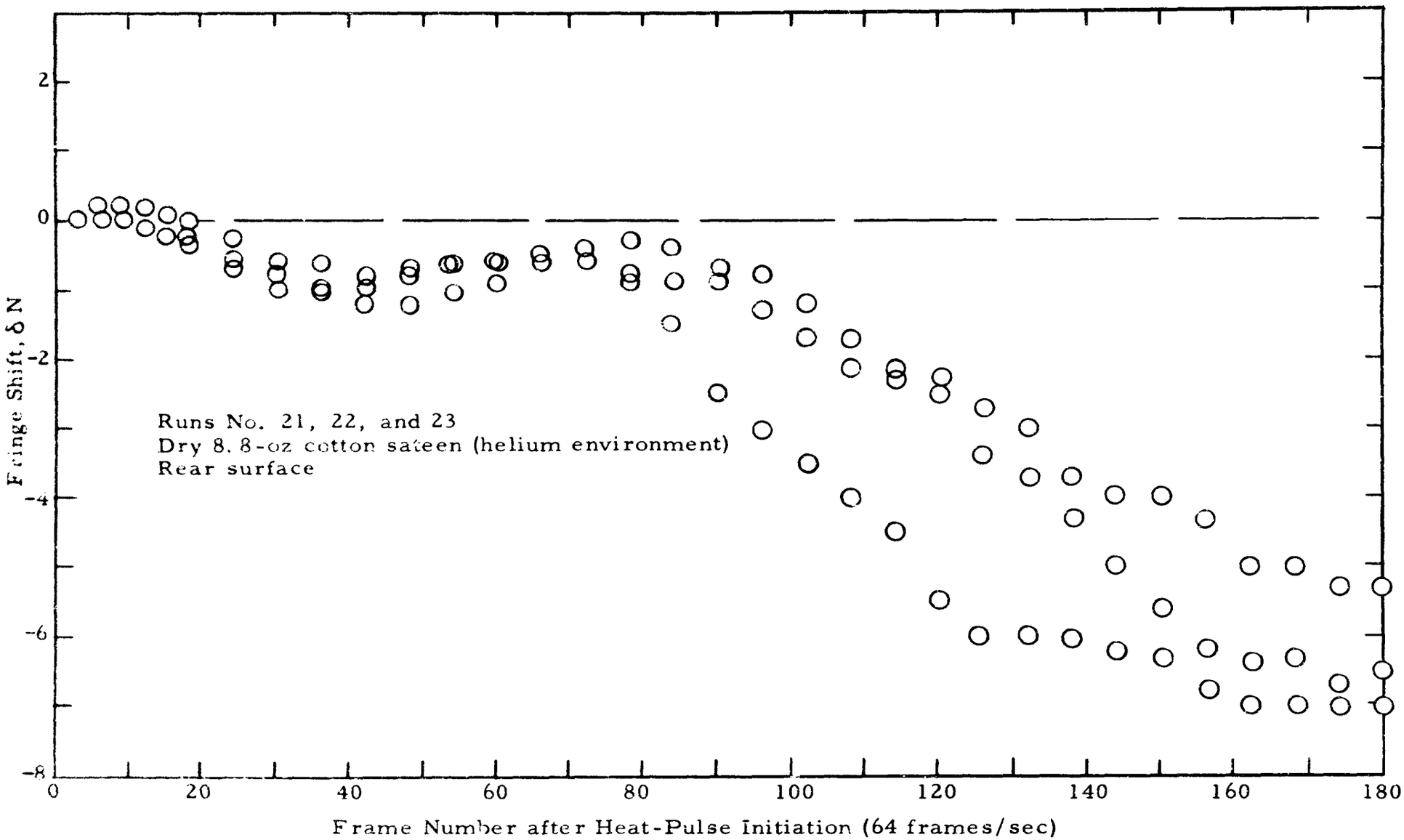

Figure 17. Fringe Shift Variations for Dry 8.8-oz Cotton Sateen in Helium Environment

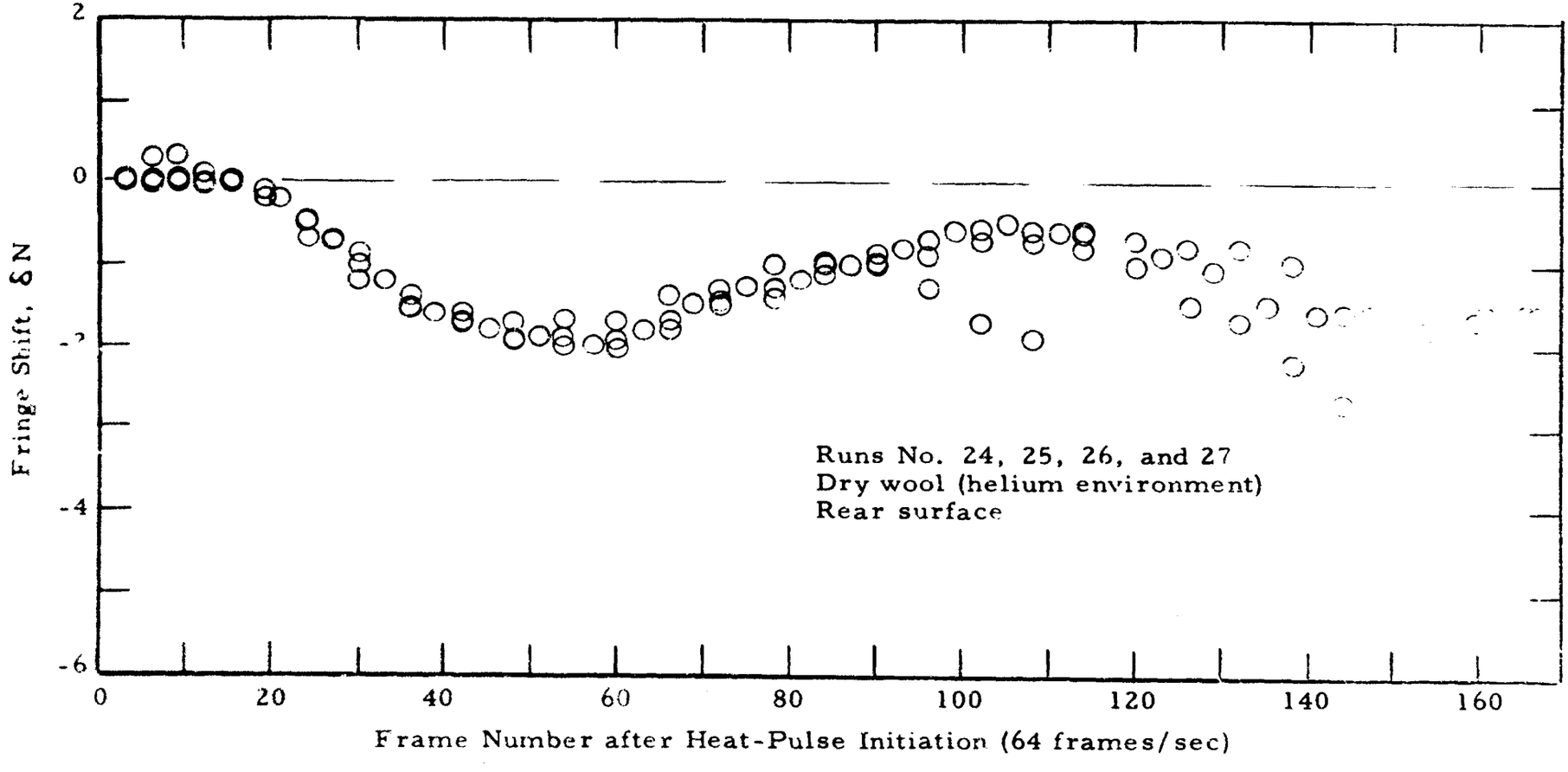

Figure 18. Fringe Shift Variations for Dry Woolin Helium Environment

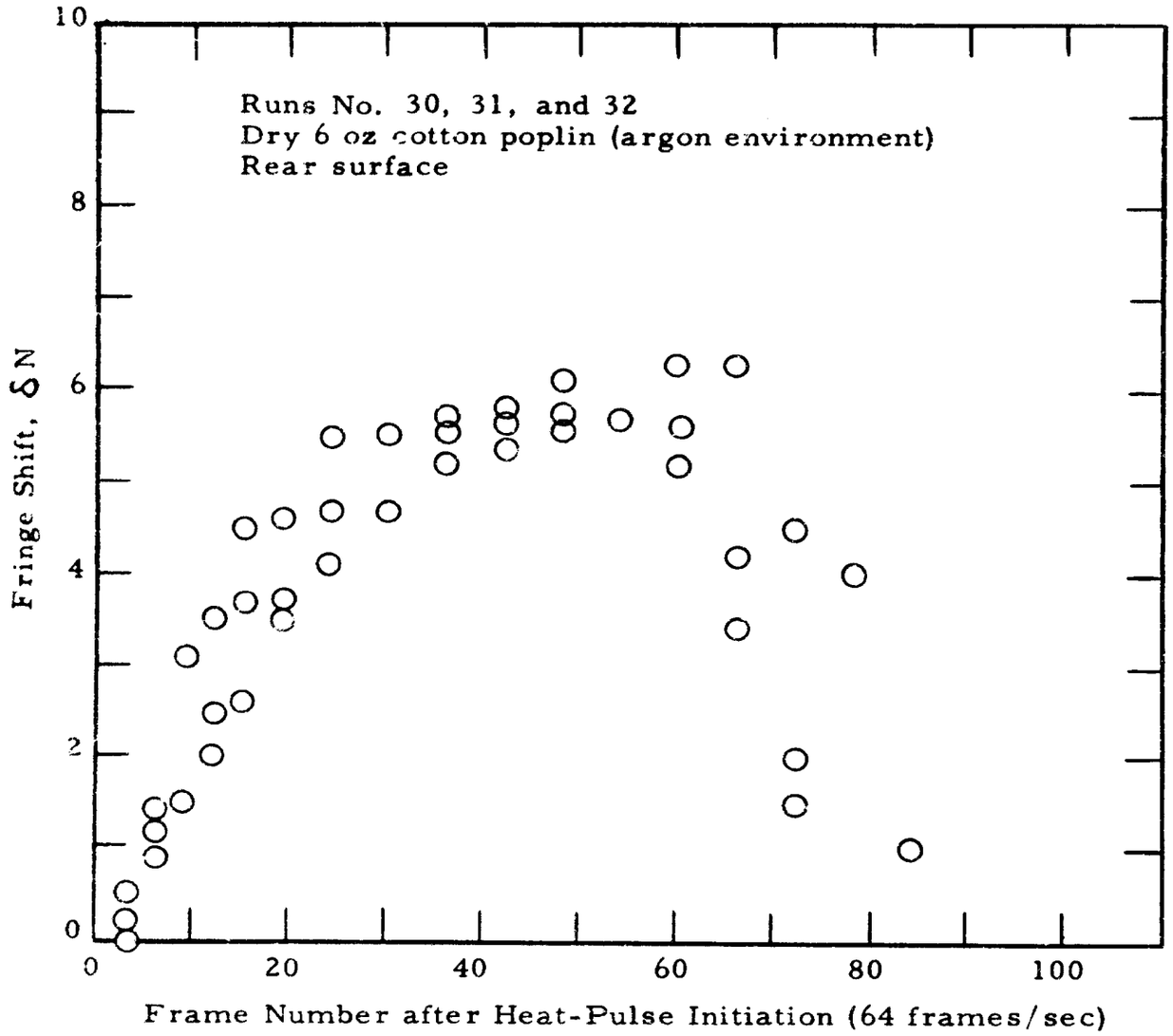

Figure 19. Fringe Shift Variations for Dry 6-oz Cotton Poplin in Argon Environment

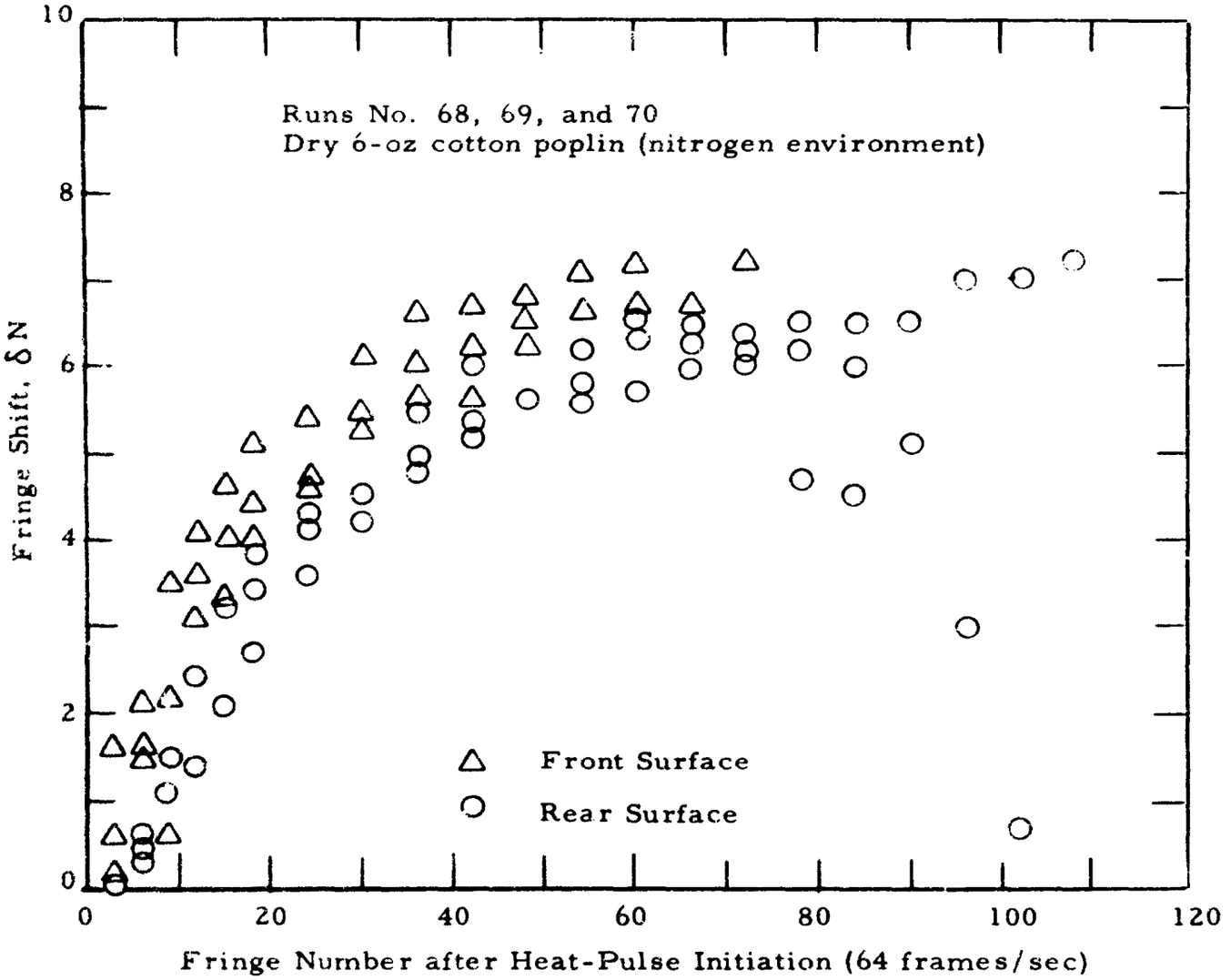

Figure 20. Fringe Shift Variations for Dry 6-oz Cotton Poplin in Nitrogen Environment

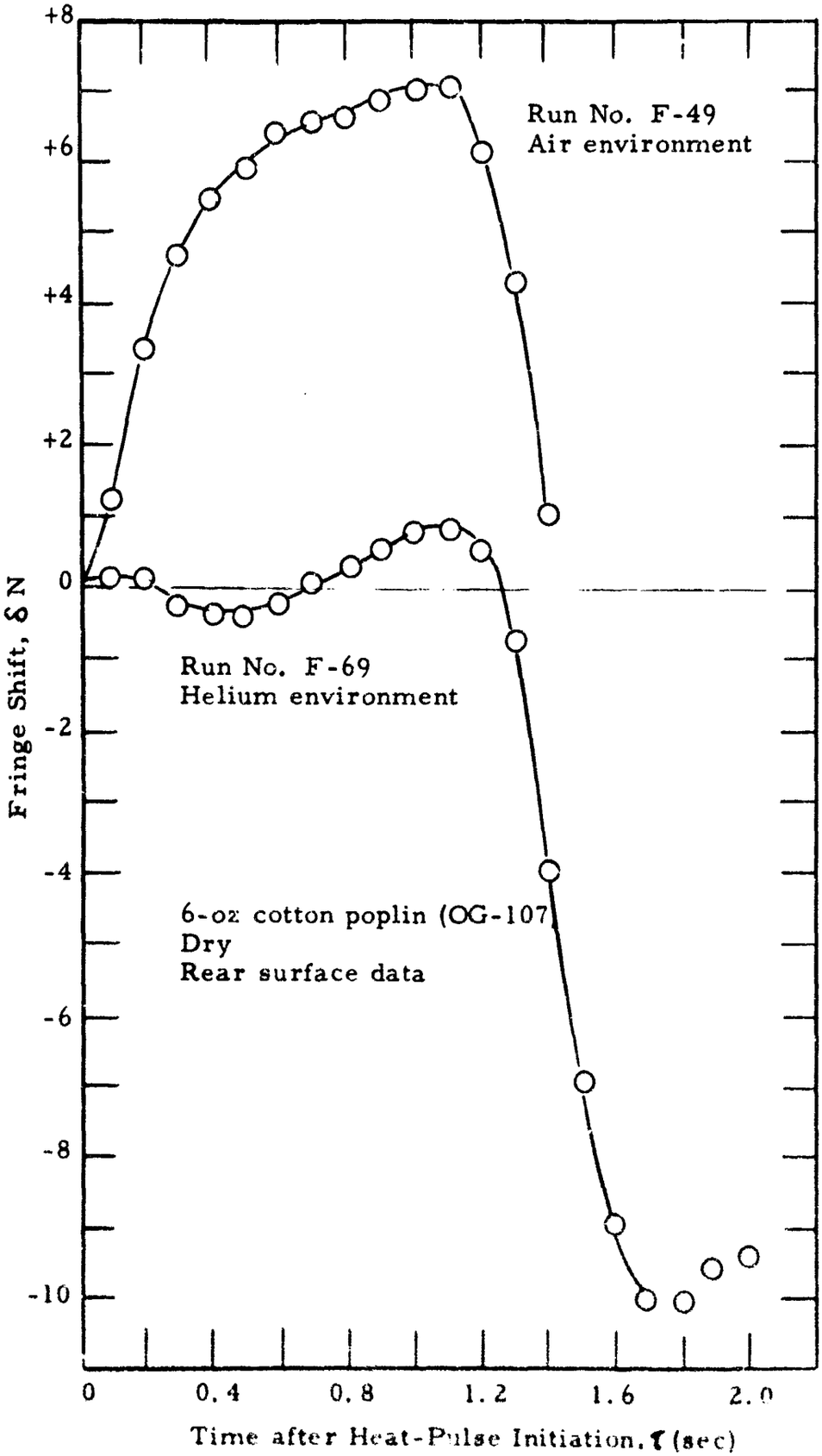

Figure 21. Fringe Shift Variations at Rear Surface of Dry, 6-oz Cotton Poplin in Both Air and Helium Environments

temperature indication, the resultant temperature error could not exceed 7°C, with the indicated temperatures more likely being higher than actual temperature by less than 5°C.

Temperature indications deviate more for heavier cotton and for the wool specimens. At approximately 30 percent relative humidity (25°C) the fiber moisture concentration or adsorption regain (Reference 19) for wool is 7.84 grams per 100 grams dry fiber, whereas cotton has a value of 3.8. As relative humidity increases the adsorption regain values increase (see Table 1). The ratio of wool to cotton interference fringe shift values in helium (lowest negative fringe values during intermediate heat stages) suggests an approximation to the ratio of moisture regain values for the two fiber materials.

Table 1. Adsorption Regains (Reference 19)
(gm adsorbed water/100 gm dry fiber)

c - Cotton (0.319 cal/gm-°C)
c - Wool (0.325 cal/gm-°C)

Relative Humidity	Adsorption Regains		
	Wool (25°C)	Cotton (25°C)	Nylon (24°C)
10	4.15	2.0	1.1
20	6.00	3.0	1.4
30	7.84	3.8	1.7
40	9.65	4.7	2.3
50	11.50	5.5	2.8
60	13.50	6.5	3.4
70	15.60	7.7	4.1
80	18.30	9.5	5.0
90	22.25	12.8	5.7

From these tests two important considerations can be noted. First, the interferometer temperature indications in air at relatively low humidity levels are not influenced greatly by fiber moisture content and may be considered reasonably accurate. Secondly, although the measurement of temperature itself is representative the effects of fiber moisture content on the temperature-time history, especially for wool, would be quite pronounced. Considering the specific heats of the fiber material and of the water, and also the heat of vaporization for the amount of water in the fiber material at a given relative humidity, the resultant heat storage and adsorption of heat during vaporization points out the influence of water. For example, the heat storage associated with 100 grams of wool (c = 0.325 cal/gm-°C) at 50 percent relative humidity when increasing the temperature from 20°C to 100°C is 24 calories for the fiber, 9.2 calories for raising the water content to 100°C and 61 calories for the subsequent vaporization.

3.3.2.3 Wet Fabric Tests

In the water-saturated fabric heating tests the fringe shift values reach a characteristic plateau at about 100°C and remain at this fringe value until the water has full, evaporated. As noted earlier, the indicated temperature level is higher by approximately 70 degrees for the condition of a saturated (100%) vapor concentration at the surface. The exact amount of water in the wetted fabric was not determined for each heating test. In environments other than air the evacuation procedure was carried out with the saturated specimen housed in the thermal test chamber. In the light 6-oz cotton specimens much of the water contained within the fibers was outgased during the evacuation processes; subsequently the heating tests on this fabric display some fringe shift irregularities. Figures 22, 23 and 24 are representative fringe shift variations for a heated fabric in the different environments.

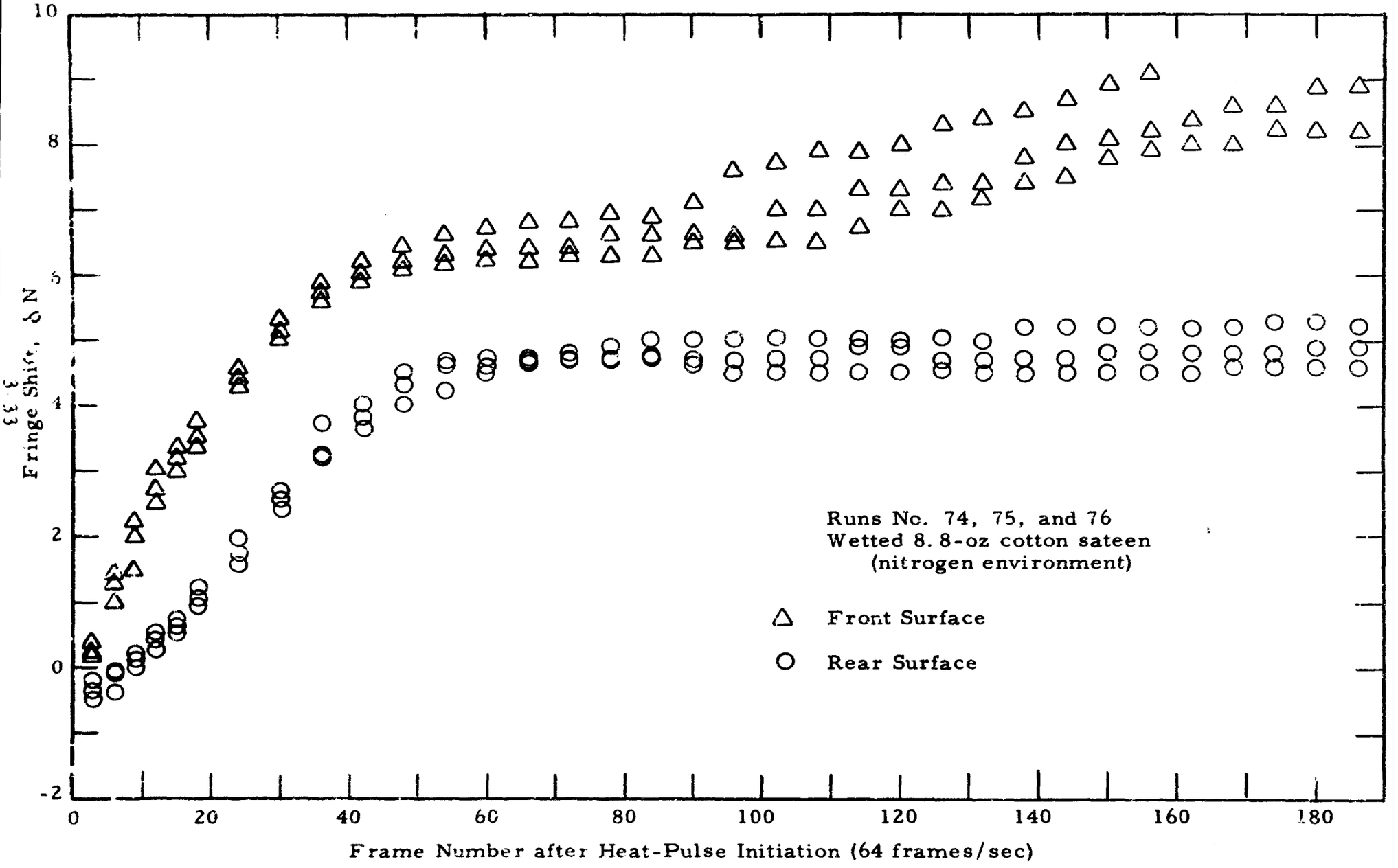

Figure 22. Fringe Shift Variations for Wetted 8.8-oz Cotton Sateen in Nitrogen Environment

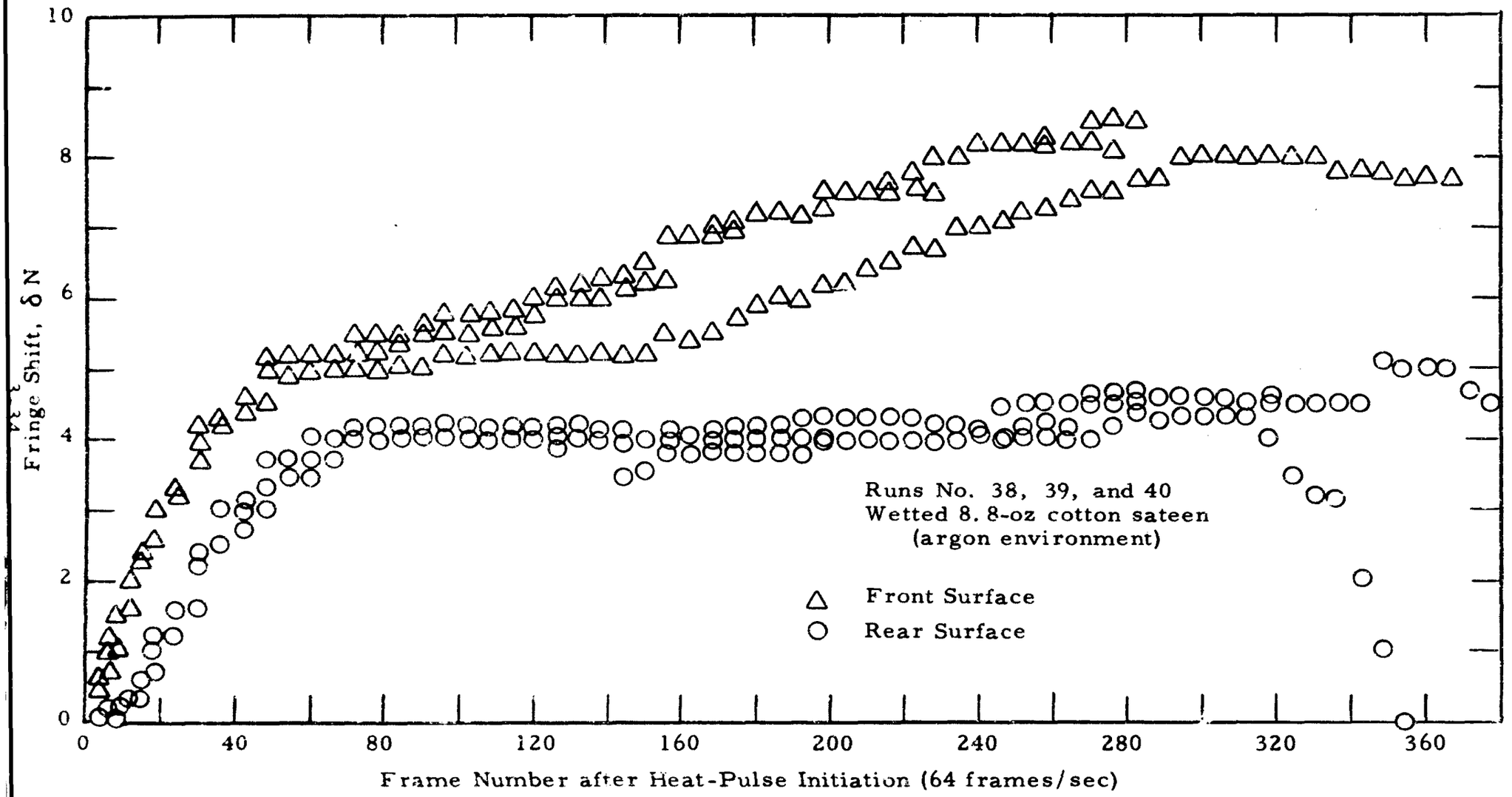

Figure 23. Fringe Shift Variations for Wetted 8.8-oz Cotton Sateen in Argon Environment

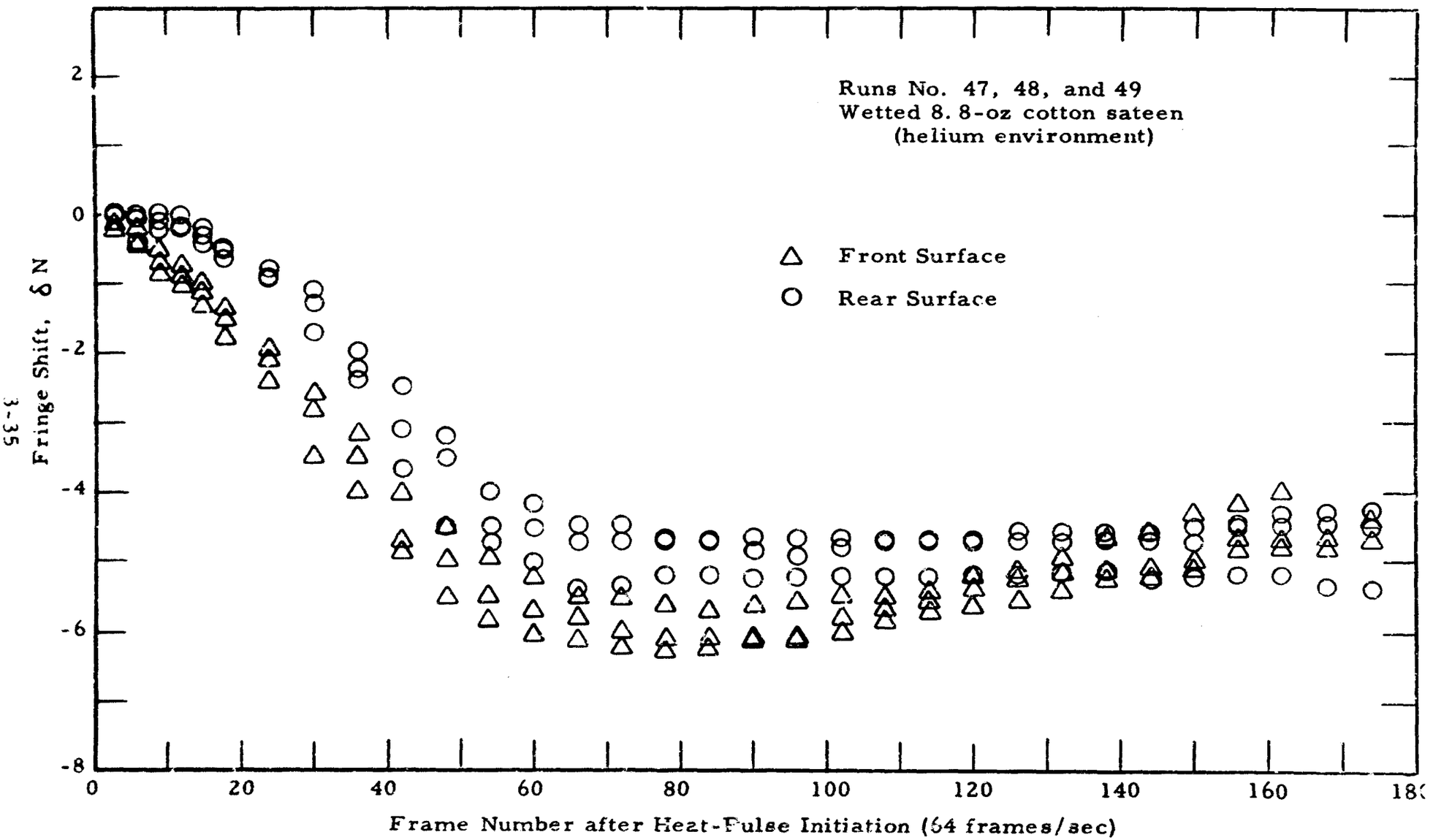

Figure 24. Fringe Shift Variations for Wetted 8.8-oz Cotton Sateen in Helium Environment

The fringe shift variations with time are plotted to show primarily the plateau regions for the various environments. Since the moisture content was not controlled the precipitation of more complete degradation after the water had been fully evaporated occurred at different times in the heating phase.

Since the molecular refractivity of water vapor is known, concentrations of vapor at the fabric surfaces, and the surface temperature can be calculated from tests in two environments. Comparisons can be made between combinations of environmental tests such as air-helium, argon-helium, and nitrogen-helium.

One such pairing (air-helium) is shown in Figure 25. Water vapor concentrations cannot accurately be predicted beyond the vaporization plateau since the amount of moisture is different in each test and the time function of fringe shift variations are not equivalent. The initial rise curve may also vary slightly due to the heat storage and dissipation associated with variable water content.

To resolve variations introduced by heat and mass transfer dissimilarities, which are functions of the environmental gases, comparisons for different gas pairs were made. Representative determinations of temperature and concentration at the rear surface for the 8-oz cotton and 8-oz wool are shown in Figures 26 and 27. Values obtained for helium and argon compare favorably with the other two pairings (helium-air, helium-nitrogen). Little difference was noted here despite the fact that argon (high molecular weight) would conceivably have different temperature and velocity boundary profiles from that of the other two environmental pairings.

One important finding can be recognized. At this level of heat loading (5 cal/cm^2-sec) the rear surface temperature of the 8-oz cotton during the vaporization plateau period is effective 100°C. This also is the temperature level for the wool (see Figure 27a); (note that the concentration of water vapor at the rear surface for wool, Figure 27b, is the same as for the cotton) For lower heat loadings the rear

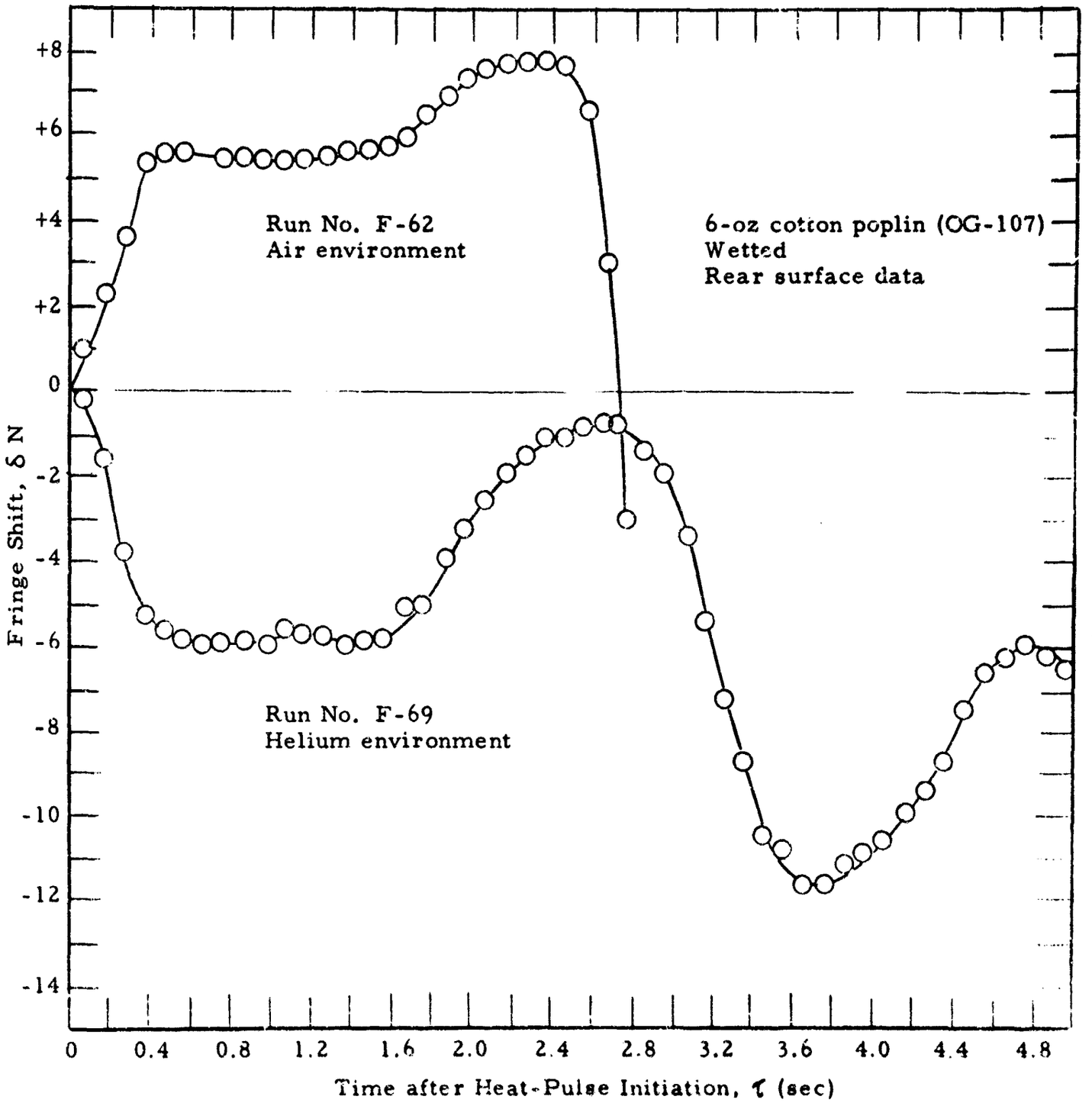

Figure 25. Fringe Shift Variations of Water-Saturated 6-oz Cotton Poplin Rear Surface in Both Air and Helium Environments

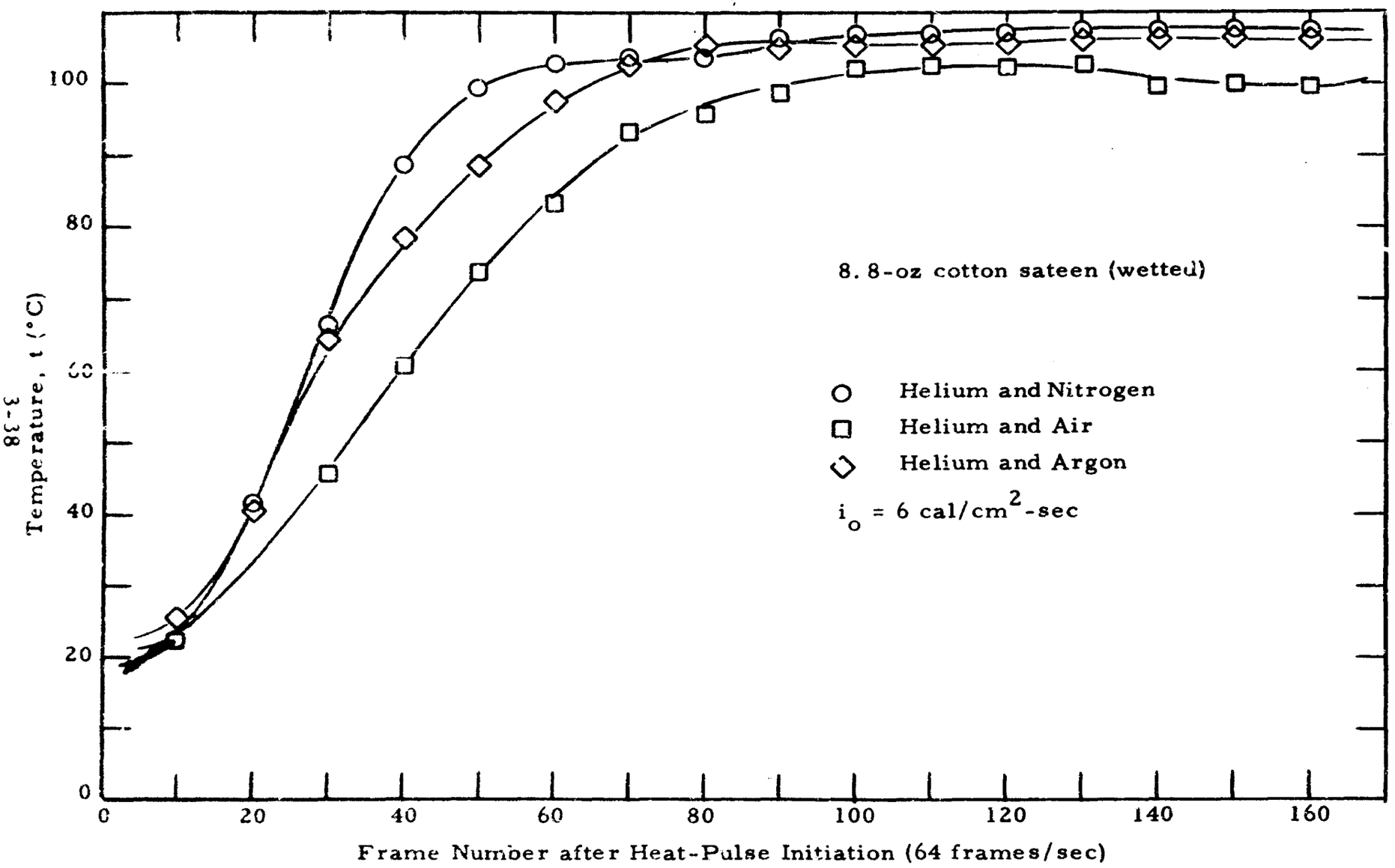

Figure 2ta. Rear Surface Temperature-Time Variations -- Comparison of Test Environment Combinations

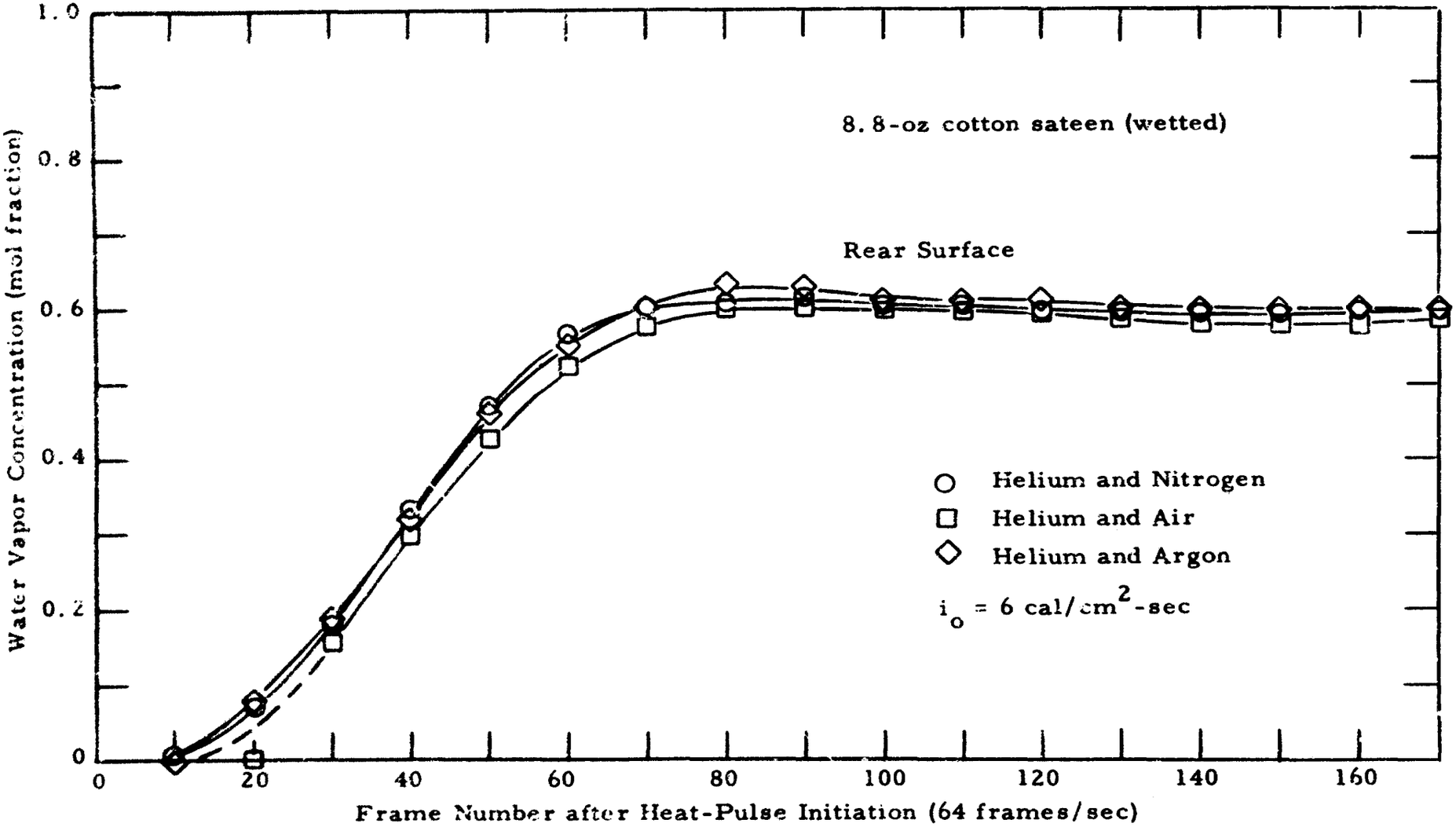

Figure 26b. Rear Surface Water Vapor Concentration-Time Variations -- Comparison of Test Environment Combinations

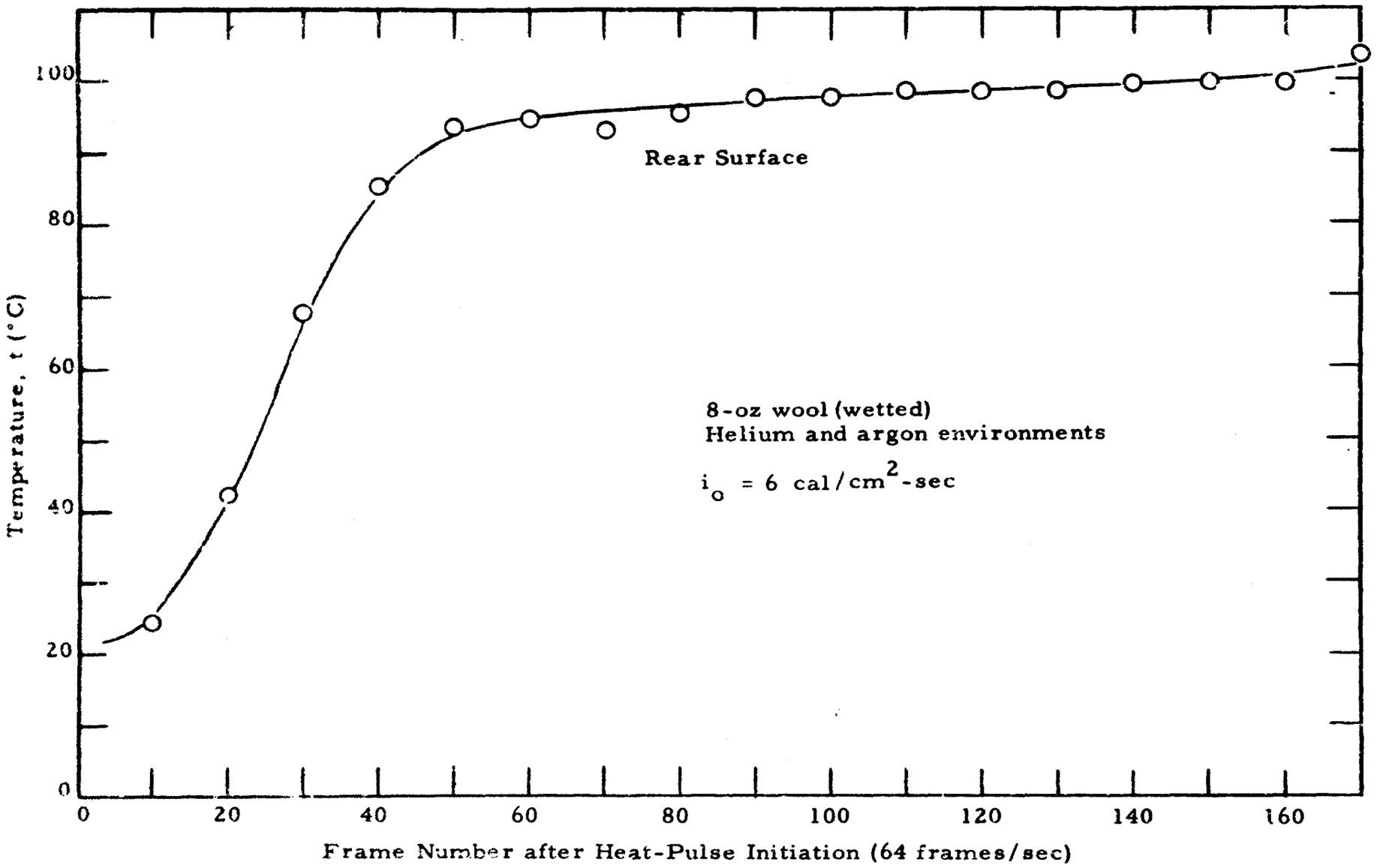

Figure 27a. Rear Surface Temperature-Time Variations Determined from Identical Tests in Helium and Argon Environments

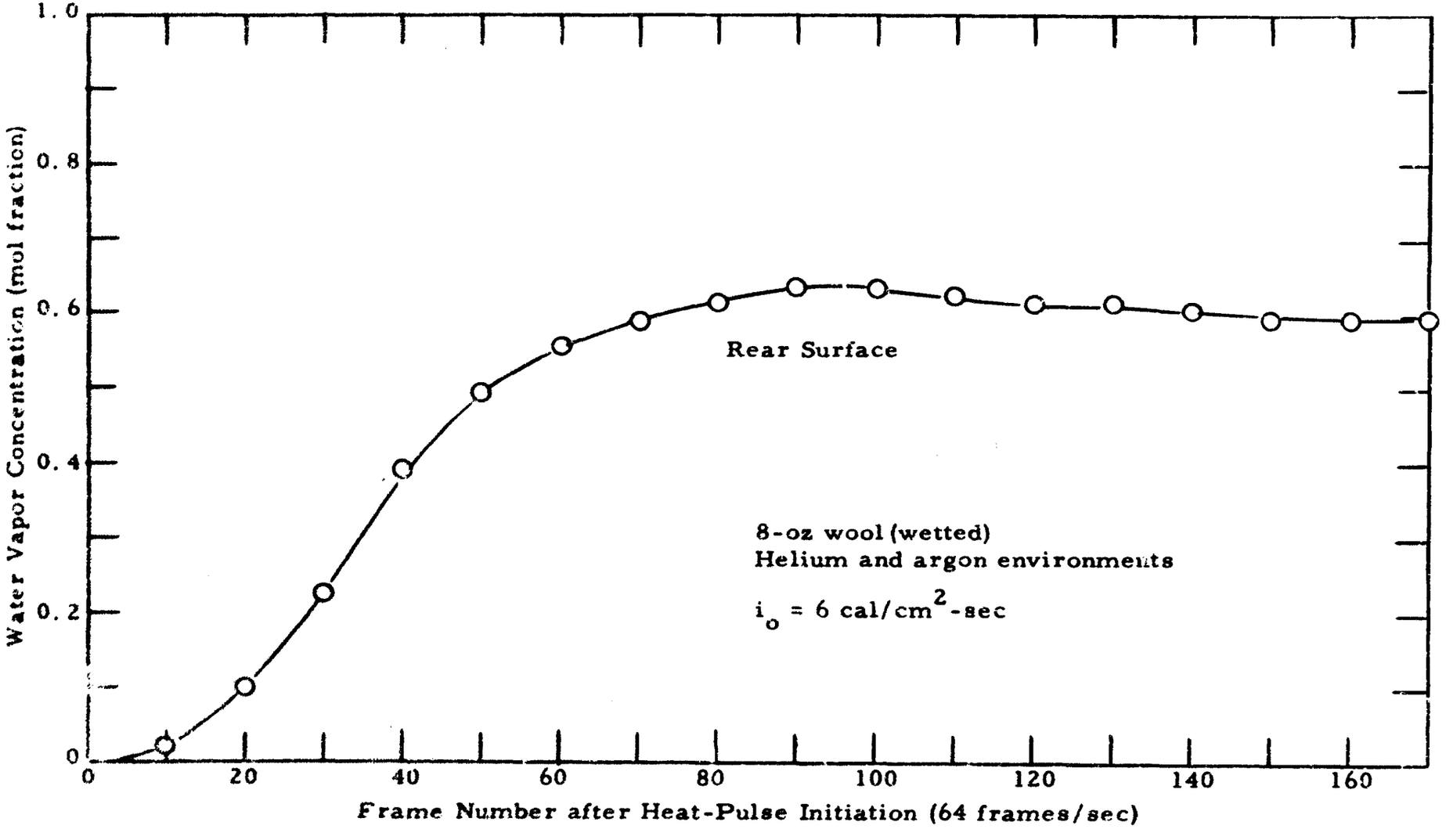

Figure 27b Rear Surface Water Vapor Concentration-Time Variations Determined from Identical Tests in Helium and Argon Environments

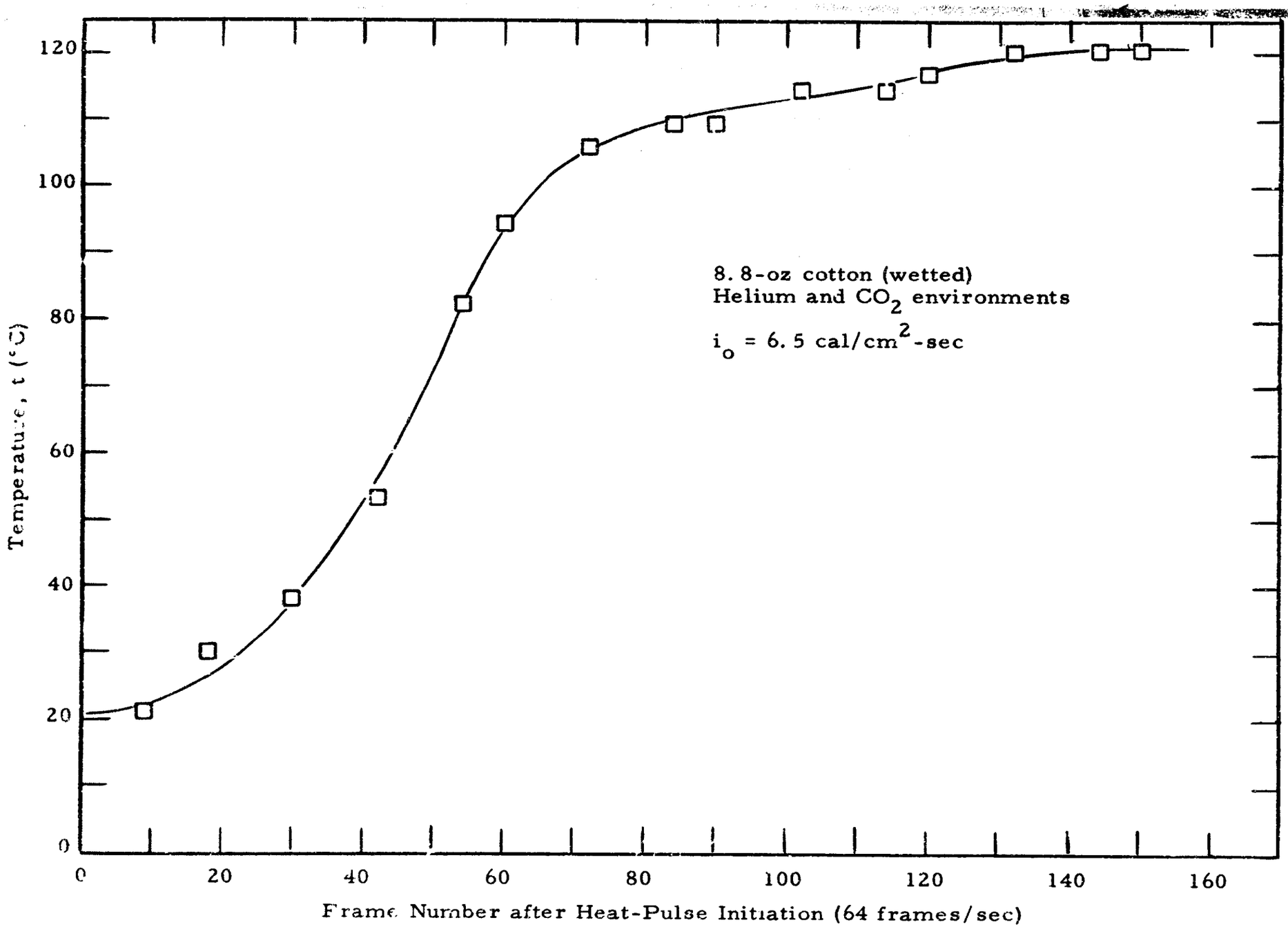

Figure 28. Rear Surface Temperature-Time Variations Determined from Identical Tests in Helium and CO_2 Environments

surface temperature during this vaporization equilibrium period is expected to be approximately 100°C also. However, as the heat flux is increased a critical input energy will be reached where higher equilibrium temperatures will be evident thereafter. In two later tests, one in helium and the other in CO_2, at incident radiant heat loads of approximately 6.5 cal/cm^2-sec, the temperature values obtained for this environmental pair were higher (Figure 28) then that determined from the earlier tests. As shown in Figure 29a, the fringe values in helium, as expected, are quite different depending on the degree of heat loading. The concentration values also are higher (Figure 29(b)) for the higher intensity radiant heat flux.

The front surface temperature and concentration values are expected to be higher than rear surface values. This was shown to be true as indicated in Figure 30.

A desired series of experiments would be to vary the heat flux under similar type experimental conditions and characterize vapor concentration values and temperature levels for a series of representative fabric materials. For the wet fabric skin complex a further experimental study could involve the important mass diffusion processes and transport mechanisms.

3.4 Measurement of Fabric Front and Rear Surface Heat Transfer Coefficients

3.4.1 General

Proper evaluation of the fabric front and rear heat transfer coefficients is necessary when comparing experimental data with theoretical predictions of the response of a fabric-skin system to a radiant heat input.

The heat-transfer model under consideration is composed of a skin layer separated from the clothing ensemble by an airspace. The flow of heat from the outer layer of the fabric to the skin is impeded

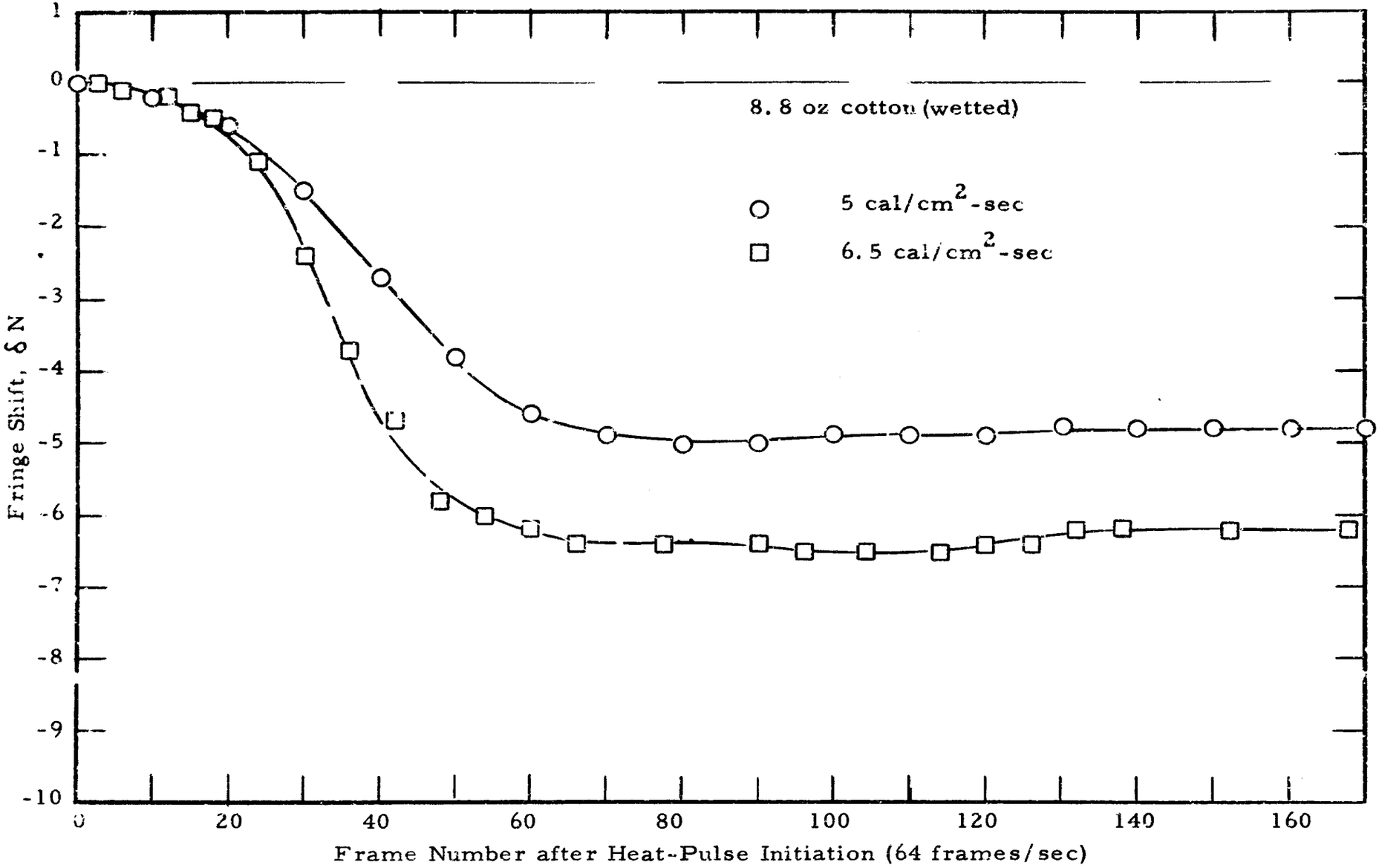

Figure 29a. Rear Surface Fringe Value Variations in Helium Environment for Two Different Heat Loadings

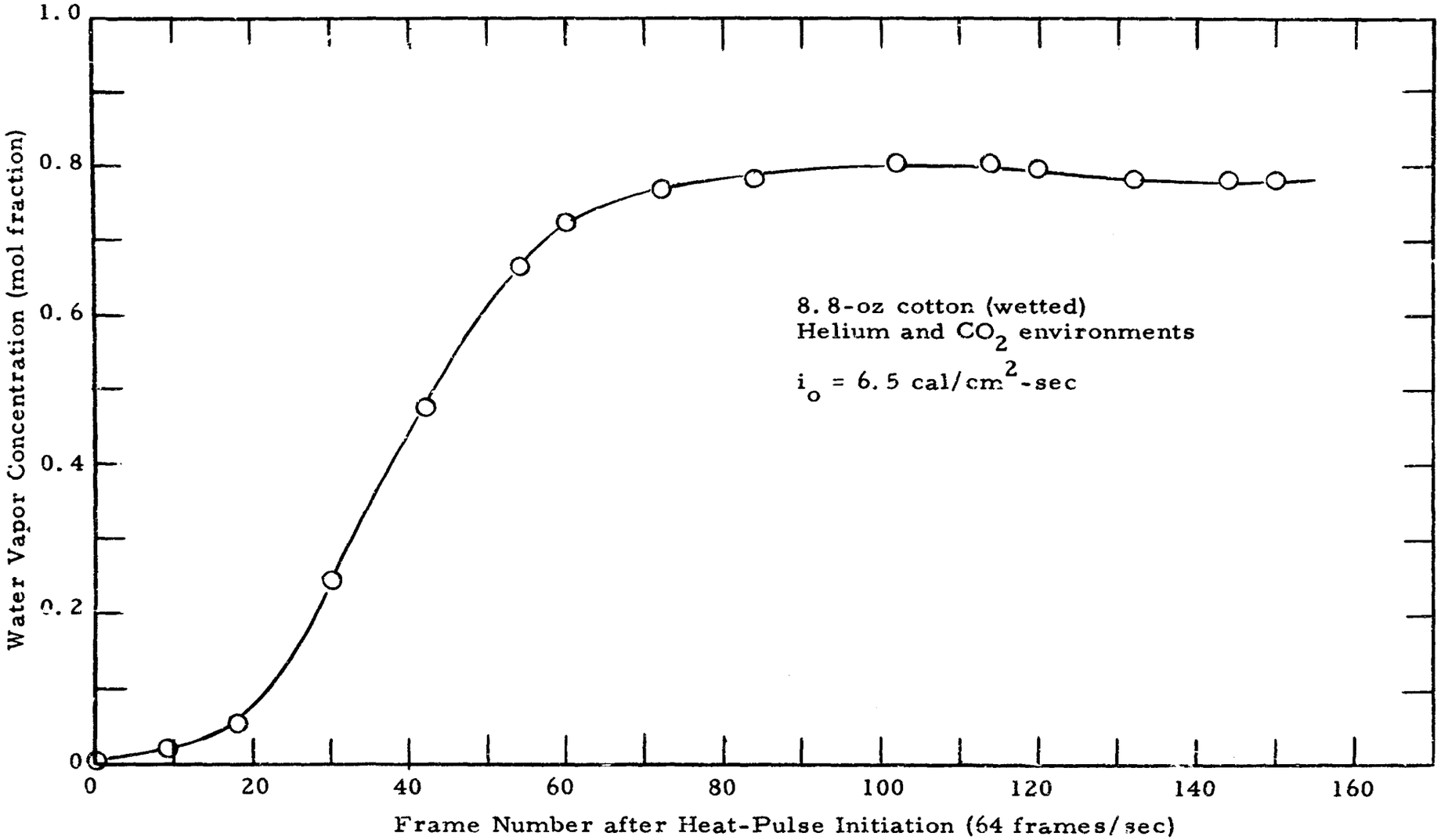

Figure 29b. Rear Surface Water Vapor Concentration-Time Variations

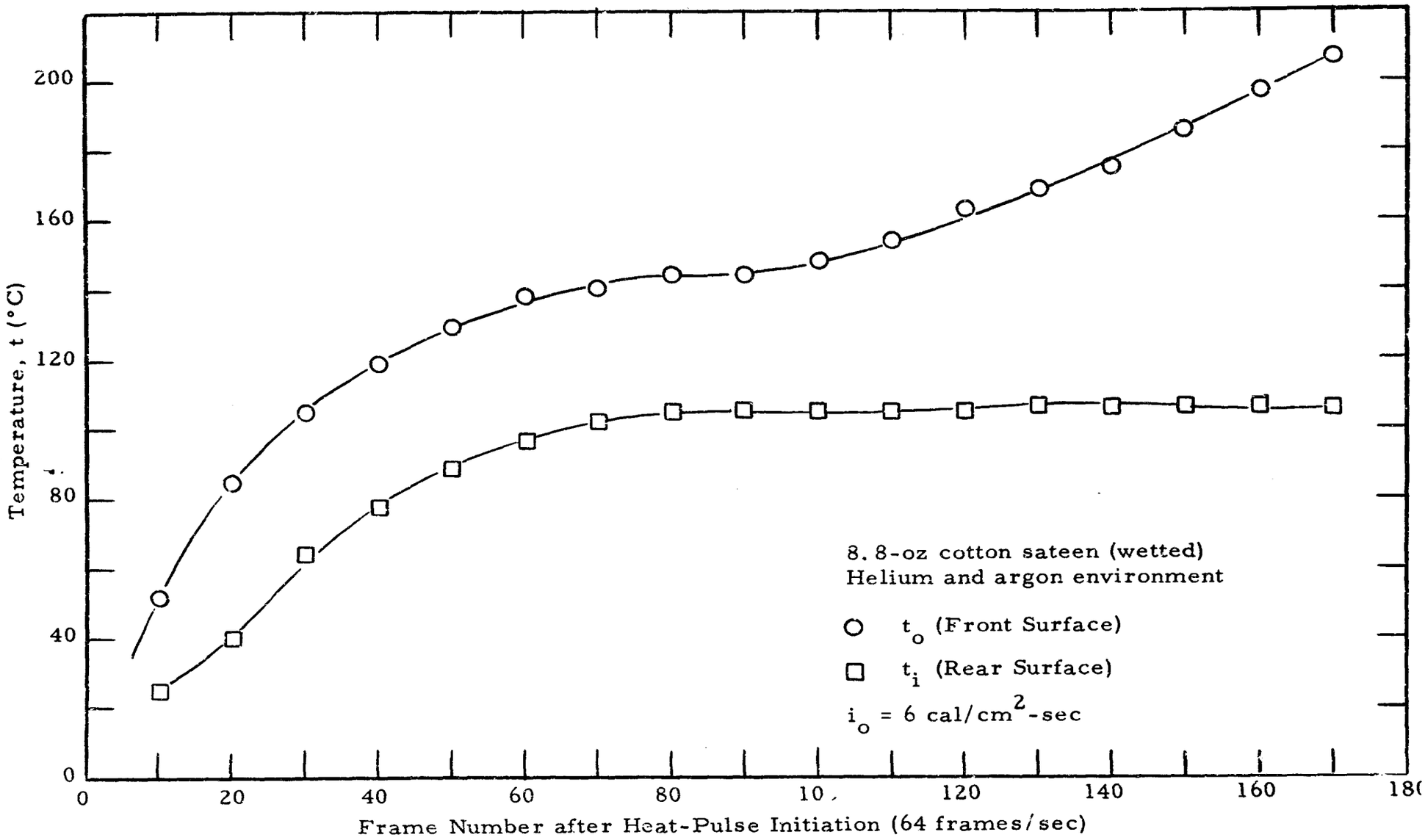

Figure 30a. Front and Rear Surface Temperature-Time Variations

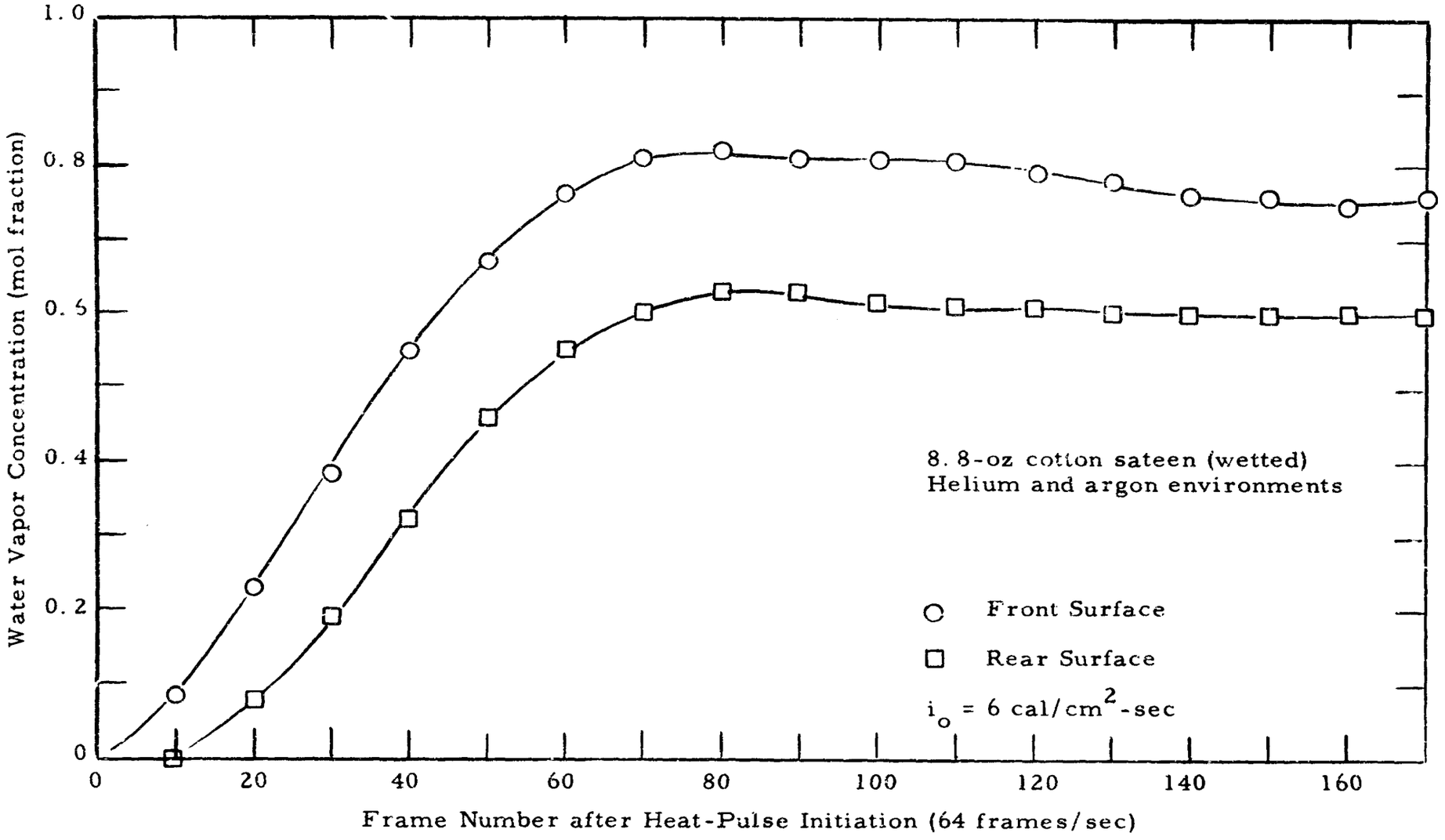

Figure 30b. Front and Rear Surface Water Vapor Concentration-Time Variations

by the insulating effects of the air layer and several layers of clothing. Heat transfer from the inner layer of the clothing to the skin is accomplished by one or a combination of several modes of heat transfer--namely, convection, conduction, and radiation. The radiation environment presented to the skin is formed by the inner layer of protective clothing. The amount of heat transferred by the mechanism is governed by the temperatures of the surfaces, by the radiation interchange coefficients, and by view factors.

The convective and conductive modes of heat transfer combine to form a fairly complicated mechanism of heat transfer. If the air between the two surfaces were still, the heat would be transferred purely by a conductive process across the air gap. The amount of heat transferred would then be a function of the temperature gradient and thermal conductivity of the air. This situation can be approximated if the warm surface or fabric is above the skin, and if no circulation of air occurs. If the fabric is below the skin, buoyancy forces can result, and free convection will occur. Forced convection has to be considered if air movement occurs laterally through the air gap.

The external environment plays an important role in fixing the amount of heat lost from the outer surfaces of the fabric by the combined transfer processes. Heat is lost from the outer layer of the clothing by a combined forced and free convection process and by radiation. The convection process is strongly influenced by air temperature and surface winds.

3.4.2 Free Convection Processes

Convection is a heat-transfer process that occurs because of the mixing of one parcel of fluid with another. Forced convection occurs when the fluid motion is produced by mechanical means, whereas free convection is the result of body forces produced on fluid particles because of differences in density. Free convection occurs when heat

is transferred to or from a surface to the adjoining fluid layer. Temperature changes in the fluid layer cause corresponding density changes, resulting in fluid movement because of the body forces created by the acceleration of gravity. Heat is then conducted through the layers and carried away by bulk motion or convection. By the use of integral methods, problems of laminar and turbulent, free convection on a vertical, flat plate have been solved. For the laminar case, the velocity and temperature-boundary layers were approximated by second-order parabolic equations. Using these methods, the following equation was developed for laminar, free convection on a vertical, flat plate:[20]

$$Nu_y = 0.508\ Pr^{1/2}\ (0.952 + Pr)^{-1/4}\ (Gr_y)^{1/4} \quad , \tag{6}$$

where:

Nu_y = Nusselt number

Pr = Prandtl number

Gr_y = Grashof number.

Considering air as an ideal gas and assuming a Prandtl number of 0.714, the following simplified relation results:

$$Nu_y = 0.378\ (Gr_y)^{1/4} \quad . \tag{7}$$

For turbulent, free convection on a vertical plate, a more complicated relationship must be used for the velocity and temperature profiles in the boundary layer. Using methods similar to those used for forced convection boundary layers, shear and heat flow conditions at the wall are modified in the light of experimental data. This method then provides the shear stress at the wall that can be converted to heat flow by use of the Reynolds analogy, and results in the following equation:[20]

$$Nu_y = 0.0295 (Gr_y)^{2/5} (Pr)^{7/5} \left[1 + 0.494 (Pr)^{2/3}\right]^{-2/5} \quad (8)$$

Using simplified relationships for air, the amount of heat loss by free convection from a vertical, flat plate can be represented by the following equation:

$$q_c = h_c \left(t_w - t_e \right) \left(\frac{cal}{cm^2 \, sec} \right) , \quad (9)$$

where the laminar and turbulent heat transfer coefficients are respectively

$$h_c = 0.27 \left(\frac{t_w - t_e}{y} \right)^{0.25}$$

and (10)

$$h_c = 0.22 \left(t_w - t_e \right)^{1/3} .$$

Laminar flow exists when the product of Grashof and Prandtl numbers is 10^5 to 2×10^7, while turbulent flow exists when it is equal to 2×10^7 to 3×10^{10}. (Reference 5).

For a gas, the Grashof number is determined from

$$G_r = \frac{g \left(t_w - t_e \right) y^3}{\nu^2 \, t_e} , \quad (11)$$

where:

g = gravitational constant

y = characteristic length

ν = [illegible] ic viscosity

t_w = wall temperature

t_e = environment temperature,

and

$$\text{the Prandtl number from Pr} = \frac{c_p \mu}{k}$$

where:

k = thermal conductivity

c_p = specific heat at constant pressure

μ = viscosity.

A more complicated situation exists when the free-convection heat-transfer process occurs in a fluid enclosed between two plane walls. For horizontal walls no free convection occurs when the upper wall is heated and the lower cooled. Here the buoyancy forces tend to stabilize the situation. Heat will be transferred by conduction only, and the temperature profile will be linear. When the lower plate is heated, however, an extremely complicated flow situation occurs. Heat now flows from the lower hot plate to the upper cooler plate, and a situation exists in which colder fluid particles are on top of warmer ones. An unstable situation thus exists, and convection currents are established when the product of Grashof and Prandtl number reaches 1700. For such a situation, Siedentopf[20] made the flow visible by tiny aluminum particles. He found that a peculiar cellular structure occurs with air moving upward in the interior of the cells and downward along the outer portions. This flow situation occurs until the Grashof-Prandtl number product reaches around 47,000. Above this value, irregular turbulence occurs.

It can be demonstrated by dimensional analysis that for an air layer enclosed between two vertical walls, the following relationship holds:

$$Nu = f(Gr_y, Pr, H/L)$$

where H/L is the ratio of air layer height to plate spacing.

The above relationship has been verified by early experiments. As reported by Carlson,[11] observations were made by different investigators of the heat transfer across plane vertical air layers, and as early as 1909 Nusselt concluded that the transfer depends on the distance between enclosed surfaces and that for wider spacings, convection effects were dominant over that of conduction. It was shown by others later that such effects as temperature difference between bounding surfaces, width to spacing ratio, and height to spacing ratio must be considered. Subsequent, empirical expressions for Nusselt number as a function of these variables were developed. These early studies were concerned with the measurement of the overall heat transfer occurring across air enclosures where a steady-state equilibrium temperature existed or where enclosed surface temperatures were maintained at different but constant values. Carlson's work was an extension of the early investigations including, in part, an examination of local heat transfer phenomena.

In a paper by Eckert and Carlson,[21] which was an extension of Carlson's thesis,[11] local heat transfer coefficients for a vertical-plate flow situation were derived from the temperature gradients in the air normal to the plate surfaces. For values of Grashof number below a certain value, a linear temperature gradient existed between the two walls and the heat was transferred only by conduction. As the Grashof number was increased, distinct boundary layers were seen to form on the two walls. The air was seen to flow in the upper direction on the heated wall and in a downward direction on the cooler wall. In the

central core between the two wall boundary layers, the temperature was found to be essentially constant in the direction normal to the walls, although it gradually increased in the vertical direction.

Various methods have been used to calculate the net flow of heat between a cold and hot surface in such a vertical arrangement. Carlson[11] showed that the boundary-layer thicknesses and heat-transfer coefficients for this situation were within 20 percent of those calculated for individual heated and cooled walls assuming as a free-stream temperature the temperature in the core. Kraussold[20] defined an equivalent heat conductivity k_E which when combined with the distance between the plate and the temperature difference allowed a fairly accurate calculation of the heat flow. A log-log plot of equivalent thermal conductivity to molecular conductivity ratio as a function of the product of Grashof and Prandtl numbers showed that the conductivity ratio remained at 0 up to an abscissa value of 3 and then steadily increased as the product was increased. This same relationship can be used for two concentric cylinders as well. This increase in effective conductivity indicates the contribution of free convection to the heat flow process.

Flow situations in which both free and forced convection exist can be extremely difficult to calculate. In addition to the Grashof number and other parameters that describe the boundaries and orientation of the flow system, a Reynolds number must also be considered. For large Reynolds numbers and small Grashof numbers the forced convection predominates, whereas with large Grashof numbers and small Reynolds numbers the free convection becomes dominant. Certain flow situations exist, however, in which neither free convection nor forced convection predominates. Eckert[20] showed that this mixed-flow region (defined as a region in which the heat transfer differs by more than 10 percent from either free- or forced-convection relations) is quite small. A rule proposed by McAdams is to calculate the heat flow by both methods and use the one that provides the larger heat flow.[20]

Bodoia and Osterle[22] studied free convection between two vertical plates for conditions when the flow was not fully developed. Such a situation exists for short plates and near the leading edges of longer plates. The equations of motion were converted to a finite difference form and programmed for solution on a digital computer. As commented on by E. M. Sparrow, the flow near the entrance to the plate is essentially one of forced convection on which is superimposed a free-convection process. This situation was studied in more detail by Pau-Cheng Lu, who investigated the case of a cylinder with its axis parallel to the direction of body forces of the fluid.[23] In two papers, Ostrach[24,25] also obtained detailed solutions for parallel-plate channels.

3.4.3 Non-Steady Heat Transfer

When conditions are changing with time, some concern has been expressed about whether the steady-state equations are applicable. Sparrow and Gregg investigated the case of free convection where surface temperature varied with time.[26] Under these conditions, heat-transfer calculations have often been made under the assumption that quasi-steady conditions prevailed. That is, it is assumed that at each moment in time an instantaneous steady-state condition exists and as a result a steady-state heat transfer relationship can be used. For a desired accuracy of 5 percent, they proposed as a criterion a parameter that must be less than a certain desired value. This parameter is a function of temperature change with time, temperature potential, distance, and free-stream temperature. For many heat-flow situations this criterion is not of concern; but for such cases as a fabric-airspace-skin system irradiated by a time-dependent heat pulse, such as from a nuclear-energy release, caution must be shown in utilizing steady-state free-convection relationships under these transient conditions. Changing ventilating flow rates due to relative motions of fabric and skin can also give rise to non-stationary effects.

Non-steady phenomena were studied experimentally by Goldstein and Eckert on a uniformly heated, vertical flat plate using a Mach-Zehnder interferometer.[27] These tests showed that the temperature field in the fluid developed initially in the same way as heat conduction into a semi-infinite solid. A short transition period then followed, and finally a steady-state condition was reached. Siegel[28] carried out a theoretical study of the same situation. He used a method of characteristics to obtain solutions to the time-dependent, free-convection equations placed in an integral form after the Karman-Pohlhausen method. This analysis predicted that the boundary layer grows initially in thickness with time and decreases before it finally settles on its steady-state value. The heat transfer coefficient also follows this change; that is, it initially decreases with time, passes to a minimum and then rises again to its steady-state value. The results obtained by Goldstein and Eckert substantiated this prediction. These studies again indicate that caution must be exercised in applying steady-state relations to transient free-convection situations.

3.4.4 Experimental Results

3.4.4.1 Fabric Surface, Air Gap, and Skin Temperatures

Our experiments involve non-steady or quasi-steady state conditions for two vertical facing surfaces using interferometry techniques. To our knowledge this configuration has not been studied previously with the interferometer. Idealized correlations of the heat transfer functions for our fabric-skin model cannot easily be made with those of the above earlier studies because of experimental dissimilarities. Early investigators chose large plate areas and electrical heat input. Our specimen size was necessarily small to permit radiant exposures of sufficient intensity. The height and width dimensions were held constant; only the space between the fabric and skin was varied. With a height dimension of 1.27 cm the height to spacing ratios were varied from 3.7 to 13.5 For a fabric exposure width of 3.18 cm the width to spacing ratios thus varied from 9.2 to 33.7.

The fabric-skin configuration is shown in Figure 31. To simulate the skin, a material to accept heat at a rate identical to that of the skin itself was chosen, which requires matching of the respective $kc\rho$ and $k/c\rho$ values. Although skin is diathermanous to thermal radiation the simulant need not be, provided the fabric is opaque. For these experiments the 8.8-oz cotton sateen, which has a reflectance of 18.8 percent, transmittance of 1.5 percent, and absorptance of 79.7 percent (for carbon-arc source) was used. The amount of energy transmitted was considered small to enable the choice of an opaque skin simulant if desired.

For human skin $kc\rho = 8.48 \times 10^{-4}$ cal^2/cm^4-sec and $k/c\rho = 1.325 \times 10^{-3}$ cm^2/sec. Pyrex and fused silica have thermal properties similar to that of skin.

Two skin simulant models, each having the same exposure area as that of the fabric, were made from quartz. The thickness of the quartz skin simulants were 0.34 cm and 0.70 cm. Experiments were made with both simulant models to determine if a semi-infinite skin assumption was valid for the heating periods studied. Heat flux was measured at 6 ± 0.5 cal/cm^2-sec. Figure 32 shows interferograms for the fabric-skin system at various time intervals and spacings. Figure 33 shows temperature-time variations for the fabric front and back surfaces, center of airgap, and the surface of the skin simulant. Measurements were made at different vertical positions in the fabric-skin system but for the present discussion we will present now temperature data at the center position of the exposed area ($y = 0.5H$).

For these tests with a blackened radiation absorbing skin, the effects of fabric diathermancy can be seen; the initial portions of the temperature rise curve at the skin surface have higher values than that of the fabric rear surface. The temperature of the skin does not increase for the short interval after heat pulse initiation to 0.1 second (conduction into airspace not felt at skin) but gradually increases thereafter (irregularly for some tests) to approximately 20 to 40°C above

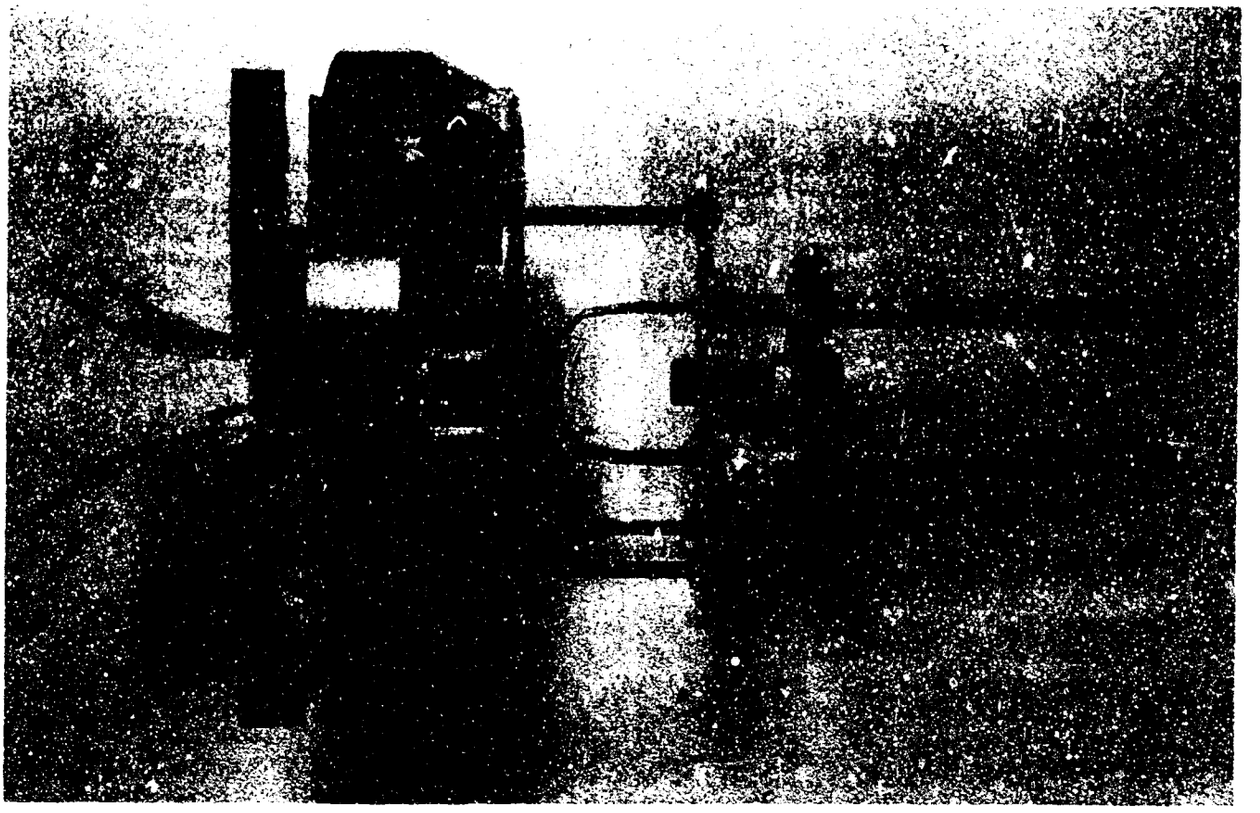

a. Photograph Showing Flux Redistributor, Sample Holder, and Fabric-Skin Model Assembly

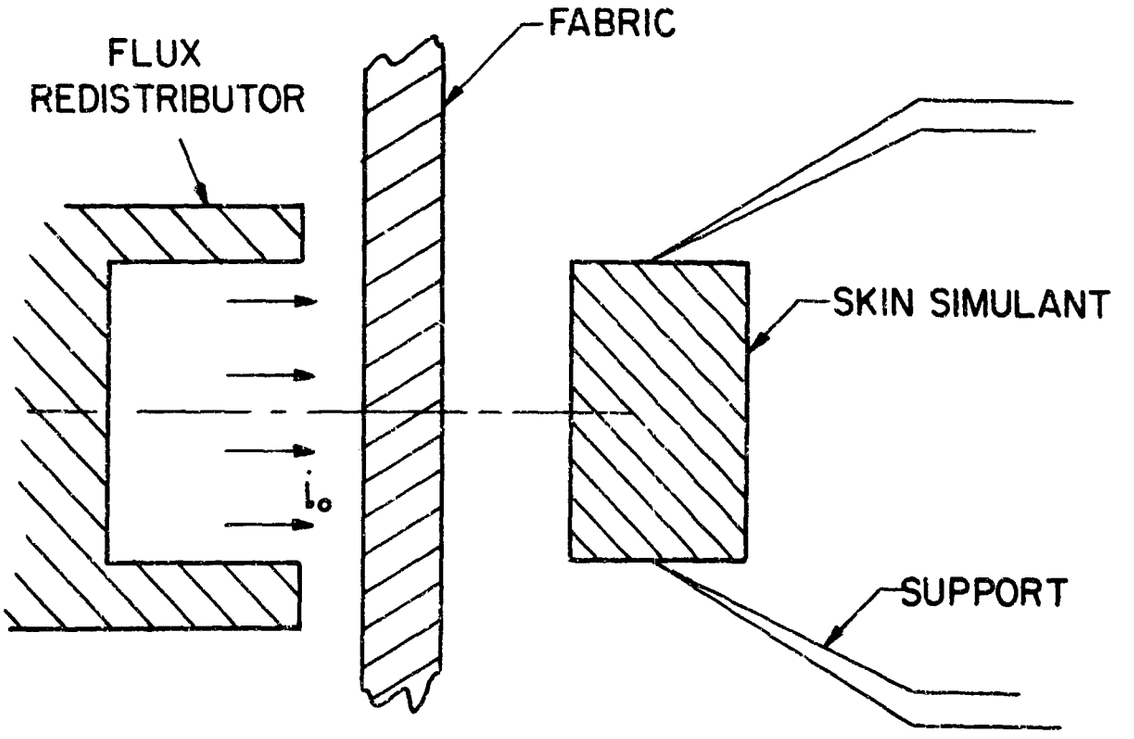

b. Schematic Drawing

Figure 31. Fabric-Skin Configuration

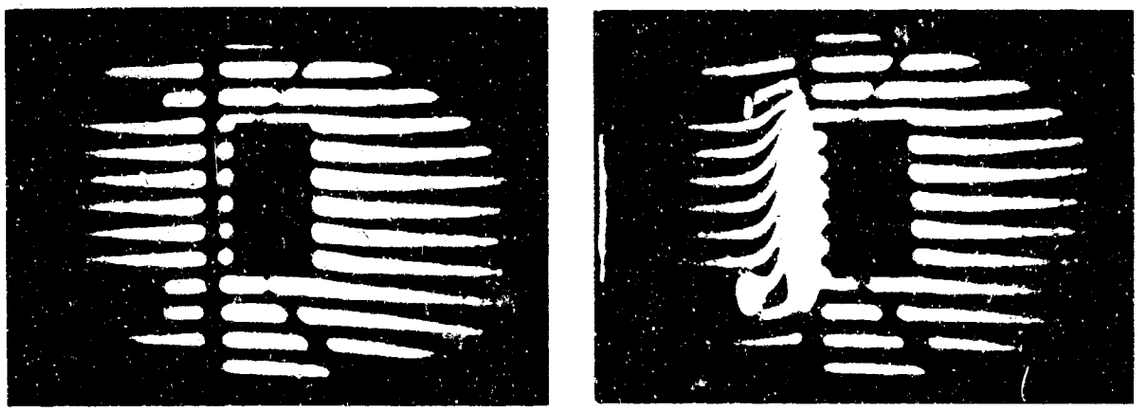

τ = 0 sec.

τ = 0.1 sec.

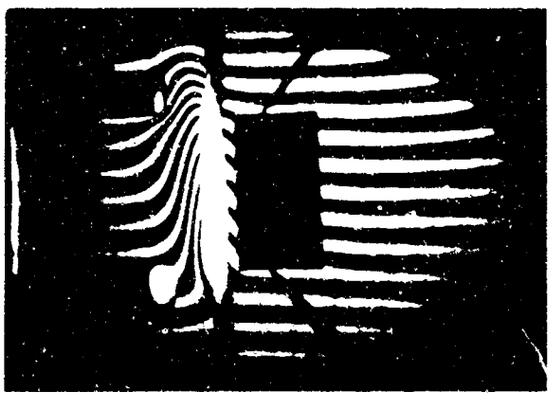

τ = 0.2 sec.

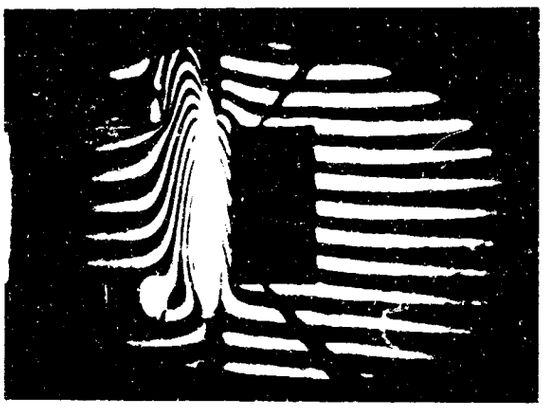

τ = 0.4 sec.

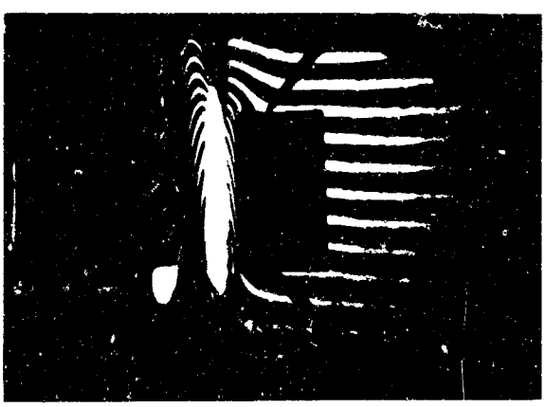

τ = 0.6 sec.

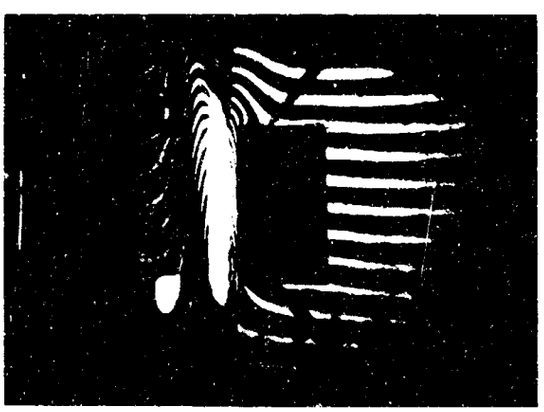

τ = 0.8 sec.

Figure 32a. Sequence of Interferograms Showing Fringe Shift Variations for Different Fabric-Skin Spacings (i_o = 6 cal/cm^2-sec) L = 0.094 cm

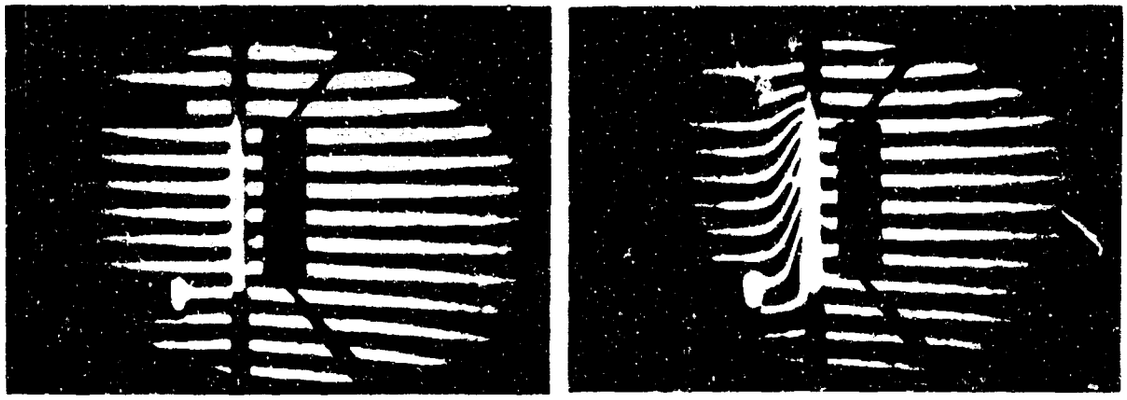

τ = 0 sec.

τ = 0.1 sec.

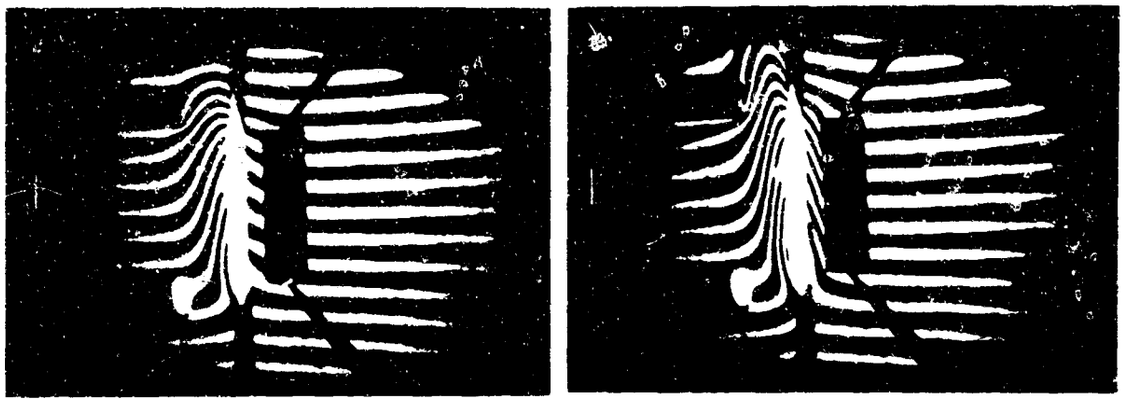

τ = 0.2 sec.

τ = 0.4 sec.

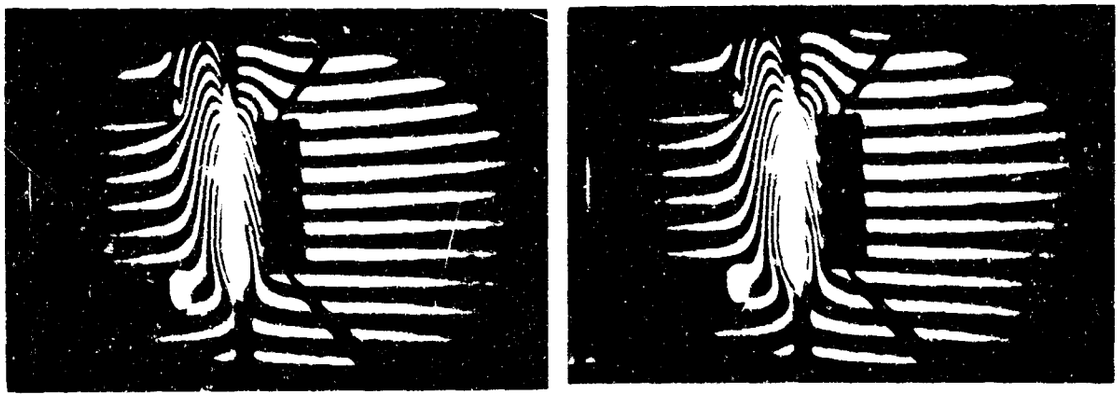

τ = 0.6 sec.

τ = 0.8 sec.

Figure 32b. Sequence of Interferograms Showing Fringe Shift Variations for Different Fabric-Skin Spacings (i_o = 6 cal/cm^2-sec) L = 0.151 cm

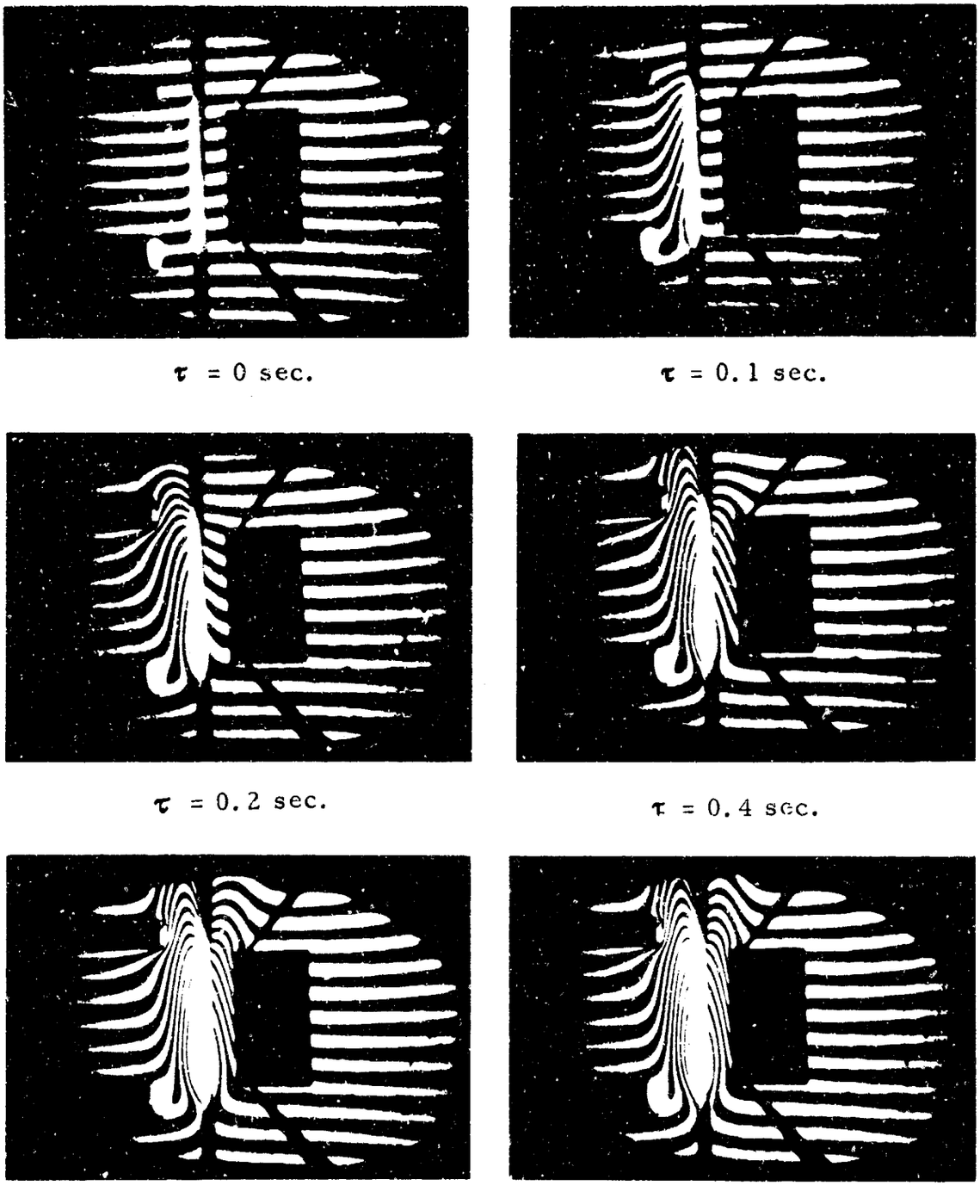

Figure 32c. Sequence of Interferograms Showing Fringe Shift Variations for Different Fabric-Skin Spacings (i_o = 6 cal/cm^2-sec) L = 0.227 cm

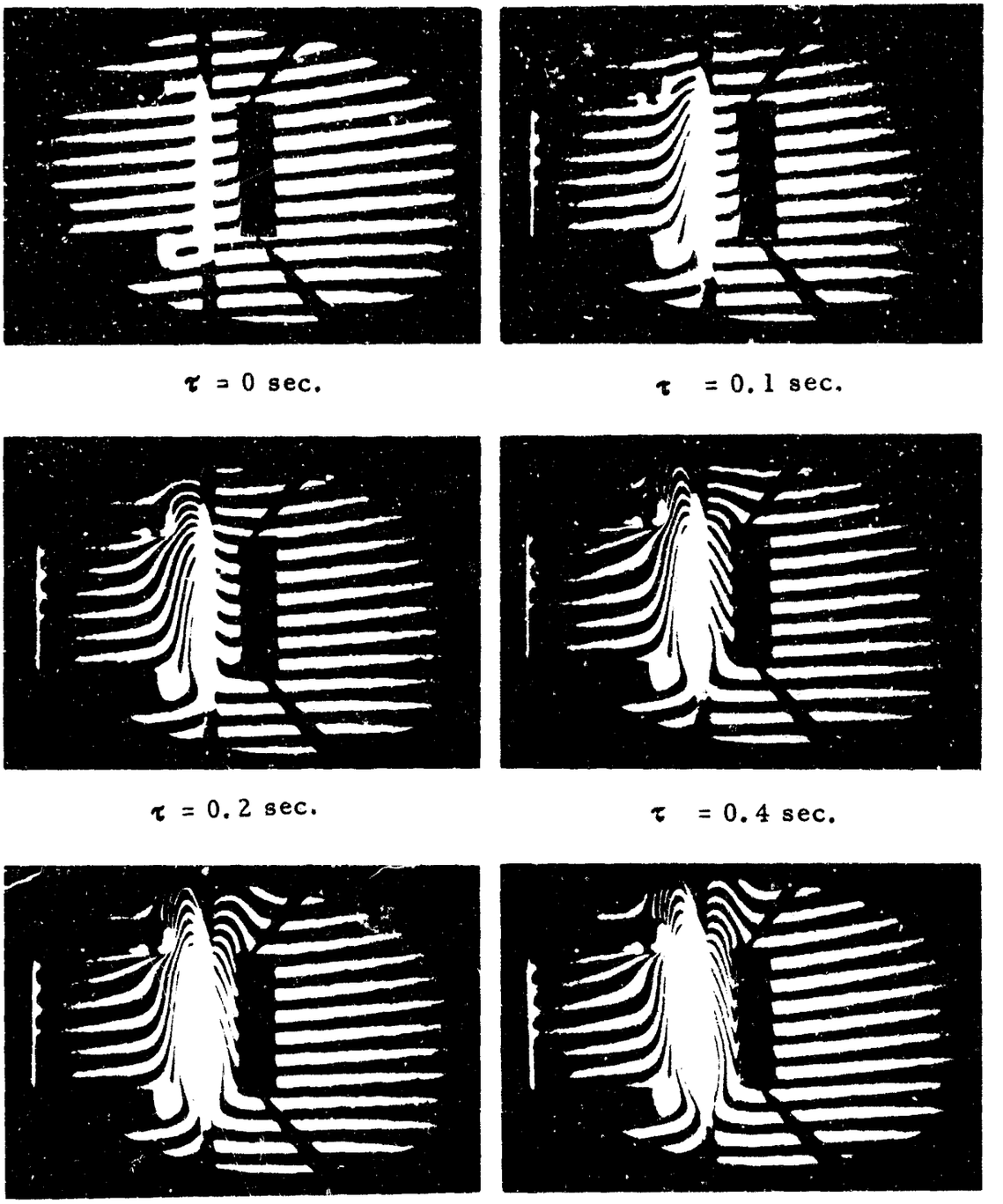

τ = 0 sec. τ = 0.1 sec.

τ = 0.2 sec. τ = 0.4 sec.

τ = 0.6 sec. τ = 0.8 sec.

Figure 32d. Sequence of Interferograms Showing Fringe Shift Variations for Different Fabric-Skin Spacings (i_o = 6 cal/cm^2-sec) L = 0.245 cm

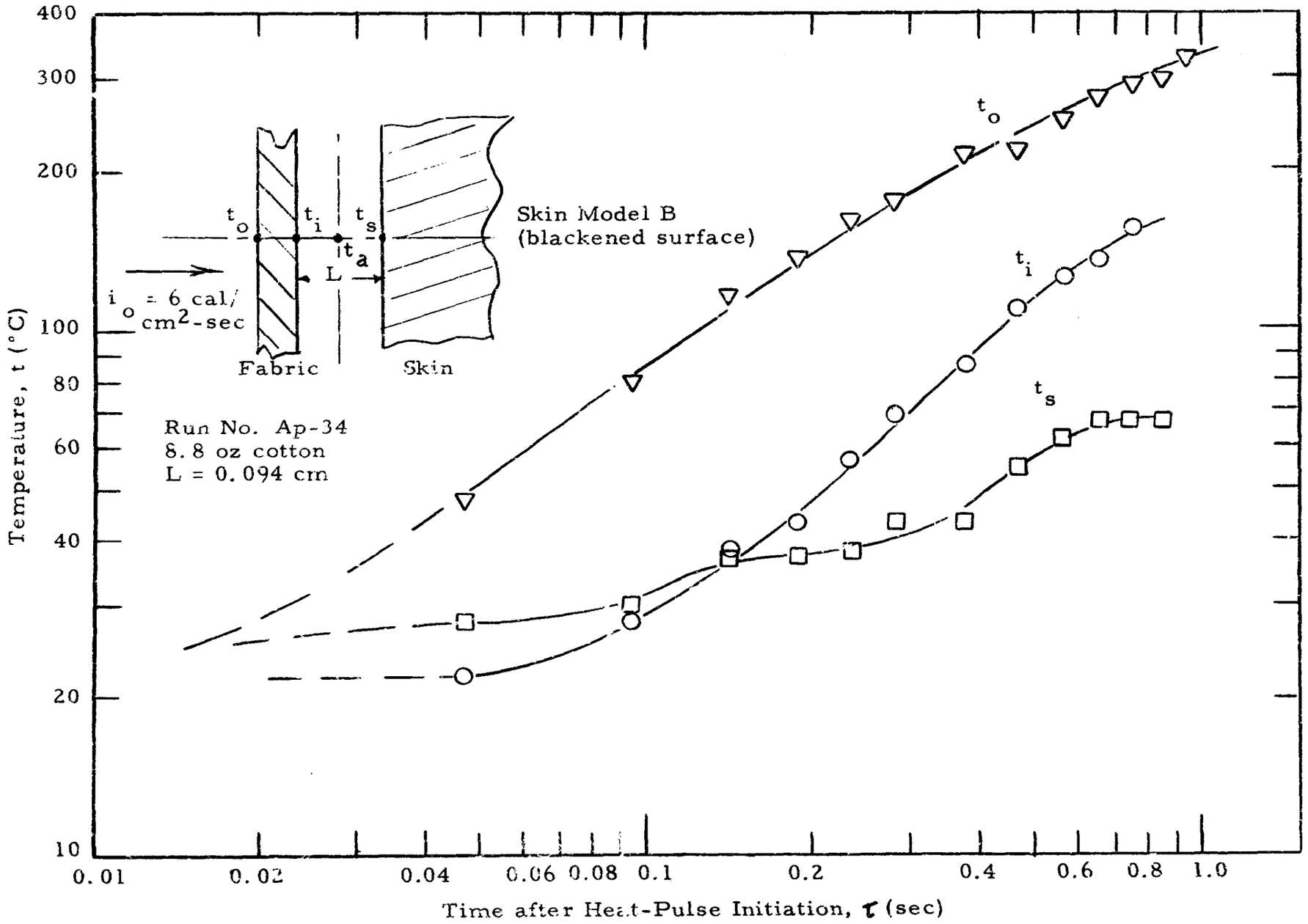

Figure 33a. Temperature-Time Variations for Heated Cotton (Comparison of Fabric-Skin Spacing)

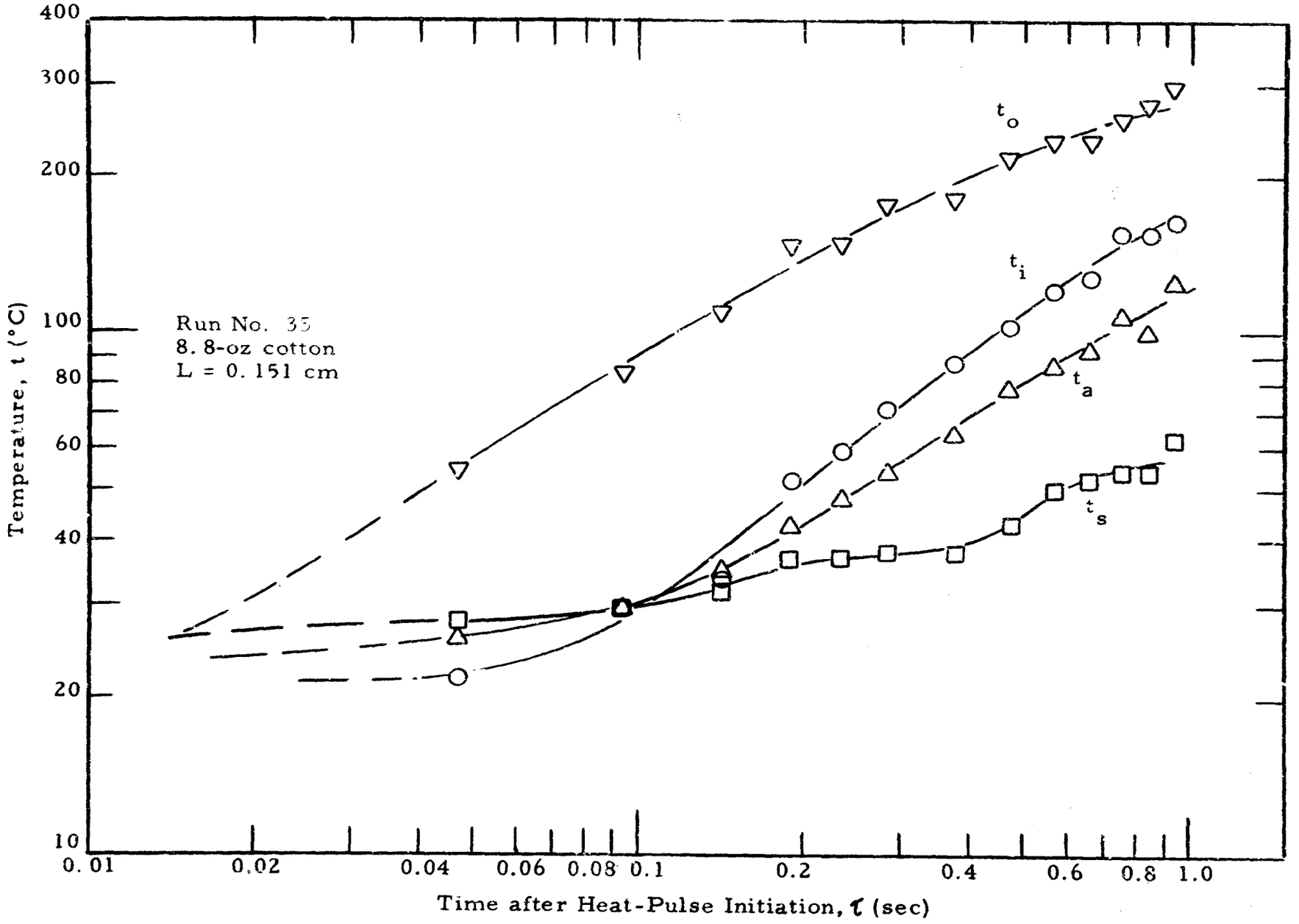
Run No. 35
8.8-oz cotton
L = 0.151 cm
t_o
t_i
t_a
t_s
Temperature, t (°C)
Time after Heat-Pulse Initiation, τ (sec)
400
300
200
100
80
60
40
20
10
0.01
0.02
0.04
0.06
0.08
0.1
0.2
0.4
0.6
0.8
1.0

Figure 33b.

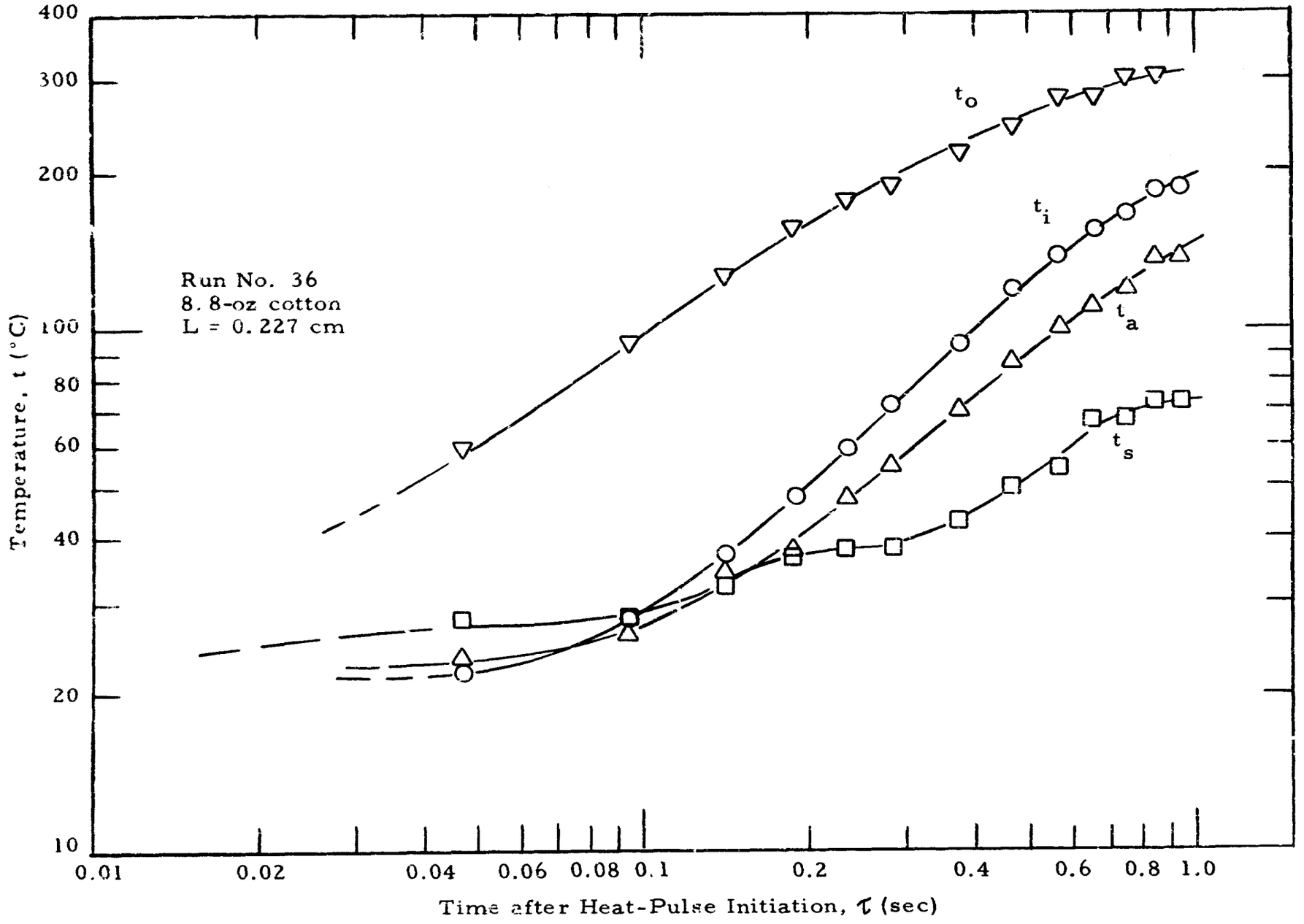
Run No. 36
8.8-oz cotton
L = 0.227 cm
t_o
t_i
t_a
t_s
Temperature, t (°C)
400
300
200
100
80
60
40
20
10
0.01
0.02
0.04
0.06
0.08
0.1
0.2
0.4
0.6
0.8
1.0
Time after Heat-Pulse Initiation, τ (sec)

Figure 33c.

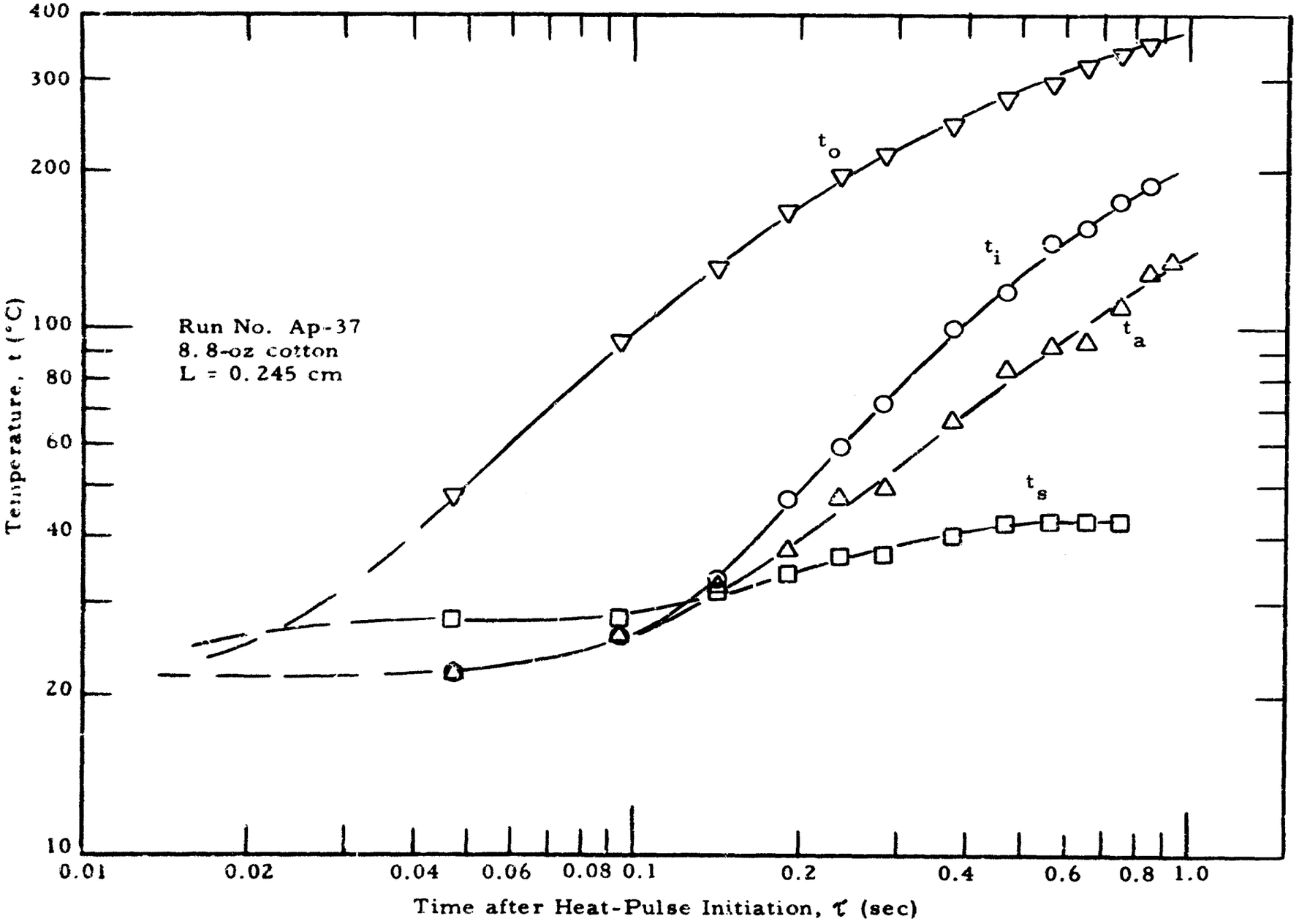
400
300
200
100
80
60
40
20
10
Temperature, t (°C)
Run No. Ap-37
8.8-oz cotton
L = 0.245 cm
t_o
t_i
t_a
t_s
0.01
0.02
0.04
0.06
0.08
0.1
0.2
0.4
0.6
0.8
1.0
Time after Heat-Pulse Initiation, τ (sec)

Figure 33d.

ambient at 0.8 second--this temperature increase depending upon spacing. The unblackened skin surface does not demonstrate an initially higher temperature level as does the camphor black coated skin but essentially responds to conduction and convection heat transfer in like manner (refer to Figure 34).

The temperature histories of the fabric surfaces and air gap are smooth curves. The skin surface did not always display a continuous temperature increase; frequently a varying rate was observed as shown in Figure 33.

The influence of fabric-skin spacing on temperature level is shown in Figure 35 with time as a parameter. The effect of a decrease in spacing is to increase the skin temperature. The fabric rear surface temperature at any instant generally was higher for increased spacing. The lower temperature values at closer spacings show further the influence of an adjacent skin.

The effects of fabric moisture content on temperature response were studied. In Figures 36a and 36b the temperature response of fabric and skin are displayed for a dry fabric specimen and for one at room humidity conditions (relative humidity 28 percent). The dry specimen had a finite but undetermined moisture content since final preparations for testing were conducted at ambient conditions. Although the moisture content of cotton at 28 percent relative humidity (3.8 percent by weight) is not appreciable, the test results show that the temperature response for a heated room humidity specimen lags that for a heated dry fabric. Temperature measurements on skin simulators reported in Reference 6 indicated a strong influence of fabric moisture content on skin response. To investigate these effects further, a more rigorously controlled series of tests were conducted. Specimens were housed for lengthy periods in a dry air environment (dew point -60°C). Upon heating, these dry air specimens did not always display higher temperature response behavior

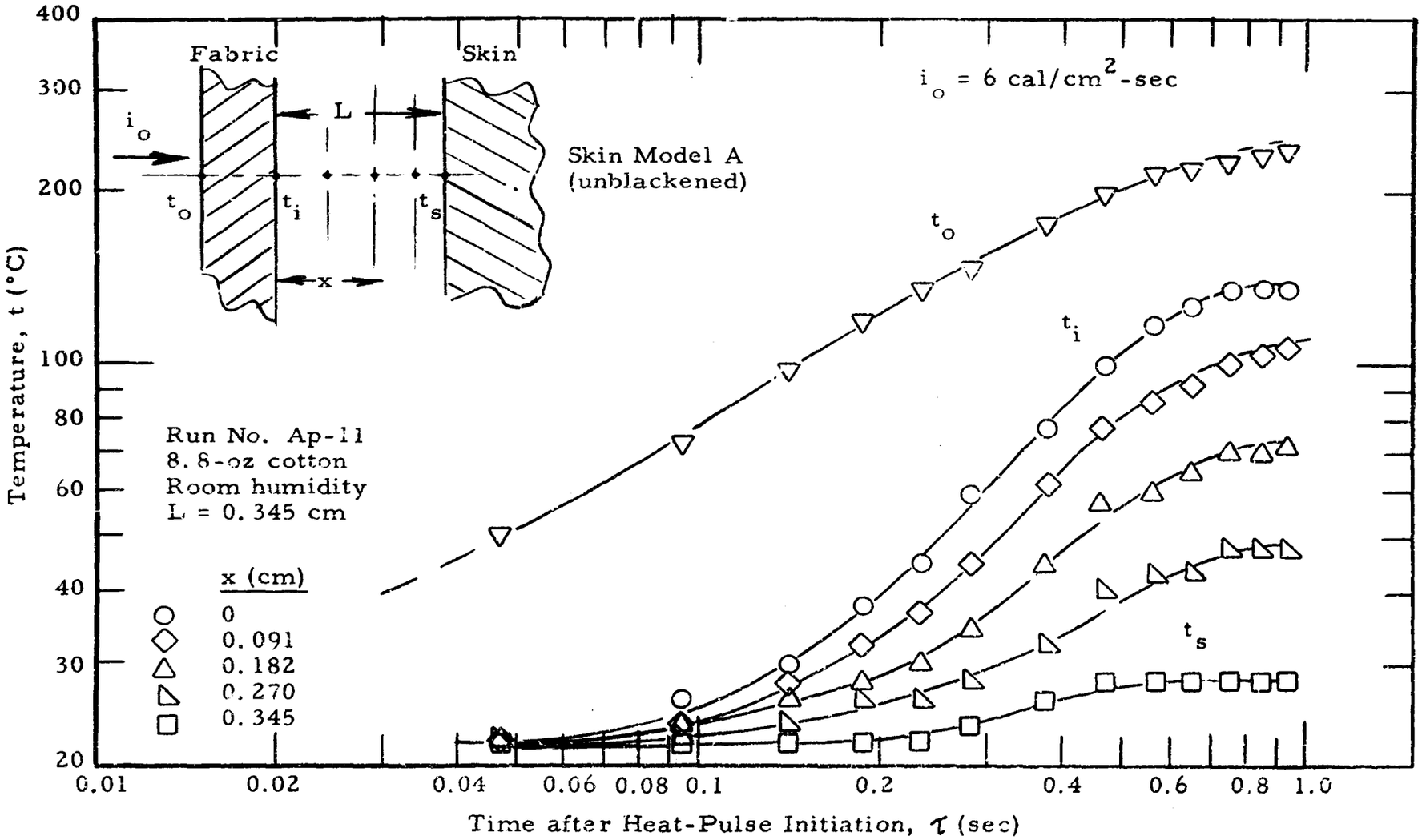

Figure 34. Temperature-Time Variations of Heated Fabric-Skin System, Unblackened Skin Surface

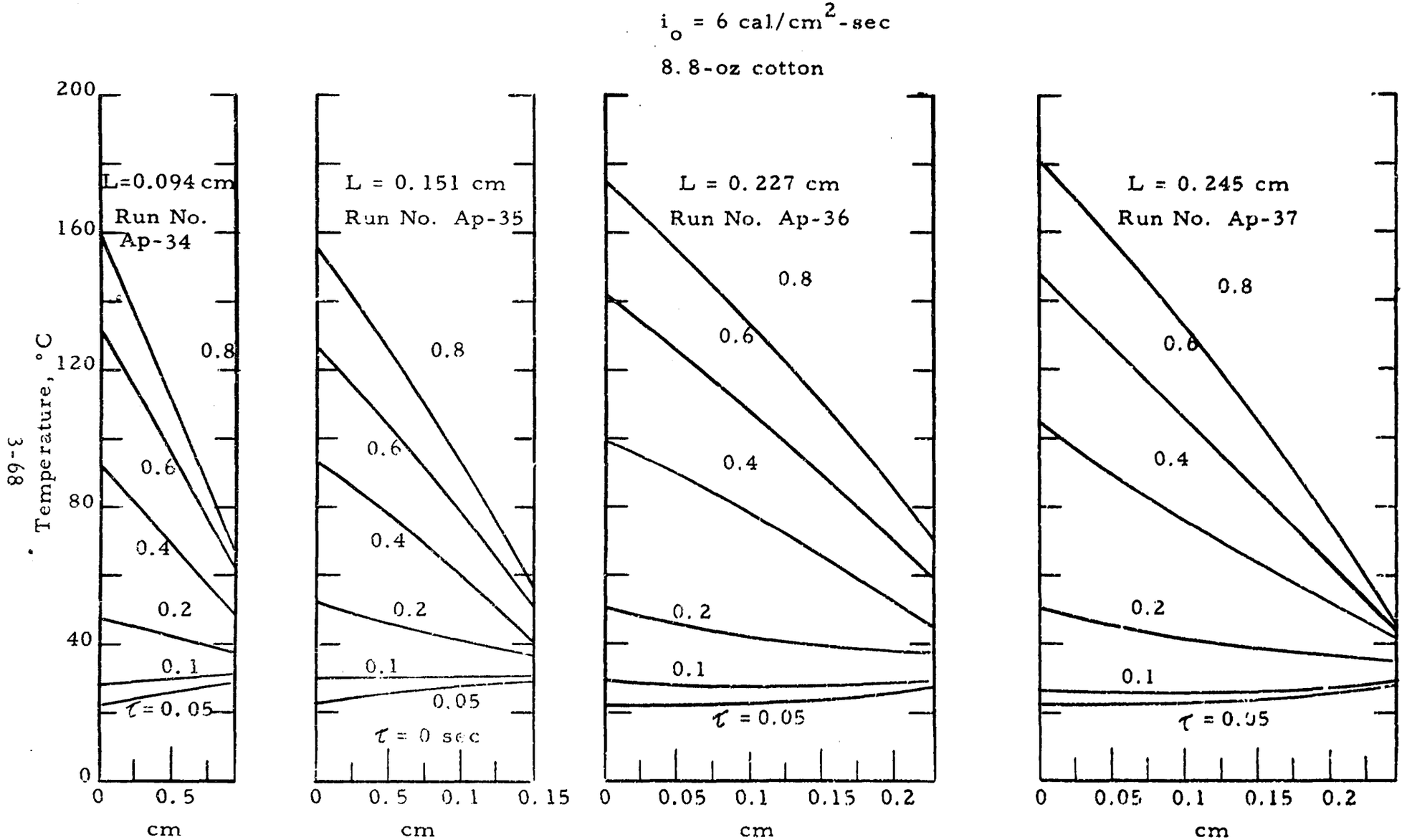

Figure 35. Fabric-Air Gap-Skin Temperature Profiles for Different Spacings (Heated 8.8-oz Cotton)

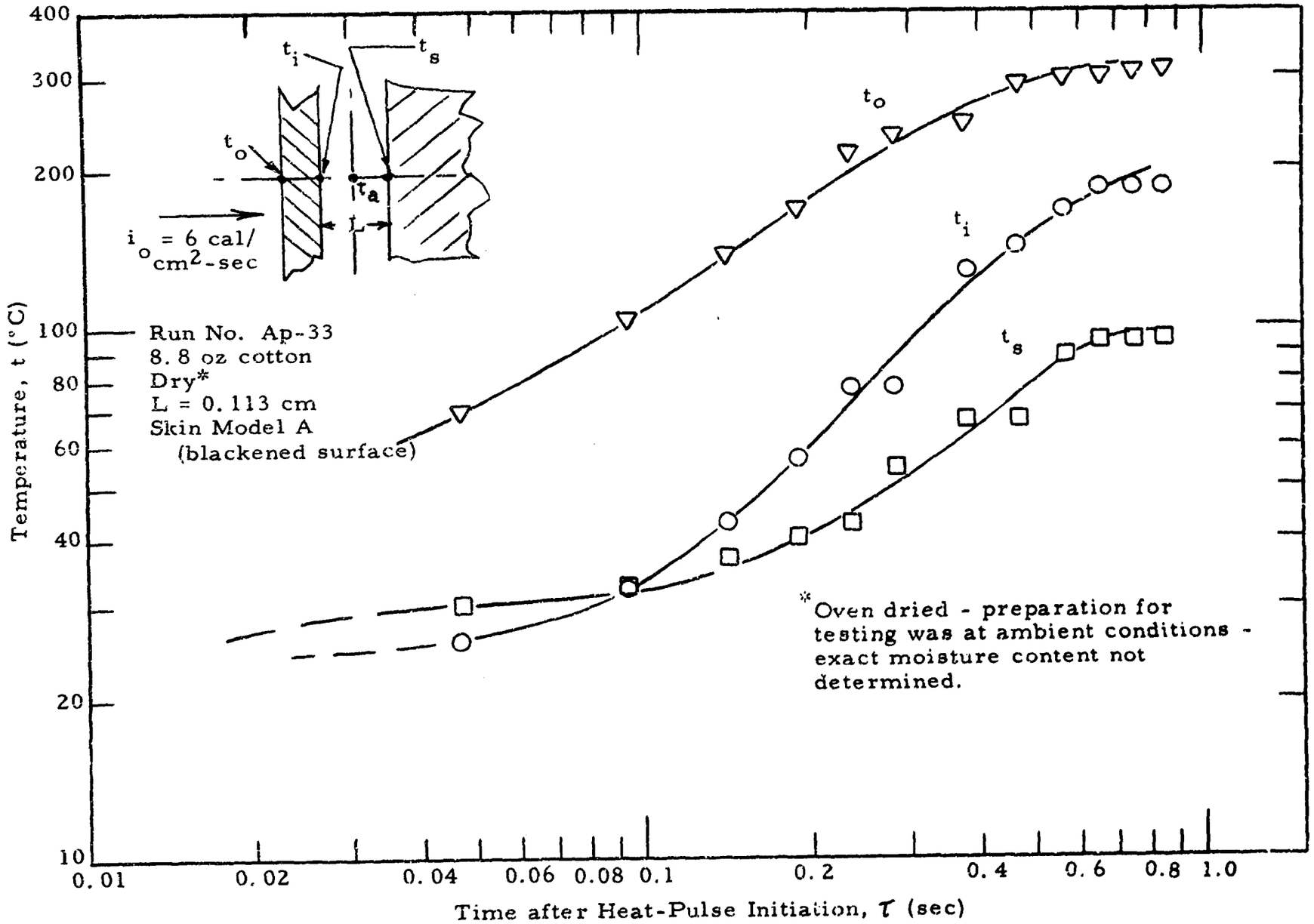

Figure 36a. Temperature-Time Variations for Dry Cotton

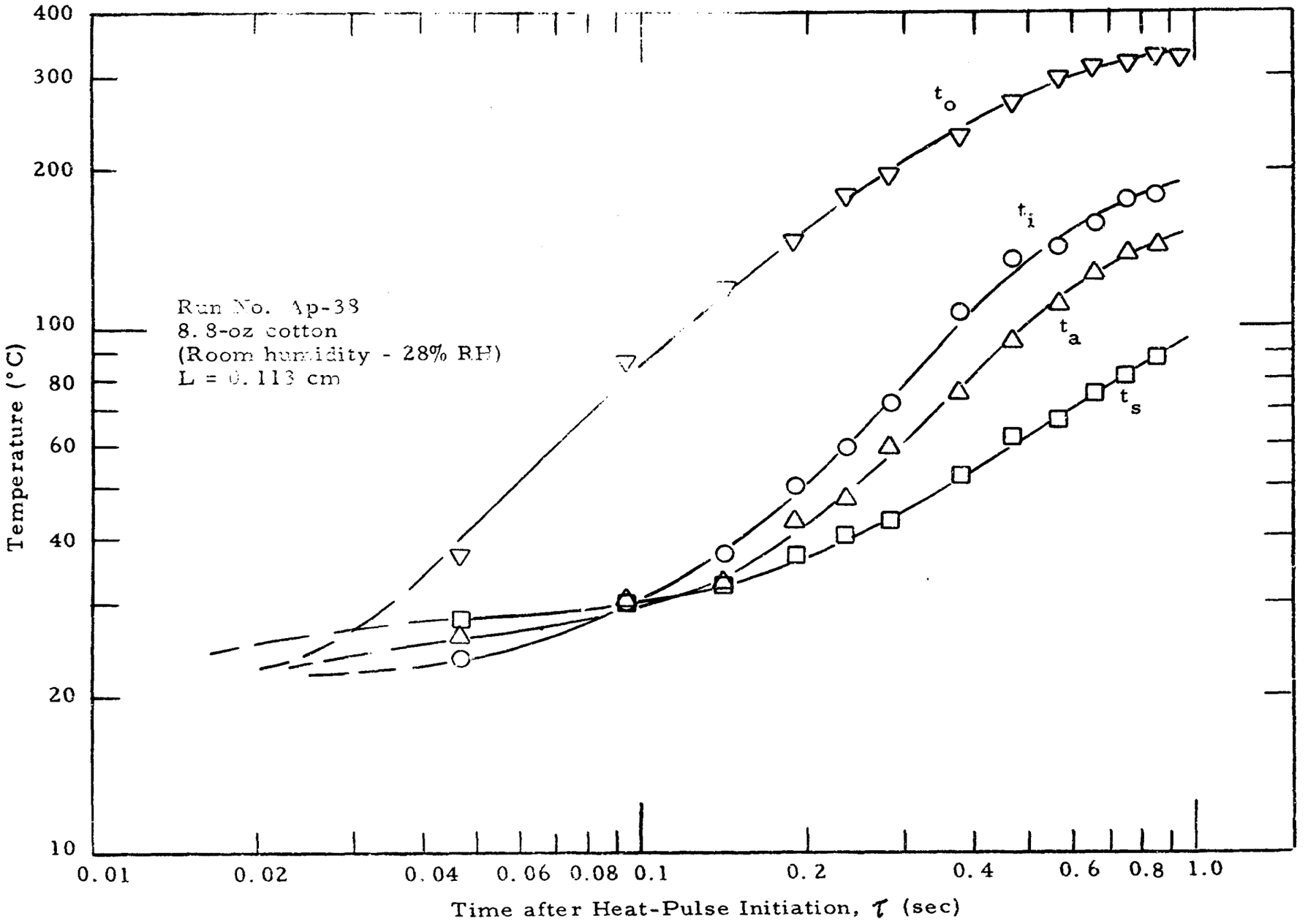

Figure 36b. Temperature-Time Variations for Undried Cotton (Room Humidity)

over that of specimens at room ambient conditions (see Figure 37). In fact, some of the room-humidity controlled specimens indicated temperature values somewhat higher than that of the dry specimens.

It must be emphasized that the temperature values for the room-humidity control tests are not corrected for the effects of water vapor. Our earlier multi-environmental test determinations demonstrate that due to the presence of water vapor (at approximately 28 percent relative humidity), the temperature indications at a considered instance (at 0.3-0.4 sec) are high by as much as 7°C. Application of such a correction for the entire profile would probably show that little statistical difference would be evident between the room humidity and the dry specimen tests.

Final conclusions as to the effect of fabric moisture content on the temperature response characteristics cannot be made at this time. However, a tentative conclusion is that the gross behavior of both dry and room humidity prepared specimens appear to be much the same, and even when compared with the wetted fabric tests, the differences in temperature response during the initial phases of heating are not as large as one might expect.

The plot of data points in Figure 37, although not demonstrating any measurable differences between dry and room-humidity specimens during the period of temperature increase, does show that combustion or more complete degradation occurs earlier for the dry samples than for the room-humidity test samples by approximately 0.2 sec. This is a significant point, although easily overlooked in the log-log profiles, since the total energy delivered prior to combustion may be different, in the different tests, by 20 percent or more. The effects of water content thus may be only evident in this manner.

From these considerations it becomes necessary to perform experimental tests over a wide range of room-humidity conditions to better assess the influence of moisture content. In addition,

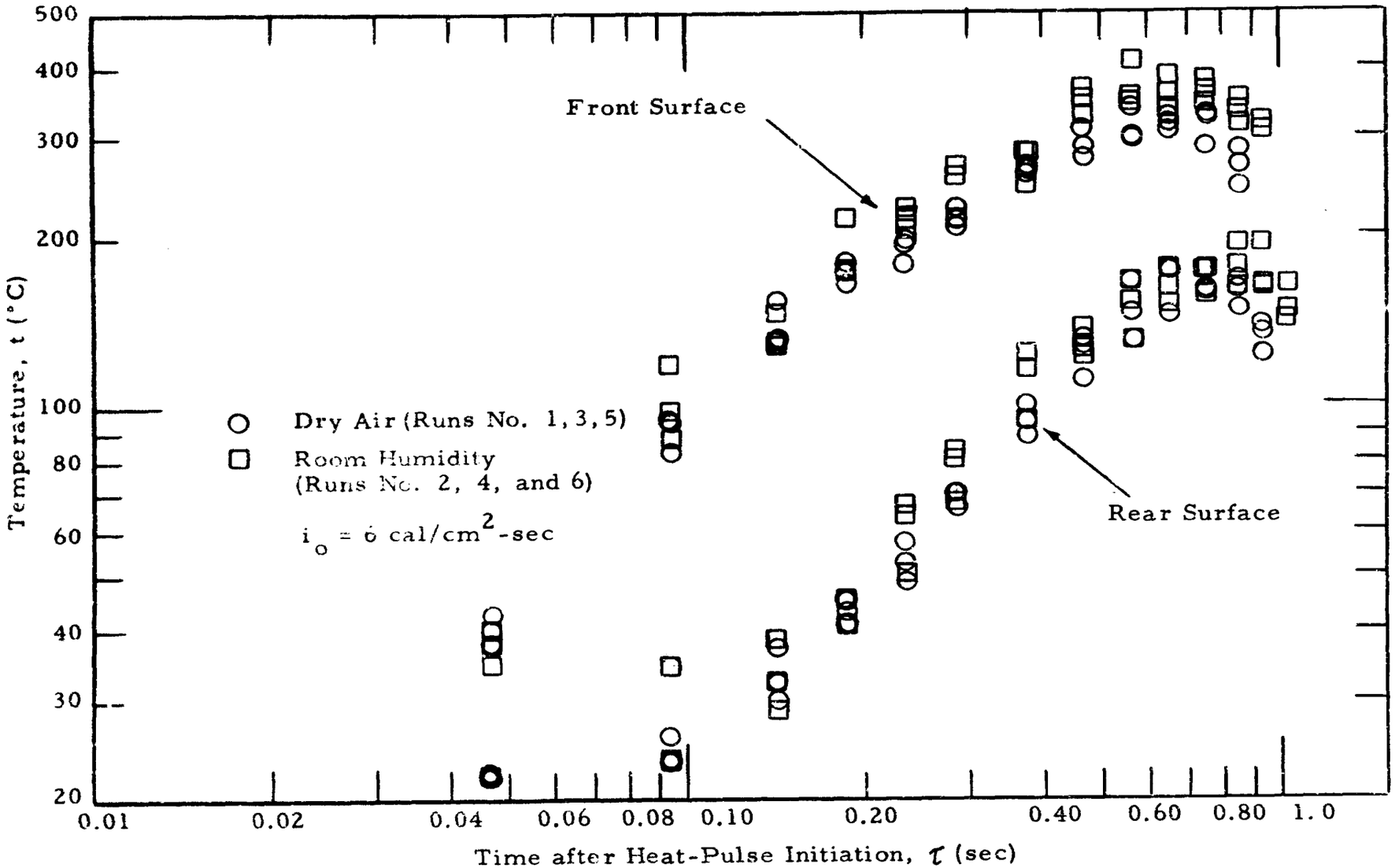

Figure 37. Temperature-Time Variations of Heated 8.8-oz Cotton Specimens at Dry and at Room Humidity Conditions

the multi-wavelength or multi-environmental interferometric techniques must be utilized to determine water vapor concentrations at the fabric surfaces and thus accurately correct indicated temperature profiles. For the multi-environmental tests, consideration must be given the water vapor diffusion processes in the different environments. A vapor concentration level at the fabric surface may be quite different in the separate environments.

The further important processes involving transfer of vapor or gaseous products from the heated fabric to the skin need to be understood. Although the influence of fabric moisture content on the temperature response of an underlying or adjacent skin (considering only heat transfer) are important, the effects of vapor or mass transfer may be equally important, and for prescribed conditions even overshadow the effects of pure conduction heat transfer. More comprehensive tests thus are needed to isolate these influencing factors.

In Figure 38 the temperature differences from fabric front to rear surfaces for two fabric-airspace-skin conditions are plotted to demonstrate the constancy of this difference beyond 0.2 second. The importance of this value and of the actual temperature recordings would be recognized if additional information on fabric diathermancy (absorption in depth) were available. Since front and rear surface temperature values can be obtained from interferometric observations it would appear that determinations of fabric diathermancy would also be possible. Using a modified flash discharge technique and the interferometer this could be accomplished. The apparent thermal diffusivity, thermal conductivity and heat capacity (important properties of the material in the absorption and dissipation of heat) can also be determined for non-homogeneous materials. These property measurements were not made during this program period although are suggested for future investigations.

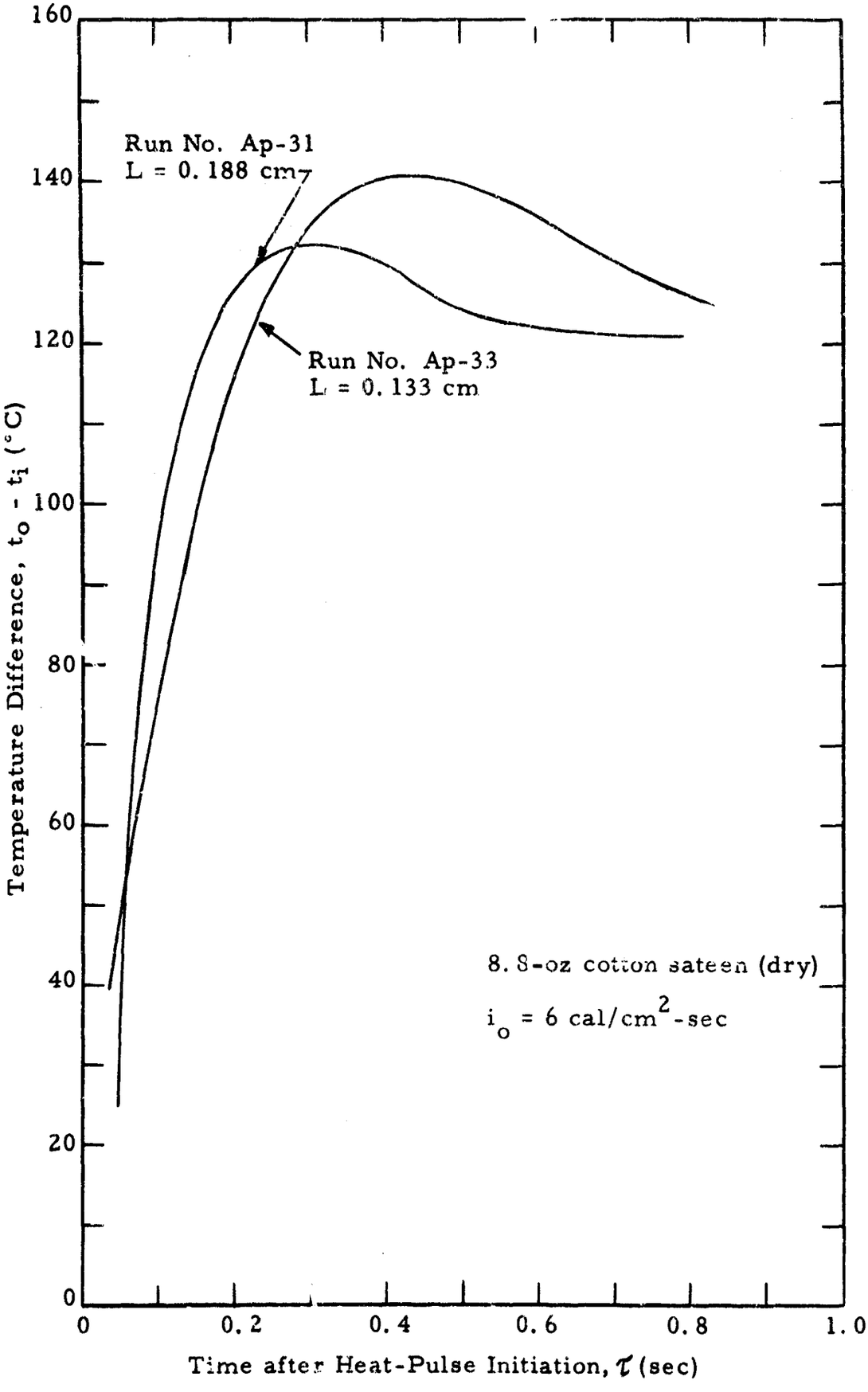

Figure 38. Fabric Front-to-Rear Surface Temperature Difference as a Function of Time

The above considerations have been applied to the center position of the vertical fabric-airspace-skin complex. At different vertical positions, the surface temperature histories and thermal boundary profiles would also be different. As shown in Figure 39, these differences are markedly evident; the fabric front surface temperature varied, for example, by as much as 100°C for an $y/H = .14$ to $y/H = .60$ at 0.6 second. In Goldstein's nonsteady state tests with a brass plate, considerable variation in temperature along the vertical plane (approximately 10 cm height) was also noted. For large vertical surface areas, the local heat losses would decrease with height up to a certain position, characterized by the flow conditions and surface temperature; thereafter increase slightly with height for some distance and finally become constant. It has been postulated that two heat transfer regimes exist: pure conduction and laminar and turbulent convection flow. Both Goldstein and Carlson,[11,12] among others, have attempted to characterize these heat flow regimes in their studies.

The degree of temperature difference with vertical dimension suggests that considerable importance must be attached to heat losses by conduction and convection even for short periods of exposure as considered in our tests. The combustion or more complete degradation occurrences were undoubtedly initiated near the top of the fabric specimen; since here the heat loss was minimum, resulting in a locally higher temperature.

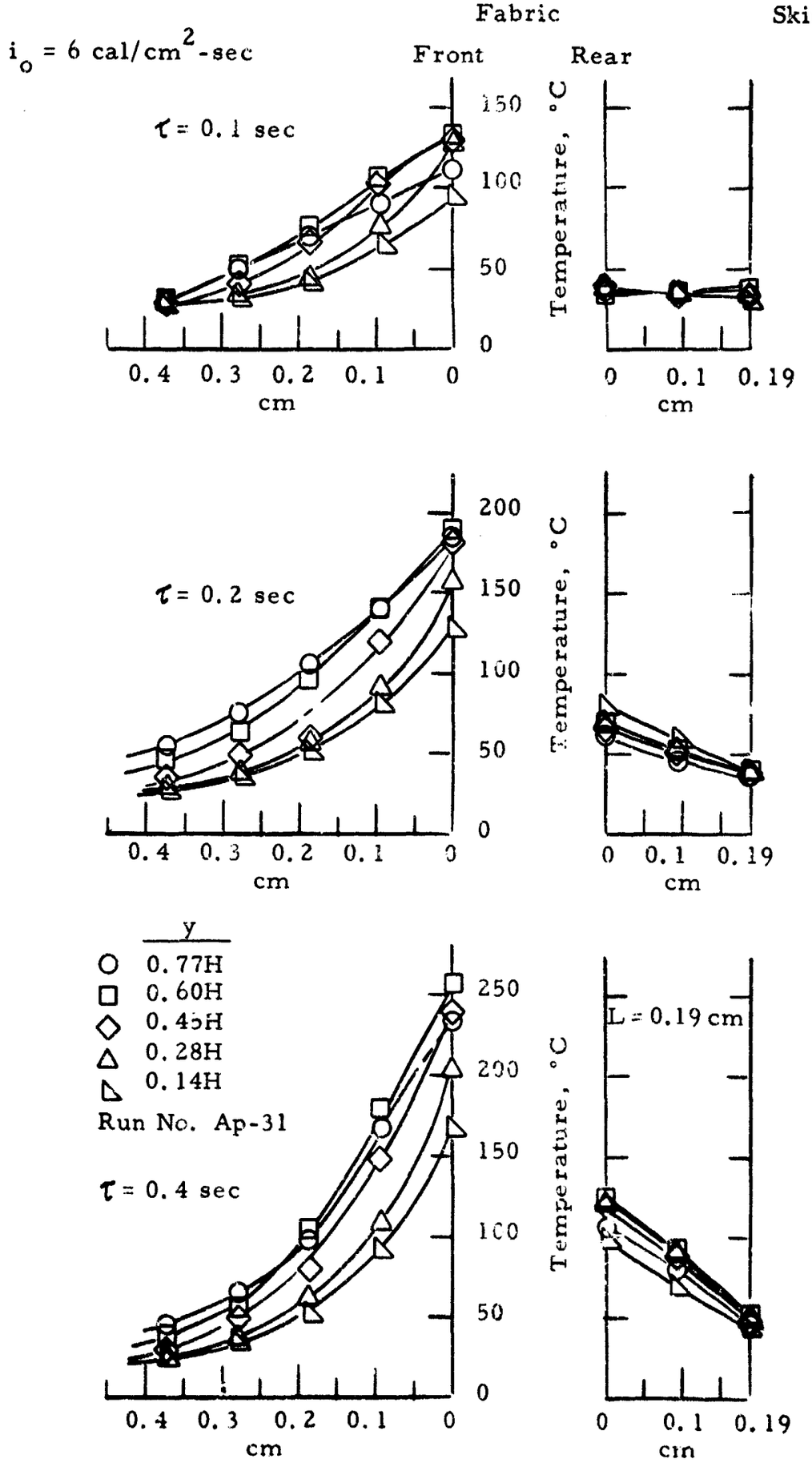

Figure 39. Temperature Distributions as a Function of Vertical Location and Time (8.8-oz Cotton)

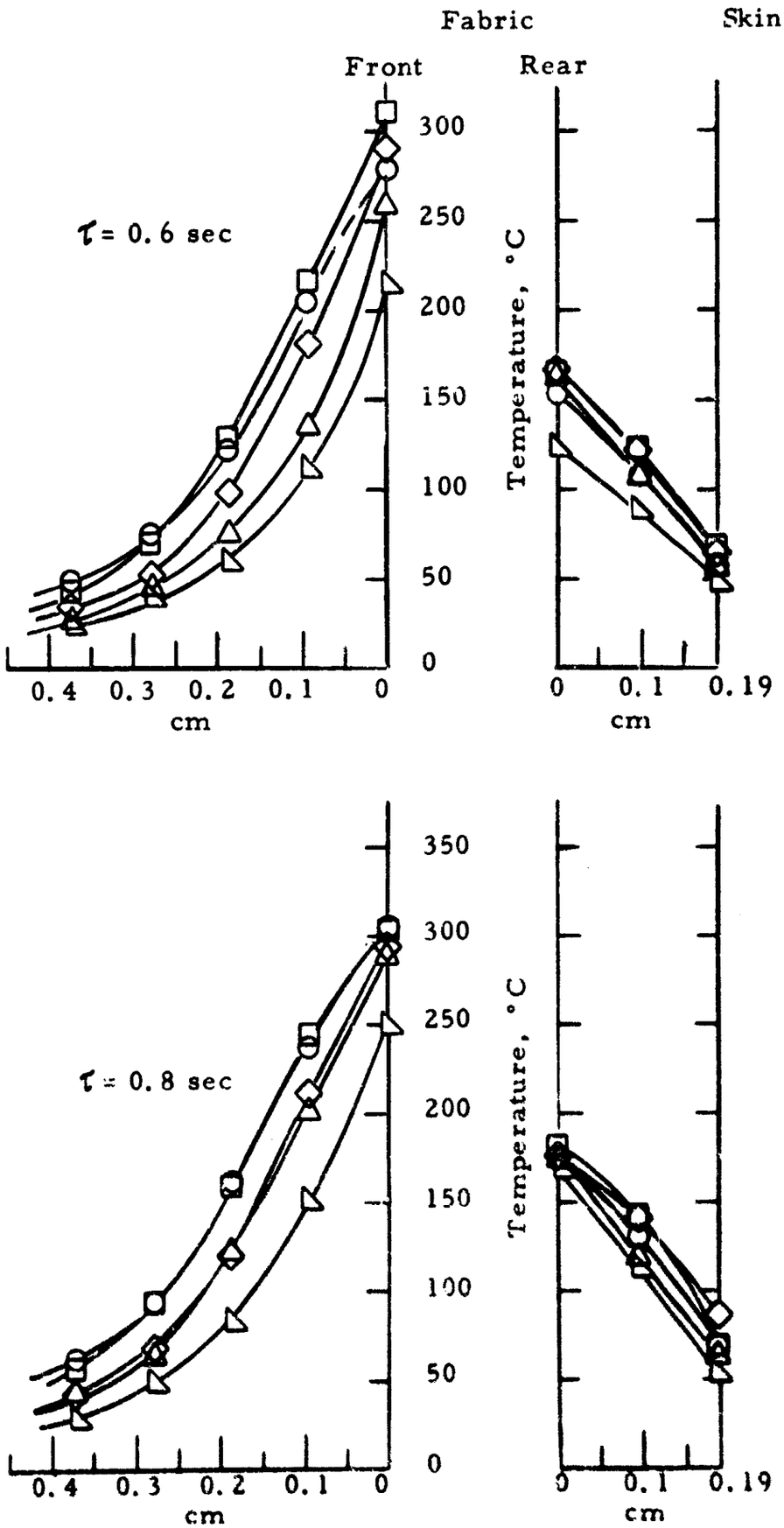

Figure 39 (continued)

3.4.4.2 Calculation of Heat Transfer Coefficients from Measured Data

3.4.4.2.1 General. - The local convective heat transfer from the fabric may be determined from the boundary layer temperature distribution at any instant. The most important value required in determining the heat loss is the film heat transfer coefficient, h, defined in the terms of the heat flow q per unit area and the temperature difference Δt.

$$q_c = h_c \Delta t . \tag{12}$$

Since the air layer at the fabric surface is at rest, the heat flow may also be calculated from the conduction equation

$$q_c = -k_w \left.\frac{dt}{dx}\right|_w \tag{13}$$

where k_w is the thermal conductivity of the air, generally considered at the wall temperature, and the $\left.dt/dx\right|_w$ the temperature gradient at the surface. By equating these expressions and setting the terms in form of the non-dimensional heat transfer coefficient, Nusselt number, we obtain

$$Nu = \frac{hy}{k_w} = \frac{y}{\Delta t} \left.\frac{dt}{dx}\right|_w \tag{14}$$

where y is a characteristic dimension.

3.4.4.2.2 Comparison with Existing Data. - Figure 40 shows a plot of h and Nusselt number variation with time for the front surface of a heated 8.8-oz cotton fabric. The characteristic length y in the Nusselt number is approximately 0.5 H at which horizontal plane the measurements were made. As shown, the coefficients decrease with

$$Nu = \frac{h_{fo} y}{k}$$

$$h_{fo} = \frac{k}{t_{fo} - t_e} \left(\frac{dt}{dx}\right)_{fo}$$

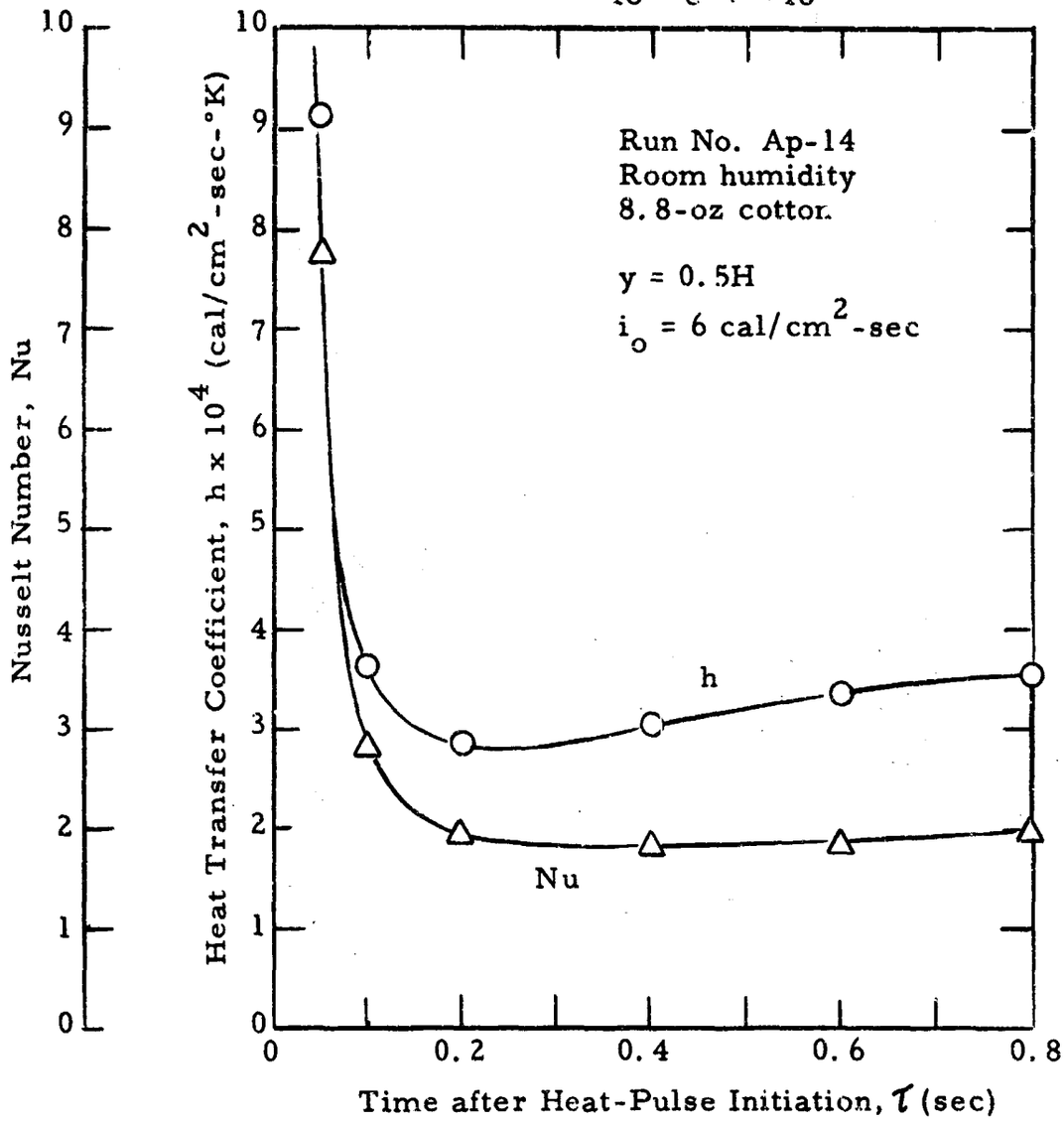

Figure 40. Variation of Surface Heat Transfer Coefficients with Time after Heat-Pulse Initiation

time during the initial pure conduction phase. Thereafter a quasi steady-state condition is reached where h is expected to increase only as Δt increases, then finally becoming constant where a true steady-state exists. A true steady-state was not obtained in our tests since the degradation processes occurred prior to equilibrium heat in-heat loss conditions. At the minimum value of h, or somewhat thereafter, the thermal boundary layer was found to have a maximum thickness, decreasing slightly from thereon to the ignition temperature.

The local non-dimensional representation of heat flow (Nu) occurring at the fabric front surface in terms of the local non-dimensional Gr_y number is plotted in Figure 41. Calculations were made at five vertical positions for times 0.1 to 0.8 second. Theoretical and empirical relationships for quasi-steady convection heat flow[11] predict for a fluid of given Prandtl number the function

$$Nu = K(Gr)^{1/4} \tag{15}$$

where K is a constant.

This relationship is not entirely evident from the plotted data points. If we chose to ignore certain points (for example, those at low values of Gr_y where theoretical and experimental agreements have been suggested as being poor) we may obtain exponent values from 1/8 to 1/3. These data may be plotted as shown in Figure 42 to examine the variation of $Nu_y/(Gr_y)^{1/4}$ from a constant value.

In providing an important non-dimensional relationship, such as this, consideration must be given the most suitable property values to use in the calculations. In calculating $Gr_y = (g\beta\Delta t\, y^3)/\nu$, the expansion coefficient of a gas β was determined directly from $1/t_e$; the kinematic viscosity ν was evaluated at t_e, whereas the wall temperature value was used for the evaluation of k. Goldstein[12] suggests that for a non-isothermal wall, as in these studies, $1/t_e$ for the expansion coefficient is appropriate; however, an evaluation of ν at wall temperature

$$Nu_y = \frac{h_{fo} y}{k} = \frac{y}{t_{fo} - t_e} \left(\frac{dt}{dy}\right)_{fo}$$

$$Gr_y = \frac{g \beta (t_{fo} - t_e) y^3}{\nu^2 t_e}$$

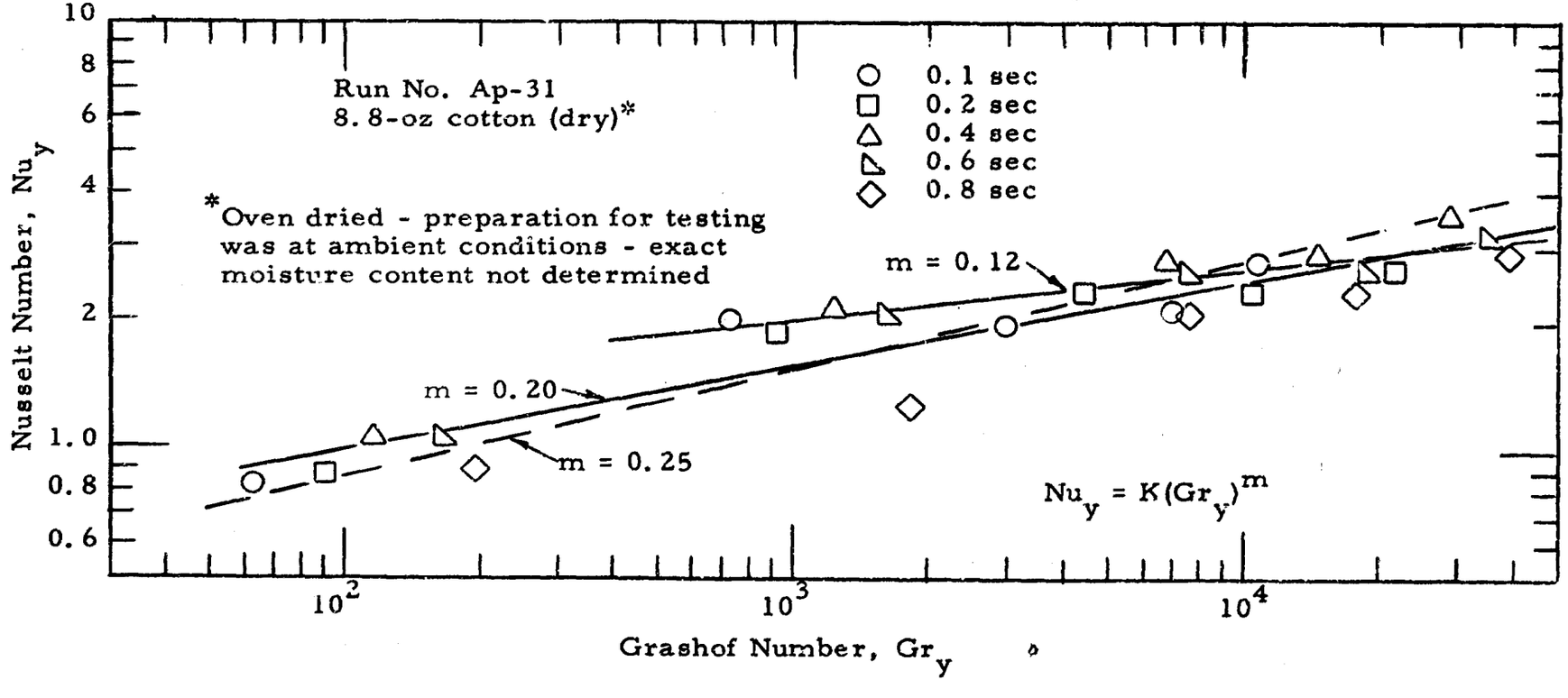

Figure 41. Variation of Front Surface Nusselt Number with Grashof Number

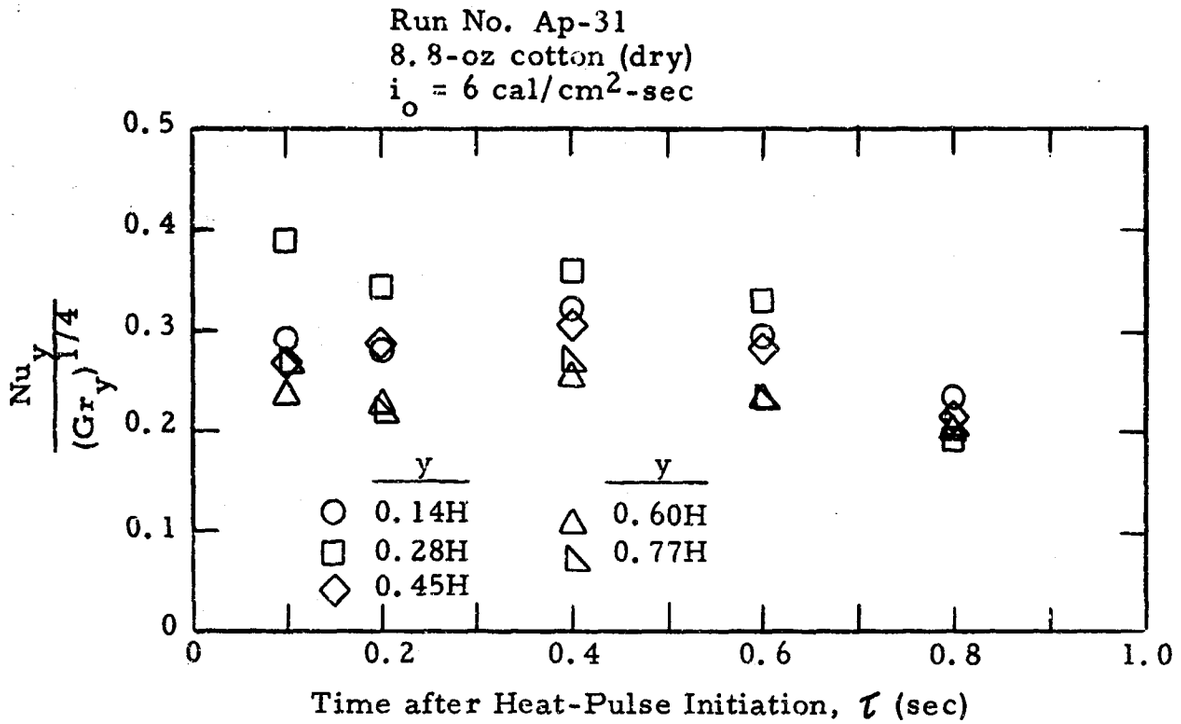

Figure 42. Variation of Front Surface Local Nondimensional Heat Transfer Parameter with Time (8.8-oz Cotton)

values would be more correct. Sparrow[12] calculated for an assumed ideal gas that in evaluating Nu_y number as a function of Gr_y the reference temperature $t_r = t_w - 0.38(t_w - t_e)$ should be used in evaluating ν, β, and k. If the above representation required further accuracy, comprehensive data could be compiled and a statistical treatment followed.

At the rear surface, for small spacings between fabric and skin, the presence of the skin surface is felt very rapidly. Conduction occurs across the air gap and fully developed convective flow does not occur. The skin surface temperature is higher for smaller spacing. A minimum heat loss from the fabric occurs at some intermediate spacing where fully developed convective flow cannot occur and where conduction is not entirely predominant. For our fabric skin spacing 0.09 to 0.35 cm the transfer of heat from the fabric rear surface was by conduction, at least along the centerline measurements. At the close spacings, top and bottom end effects were also negligible; conduction heat transfer occurring entirely.

For a fabric spacing of 0.181 cm the local fabric rear surface non-dimensional heat transfer coefficient Nu_y has been calculated for five different vertical positions and different time instances as a function of Gr_y. The predicted relationship $Nu_y/(Gr_y)^{1/3}$ approaches a constant at 0.6 to 0.8 second (steady-state) as shown in Figure 43. At 0.2 second the exponent m = 1/3 already holds precisely since Nu_y (for pure conduction) is equal to $(Gr_y/Gr_L)^{1/3}$. If the characteristic length in the non-dimensional coefficient were chosen to be the fabric-skin spacing dimension L, then $Nu_L = 1$ for all values of Gr_L within the pure conduction regime. If the spacing had been greater (values of Gr_L greater than 10^3) then $Nu_y = K(Gr_L)^{1/3}$.

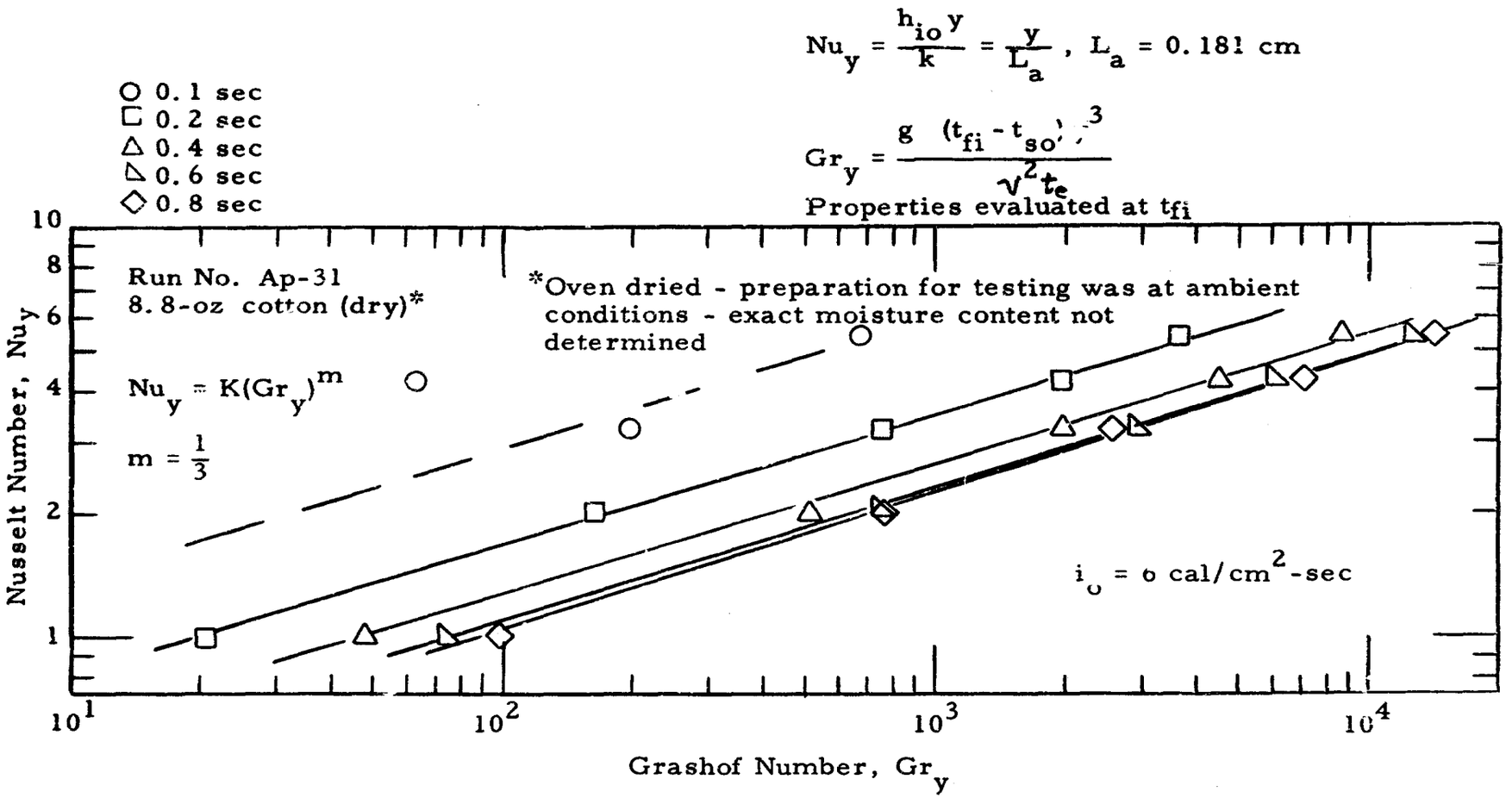

Figure 43. Variation of Rear Surface Nusselt Number with Grashof Number

3.4.4.2.3 Measurement of Non-Dimensional Heat Transfer Coefficients for Utilization in Theoretical Development

As presented in Appendix A, the fabric front and rear surface heat transfer coefficients were non-dimensionalized as follows:

$$H_{fo} = \frac{h_{fo} L_f}{k_f} \tag{16}$$

and

$$H_{io} = \frac{ha_{eff} L_f}{k_f} \tag{17}$$

It is to be noted that in the above relationships the thermal conductivity k_f is that of the fabric rather than air. In addition, the characteristic length is the fabric thickness, L_f. In this form (Biot number), the process of heat transfer from air to fabric is more intimately related to conduction heat transfer in the fabric because of the conductivity. The variations of these coefficients with time (and for the rear surface, the variation with air gap spacing also) may be determined. Figure 44 is a plot of the non-dimensional front surface heat transfer coefficient H_{fo} (Biot number) for three separate heating tests on the 8.8-oz cotton sateen. The film heat transfer coefficient h_{fo} was determined from the expression

$$h_{fo} = \frac{k}{t_{fo} - t_e} \left(\frac{dt}{dx}\right)_{fo}$$

where k was chosen at t_e.

The effective fabric value for k_f / L_f was taken as a constant.[4] (No variation with fabric temperature was assumed.) The plot follows the predicted variation for the different heat transfer regimes.

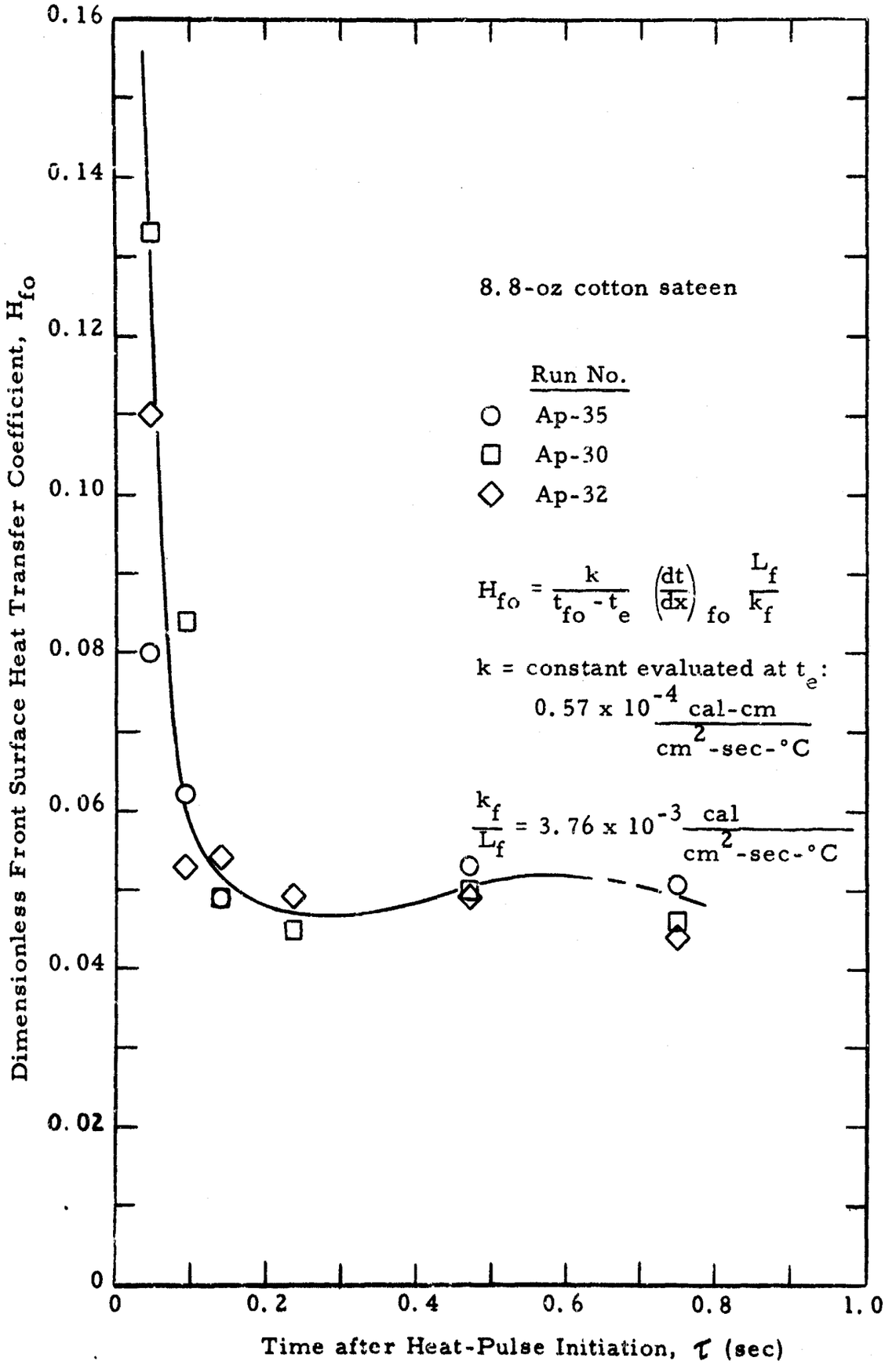

Figure 44. Variation of Front Surface Convective Heat Transfer Coefficient (Biot Number) with Time (k evaluated at t_e)

For values of k, in the above calculations, taken at t_{fo} instead of at t_e, the more representative but similar variation of h_{fo}, Figure 45, would result.

In Figure 46 the rear surface values of H_{io} are plotted to show variations with time and with spacing. Since a conduction flow regime exists for the small fabric skin spacings, the non-dimensional coefficient is calculated as

$$H_{io} = \frac{k}{L_a}\left(\frac{L_f}{k_f}\right) . \qquad (18).$$

It should be noted that for high fabric rear surface temperatures the heat conductivity change is sufficient to prevent the formation of a linear temperature gradient for a truly one-dimensional heat flow situation. As the deviations from a linear distribution are not as large as would be expected for the higher temperatures, it is possible that localized areas of free convection may be occurring.

3.5 Comparison of Measured Temperature-Time Variation with Theory

In Appendix A four sample calculations are presented for the following conditions:

1) Case I. Opaque Fabric-Airspace-Skin System

2) Case II. Diathermaneous Fabric-Airspace-Skin System

3) Case III. Flat Plate Radiating to a Deep Space Environment

4) Case IV. Flat Plate Irradiated by a Time-Dependent Heat Pulse.

These calculations were performed to allow a comparison with results of Reference 4 (Case I and Case II), Reference 29 (Case III), and

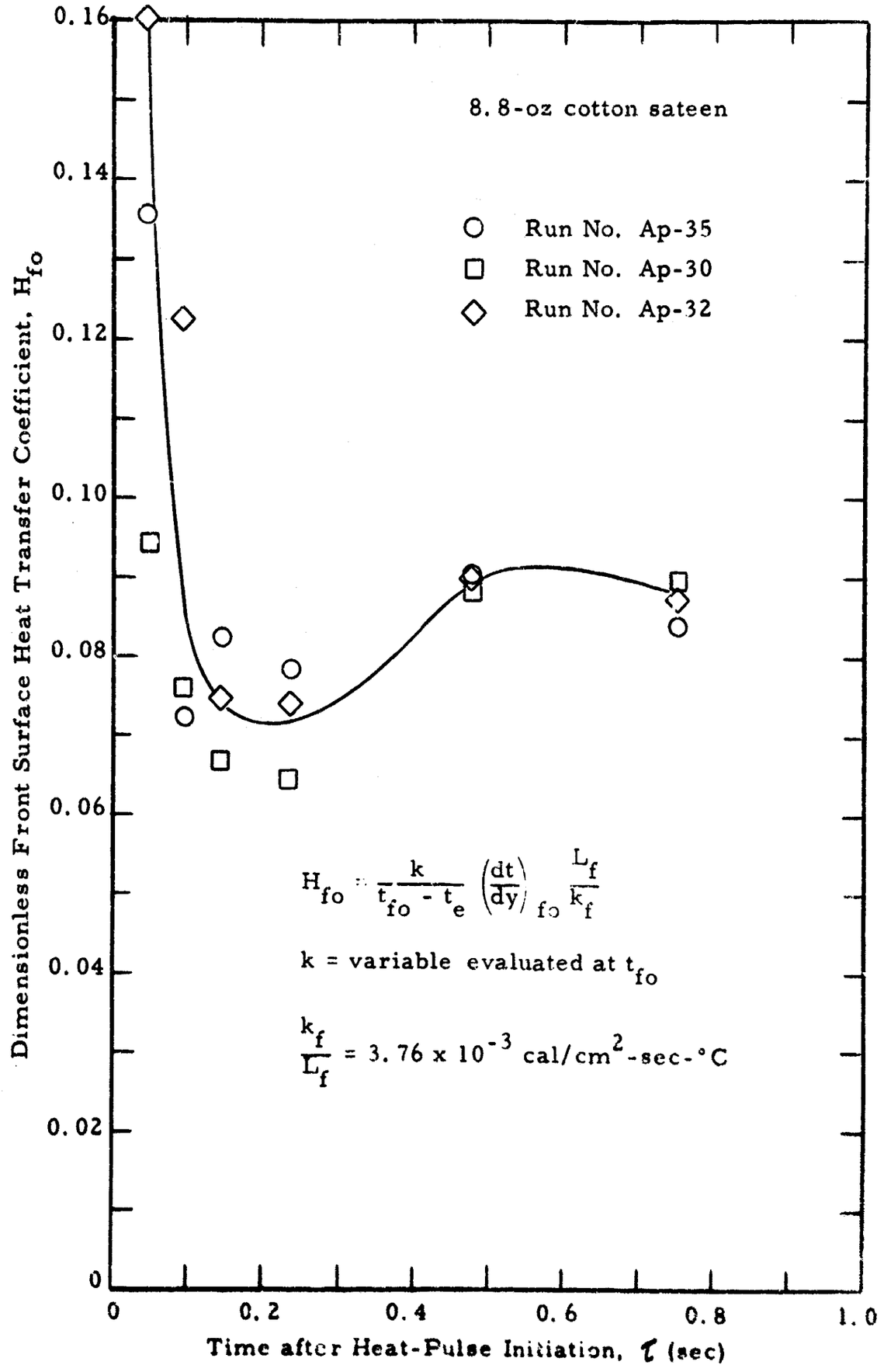

Figure 45. Variation of Front Surface Convective Heat Transfer Coefficient (Biot Number) with Time (k evaluated at t_{fo})

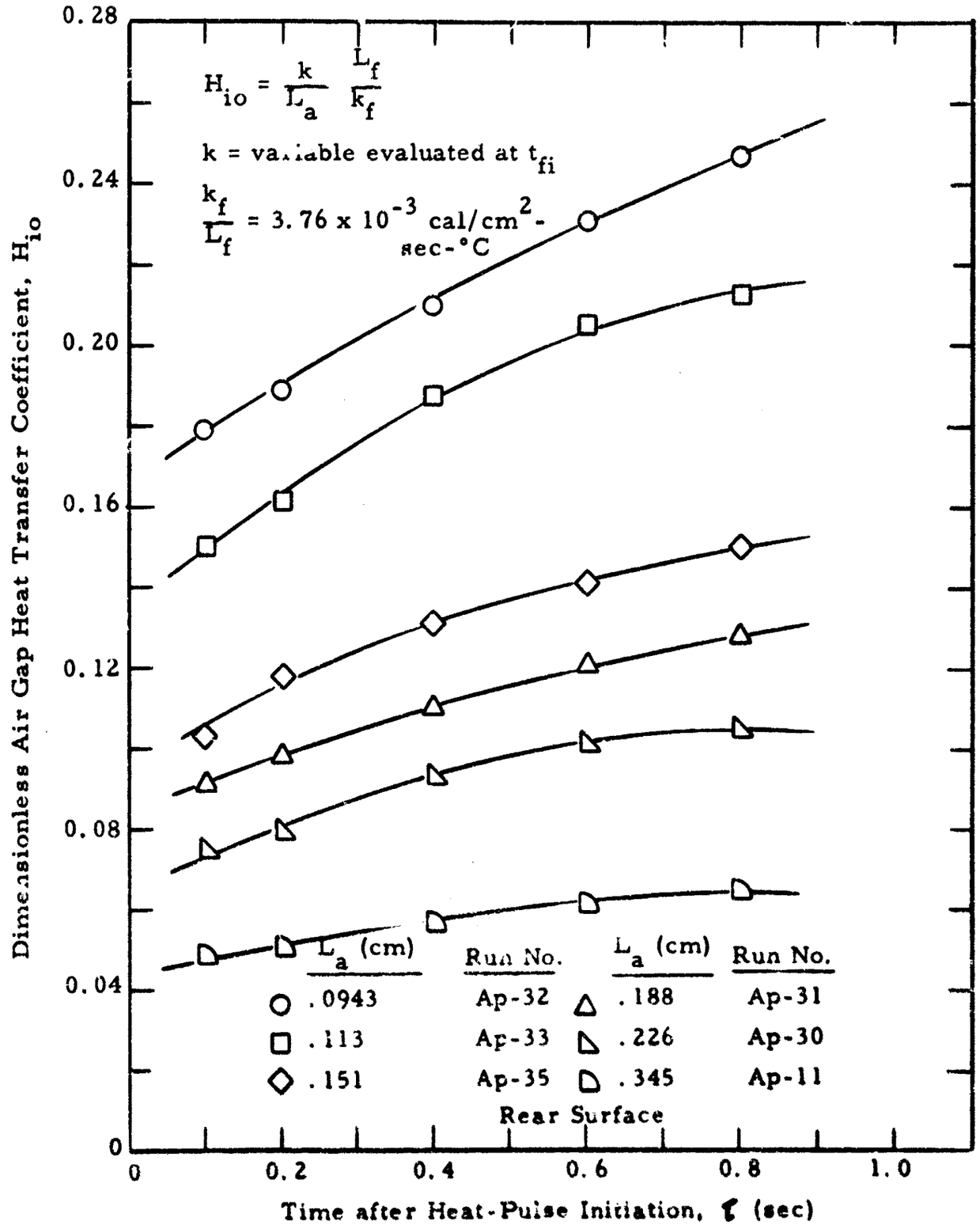

Figure 46. Variation of Rear Surface Convective Heat Transfer Coefficient (Biot Number) with Time

References 30 and 31 (Case IV). A limited parameter study (Case V) is also presented to show the effects of variation of the various heat transfer coefficients.

To our knowledge, no experimental verification has existed previously pertaining to the fabric response. For instance, in the study reported in Reference 4, complete attention was shown to the skin simulant response due to lack of an accurate method of measuring fabric surface temperatures. The interferometric techniques described herein have allowed measurement of the fabric response. For this reason, major emphasis is shown to the fabric behavior and a skin simulant is only needed to properly fix the rear surface heat losses.

Presented in Figure 47 are experimental results for fabric-skin simulant responses at ambient and dry moisture conditions. Particular care was exercised in conditioning the fabrics for these tests. Shown also for comparison are theoretical predictions for our particular test conditions (refer to Appendix A for details of the theoretical calculations).

Results for both test conditions fall below the theoretical predictions for the fabric response with reasonable agreement between theory and experiment. A similar agreement exists for the skin simulant response, with the experimental data being above the theoretical curve. The experimental data tend to level off as the ignition point is approached, while the theoretical predictions, which are based on inert behavior, keep on increasing.

These results indicate that additional modifications are needed in the present mathematical model. Further, other effects which cannot be identified at this time, tend to mask deviations in fabric response caused by moisture content. Additional experiments at various heating rates, fabric moisture content, and fabric-skin simulant spacings, are required to properly describe the observed behavior.

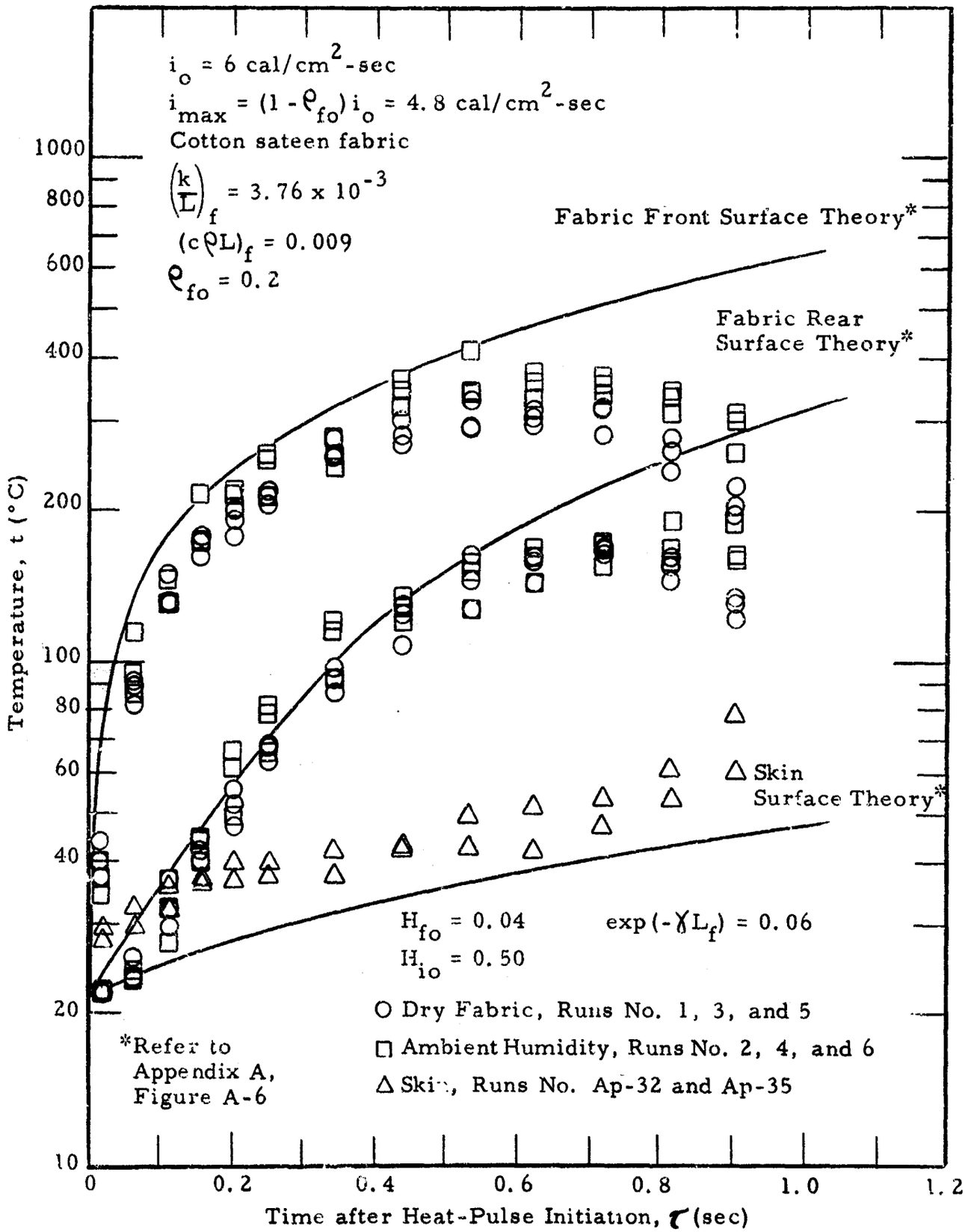

Figure 47. Temperature-Time Variations for Heated Fabric-Skin Model

4. SUMMARY AND CONCLUSIONS

The general objective of the study reported herein was to determine the physical properties required in a new material that could be used as a clothing fabric for protection against intense thermal radiation. To accomplish this objective, a five-year research program was planned. A curtailment of funds, however, terminated the program after three years of research efforts. This Final Report summarizes findings reported in the first two Annual Reports, and includes a detailed description of the third year's efforts.

A combined theoretical and experimental approach was followed to allow attainment of the program objectives. The studies that have been carried out have isolated many of the salient features of the behavior of a fabric-airspace-skin system when exposed to intense thermal radiation. During this program the following tasks were accomplished:

4.1 Theoretical Studies

1) An extensive and critical review of previous theoretical and experimental studies reported in the literature was undertaken. This study was continued during the second and third years of the program.

2) To obtain a basic insight into the heat flow processes involved, a simplified mathematical model was chosen and the heat flow equations were solved using an explicit finite difference technique. This procedure was programmed for solution on a Control Data G-15D digital computer. Considered in the analysis are a time-dependent heat input, fabric diathermancy, and non-linear radiation and convection boundary conditions.

3) Portions of the computer program were examined by comparing our results with those existing in the literature. Included in the calculations are the temperature-time responses of opaque and diathermanous fabric-skin systems irradiated by a constant heat pulse, a flat plate radiating to a heat sink environment, and a flat plate irradiated by a time-dependent heat pulse.

In addition, calculations were performed for an opaque fabric-skin system exposed to a constant heat input assuming various values of the heat transfer coefficients. Envelopes showing the limits of these responses for order of magnitude changes of the heat transfer coefficients were obtained.

4) A critical examination was made of the flash technique as a means of measuring thermal properties of materials. We extended this method, as originally developed at NRDL, for application to diathermanous materials such as fabrics. In addition, the theory was improved to allow consideration of radiative and/or convective front surface heat losses.

4.2 Experimental Studies

1) Interferometer techniques were perfected for study of fabric materials exposed to high intensity thermal radiation. Combined with high speed photographic methods, these techniques allow both qualitative and quantitative measurements during the initial phases of heating, as degradation processes were initiated, and when combustion occurred.

2) Interferometric temperature measurements at the fabric surfaces, in the air gap, and at the skin simulant surfaces, were obtained for various fabric-skin spacings, fabric water content, and fabric types. Radiant energy pulses from an arc-image furnace provided constant intensity heat loadings up to 7 cal/cm^2 sec.

3) The temperature data were utilized to calculate fabric front surface and air gap convective heat transfer coefficients. Instantaneous values of these coefficients during the heating phases were calculated, allowing determination of the effects of transient flow conditions. The experimentally obtained temperature-time data for the fabric-skin systems were further utilized in preliminary comparisons of the theoretically predicted values.

4) Multi-environment and multi-wave length interferometer techniques were studied and utilized as methods of detecting the release and determining the concentrations of fabric degradation products. Comprehensive heating tests on dry and oil wetted cotton and wool

fabrics in separate inert gas environments of helium, nitrogen, argon and CO_2 allowed separation of temperature and water vapor concentration at fabric front and rear surfaces. To conduct these tests a special fabric test chamber was designed and fabricated which provided a controlled environment and made possible the optical observation of fabric samples while exposed to radiation from the arc-image furnace.

5) The flash discharge technique, originally developed at NRDL, was perfected in our laboratories. Measurements of thermal diffusivity were made initially on opaque electrically-conducting samples. The studies were then extended to include opaque non-conductors and finally, diathermanous materials.

As a result of the theoretical and experimental investigations, the following conclusions have been reached:

1) Information obtained during our studies indicate that separation of the inert behavior of an "ideal" fabric from the true behavior of an actual fabric is not realistic. A coupling of the semi-ideal response of a dry fabric during the early phases of heating with the actual performance of a real fabric during degradation and eventual combustion must be accomplished. Only then will a true understanding of the behavior of a clothing fabric under field conditions be possible.

2) Studies of the heat flow processes in a fabric-airspace-skin system irradiated by an intense source, indicated the usefulness of the Mach-Zehnder interferometer in providing experimental data previously unobtainable. We are able to gain information pertaining to the fabric surface temperatures, free convection flow processes at the fabric surfaces and in the air gap, degradation phenomena, and a description of eventual combustion. From these measurements maximum temperature and critical energy levels of fabric systems can be determined. Thermal diffusion processes through multi-layer fabrics and the behavior and interaction of fabric types on heat flow can be assessed.

3) The multi-wavelength and multi-environment interferometric techniques show promise in identifying degradation products and determining concentrations.

Eventual perfection of techniques such as these will allow measurement of the mass diffusion and transfer processes and provide chemical effect evaluations.

4) Other techniques such as differential thermal analysis are needed to complement interferometric methods in providing additional information pertaining to exothermic and endothermic reactions which occur in fabrics during heating. Important also would be a study of reaction rates, both for steady-state conditions, and as a function of temperature changes with time. Further experimental efforts must be expended to provide a full description of the heat flow processes. Variations in heat loading, fabric type and configuration, conditions of moisture content and chemical addition, and ventilation effects and layer-spacing systems are a few of the desired experimental considerations.

5) The mathematical model should be improved to include consideration of exothermic and endothermic chemical effects and other real fabric behavior. Until this information is available, other improvements in the model are not feasible, as the chemical effects overpower the "ideal" behavior assumed in present analyses. The initiation of effective heat "sources" and "sinks" caused by chemical effects can be incorporated into the finite difference calculation algorithm.

Additional theoretical and experimental studies are required before a proper understanding of the complicated fabric heating processes is obtained. An integrated program combining the research efforts of specialists in physical chemistry, heat transfer, mathematical analysis, and instrumentation is required. The necessary experimental and theoretical techniques have now been sufficiently developed to allow reasonable expectation of success in the near future.

5. REFERENCES

1) General Mills, Inc. Electronics Division. Report 2409. Annual progress report on thermal-physical parameters of materials, by S. Steinberg, R. E. Larson and A. R. Kydd. Contract DA-19-129-QM-1998 (OI 6082) (July 12, 1963).

2) Litton Systems, Inc. Applied Science Division. Report no. 2598. Second annual progress report on thermal-physical parameters of materials, by R. E. Larson, et al. Contract DA-19-129-QM-1998 (OI 6082) (August 5, 1964).

3) Carslaw, H. S. and J. C. Jaeger. Conduction of heat in solids. Oxford, Clarendon Press, 1947.

4) Massachusetts Institute of Technology. Fuels Research Laboratory. Heat transfer to skin through thermally-irradiated cloth, by N. Y. Chen and W. P. Jensen. Contract Nonr 1841(37). Technical Report No. 6 (July 1958). AD 200, 210.

5) McAdams, W. H. Heat transmission. 3rd ed. N. Y., McGraw-Hill, 1954.

6) -----. Transient heat and moisture transfer to skin through thermally-irradiated cloth, by H. C. Hottel, et al. Contract DA-19-129-QM-1592. Technical Report No. 8 (Dec. 26, 1961).

7) Armour Research Foundation. Investigation of means and materials to combat thermal radiation flash burns, by A. Goldsmith, A. N. Takata and I. B. Fieldhouse. Contract DA-19-129-QM-187. Final Report (Jan. 1957).

8) Little, Arthur D , Inc. Development of a means of neutralize intense thermal radiation. Contract DA-19-129-QM-1087. Final Report (Oct. 1960). AD 255, 690.

9) Eckert, E. R. G. and E. Soehngen. Interferometric studies on stability transition to turbulence of free convection boundary layer. In Institution of Mechanical Engineers. Proceedings of the general discussion on heat transfer, Sept. 11-13, 1951.

10) Kennard, R. B. An optical method for measuring temperature distribution and convective heat transfer. J. Res. Nat. Bur. Std. 8: 787-805 (1932).

11) Carlson, W. D. Interferometric studies of convective flow phenomena in vertical, plane enclosed air layers. Ph. D. Thesis, University of Minnesota (1956).

12) Goldstein, R. J. Interferometric study of the steady state and transient free convection thermal boundary layers in air and in water about a uniformly heated vertical flat plate. Ph.D. Thesis, University of Minnesota (March 1959).

13) Novotny, J. L. Interferometric study of laminar convection in a vertical parallel plate channel with uniform heat sources in the fluid. Ph.D. Thesis, University of Minnesota (1963).

14) Bevans, J. T. Vertical free convection from an isothermal surface. Ind. Eng. & Chem. 49, 1: 114-19 (Jan. 1957).

15) Azami, B. Ali. Determination of the temperature distribution in a water film adhering to a vertical heated surface and the local heat transfer coefficient. Ph.D. Thesis, University of Minnesota (1956).

16) McLean, E. A., V. E. Scherrer, C. A. Nanney and C. E. Fancuff. Interferometer used to study transient heating of water. The Rev. Sci. Inst. 29, 3: 225-28 (1958).

17) Schneider, B. M. E. Interferometer study of effects of mass addition by transpiration on heat transfer from a vertical plate in free convection. M.S. Thesis, Air Force Institute of Technology, Air University (June 1961).

18) Canada. Defense Research Medical Laboratories. Report no. 123-5. Temperature measurement of textile fabrics under intense thermal irradiation, by L. E. MacHattie (Oct. 1961).

19) Harris, M. Handbook of textile fibers. Harris Research Laboratories, Inc., Washington, D. C. (1954).

20) Eckert, E. R. G. and R M. Drake. Heat and mass transfer. 2nd ed. N. Y., McGraw-Hill, 1959.

21) Eckert, E. R. G. and W. O Carlson. Natural convection in an air layer enclosed between two vertical plates with different temperatures. Intern. J. Heat Mass Transfer 2: 106-20 (1961).

22) Bodoia, J R. and J. F. Osterle. The development of free convection between heated vertical plates. ASME Trans. 84C: 40-44 (1962).

23) Lu, Pau-Chang. Combined free and forced-convection heat-generating laminar flow inside vertical pipes with circular sector cross sections. ASME Trans 82C: 227-32 (1960).

24) National Advisory Committee for Aeronautics. Technical Note 3141. Combined natural- and forced-convection laminar flow and heat transfer of fluids with and without heat sources in channels with linearly varying wall temperatures, by S. Ostrach (1954).

25) -----. Technical Note 3458. Unstable convection in vertical channels with heating from below, including effects of heat sources and frictional heating, by S. Ostrach (1955).

26) Sparrow, E. M. and J. L. Gregg. Nearly quasi-steady free convection heat transfer in gases. ASME Trans. 82C: 268-60 (1960).

27) Goldstein, R. J. and E. R. G. Eckert. The steady state and transient free convection boundary layer on a uniformly heated vertical plane. Intern. J. Heat Mass Transfer 1: 208-18 (1960).

28) Siegel, R. Transient free convection from a vertical flat plate. ASME Trans 80: 347-59 (1958).

29) Fairall, R. S., R. A. Wells and R. L. Belcher. Unsteady-state heat transfer in solids with radiation at one boundary. ASME Transactions 84C: 266-67 (1962).

30) Technical Operations, Inc. Report No. 58-7. Transient effects of a time varying thermal pulse Part II, by J. F. Bratter. Contract DA-29-044-XZ-587 (March 1958). AD 158,776.

31) Massachusetts Institute of Technology. Temperature response of six plates exposed to radiant heat pulses, by J. C Soria and L. Schmidt. Contract AF 33(616)-3259 (July 25, 1956), WADC Technical Report 56-149. AD 97,295.

APPENDIX A

HEAT TRANSFER ANALYSIS OF A FABRIC-SKIN SYSTEM IRRADIATED BY A TIME DEPENDENT HEAT PULSE

I. SELECTION OF COMPUTATION METHOD

The heat flow equation and boundary conditions describing the fabric-skin heat transfer processes as presented in Section 2.3 are as follows:

A. Heat Flow Equations in Fabric and Skin

1. Fabric

$$(\rho c)_f \frac{\partial t}{\partial \tau} = k_f \frac{\partial^2 t}{\partial x^2} - i \frac{\partial}{\partial x} \left[\exp(-\gamma x)\right] \qquad (A-1)$$

2. Skin

$$(\rho c)_s \frac{\partial t}{\partial \tau} = k_s \frac{\partial^2 t}{\partial x^2} \qquad (A-2)$$

B. Boundary Conditions

1. At the Outer Surface of the Fabric

$$k_f \frac{\partial t}{\partial x}\Bigg]_{x_f = 0} - h_{fo}(t_{fo} - t_e) - \epsilon_{fo}\,\sigma\,(t_{fo}^4 - t_e^4) + iD = 0 \qquad (A-3)$$

2. At the Inner Surface of the Fabric

$$k_f \frac{\partial t}{\partial x}\Bigg]_{x_f = L_f} + h_{a_{eff}}(t_{fi} - t_{so}) + F_{f-s}\,\sigma\,(t_{fi}^4 - t_{so}^4) = 0 \qquad (A-4)$$

3. At the Skin Layer

$$k_s \frac{\partial t}{\partial x}\Bigg]_{x_s = 0} + h_{a_{eff}}(t_{fi} - t_{so}) + F_{f-s}\,\sigma(t_{fi}^4 - t_{so}^4) + i\alpha_{so}\exp(-\gamma L_f) = 0 \qquad (A-5)$$

The system of equations and boundary conditions under present consideration is not subject to exact solution by known analytic techniques. If the problem is attacked in its most general form, the combination of nonlinear boundary conditions and temperature-dependent physical properties is sufficient to force the use of numerical methods. When an analytical solution of the heat-flow equation is possible, temperature can be expressed as a continuous function of the time and space variables. In a numerical solution, the differential representation is replaced by a discrete or finite representation. A method of spatial subdivision is chosen, and temperatures are calculated only for certain pre-selected points that are assumed to be representative of the region, including the point. In a transient heat-flow problem proper subdivisions must also be made in the time variable.

Over the years, various computation systems have been developed for numerical analysis of transient heat-flow problems. In three of these methods, the partial differential equations, and the boundary and initial conditions are replaced totally or partially by difference representation of space and time variables. In one method, the partial differential equations are replaced by a system of equations with a difference representation of the space variable, while the time variable remains in differential form.[1] The other two methods utilize difference representations of both the space and time variables. The first of these, the explicit method, allows calculation of the temperature at a future time on the basis of temperatures and heat inputs or heat generation existing during the present time increment.

The finite difference form of Equation (A-2) can be obtained by performing a heat balance on an internal element, as shown in Figure A-1. The net heat transferred to an element can be equated to the change of elemental heat content. In a solid, the heat added to a body is equal to its increase in enthalpy, which for a constant specific heat can be expressed as a product of specific heat and temperature change. For internal points in the system, the primary mechanism

of heat transfer to and from the element is by conduction, except when the material is diathermanous, and the temperatures are high enough to cause interelement radiation interchange. If heat is being generated in the element due to chemical reaction or diathermancy, an additional term must be included in the calculation. For the case of conduction heat transfer only and no heat generation,

$$k \frac{(t_{j-1}^{n} - t_{j}^{n})}{\Delta x} + k \frac{(t_{j+1}^{n} - t_{j}^{n})}{\Delta x} = c \rho \frac{\Delta x}{\Delta \tau} (t_{j}^{n+1} - t_{j}^{n}) \qquad \text{(A-6)}$$

where Δx and $\Delta \tau$ are increments of the space and time variables and the set of points in the x, τ plane are given by $x = j\Delta x$ and $\tau = n\Delta\tau$. Rearranging slightly,

$$t_{j-1}^{n} - 2 t_{j}^{n} + t_{j+1}^{n} = \left(\frac{c \rho}{k}\right) \frac{\Delta x^2}{\Delta \tau} (t_{j}^{n+1} - t_{j}^{n}) \qquad \text{(A-7)}$$

Equation (A-7) is an explicit representation of Equation (A-2) using forward time differences; i.e., the temperatures at the beginning of the time increment $\Delta\tau$ are used to calculate the temperature at the end of the time increment. The second, or implicit method, includes consideration of conditions at the end of the time increment. Expressing Equation (A-2) in an implicit form utilizing backward time differences we obtain

$$t_{j-1}^{n+1} - 2t_{j}^{n+1} + t_{j+1}^{n+1} = \left(\frac{c \rho}{k}\right) \frac{\Delta x^2}{\Delta \tau} (t_{j}^{n+1} - t_{j}^{n}), \qquad \text{(A-8)}$$

which is similar in form to Equation (A-7), except that the second derivative in space is taken at the end of the time increment. Application of this method requires solution of a set of simultaneous equations at each step in time.

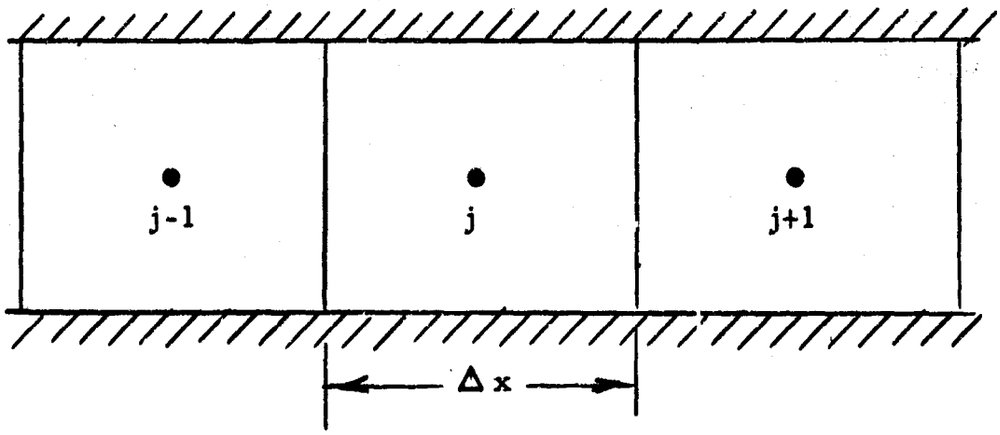

a) Internal Element

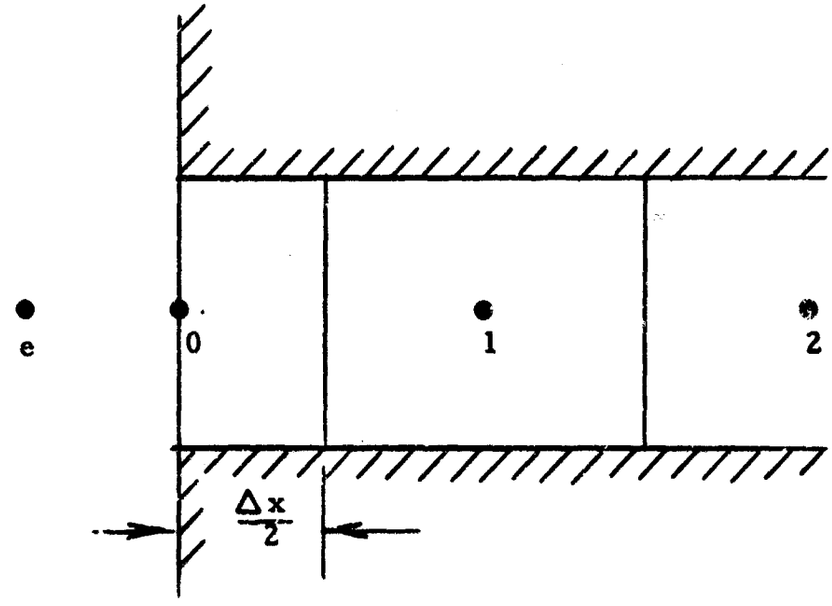

b) Boundary Subdivision

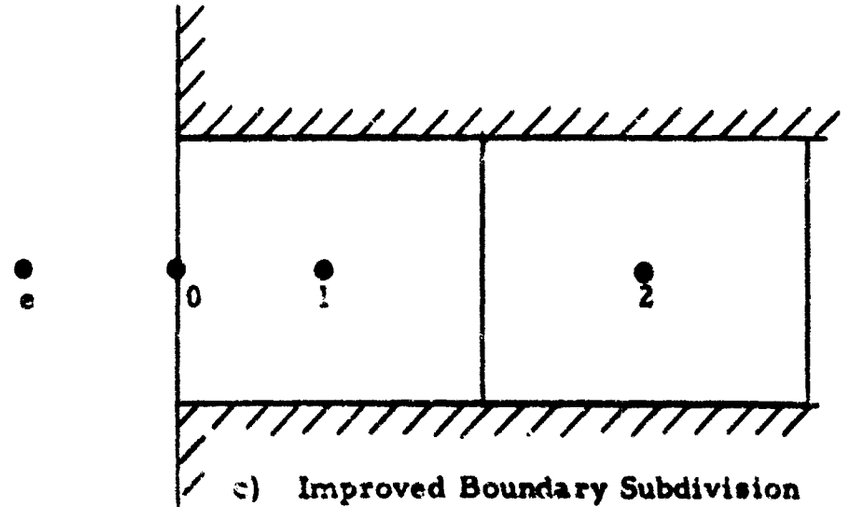

c) Improved Boundary Subdivision

Figure A-1. Finite Difference Subdivisions

Considering further the explicit finite difference method and solving for t_j^{n+1} in Equation (A-7), one obtains

$$t_j^{n+1} = \frac{t_{j-1}^n + t_{j+1}^n - 2t_j^n + Mt_j^n}{M} \qquad \text{(A-9)}$$

where

$$M = \left(\frac{c\rho}{k}\right) \frac{\Delta x^2}{\Delta \tau} \quad , \qquad \text{(A-10)}$$

a dimensionless modulus. If a value of 2 is chosen for the modulus M, the temperature of the element at the end of the time increment $\Delta\tau$ is simply the average of the previous temperatures of the adjoining elements. The calculation can then be carried out graphically using the familiar Binder-Schmidt method.[2] Nessi and Nissole[3] discussed the use of other moduli, and Dusinberre[4] presented a graphical construction for M = 4. Paul[5] showed how the method could be generalized even further for other moduli.

It is known that implicit analogs are stable for all division of space and time while the semi-discrete analog is stable for all divisions of the space increment and allows the use of continuous or analog time computers for certain heat flow problems.[1] Explicit calculations, however, are subject to several restrictions to insure stability. The stability condition is defined as

$$\left(\frac{c\rho}{k}\right) \frac{\Delta x^2}{\Delta \tau} \geq 2 \quad .$$

If stability restrictions are not observed, large undamped fluctuations can sometimes appear in the solution that make the calculation worthless. Calculations are usually made with a finite net size; if the calculation system is unstable, the symptoms appear early. The stability condition equation indicates that making the space divisions small without also decreasing the time increment could cause instability problems.

At the boundary, an additional restriction can be placed on M, depending on the method of subdivision. If convective heat transfer is occurring at the surface and a division like that in Figure A-1b is used, the heat balance is

$$k\frac{(t_1 - t_o)}{\Delta x} - h(t_o - t_e) = c\rho \frac{\Delta x}{2\Delta\tau}(t_o' - t_o) \quad . \qquad \text{(A-11)}$$

To simplify the notation, the temperature at the end of the time increment is designated by a prime and the unprimed values represent temperatures at the beginning of the increment. Solving for t_o', one obtains

$$t_o' = \frac{2Bi\, t_e + 2t_1 + t_o (M - 2Bi - 2)}{M} \qquad \text{(A-12)}$$

where the Biot number Bi, is defined as $\frac{h\Delta x}{k}$. Equation (A-12) introduces the requirement that $M \geq (2Bi + 2)$. If this requirement is not met (according to Dusinberre[4]), an absurd physical situation develops, namely, the warmer region 0 is, the colder it will be after the time interval $\Delta\tau$.

The above limitiation can be circumvented if a subdivision suggested by Dusinberre[4] and shown in Figure A-1c is used. As no heat capacity is associated with point 0, the surface temperature is calculated using a steady state relationship, or,

$$2k\frac{(t_1 - t_o)}{\Delta x} - h(t_o - t_e) = 0 \qquad \text{(A-13)}$$

and

$$t_o = \frac{t_e + 2t_1/Bi}{1 + 2/Bi} \qquad \text{(A-14)}$$

This t_o is then used to calculate the transient t_1 after the time increment $\Delta\tau$.

Thought must be given not only to stability considerations but also to other errors which can arise. Truncation error arises because the difference representation differs from the original problem, a fact which places the mathematical burden on the user, who must prove that the solution of the difference equation converges to that of the differential equation as the space and time increments are refined. Round off error appears because the difference equation is not solved exactly, the computation being accomplished with numbers of finite length. Rounding errors are not usually of much consequence. If stable equations are used, the rounding errors are not amplified with time and accumulate roughly as the square root of the number of calculation steps.[6]

Analytical formulation of stability criteria and truncation error estimates for a finite difference approximation of the heat flow equation depend upon the particular computing algorithm used. If an analytical solution is available or if experimental data are taken in such a way as to satisfy all requirements of the original equations, a good insight into these errors can be obtained. If sufficient computer time is available, the rate of convergence of the finite difference approximation to the "true" solution can be studied by refining the calculation net. System instability can easily be seen by examination of the temperature-time curves. The major danger in consideration of the appropriateness of the finite difference approximation is to assume that refinement of the calculation mesh is a sufficient condition to insure accuracy of solution. Even though the exact solution closely approaches the difference results as the space and time increments are refined, it is possible that the exact solution of the difference equations can depart considerably from the true solution of the initial value problem.[6]

The choice of whether to use an explicit or implicit method of calculation depends mainly on the problem to be solved and the availability of high-speed computers. Very often stability requirements

imposed on explicit methods dictate that an excessive number of time and space increments must be used to provide a meaningful solution. Then hand calculations become impossible and even machine computation time must be considered. It is then possible that an implicit scheme could be utilized with more efficiency. In many cases the advantage of fewer increments in time and space because of less rigid stability requirements overrides the disadvantage of more complex calculations at each time increment.

In the results reported in Reference 7, a graphical explicit finite difference technique was emphasized, and the results so obtained were in good agreement with the experiments. Our initial requirements were also satisfied by an explicit technique designed for computer solution, but it is felt that an implicit technique would allow easier handling of temperature-dependent properties by relaxing the stability restrictions. The details of transforming the heat flow equations into an explicit finite difference form are presented as follows.

II. EXPLICIT FINITE DIFFERENCE EQUATIONS

A. Development of Equations

To uncover the important parameters describing the fabric-skin heat transfer situation, and to obtain an insight into the salient features of finte-difference techniques, a simplified explicit finite-difference procedure was chosen for our initial studies. The stability restrictions imposed on this method tend to counterbalance its main virtue of simplicity by requiring an excessively large number of calculation steps with small time increments. The stability of such a technique, for conditions of variable properties, is also open to question. For the above reasons, it is felt that an implicit procedure would be more suitable for future studies. However, the insight obtained into the relative importance of the various parameters and heat transfer boundary conditions more than compensate for the effort expended.

For the present problem the boundary subdivision shown in Figure A-2 is used. In addition to convection at the surface 0, radiant input and reradiation as a function of surface temperature are considered. In addition, a moderate amount of fabric diathermancy is assumed. The radiation absorbed by element 1 is assumed to be released as heat at the surface 0 and is included in the heat balance. For the other elements the absorbed radiation is assumed to be released at their centers.

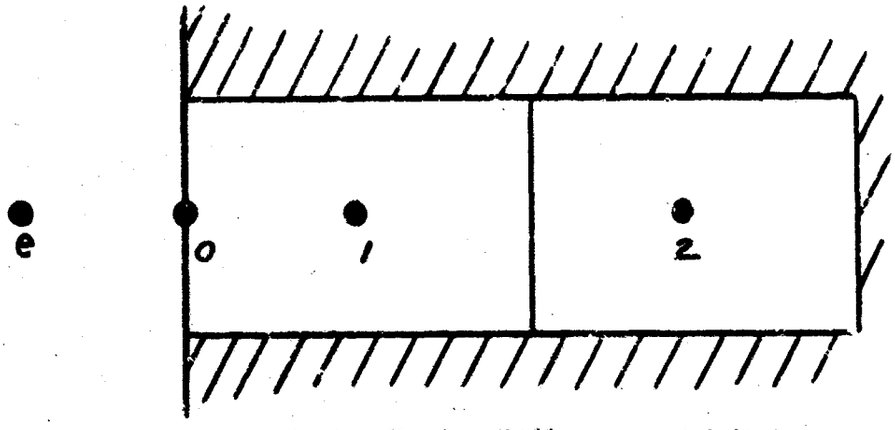

Figure A-2. Finite Difference Subdivisions

In the revised Schmidt graphical method,[2] a half slice having no heat capacity is added outside the surface. The temperature at the outer surface of this element is obtained graphically as a function of surface and environmental temperatures. This procedure is discussed in detail in References 2 and 7 and will not be presented here. This concept allows a simple graphic determination of the transient temperatures of element 1, as a function of the fictional element surface temperature and element 2 temperature, using the familiar Schmidt representation. The accuracy of this method is compromised somewhat because in the calculation of t_1' the fictional element is assumed to possess the thermal properties of the real system. This assumption enters implicitly when Equation (A-9) is used to calculate t_1'. In addition, the initial surface temperature is assumed equal to the environmental temperature, which is not completely compatible with the other assumptions made. A steady state heat balance is made at the surface, which has no heat capacity, and which should immediately sense any heat transfer and react instantaneously.

The method used in Reference 7 is essentially as discussed above, except that the initial surface temperature is allowed to seek a value different from the environmental value, which tends to counterbalance the error arising in the calculation of t_1', using the Schmidt equation.

With a modulus of 2, it can be shown that the equations for the surface temperature and transient temperatures for element 1 derived herein are equivalent to those presented in Reference 7, although some of the assumptions and internal details of the developments differ slightly. The method presented herein is not intended for graphical solution and allows the use of moduli other then 2.

The heat balance at the outer surface becomes (see Figure A-3)

$$2k_f \frac{(t_1 - t_o)_f}{\Delta x_f} - h_{fo}(t_{fo} - t_e) - \epsilon_{fo}\sigma(t_{fo}^4 - t_e^4) + i\left[1 - \left(\exp(-\beta \Delta x_f)\right)\right] = 0 \qquad \text{(A-15)}$$

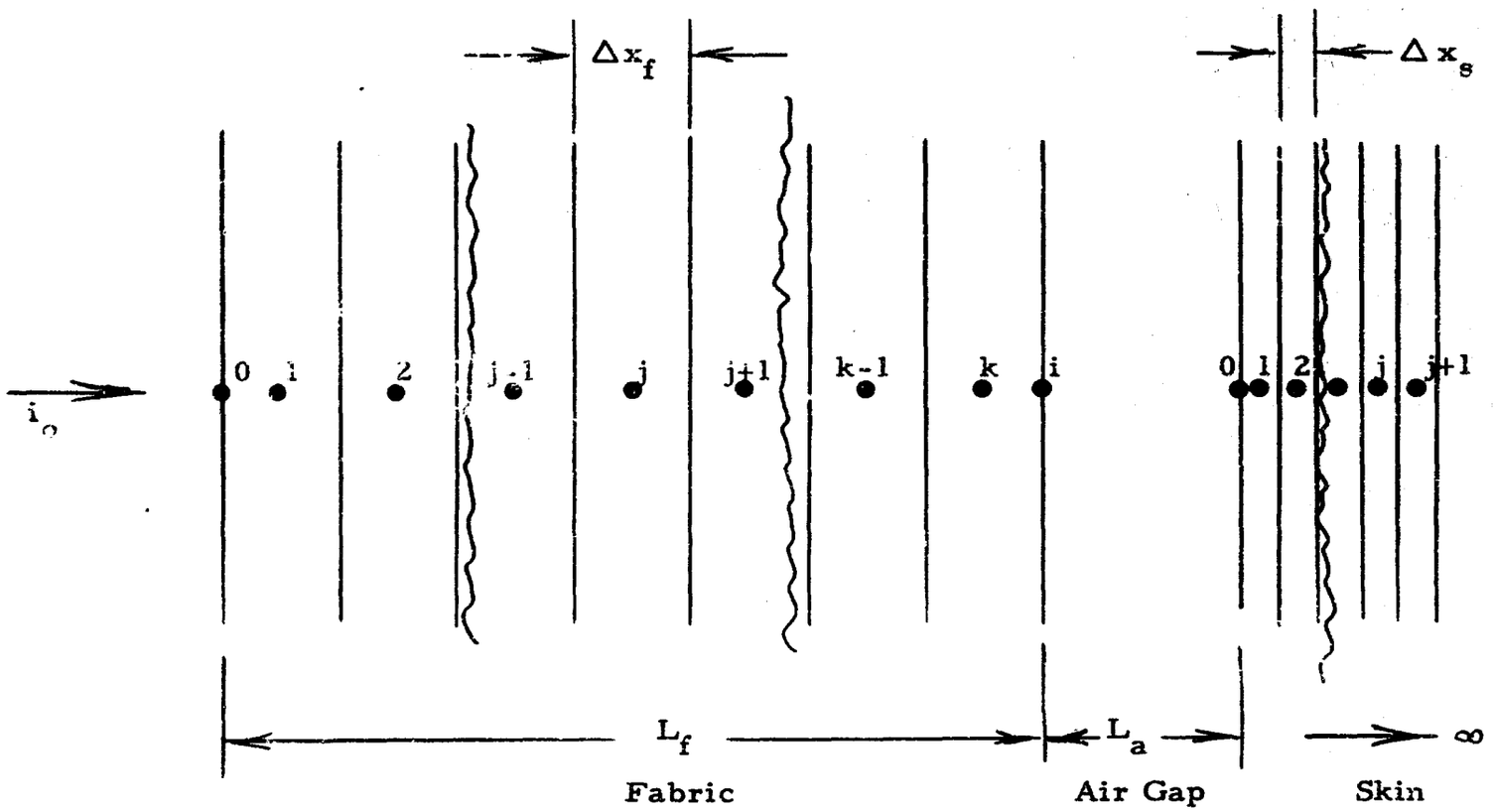

Figure A-3. Fabric-Air Gap-Skin System

which is the finite difference form of Equation (A-3). The finite difference form of Equation (A-1) for element 1 is

$$2k_f \frac{(t_o - t_1)_f}{\Delta x_f} + k_f \frac{(t_2 - t_1)_f}{\Delta x_f} = (c\rho)_f \left[\frac{\Delta x}{\Delta \tau}\right]_f (t_1' - t_1)_f \quad . \tag{A-16}$$

For element 2 and all others in the fabric the diathermancy term is included. For all elements except the rear element the general or jth term is

$$k_f \frac{(t_{j-1} - t_j)_f}{\Delta x_f} + k_f \frac{(t_{j+1} - t_j)_f}{\Delta x_f} + i \exp\left[-(j-1)\gamma\Delta x_f\right]\left[1-\exp(-\gamma\Delta x_f)\right]$$

$$= (c\rho)_f \left[\frac{\Delta x}{\Delta \tau}\right]_f (t_j' - t_j)_f \quad . \tag{A-17}$$

The last or kth element equation is of the form of Equation (A-17) except that the first term is multiplied by 2, as in Equation (A-16), because of the half increment distance used in the subdivision:

$$2k_f \frac{(t_i - t_k)_f}{\Delta x_f} + k_f \frac{(t_{k-1} - t_k)_f}{\Delta x_f} + i \exp\left[-(k-1)\gamma\Delta x_f\right]\left[1-\exp(-\gamma\Delta x_f)\right]$$

$$= (c\rho)_f \left[\frac{\Delta x}{\Delta \tau}\right]_f (t_k' - t_k)_f \quad . \tag{A-18}$$

The heat balance at the inner surface of the fabric, Equation (A-18), in finite difference form is

$$2k_f \frac{(t_i - t_k)_f}{\Delta x_f} + h_{a_{eff}} (t_{fi} - t_{so}) + F_{f-s}\,\sigma (t_{fi}^4 - t_{so}^4) = 0 \tag{A-19}$$

where the radiation interchange term is calculated on the basis of parallel infinite flat plates radiating as grey bodies (refer to Table A. 1).

Table A.1 Dimensionless Groups

	Fabric	Skin
Distance	$X_f = \frac{x_f}{L_f}$	$X_s = \frac{x_s}{L_f}\frac{k_f}{k_s}$
Time	$\theta_f = (\frac{k}{c\rho})_f \frac{\tau_f}{L_f^2}$	$\theta_s = (\frac{k}{c\rho})_s \frac{\tau_s}{L_f^2}\left[\frac{k_f}{k_s}\right]^2$
Temperature	$T_f = \frac{k_f t_f}{i_{max} L_f}$	$T_s = \frac{k_f t_s}{i_{max} L_f}$
Modulus	$M_f = (\frac{c\rho}{k})_f (\frac{\Delta x_f}{\Delta \tau_f})^2 = \frac{\Delta X_f^2}{\Delta \theta_f}$	$M_s = (\frac{c\rho}{k})_s (\frac{\Delta x_s}{\Delta \tau_f})^2 = \frac{\Delta X_s^2}{\Delta \theta_s}$
Radiation coefficient for front surface of fabric	$R_{fo} = \frac{\sigma \epsilon_{fo} i_{max}^3 L_f^4}{k_f^4}$	
Radiation interchange coefficient between fabric and skin	$R_{io} = \sigma F_{f-s} \frac{i_{max}^3 L_f^4}{k_f^4}$, where $F_{f-s} = \frac{1}{1/\epsilon_{fi} + 1/\epsilon_{so} - 1}$	
Heat transfer coefficient for front surface of fabric	$H_{fo} = \frac{h_{fo} L_f}{k_f}$	
Heat transfer coefficient for air gap	$H_{io} = \frac{h_{a_{eff}} L_f}{k_f}$	
Radiation input into system	$I = \frac{i}{i_{max}}$, where $i = i_o (1 - \rho_{fo})$	

At the skin surface Equation (A-19) becomes

$$2k_s \frac{(t_1 - t_o)_s}{\Delta x_s} + h_{a_{eff}} (t_{fi} - t_{so}) + F_{f-s}\, \sigma (t_{fi}^4 - t_{so}^4) + i\alpha_{so} \exp(-\gamma L_f) = 0 \quad \text{(A-20)}$$

Because the skin is assumed to be opaque, all of the transmitted radiation is absorbed or reflected at the surface. For these calculations, the reflected part is neglected. The equation for the first skin element is

$$2k_s \frac{(t_o - t_1)}{\Delta x_s} + k_s \frac{(t_2 - t_1)_s}{\Delta x_s} = (c\rho)_s \left(\frac{\Delta x}{\Delta \tau}\right)_s (t_1' - t_1)_s \,. \quad \text{(A-21)}$$

The equations for all succeeding elements are of the form

$$k_s \frac{(t_{j-1} - t_j)_s}{\Delta x_s} + k_s \frac{(t_{j+1} - t_j)_s}{\Delta x_s} = (c\rho)_s \left(\frac{\Delta x}{\Delta \tau}\right)_s (t_j' - t_j)_s \,. \quad \text{(A-22)}$$

If the properties are allowed to vary with temperature, the finite difference calculations must be made with the above equations. If the properties are assumed constant, the solution can be made more general by nondimensionalizing the equations with a group of dimensionless parameters. Unfortunately, the diathermancy term γL_f remains explicitly in the equations. As shown in Section III, separate calculations also have to be made for various bomb yields when a time-dependent heat input from a nuclear energy release is considered. Introducing the dimensionless groups presented in Table A. 1, the equations for the fabric and skin become

1) Fabric outer surface

$$\frac{2(T_1 - T_o)_f}{\Delta X_f} - H_{fo}(T_{fo} - T_e) - R_{fo}(T_{fo}^4 - T_e^4) + I\left[1 - \exp(-\gamma \Delta X_f L_f)\right] = 0 \quad \text{(A-15a)}$$

2) First element of fabric

$$2(T_o - T_1)_f + (T_2 - T_1)_f = \frac{\Delta X_f^2}{\Delta \theta_f} (T_1' - T_1)_f \qquad \text{(A-16a)}$$

3) General fabric element

$$(T_{j-1} - T_j)_f + (T_{j+1} - T_j)_f + \Delta X_f \, I \exp\left[-(j-1)\gamma \Delta X_f L_f\right]\left[1-\exp(-\gamma \Delta X_f L_f)\right]$$

$$= \frac{\Delta X_f^2}{\Delta \theta_f} (T_j' - T_j)_f \qquad \text{(A-17a)}$$

4) Last fabric element

$$2(T_i - T_k)_f + (T_{k-1} - T_k)_f + \Delta X_f \, I \exp\left[-(k-1)\gamma \Delta X_f L_f\right]\left[1-\exp(-\gamma \Delta X_f L_f)\right]$$

$$= \frac{\Delta X_f^2}{\Delta \theta_f} (T_k' - T_k)_f \qquad \text{(A-18a)}$$

5) Fabric inner surface

$$\frac{2(T_i - T_k)_f}{\Delta X_f} + H_{io}(T_{fi} - T_{so}) + R_{io}(T_{fi}^4 - T_{so}^4) = 0 \qquad \text{(A-19a)}$$

6) Skin surface

$$\frac{2(T_1 - T_o)_s}{\Delta X_s} + H_{io}(T_{fi} - T_{so}) + R_{io}(T_{fi}^4 - T_{so}^4) + I\alpha_{so} \exp(-\gamma L_f) = 0 \qquad \text{(A-20a)}$$

7) First element of skin

$$2(T_o - T_1)_s + (T_2 - T_1)_s = \frac{\Delta X_s^2}{\Delta \theta_s} (T_1' - T_1)_s \qquad \text{(A-21a)}$$

8) General skin element

$$(T_{j-1} - T_j)_s + (T_{j+1} - T_j)_s + \frac{\Delta X_s^2}{\Delta \theta_s} (T_j' - T_j)_s \qquad \text{(A-22a)}$$

When the fabric is in good thermal contact with the skin, which is assumed to be opaque, any radiation transmitted through the fabric will be released as heat at the interface. The steady-state heat balance at the interface i is,

$$2k_f \frac{(t_k - t_i)_f}{\Delta x_f} + 2k_s \frac{(t_l - t_i)_s}{\Delta x_s} + i\alpha_{so} \exp(-\gamma L_f) = 0 \qquad \text{(A-23)}$$

It might be noted here that transmitted short-wavelength radiation reflected from the skin is again assumed negligible and is not considered in the fabric heat balances. The above equation in dimensionless form is

$$\frac{2(T_k - T_i)_f}{\Delta X_f} + \frac{2(T_l - T_i)_s}{\Delta X_s} + I\alpha_{so} \exp(-\gamma L_f) = 0 \qquad \text{(A-23a)}$$

For this configuration the above equation replaces Equations (A-19a) and (A-20a).

B. Solution of Equations

Equations (A-16a), (A-17a), (A-18a), (A-21a), and (A-22a) are in an explicit finite difference form. That is, the temperatures at the end of the time increment $\Delta\theta$ are based on conditions existing at the beginning of the time increment. The boundary conditions, as represented by Equations (A-15a), (A-19a), and (A-20a) are of a steady-state form. This comes about because of the particular method of boundary subdivision utilized. As shown in Figure A-1, no heat capacity is

associated with surface 0. Thus, the heat balance for this surface does not include consideration of a heat storage term, and the surface temperature is a function of the heat transfer occurring at the same instant in time.

Equations (A-15a), (A-19a), and (A-20a) being nonlinear were solved using the Newton-Raphson[8] method of determining roots. This is an iterative scheme which converges quite rapidly for our particular problem because of the smoothness of the temperature-time function. Equation (A-15a) involves only one variable, while Equations (A-19a) and (A-20a) must be solved simultaneously as the fabric and skin temperatures both appear in each equation. The Newton-Raphson method utilizes a recurrence formula of the type

$$x^{k+1} = x^{k} - \frac{f(x^{k})}{f'(x^{k})} \qquad \text{(A-24)}$$

to obtain a real solution of an equation of the form

$$f(x) = 0 \quad . \qquad \text{(A-25)}$$

Successive applications of this iteration result in a value of x which satisfies Equation (A-25). This method was applied to obtain a solution for Equation (A-15a).

The above method was also used to obtain solutions for the two simultaneous equations represented by Equations (A-19a) and (A-20a). These equations are of the form

$$f(x, y) = 0 \qquad \text{(A-26)}$$

$$g(x, y) = 0 \qquad \text{(A-27)}$$

If x^{k} and y^{k} represent initial values and x^{k+1} and y^{k+1} represent corrected values, these terms are related by the corrections m and n, or

$$x^{k+1} = x^k + m \tag{A-28}$$

$$y^{k+1} = y^k + n \tag{A-29}$$

These values are inserted in Equations (A-26) and (A-27) and expanded by Taylor's theorem for a function of two variables. Neglecting all non-linear terms, the resulting simultaneous equations can be solved by determinants to yield the corrections m and n.

$$m = \frac{\begin{vmatrix} -f(x^k, y^k) & \left(\frac{\partial f}{\partial y}\right)^k \\ -g(x^k, y^k) & \left(\frac{\partial g}{\partial y}\right)^k \end{vmatrix}}{J} \tag{A-30}$$

$$n = \frac{\begin{vmatrix} \left(\frac{\partial f}{\partial x}\right)^k & -f(x^k, y^k) \\ \left(\frac{\partial g}{\partial x}\right)^k & -g(x^k, y^k) \end{vmatrix}}{J} \tag{A-31}$$

where

$$J = \begin{vmatrix} \left(\frac{\partial f}{\partial x}\right)^k & \left(\frac{\partial f}{\partial y}\right)^k \\ \left(\frac{\partial g}{\partial x}\right)^k & \left(\frac{\partial g}{\partial y}\right)^k \end{vmatrix}. \tag{A-32}$$

Successive applications of Equations (A-30) and (A-31) result in values of x and y which satisfy Equations (A-26) and (A-27).

Applying Equation (A-24) to Equation (A-15a) and Equations (A-30) and (A-31) to Equations (A-19a) and (A-20a) and solving Equations (A-16a), (A-17a), (A-18a), (A-21a) and (A-22a) for temperature at the end of the time increment, the following system of equations results:

1) Fabric outer surface

$$T_{fo}^{k+1} = T_{fo}^{k} + \frac{2(T_1 - T_o^{k})_f - \Delta X_f \left\{ H_{fo} \left[T_o^{k} - T_1 \right]_1 + R_{fo} \left[(T_{fo}^{k})^4 - (T_e)^4 \right] - I \right\}}{2 + \Delta X_f \left[H_{fo} + 4R_{fo} (T_{fo}^{k})^3 \right]}$$

$$- \frac{\Delta X_f \left\{ I \exp(-\gamma \Delta X_f L_f) \right\}}{2 + \Delta X_f \left[H_{fo} + 4R_{fo} (T_{fo}^{k})^3 \right]} \qquad \text{(A-33)}$$

2) First element of fabric

$$T_{f1}' = T_{f1} + \frac{1}{M_f} 2 \left[T_o - 3 T_1 + T_2 \right]_f \qquad \text{(A-34)}$$

3) General fabric element

$$T_{fj}' = T_{fj} + \frac{1}{M_f} \left[T_{j-1} - 2 T_j + T_{j+1} \right]_f$$

$$+ \frac{1}{M_f} \left\{ \Delta X_f I \exp \left[-(j-1) \gamma \Delta X_f L_f \right] \left[1 - \exp(-\gamma \Delta X_f L_f) \right] \right\} \qquad \text{(A-35)}$$

4) Last fabric element

$$T_{fk}' = T_{fk} + \frac{1}{M_f} \left[T_{k-1} - 3 T_k + 2 T_i \right]$$

$$+ \frac{1}{M_f} \left\{ \Delta X_f I \exp \left[-(k-1) \gamma \Delta X_f L_f \right] \left[1 - \exp(-\gamma \Delta X_f L_f) \right] \right\} \qquad \text{(A-36)}$$

5) Interface boundary conditions

a) Fabric inner skin

$$T_{fi}^{k+1} = T_{fi}^{k} + \frac{-G_{T_{so}} F + F_{T_{so}} G}{J} \qquad \text{(A-37)}$$

b) Skin surface

$$T_{so}^{k+1} = T_{so}^{k} + \frac{G_{T_{fi}} F - F_{T_{fi}} G}{J} \qquad \text{(A-38)}$$

where

$$F = 2(T_i - T_k)_f + \Delta X_f \left[H_{io} (T_{fi} - T_{so}) + R_{io} (T_{fi}^4 - T_{so}^4) \right] \qquad \text{(A-39)}$$

$$G = 2(T_1 - T_o)_s + \Delta X_s \left[H_{io} (T_{fi} - T_{so}) + R_{io} (T_{fi}^4 - T_{so}^4) \right] + I\alpha_{so} \exp(-\gamma L_f) \qquad \text{(A-40)}$$

The subscript notations on the above functions represent partial derivatives with respect to the subscript, or

$$F_{T_{fi}} = \frac{\partial F}{\partial T_{fi}}, \quad F_{T_{so}} = \frac{\partial F}{\partial T_{so}}, \quad G_{T_{fi}} = \frac{\partial G}{\partial T_{fi}}, \text{ and } G_{T_{so}} = \frac{\partial G}{\partial T_{so}}$$

and

$$J = F_{T_{fi}} G_{T_{so}} - F_{T_{so}} G_{T_{fi}}$$

6) First element of skin

$$T_{s1}' = T_{s1} + \frac{1}{M_s}\left[2\,T_o - 3\,T_1 + T_2\right]_s \qquad \text{(A-41)}$$

7) General skin element

$$T_{sj}' = T_{sj} + \frac{1}{M_s}\left[T_{j-1} - 2\,T_j + T_{j+1}\right]_s \qquad \text{(A-42)}$$

The validity of the proposed model and system of equations presented herein can be determined only if experimental results obtained under equivalent conditions are available for comparison. The uncertainties regarding values of the heat transfer coefficients and temperature dependence of the thermal and optical properties remain yet to be resolved. For fabrics which have a low value of thermal conductivity, front surface degradation effects due to the high local temperatures can greatly change the optical properties. In our flash tube experiments on plastics, it was found that these effects did occur. These findings were substantiated by the theoretical predictions of Reference 9, which indicated a maximum front surface temperature of around 600 C.

A computer program utilizing the Daisy interpretive routines for the Control Data G-15 computer was written to obtain solutions for the system of finite difference equations represented by Equations (A-33) through (A-42). The program is entirely general and allows variation of all the nondimensional parameters presented in Table A.1 for any one calculation. In addition, the initial temperature conditions and environmental temperature can vary. However, for diathermanous calculations, the particular way in which the energy is assumed to be absorbed in depth restricts the calculation to opaque or only slightly diathermanous materials. The modification required to handle highly diathermanous materials is minor, but for the present this limitation will be observed.

A schematic of the program is shown as Figure A-4.

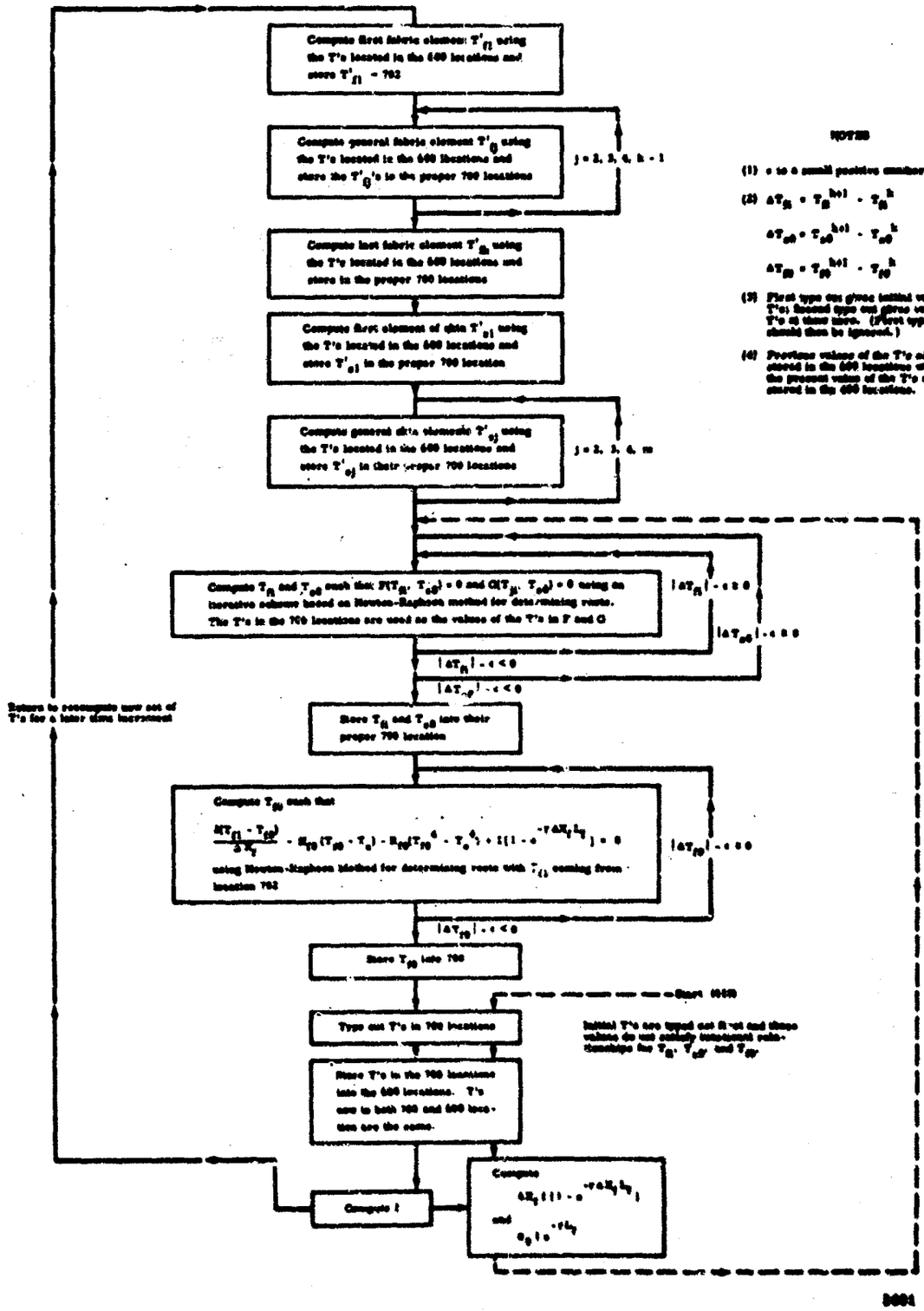

Figure A-4. Flow Diagram of Computer Program

III. COMPARISON OF PRESENT CALCULATION PROCEDURE WITH OTHER RESULTS

Although experimental data are limited, it was possible to check out various portions of our total computer program by comparison with other theoretical results available. In Reference 7, computer solutions were presented both for opaque fabric and diathermanous fabric-airspace-skin systems. In this study, the radiation and convection heat exchange coefficients were linearized into a single term and a square-wave radiation heat input term was assumed. The fabric was divided into six slices and the modulus M, defined as $\Delta X^2/\Delta\theta$, was the same in both the cloth and skin. As the actual time increments were also selected as being equal, the ΔX ratio of fabric to skin was found to be inversely proportional to the square root of the $k/c\rho$ ratio of skin to fabric. The same conditions were assumed to perform the following calculations.

A. Case I. Opaque Fabric-Airspace-Skin System

1. Initial Conditions

$$T_1 = T_2 = T_3 \ldots\ldots \text{etc.} = 0$$

$$T_e = 0$$

$$T_{fo} > 0$$

2. Values of Parameters

$$R_{fo} = F_{io} = 0$$

$$e^{-\gamma L_f} = 0$$

$$H_{fo} = 0.04$$

$$H_{io} = 0.50$$

$$I = 1$$

$$\Delta X_f = 1/6, \quad \Delta X_s = 1/30$$

$$M_f = M_s = 2, \quad \Delta\theta_f = \frac{\Delta X_f^2}{2} = 1/72$$

These calculations and equivalent points from the MIT calculations[7] are shown in Figure A-5 for comparison.

B. Case II. Diathermanous Fabric-Airspace-Skin System

1. Initial Conditions

$$T_1 = T_2 = T_3 \ldots\ldots \text{etc.} = 0 \text{ (only internal points)}$$

$$T_e = 0$$

$$T_{fo} > 0, \quad T_{fi} > 0, \quad T_{so} > 0$$

2. Values of Parameters

$$R_{fo} = R_{io} = 0$$

$$e^{-\gamma L_f} = 0.06$$

$$H_{fo} = 0.04$$

$$H_{io} = 0.50$$

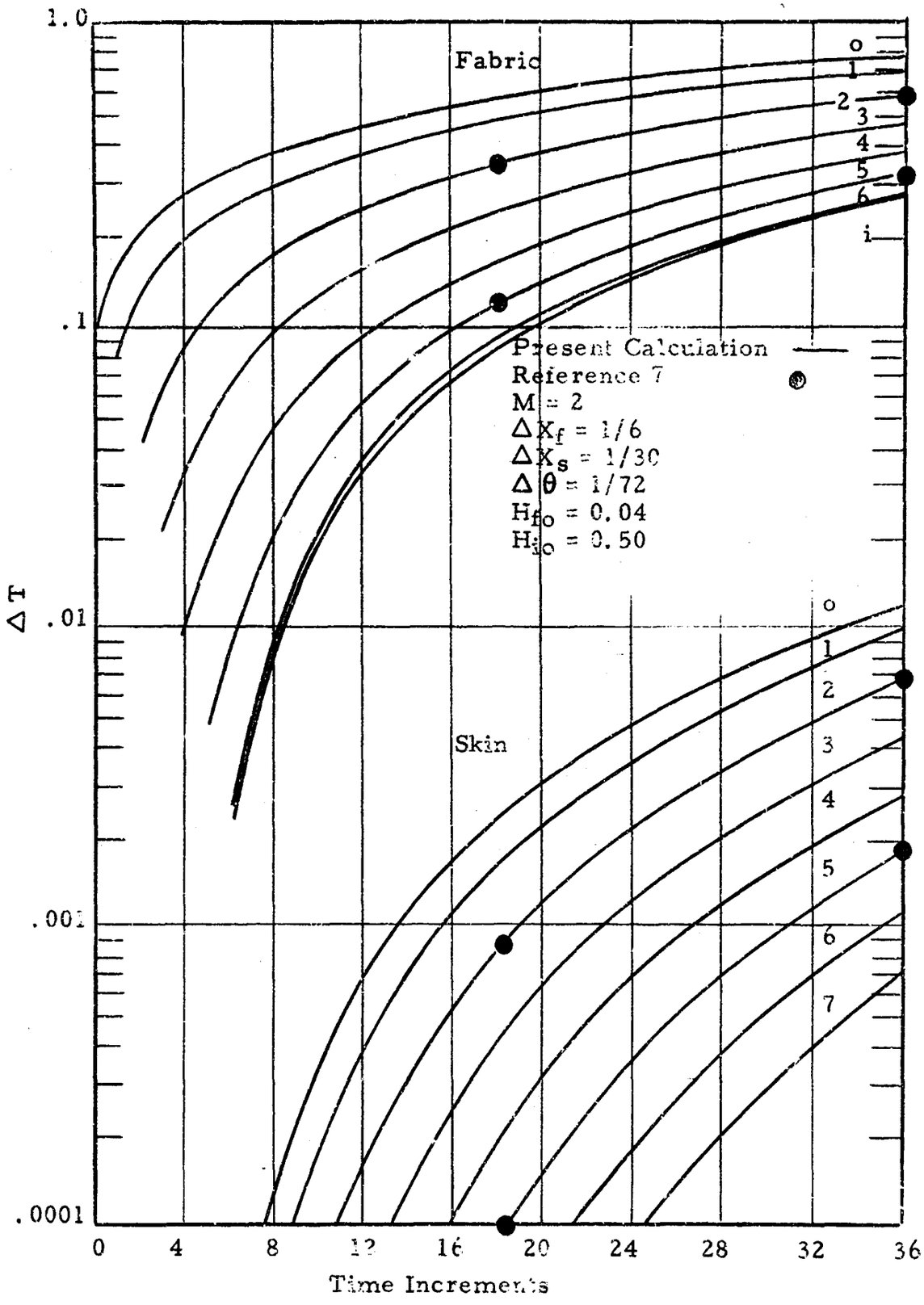

Figure A-5. Temperature History within an Opaque Fabric-Skin System

$$l = 1$$

$$\Delta X_f = 1/6, \quad \Delta X_s = 1/30$$

$$M_f = M_s = 2, \quad \Delta\theta_f = \frac{\Delta X_f^2}{2} = 1/72$$

These calculations and equivalent points from the MIT calculations are shown in Figure A-6 for comparison.

The good agreement between the present results and the MIT data was sufficient to show that the calculation procedures are equivalent. Because of close correlation between both sets of data during the earlier phases of the temperature-time history, it was not felt necessary to continue the calculation.

A good insight into the effects of the nonlinear radiation term was provided by comparison with the recent data of Reference 10. In this study, a finite difference technique adapted for computer solution was utilized to present front and back surface temperature variation as a function of time for a flat plate radiating into deep space with an insulated back surface. For this comparison the following calculation was performed.

C. Case III. Flat Plate Radiating to a Deep Space Environment

1. Initial Conditions

$$T_1 = T_2 = T_3 \ldots \text{etc.} = 1$$

$$T_e = 0$$

$$T_{fo} < 1$$

2. Values of Parameters

$$R_{io} = H_{fo} = H_{io} = 0$$

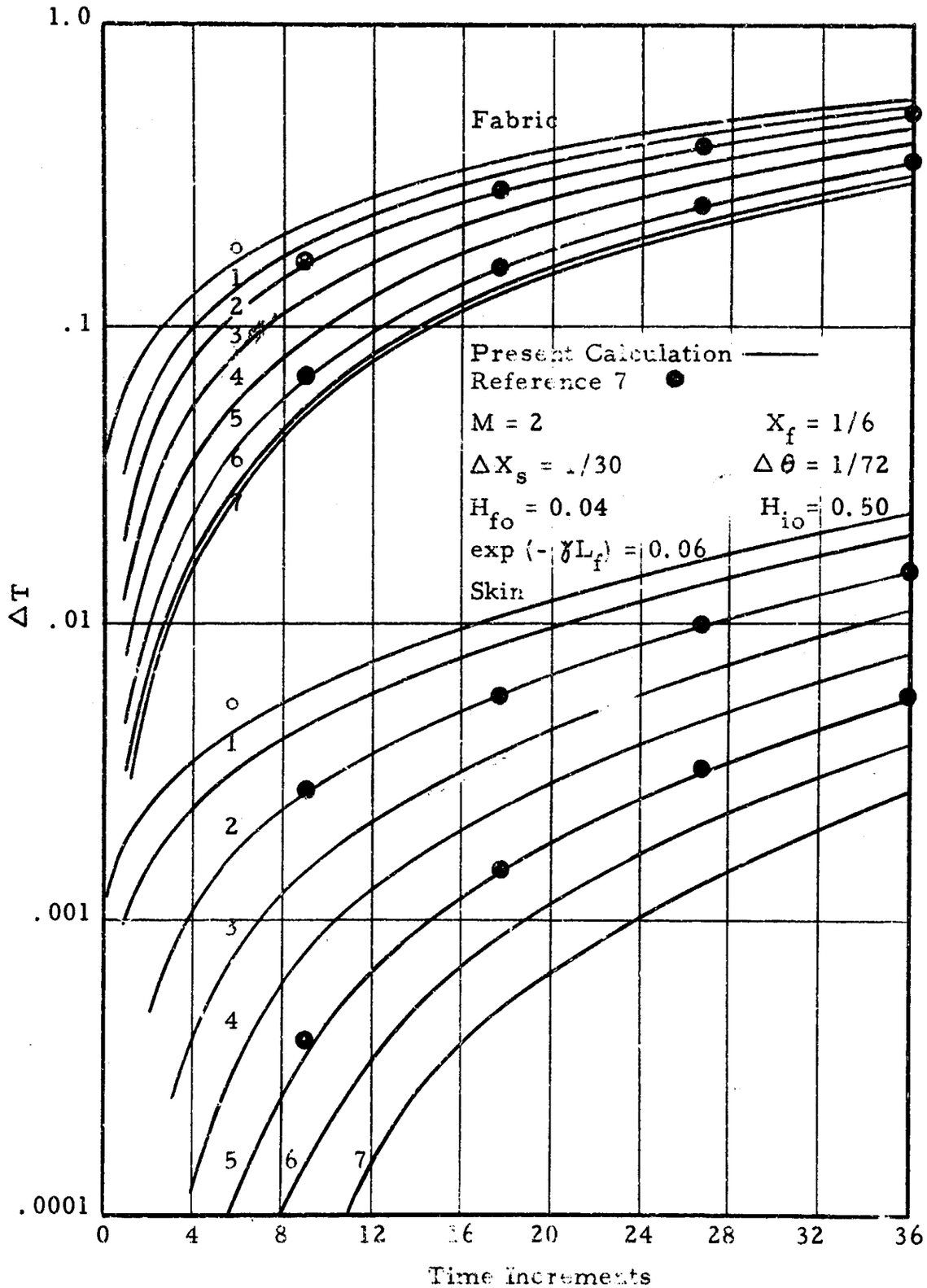

Figure A-6. Temperature History within a Diathermanous-Fabric-Skin System

$$e^{-\gamma L_f} = 0$$

$$I = 0$$

$$\Delta X_f = 1/10$$

$$M_f = 2, 3$$

$$R_{fo} = 0.1,\ 0.2,\ 0.4,\ 1.0,\ 2.0,\ 4.0,\ 10.0,\ \text{and } 20.0.$$

This calculation is presented in Figure A-7, where T_{fo} is t_f/t_i.

Neither the modulus M_f nor number of plate subdivisions ΔX_f were specified in Reference 10, so values of 2 and 1/10, respectively, were initially chosen. The resulting curves indicate that as the radiation coefficient increases, an instability appears in the solution which gets progressively worse for each increase in R_{fo}. However, the instability is damped out after a certain number of nondimensional time increments. For $R_{fo} = 20$, the modulus was increased to 3, which improved the accuracy of the calculation. Division of the plate into a larger number of increments also increases the stability of the calculation. This calculation was performed for values of R_{fo} much larger than those to be encountered in a fabric heat exchange situation, and the instability would not normally be a problem. However, the results obtained bring to light a basic feature of finite difference calculations as regards instabilities and boundary subdivisions.

D. Case IV. Flat Plate Irradiated by a Time Dependent Heat Pulse

1. Initial Conditions

$$T_o = T_1 = T_2 = T_3 \ldots\ldots \text{etc.} = 0$$

$$T_e = 0$$

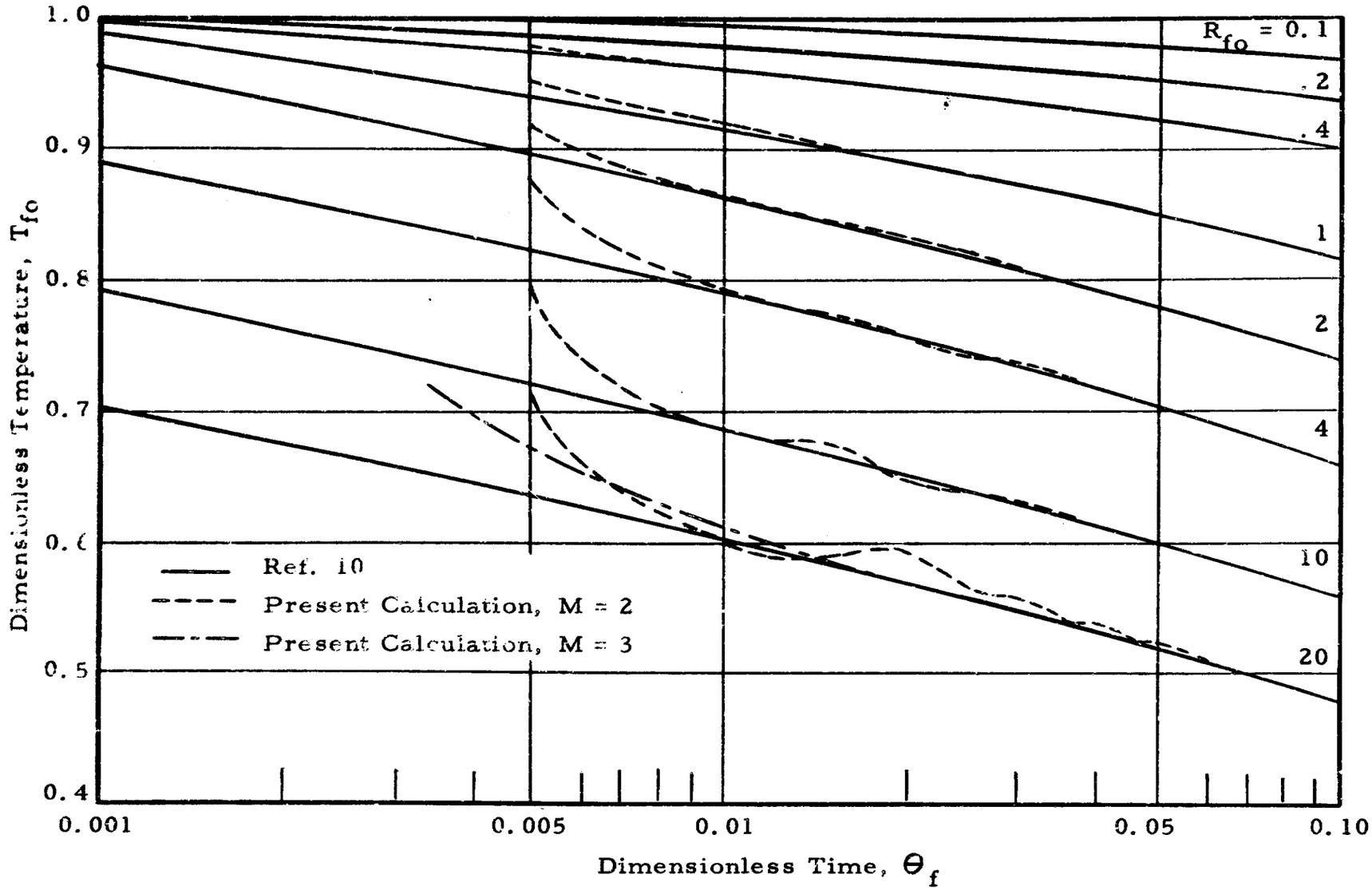

Figure A-7. Temperature Change on Outer Surface of Plate Radiating to Outer Space

2. Values of Parameters

$$R_{fo} = R_{io} = 0$$

$$e^{-\gamma L_f} = 0$$

$$H_{fo} = 0.10$$

$$H_{io} = 0$$

$$I = I(A\theta)$$

$$A = 1$$

$$\Delta X_f = 1/6$$

$$M_f = 2, \Delta\theta_f = \frac{\Delta X_f^2}{2} = 1/72$$

A calculation was performed to investigate the behavior of the explicit finite difference calculation procedure for the case of a time dependent heat input. The dimensionless presentation of radiation intensity variation with time for a nuclear energy release[11] is given by the following equations:

Region	Equation
$0 \leq A\theta \leq 0.3$	$I = 0.565\ A\theta$
$0.3 \leq A\theta \leq 0.65$	$I = 1.72\ A\theta - 0.347$
$0.65 \leq A\theta \leq 1.4$	$I = 1 - 1.42(A\theta - 1.05)^2$
$1.4 \leq A\theta \leq 10$	$I = 1.434(A\theta)^{-1.64}$

where A is the reciprocal of the Fourier number evaluated at τ_{max}, or,

$$A = \frac{L_f^2}{\tau_{max}} \left(\frac{c\rho}{k}\right)_f$$

and

$$A\theta = \frac{\tau}{\tau_{max}}$$

Batter[11] presented plotted data for a flat plate with an insulated back surface irradiated by a heat pulse with a shape described by the above equations. Comparison of the present method with these results was made for a selected A (proporational to explosion yield) of 1.0 and a front surface heat loss parameter, H_{fo} of 0.10. This comparison is presented in Figure A-8 along with data of Loria and Schmit[12] who used a method very similar to Batter's.[11] Presented are the front surface, back surface and center temperatures of the plate.

An initial parameter study was performed to obtain a better understanding of the relative significances of the various parameters isolated earlier in this appendix.

To reduce the scope of the study, only a constant-time heat input and an opaque fabric were considered. To isolate and study the radiation and convection heat-transfer processes separately, we retained the nonlinear boundary conditions. This complicates the calculation because temperature levels, as well as temperature differences, must then be considered. Recall that when linear heat-transfer terms are used, differences only need be considered, and the initial or environmental temperature can be chosen as zero. This restriction reduces the generality of the solution. Consideration of Equation (A-33) and Table A.1, shows that the environmental temperature t_e, maximum values of radiation input i_{max}, thermal conductivity k_f, and thickness L of the fabric must be considered to properly select the non-dimensional environmental (and initial) temperatures.

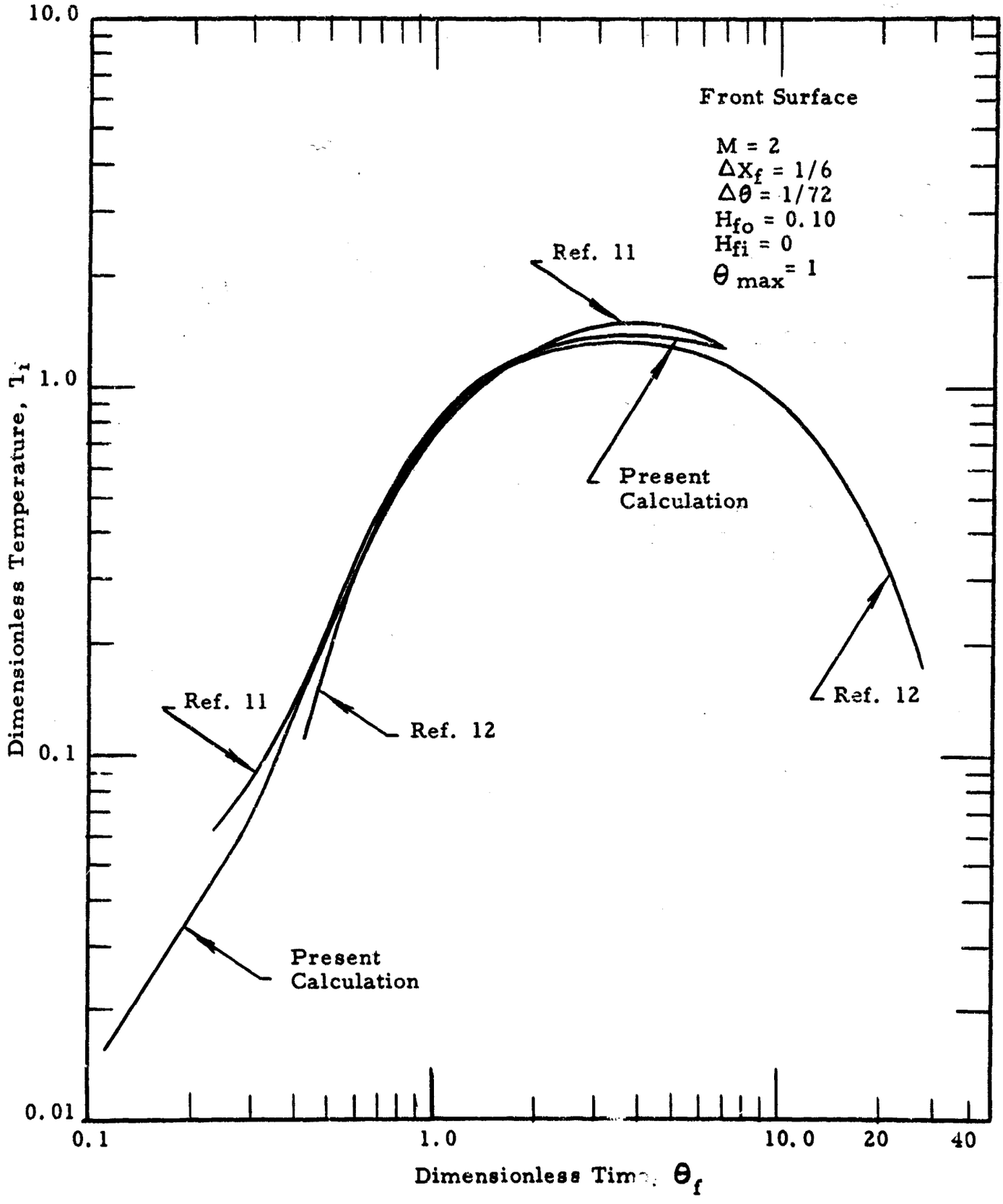

Figure A-8a . Temperature Response of a Semi-Infinite Slab (with Front Surface Heat Loss) Irradiated by a Time-Dependent Heat Pulse

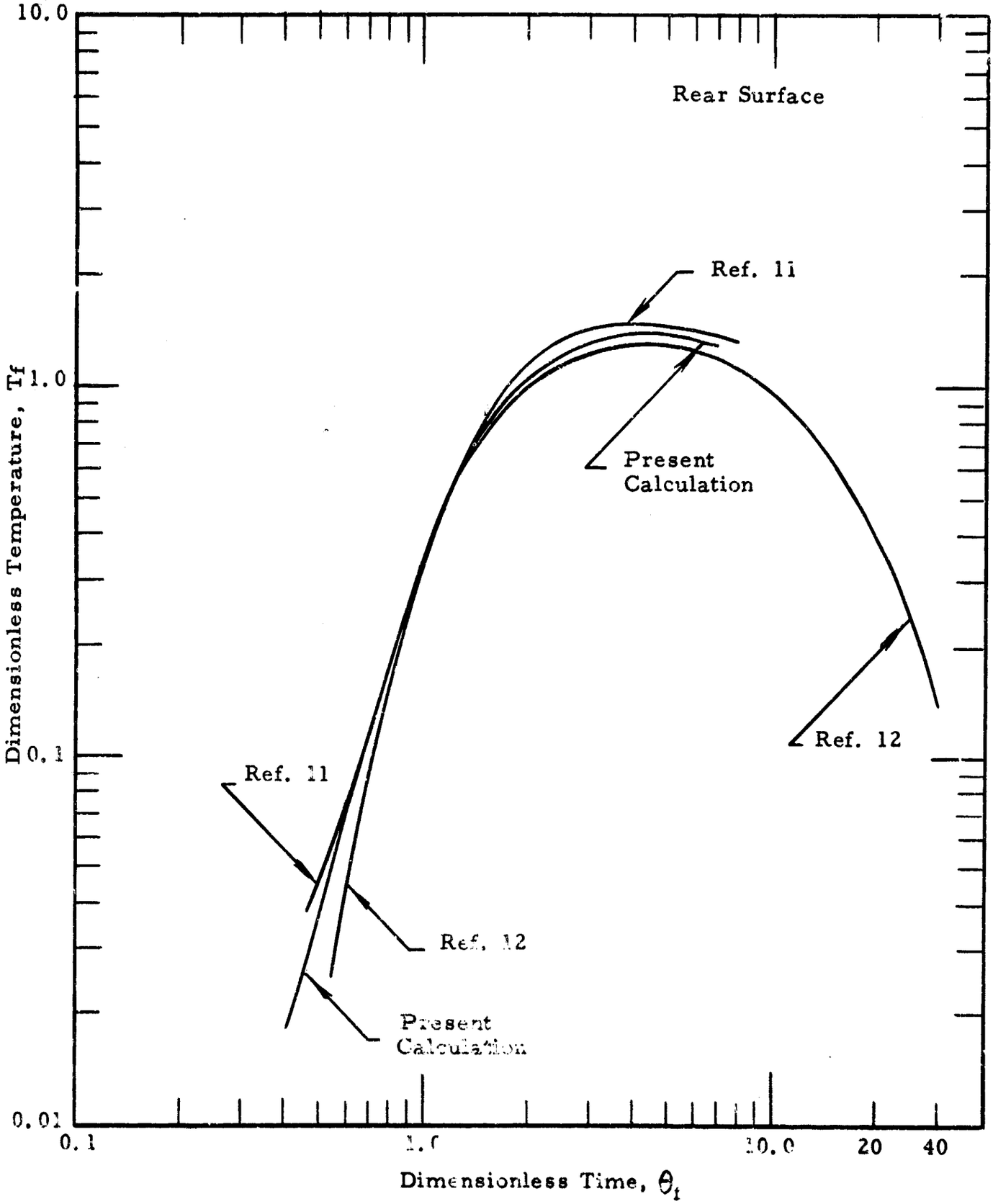

Figure A-8b. Temperature Response of a Semi-Infinite Slab (with Front Surface Heat Loss) Irradiated by a Time-Dependent Heat Pulse

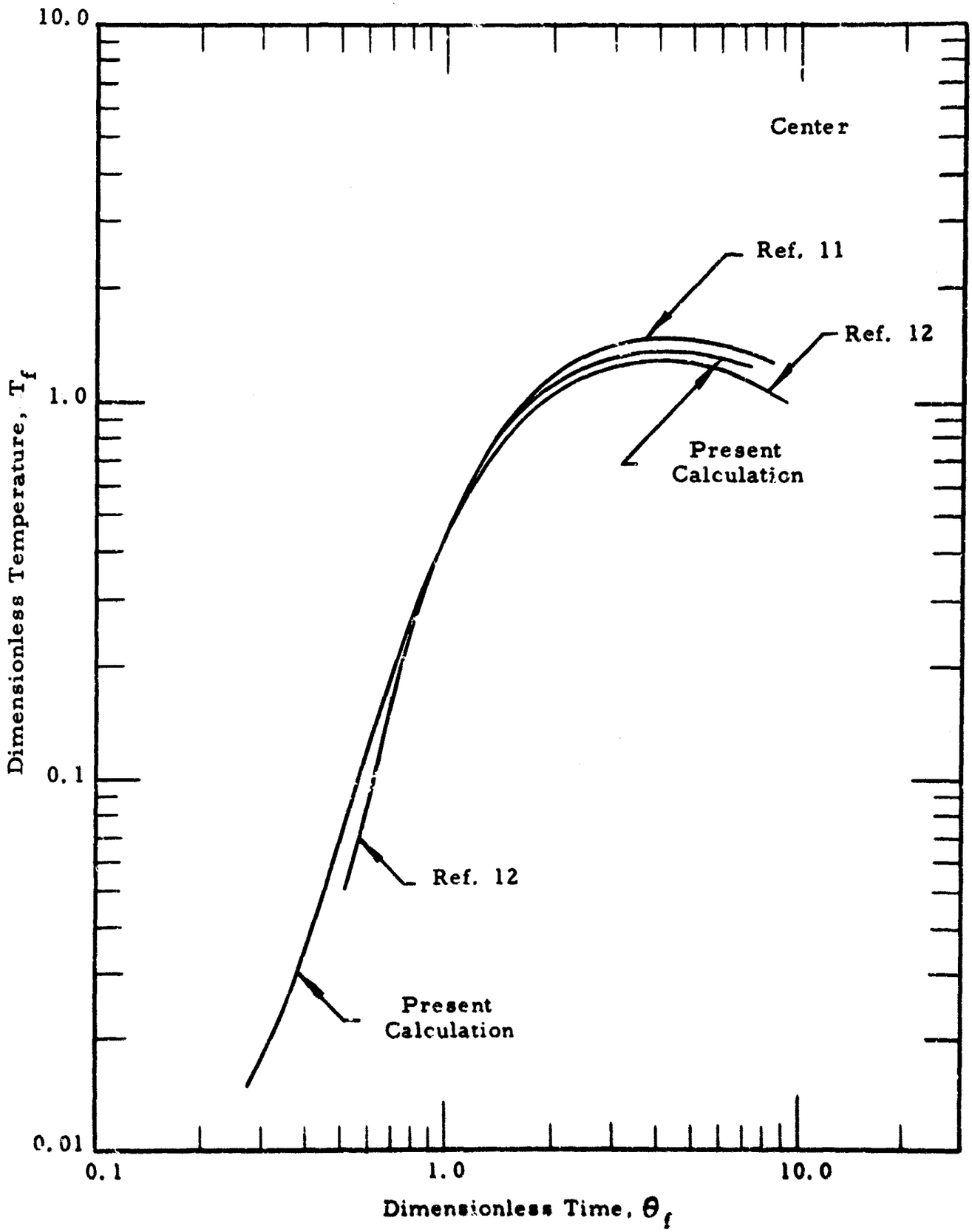

Figure A-8c . Temperature Response of a Semi-Infinite Slab (with Front Surface Heat Loss) Irradiated by a Time-Dependent Heat Pulse

In addition, the non-dimensional front- and rear-surface radiation and convection heat-transfer coefficients must be specified separately.

Because of the appreciable time involved for each calculation, owing to the relatively limited capacity of our computer, the parameter variations selected for the computations were chosen to satisfy only our immediate requirements. Since the fabric- and skin-surface radiation heat-transfer coefficients were not linearized, and also were separated from the convection terms, the solutions are more specific than the generalized non-dimensional solution. Further, temperature levels, as well as temperature differences, must be considered.

For this calculation, the following conditions were chosen.

E. Case V. Opaque Fabric-Airspace-Skin System (Variation of Heat Transfer Coefficients

1. Initial Conditions

$$T_1 = T_2 = T_3 \ldots\ldots \text{etc.} = T_e$$

$$T_e = 0.108$$

$$T_{fo} > T_e$$

2. Values of Constant Parameters

$$e^{-\gamma L_f} = 0$$

$$I = 1$$

$$\Delta X_f = 1/6$$

$$\Delta X_s = 1/30$$

$$M_f = M_s = 2$$

$$\Delta\theta_f = \Delta X_f^2/2 = 1/72$$

3. Values of Variable Parameters (Heat-Transfer Coefficients)

$$R_{fo} = 1, 10$$

$$R_{io} = 1, 10$$

$$H_{fo} = 0.01, 0.10$$

$$H_{io} = 0.10, 1$$

Because of the nonlinear radiation term, a non-zero value of the non-dimensional environmental temperature must be chosen. Referring to Table A.1, the non-dimensional representation of T_e is

$$T_e = \frac{k_f t_e}{i_{max} L_f}$$

This was evaluated by selecting a constant radiation input of $i_{max} = 10$ cal/cm^2 sec, an environmental temperature of $t_e = 15°C$, and assuming a 9 oz "standard" cotton-sateen cloth having $k_f/L_f = 3.76 \times 10^{-3}$ cal/cm^2 sec °C. This combination resulted in a T_e of 0.108.

The non-dimensional heat-transfer coefficients (R_{fo}, R_{io}, H_{fo}, and H_{io}) were selected in a similar manner, using the best available information pertaining to the dimensional convection coefficients. Utilizing the above selected values, the radiation coefficients are of the order of 5, the fabric front- and rear-surface convection coefficents are of the order of 0.05 and 0.50, respectively.

For our calculations, only envelopes of fabric front- and rear-surface and skin front-surface response are presented (Refer to Figure A-9). They show the effects of order-of-magnitude changes of the transfer coefficients, selecting as a parameter the extreme values of each coefficient. Variation of the other parameters in any manner within the prescribed limits results in curves lying within the envelopes. A presentation such as this allows a quicker understanding of the significance of each heat-transfer parameter, without the necessity of considering a vast number of curves resulting from incremental changes in the parameters.

An appreciation and an understanding of the curves shown in Figure A-9 can be obtained by referring to the Nomenclature on page A-47 and the non-dimensional parameters presented in Table A. 1. The dimensionless representation is necessary to allow implicit consideration of many possible temperature responses for various heat inputs and combinations of thermal and optical properties, and surface heat loss rates. The exact response for a particular configuration can be obtained by inserting the proper thermal and optical properties in the various parameters.

One obvious feature of these curves is that, when the fabric front-surface radiation coefficient (R_{fo}) is fixed, the envelope for ΔT_{fo} is very small, which indicates that the front-surface temperature depends largely on the radiation coefficient. Other conclusions can be drawn as well. In most cases, the percentage change in the skin response is larger than the fabric responses, except for $H_{io} = 1$, where they are approximately equal. The size of the envelope increases progressively from the fabric outer surface to the inner surface and skin surface, except for $H_{io} = 1$, where they are of the same order.

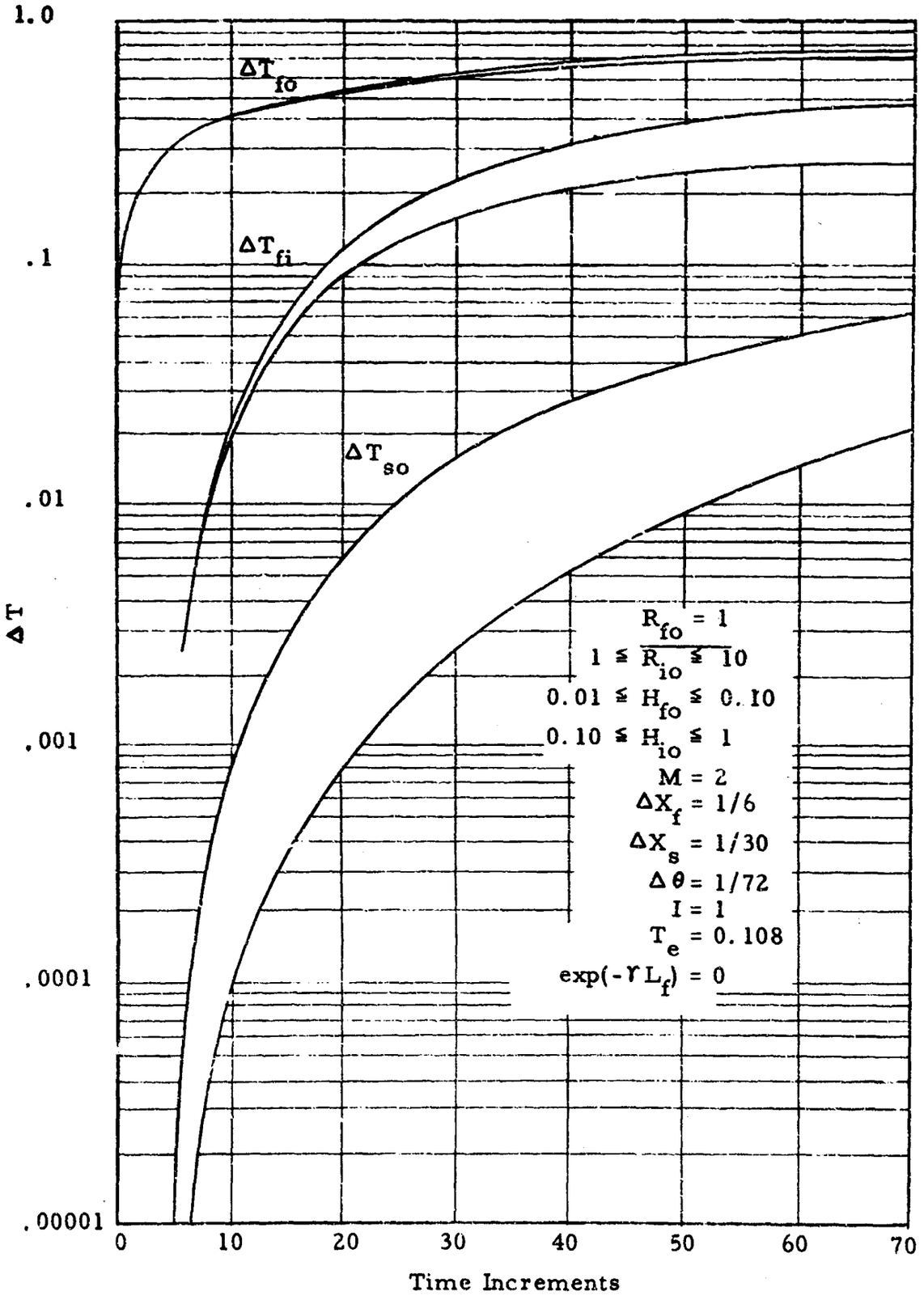

Figure A-9a. Envelopes of Temperature Response of an Opaque Fabric Skin System

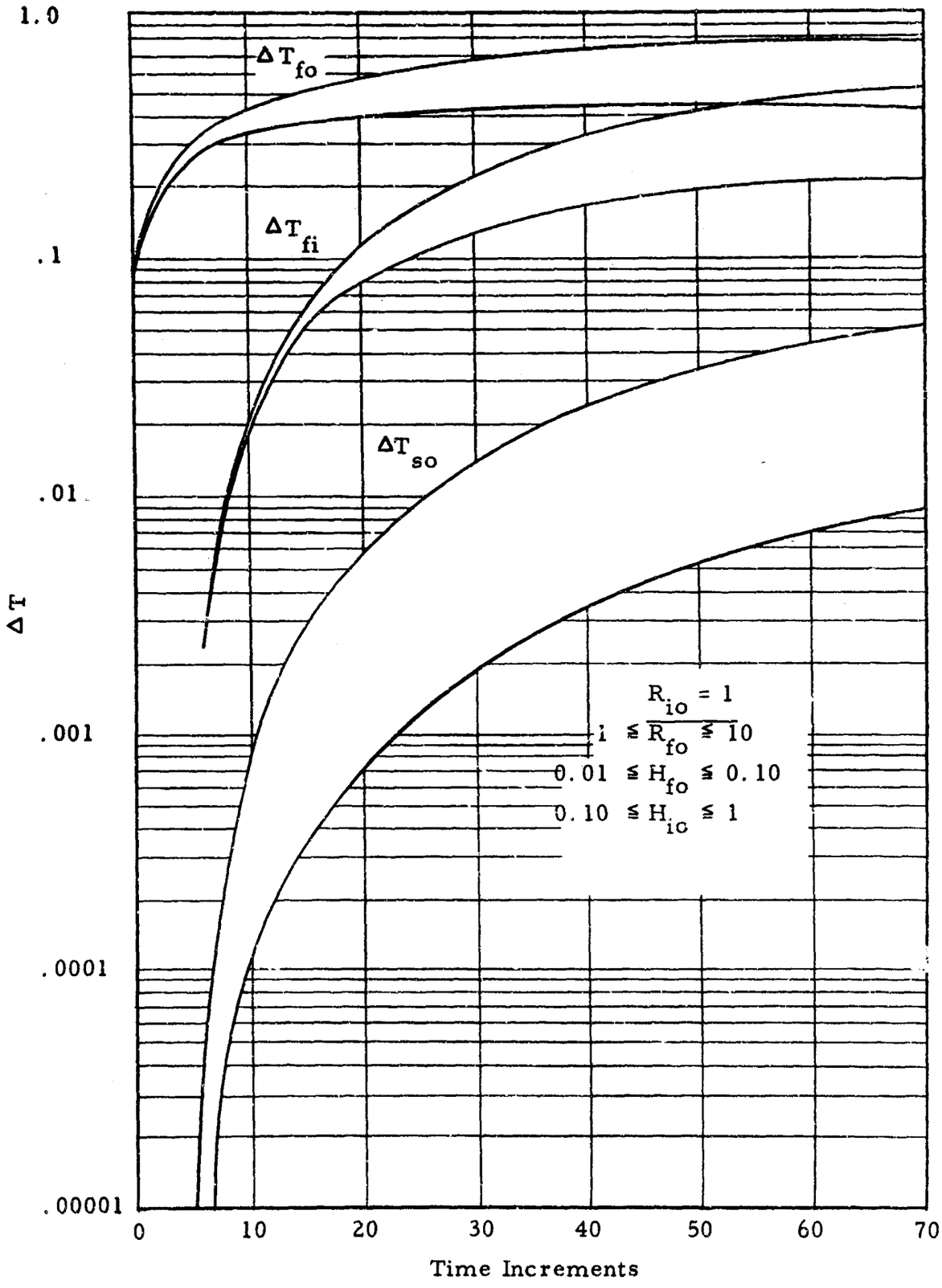
1.0
.1
.01
.001
.0001
.00001
ΔT
ΔT_fo
ΔT_fi
ΔT_so
R_io = 1
1 ≤ R_fo ≤ 10
0.01 ≤ H_fo ≤ 0.10
0.10 ≤ H_ic ≤ 1
0
10
20
30
40
50
60
70
Time Increments

Figure A-9b.

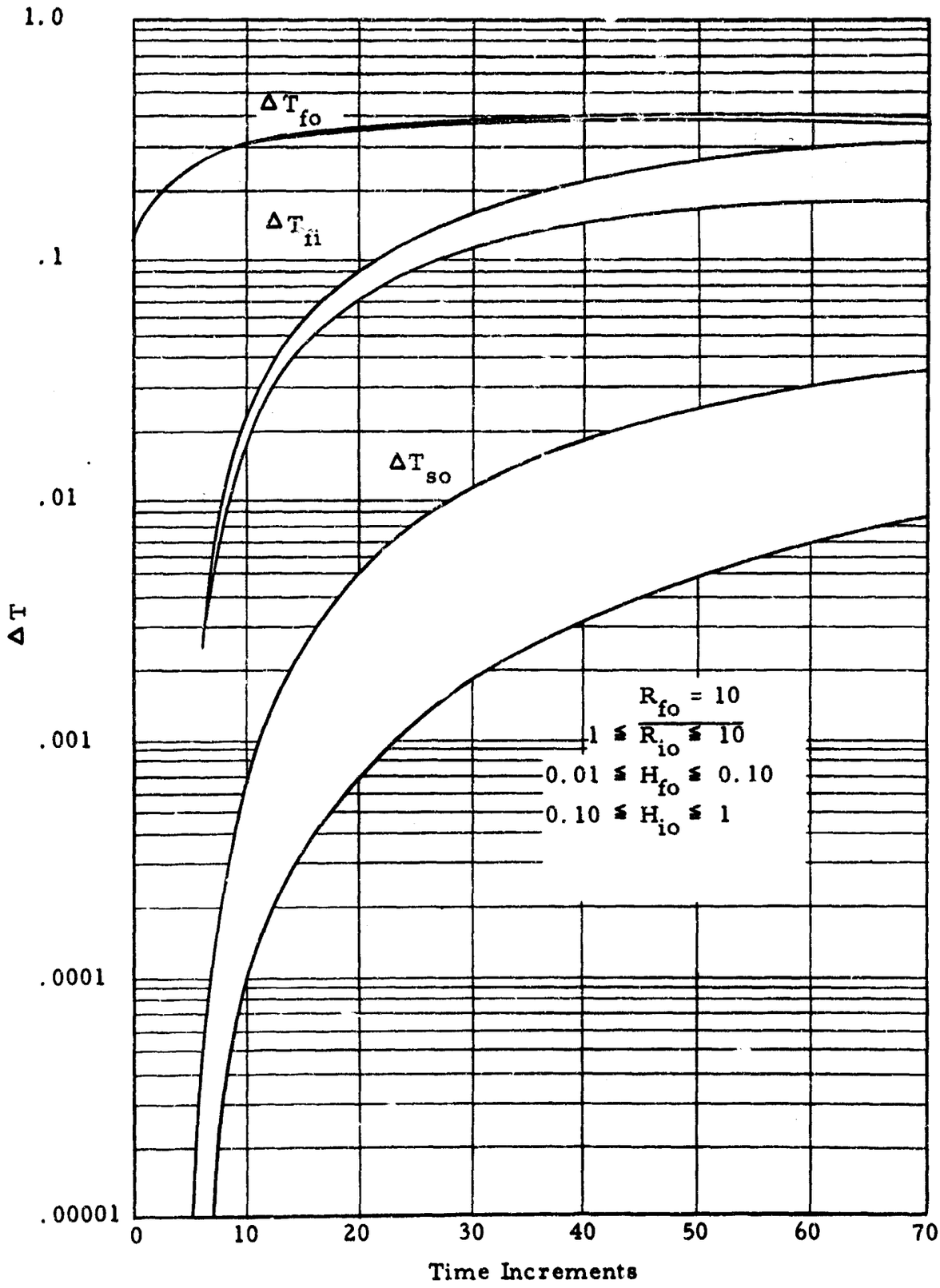
1.0
.1
.01
.001
.0001
.00001
ΔT
ΔT_fo
ΔT_fi
ΔT_so
R_fo = 10
1 ≤ R_io ≤ 10
0.01 ≤ H_fo ≤ 0.10
0.10 ≤ H_io ≤ 1
0
10
20
30
40
50
60
70
Time Increments

Figure A-9c.

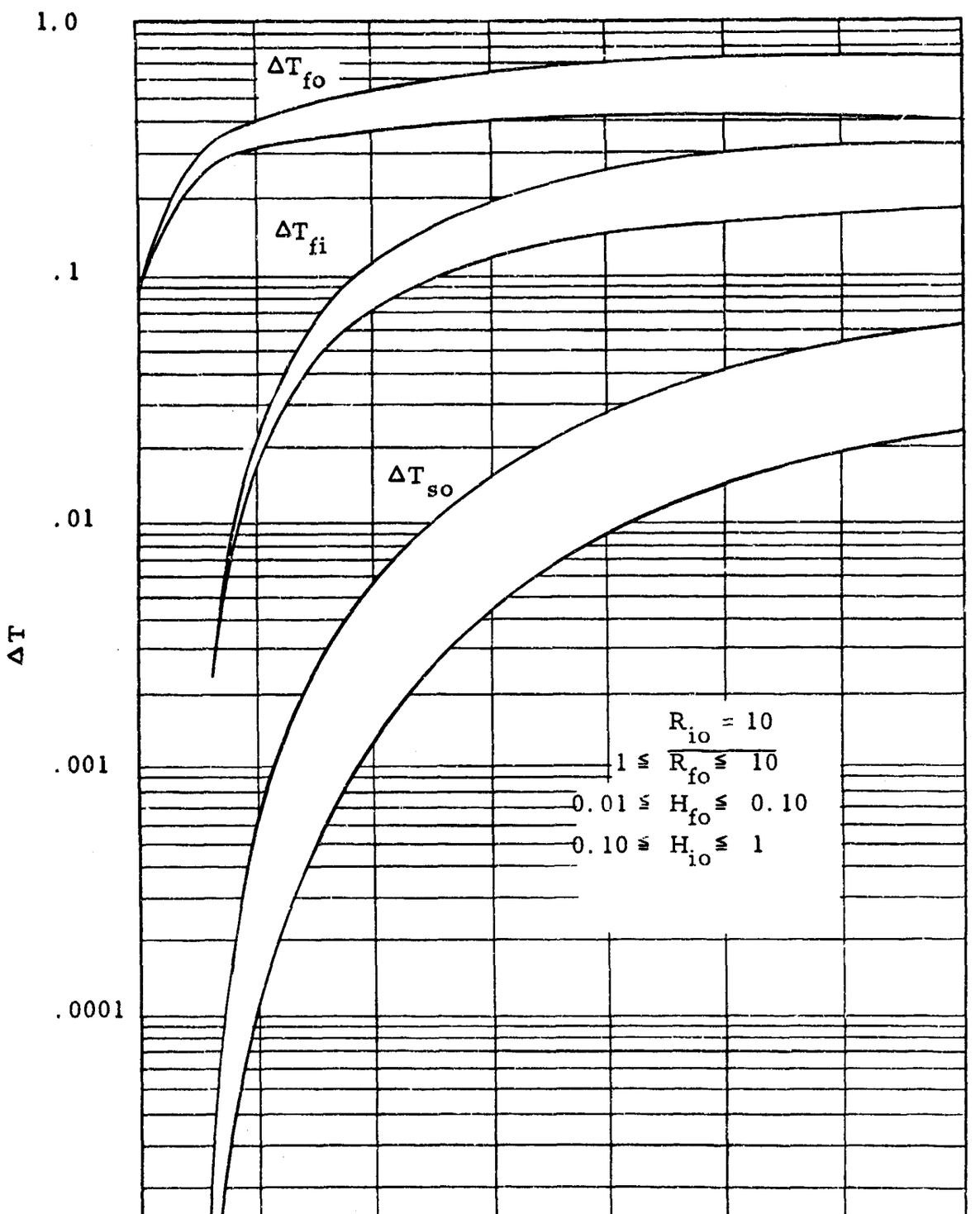
1.0
.1
.01
.001
.0001
.00001
ΔT
ΔT_fo
ΔT_fi
ΔT_so
R_io = 10
1 ≤ R_fo ≤ 10
0.01 ≤ H_fo ≤ 0.10
0.10 ≤ H_io ≤ 1
0
10
20
30
40
50
60
70
Time Increments

Figure A-9d.

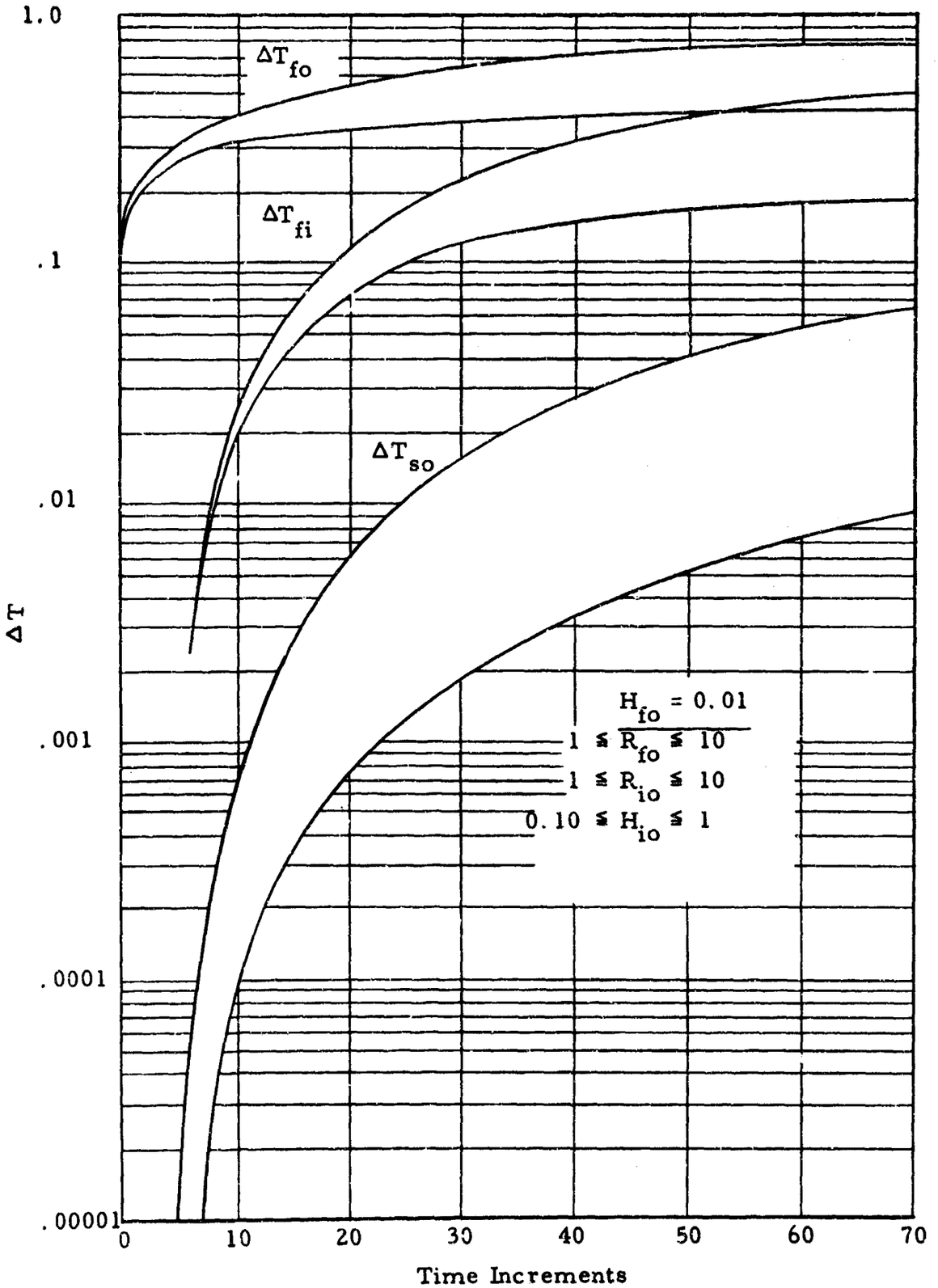
1.0
.1
.01
.001
.0001
.00001
ΔT
ΔT_fo
ΔT_fi
ΔT_so
H_fo = 0.01
1 ≤ R_fo ≤ 10
1 ≤ R_io ≤ 10
0.10 ≤ H_io ≤ 1
0
10
20
30
40
50
60
70
Time Increments

Figure A-9e.

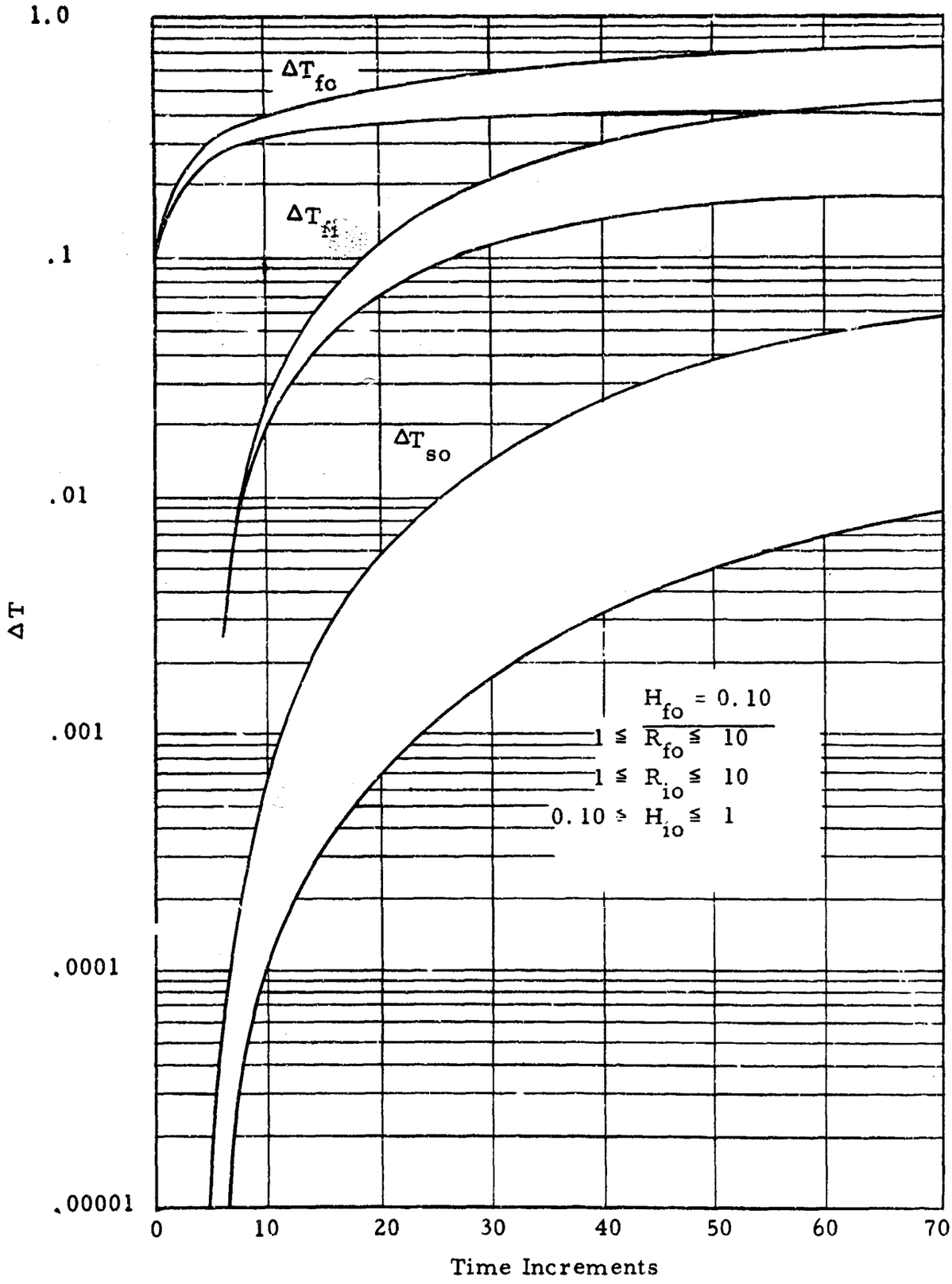
1.0
.1
.01
.001
.0001
.00001
ΔT
ΔT_{fo}
ΔT_{fi}
ΔT_{so}
$H_{fo} = 0.10$
$1 \leq R_{fo} \leq 10$
$1 \leq R_{io} \leq 10$
$0.10 \leq H_{io} \leq 1$
0
10
20
30
40
50
60
70
Time Increments

Figure A-9f.

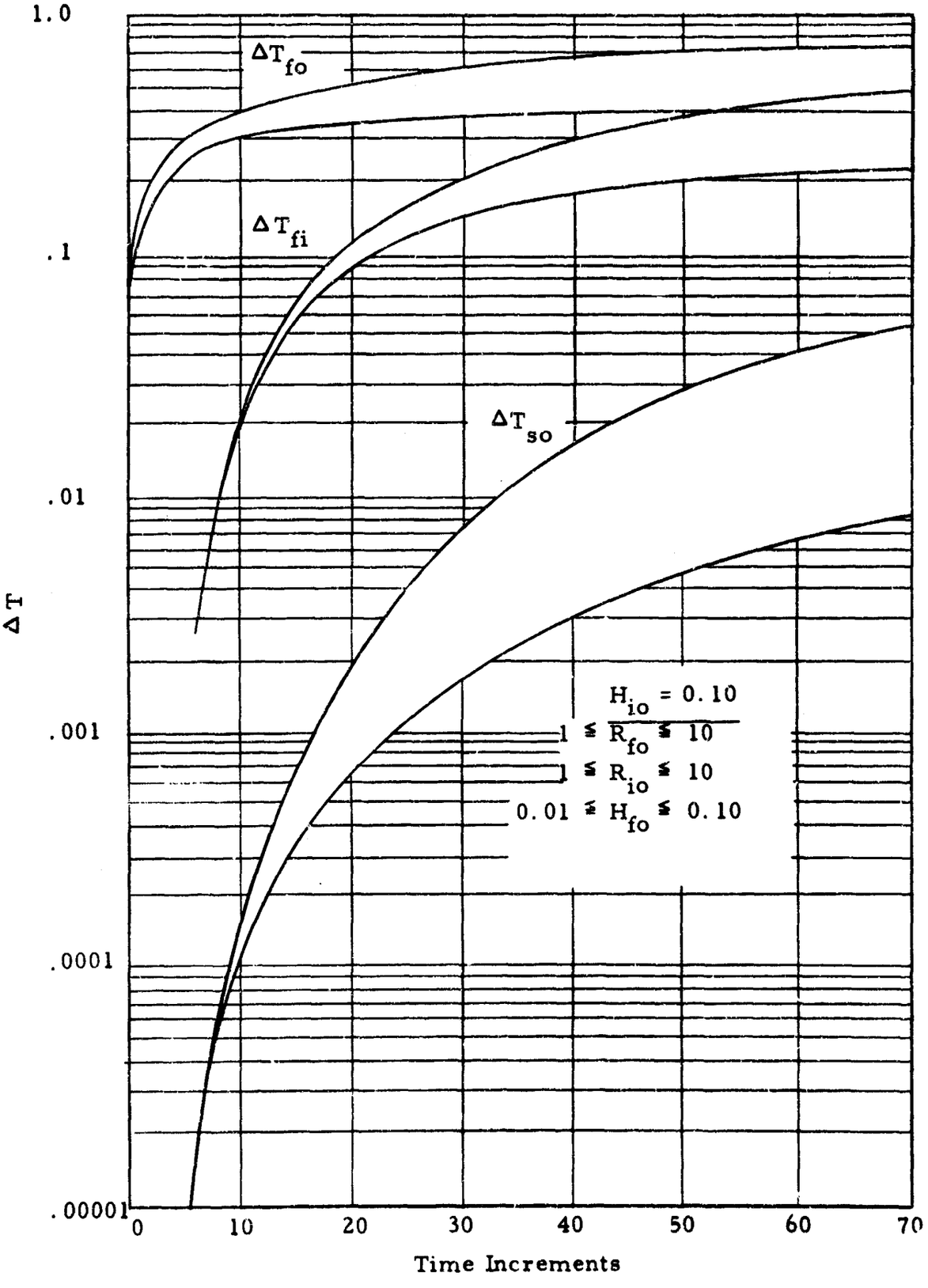
1.0
.1
.01
.001
.0001
.00001
ΔT
ΔT_fo
ΔT_fi
ΔT_so
H_io = 0.10
1 ≤ R_fo ≤ 10
1 ≤ R_io ≤ 10
0.01 ≤ H_fo ≤ 0.10
0
10
20
30
40
50
60
70
Time Increments

Figure A-9g.

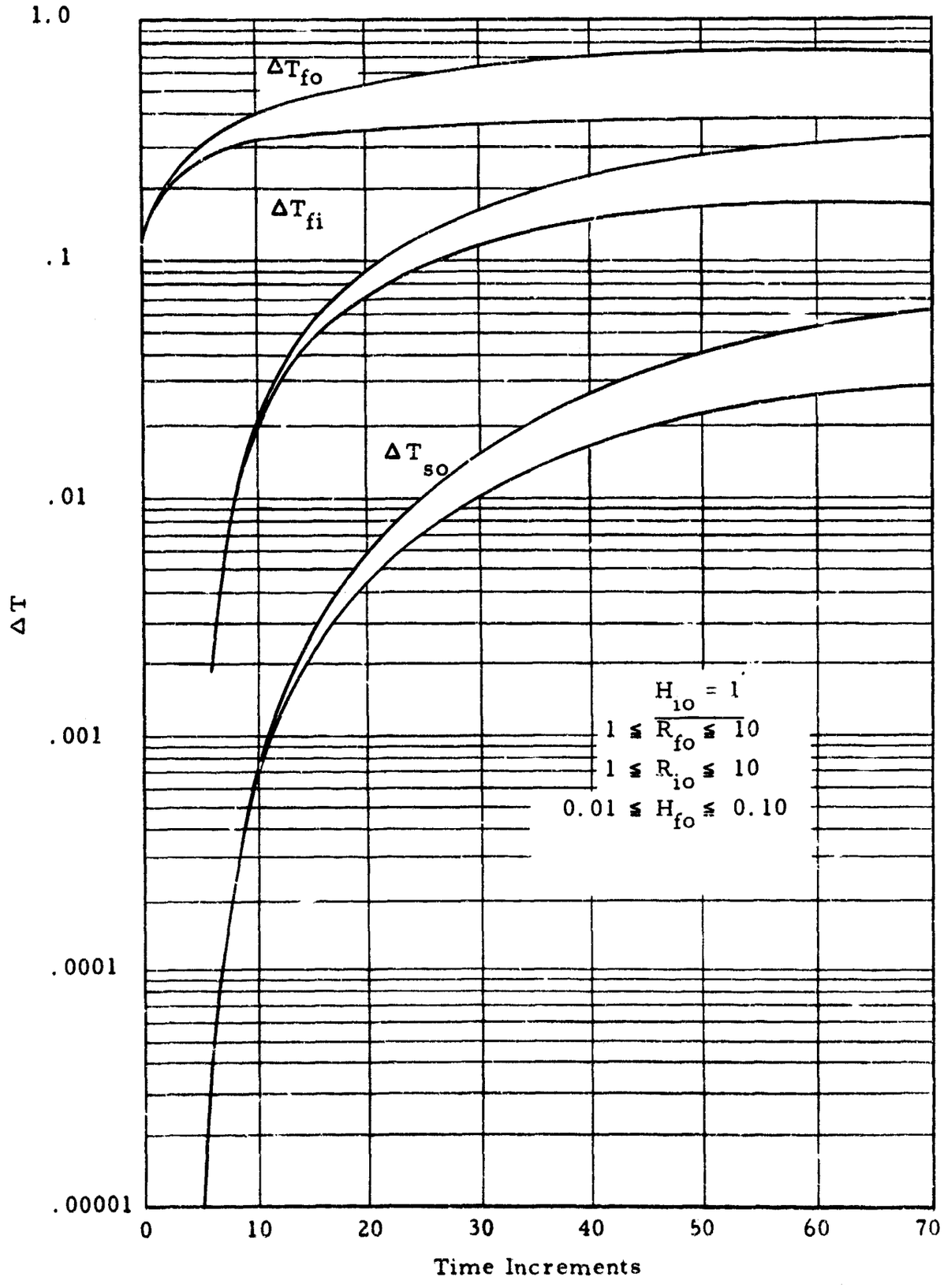
1.0
.1
.01
.001
.0001
.00001
ΔT
ΔTfo
ΔTfi
ΔTso
H1o = 1
1 ≤ Rfo ≤ 10
1 ≤ Rio ≤ 10
0.01 ≤ Hfo ≤ 0.10
0
10
20
30
40
50
60
70
Time Increments

Figure A-9h.

SYMBOLS AND ABBREVIATIONS

Symbol	
Bi	Biot number
c	specific heat
D	diathermancy factor
F_{f-s}	radiation interchange factor between fabric and skin
Fo	Fourier number
h	heat transfer coefficient
i	radiant heat flux
J	Jacobian
k	heat conductivity
L	fabric or air gap thickness or characteristic length
M	dimensionless modulus
m	iteration correction factor
n	iteration correction factor or series term
t	temperature
x	distance
α	absorptivity or diffusivity
γ	extinction coefficient
Δ	time or distance increment
ϵ	emissivity
ρ	density or reflectivity
σ	Stefan-Boltzmann constant
τ	time or transmissivity

Subscript

a	air gap or air
e	environment
eff	effective
f	fabric
i	inner surface of fabric or initial value
j	general space increment
k	last fabric element
max	maximum
o	outer surface or impinging radiation
s	skin

Superscript

'	conditions at end of time increment
k	first approximation in iteration
n	general time increment

IV. REFERENCES

1) Friedmann, N. E. The truncation error in a semi-discrete analog of the heat equation. J. Math. Phys. 35: 299-308 (1956).

2) McAdams, W. H. Heat transmission. 3rd ed. N. Y., McGraw-Hill, 1954.

3) Nessi, A. and L. Nissolle. Methodes graphiques pour l'étude des installations de chauffage et de refrigeration et régime discontinué. Paris, Dunod, 1929.

4) Dusinberre, G. M. Heat-transfer calculations by finite differences. Scranton, Pa., International Textbook Co., 1961.

5) Paul, B. Generalization of the Schmidt graphical method for transient heat conduction. ARS J. 32: 1098-99 (1962).

6) Richtmyer, R. D. Difference methods for initial-value problems. N. Y., Interscience, 1958.

7) Massachusetts Institute of Technology. Fuels Research Laboratory. Heat transfer to skin through thermally-irradiated cloth, by N. Y. Chen and W. P. Jensen. Contract Nonr 1841(37). Technical Report No. 6 (July 1958). AD 200,210.

8) Scarborough, J. B. Numerical mathematical analysis. 3rd ed. Baltimore, Johns Hopkins Press, 1955.

9) U. S. Naval Radiological Defense Laboratory. A flash method for determining thermal diffusivity over a wide temperature range, by R. J. Jenkins and W. J. Parker (June 1961). AD 268,752; WADD Tech. Report 61-95.

10) Fairall, R. S., R. A. Wells and R. L. Belcher. Unsteady-state heat transfer in solids with radiation at one boundary. ASME Trans. 84C: 266-67 (1962).

11) Technical Operations, Incorporated. Report no. 58-7. Transient effects of a time varying thermal pulse, Part 2, by J. F. Batter, Contract No. DA-29-044-XZ-587 (Mar. 1958). AD 158,776.

12) Massachusetts Institute of Technology. The temperature response of thick plates exposed to radiant heat pulses, by J. C. Loria and L. A. Schmit. Contract AF 33(616)-3259 (July 25, 1956). WADC Technical Report 56-149; AD 97,295.

APPENDIX B

INTERFEROMETER THEORY, EQUIPMENT, AND CALIBRATION

(Including Discussion of Errors)

I. INTERFEROMETER THEORY

In the Mach-Zehnder instrument, shown in Figure B-1, the wave fronts from two separated beams of light, both emanating from a single source, are made to interfere with one another. The interference phenomena produces bright or dark bands on the image plane as reflected by phase cancellation or amplification of the beams wherever the wave fronts are in or out of phase. If the light beam passing through the test region of interest is retarded (or advanced) because of changes in the refractive index in that region, the interference fringes can be seen to shift. Localized fringe shifting occurs near a heated body since the temperature or density gradient in a thermal boundary layer surrounding the heated body produces a direct change in the refractive index. In gases the simple relationship $\eta - 1 = C$, as shown by Lorenz-Lorentz describes the dependency of density ρ on the index of refraction η. The Gladestone-Dale constant C maintains its constancy for gas over a wide range of pressure and temperature.

Since the degree of fringe displacement is dependent on total path length through which the refractive effects are occurring, among other things, an equation or equations can be derived expressing the variables to whatever determinant or quantity desired. For example, to calculate temperature at any location where refractive variances are restricted to a two-dimensional plane (no variation occurs along the light path) the following equation may be used:

$$t_2 = t_1 \left[\frac{1}{1 - \frac{\delta N \lambda R t_1}{CZP}} \right]$$

where:

t_1 = ambient temperature

δN = fringe shift

λ = wavelength of light

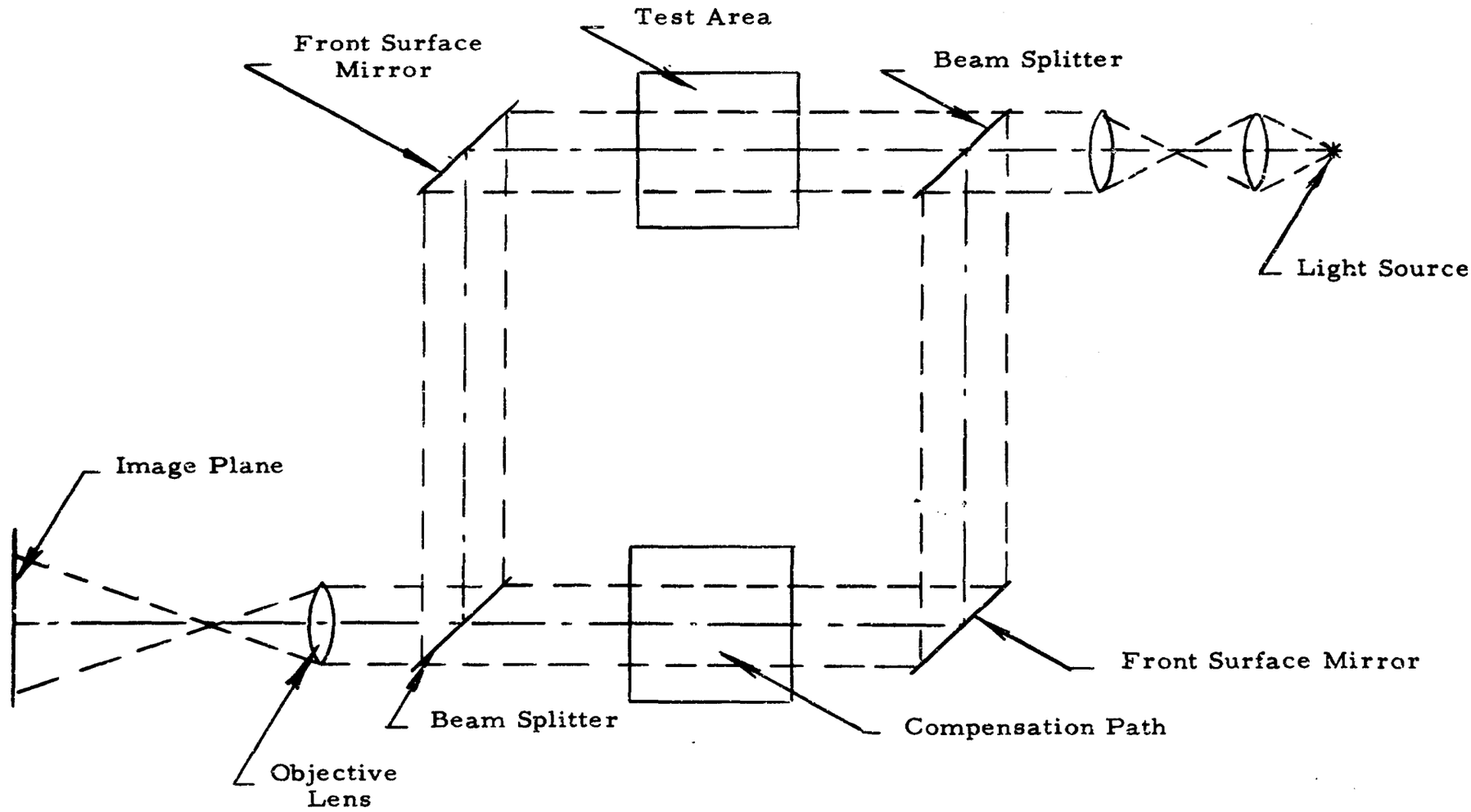

Figure B-1. Mach-Zehnder Interferometer

C = Gladstone-Dale constant

Z = interference path length

P = pressure.

The derivation of the basic interferometer equations are presented in Reference 1. Included also is a discussion of measurement errors. A complete description of the interferometer, its light source, alignment procedures, related equipment and system of measurements is also included in the above reference.

II. DEVELOPMENT OF EQUATIONS

A geometrical understanding of wave-front interference phenomena can be obtained for the condition of "finite" fringe adjustment of the interferometer. Consider that one of the beam-splitters has been rotated by a small angle in a given plane. The emergent coherent beams are now not parallel but intersect such that phase differences in the two beams appear as parallel dark or light fringes everywhere along the intersection plane (see Figure B-2). The width between fringes will depend on the angle of rotation.

For analysis purposes, the wave fronts can be made to intersect so that horizontal fringes will be projected across the field of view; this creates a two-dimensional representation of fringe shifts in the x-y plane permitting easier study. With appropriate adjustment of the optical elements, the intersection of wave fronts can also be made to occur within the test region where refraction effects take place (see Reference 1 for alignment procedures). Analysis is made with the assumption that variations in the z direction do not exist.

For a heated body the fringes are observed to bend as shown in Figure B-3. The direction of fringe bending (up or down) depends on the rotation direction of the beam-splitter. The optical path difference δQ for two light paths (projected at points 1 and 2) traveling in the z plane a distance Z is given as

$$\delta Q = (\eta_1 - \eta_2) Z ,$$

where Z is the length of heated body (z direction), and η_1 and η_2 are the indices of refraction of gas along the undisturbed path and along the shifted or deviant path, respectively. The difference in wavelengths δN from point 1 to point 2 can be shown equal to:

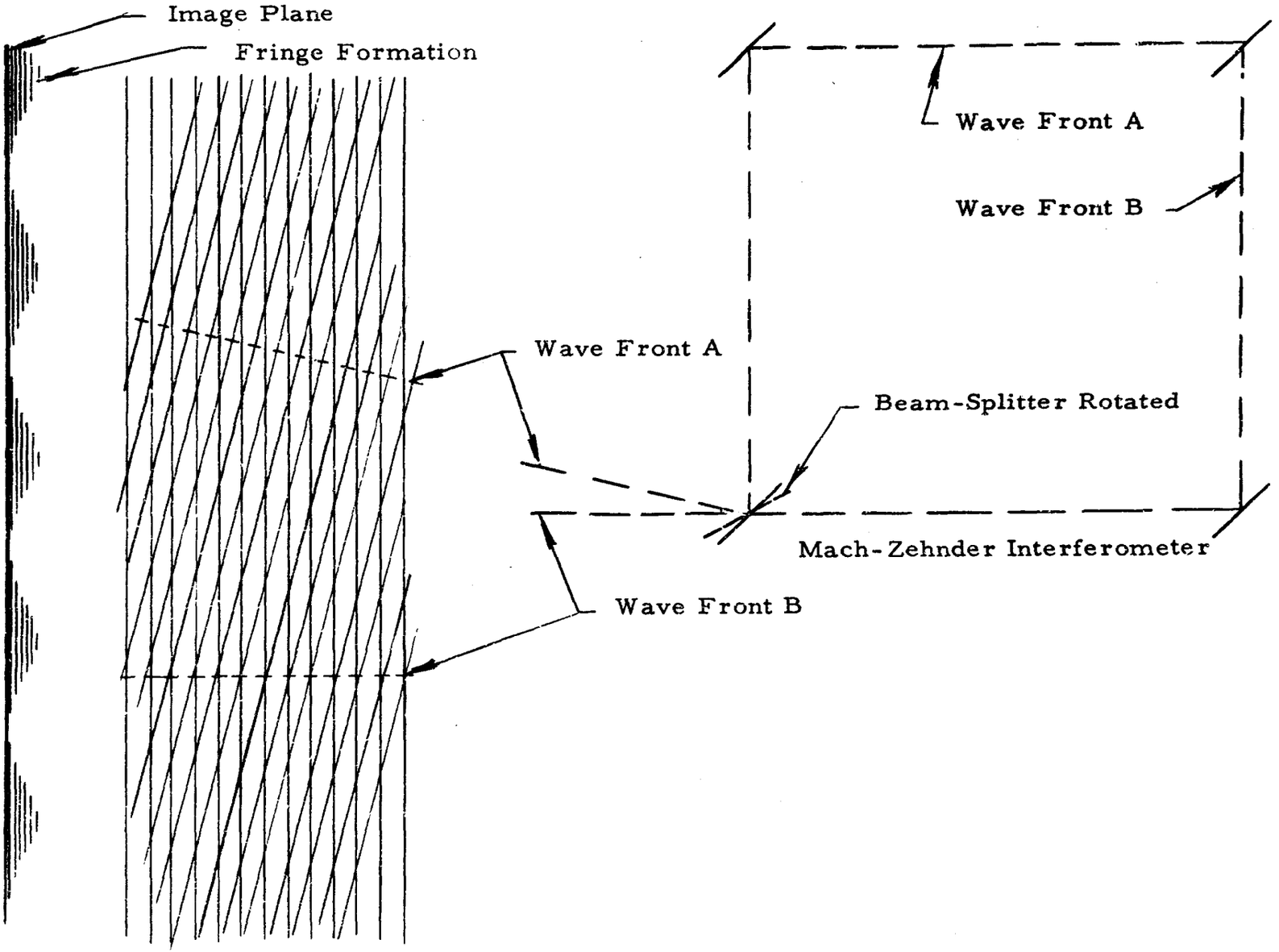

Figure B-2. Wave Front Interference and Formation of Fringes

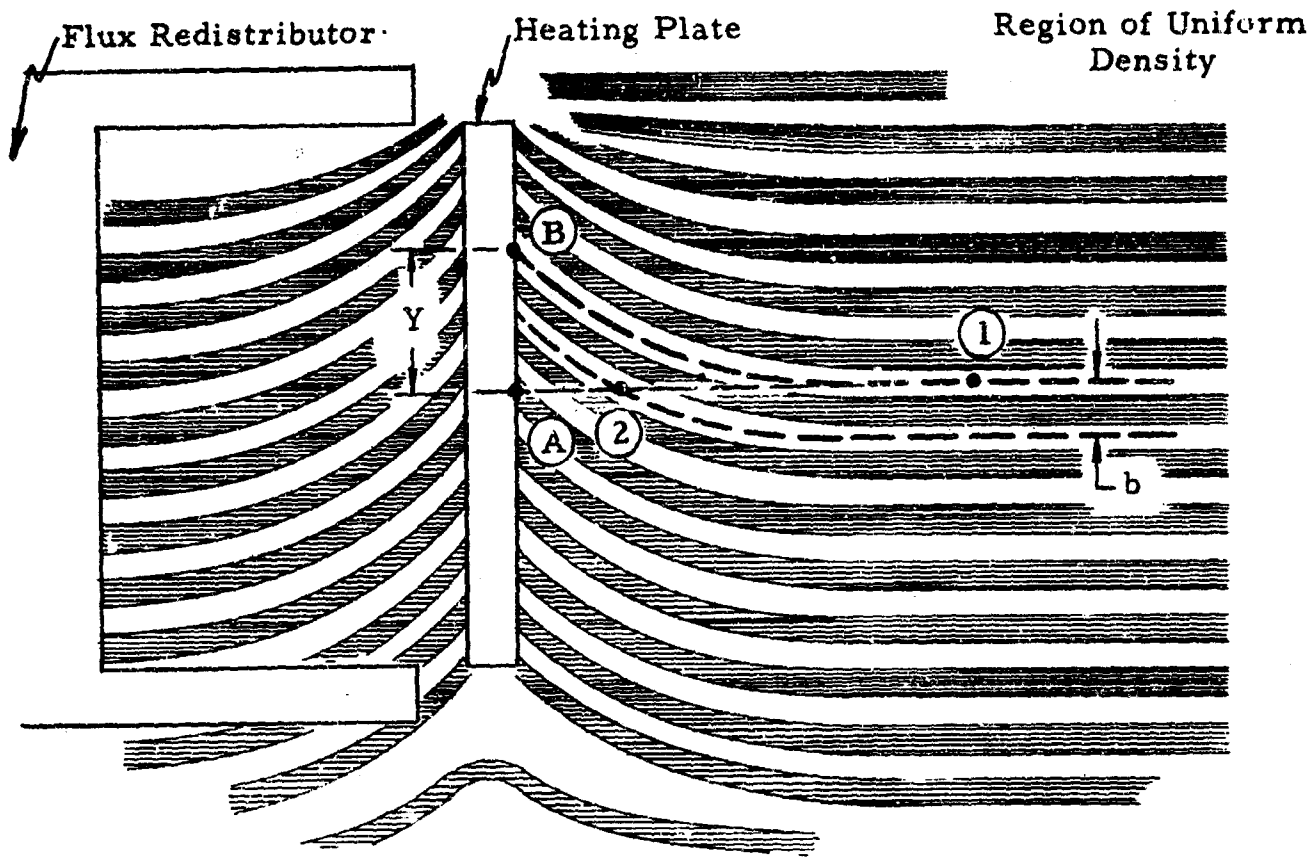

Figure B-3. Measurement of Fringe Shift Number

$$\delta N = \frac{\delta Q}{\lambda} ,$$

where λ is the wavelength of light in a vacuum.

Considering the fringe bending, point 2 represents one whole fringe shift from the uniform undisturbed field at point 1, which indicates that the optical path at point 2 is 1 wavelength different from that at point 1. The number of wavelengths reaching each point, for light traveling distance Z, is given as:

$$N_1 = \frac{Z}{\lambda_1} ; \quad N_2 = \frac{Z}{\lambda_2} ,$$

where λ_1 and λ_2 represent the wavelengths corresponding with light traveling the undisturbed and the deviant paths, respectively. The difference in the number of waves is expressed as:

$$\delta N = N_1 - N_2 = Z \left(\frac{1}{\lambda_1} - \frac{1}{\lambda_2}\right) .$$

Since the index of refraction is

$$\eta_1 = \frac{\lambda}{\lambda_1} ; \quad \eta_2 = \frac{\lambda}{\lambda_2} .$$

The wavelength difference can then be written as

$$\delta N = \frac{Z}{\lambda} (\eta_1 - \eta_2) = \frac{\delta Q}{\lambda} .$$

Independently, Lorenz (using the elastic-solid theory) and Lorentz (using the electromagnetic theory) arrived at the same theoretical law related density of gas with the refractive index.

$$\rho \times \text{constant} = \frac{\eta^2 - 1}{\eta^2 + 2} = \frac{\eta + 1}{\eta^2 + 2}(\eta - 1)$$

where the constant depends upon the molecular nature of the gas. Since most gases have a refractive index very nearly 1, the factor $(\eta + 1)/(\eta^2 + 2)$ is nearly constant and the above equation can be simplified to:

$$C = \frac{\eta - 1}{\rho} ,$$

where C (Gladstone-Dale constant) maintains its constancy for a gas over a wide range of pressure and temperatures.

Between points 1 and 2 in our interference field

$$\frac{\eta_1 - 1}{\rho_1} = \frac{\eta_2 - 1}{\rho_2} = C$$

or

$$(\eta_1 - \eta_2) = C(\rho_1 - \rho_2) .$$

The optical path difference δQ may be written as:

$$\delta Q = Z(\eta_1 - \eta_2) = CZ(\rho_1 - \rho_2)$$

and the wavelength difference or fringe shift number δN is then related to density as

$$\delta N = \frac{CZ}{\lambda}(\rho_1 - \rho_2) .$$

Fringe shift number can be measured at any point in the field directly from the interferogram. For density measurement at the face of a heated body (point A in Figure B-3), fringe crossings can be counted from the undisturbed field along a line parallel to the undisturbed fringes with interpolation made between adjacent fringes intercepting the surface.

Fringe count can also be made from A to B, which gives the same density value at A as when counting directly across from the undisturbed field at 1. The density at B, however, may be different from that at A and a separate determination is necessary at that point.

Since the difference in one fringe shift is equivalent to a difference of one wavelength, another technique is to take the ratio of physical distance Y, e.g., from A to B, to actual fringe width b, which gives the equivalent:

$$\frac{Y}{b} = \delta N = \frac{CZ}{\lambda} (\rho_1 - \rho_2) .$$

The measurement in this instance is for point B. The advantage of this technique is that for adjustment of widely spaced fringes, the physical measurements of Y and b can be made more accurately than with narrow fringe adjustment. (Note that fringe count would be the same regardless of fringe spacing.) The choice of fringe spacing depends on the degree of refraction occurring in the test region and on the field of view available for measurements.

Since, in our measurements, we are actually interested in the temperature boundary field near a heated object rather than density, the gas law equation can be applied. Any convective flow of gas near the heated body is of sufficiently low velocity that pressure can be assumed constant throughout, and we arrive at the expression:

$$\delta N = \frac{CZ\ \rho_1}{\lambda} (1 - \frac{t_1}{t_2})$$

or, in terms of the unknown temperature t_2

$$t_2 = t_1\left[\frac{1}{1 - \frac{\delta N \lambda}{CZ\rho_1}}\right] = t_1\left[\frac{1}{1 - \frac{\delta N \lambda R t_1}{CZP}}\right],$$

where R is the gas constant and P the ambient pressure. For a given gas and for monochromatic light of given wavelength, $\lambda R/C$ is constant. Ambient pressure, temperature, and body length are measured to solve the expression for unknown temperature t_2. When the quantity $(\delta N \lambda R t_1)/(CZP)$ is small compared to 1, it is convenient for computational purposes to convert the bracketed expression in the above equation into a series expansion

$$t_2 = t_1\left[1 + \left(\frac{\delta N \lambda R t_1}{CZP}\right) + \left(\frac{\delta N \lambda R t_1}{CZP}\right)^2 + \left(\frac{\delta N \lambda R t_1}{CZP}\right)^3 + \ldots\right].$$

The above relationships permit a localized density or temperature determination in the two-dimensional plane from a single interferogram taken while the refractive variances are occurring. The undisturbed interference field to the right of the heated body is the reference region of uniform density. However, if the test region is enclosed and pressure or temperature changed uniformly throughout, the region of uniform density cannot then be taken as an absolute reference. The entire fringe field will shift and reference must necessarily be made to the optical path length in the external compensating beam.

If the fringe shift in the uniform density field can be observed and measured (assume that a temperature change occurs in the test chamber), then temperature t_2 can again be determined by the equation:

$$t_2 = t_r\left[\frac{1}{1 - \frac{\delta N \lambda R t_r}{CZP}}\right],$$

where the reference t_r, is itself determined from the same equation; thus,

$$t_r = t_c \left[\frac{1}{1 - \frac{(\delta N)_c \lambda R t_c}{C Z_{TC} P}} \right],$$

where $(\delta N)_c$ is the fringe shift in the uniform field with respect to the compensating optical path, t_c is the external temperature in the compensated path, and Z_{TC} is the path length through the test chamber.

With monochromatic light the fringe shift in a uniform field is difficult to measure since all fringes are alike, indistinguishable one from another. The use of white-light makes this measurement possible since each fringe can be identified and a shift in the uniform density field can easily be determined.

The interferometer equation for predicting temperature can be plotted for different plate lengths Z. From these plots (and, as shown by equations) the sensitivity and accuracy of the interferometer to predict high temperature decreases. From the above developed equations when

$$\frac{\delta N \lambda R t}{C Z P} = 1$$

the predicted temperature would become infinite. The fringe shift number δN has a discrete maximum value for a given plate length Z.

III. DISCUSSION OF ERRORS

Deviation from 100 percent correlation is shown for the fringe shift temperature prediction versus the thermocouple-measured temperature in Figures B-4 and B-5. In practice the calibration curve would suffice to determine interferometric fringe-shift temperature. However, since errors such as end effects and refraction effects have been treated extensively in the literature, these and other errors must be considered.

A. Fringe Shift Measurement

The scatter of data points from a mean datum line is attributed to fringe count accuracy. Our measurements were made by projecting the original interferogram negative onto a screen. From the enlarged interference field (25-50X scale) extrapolations between fringe lines were made with a ruled scale. Variation between separate readings or between readings made by different individuals was ±0.1 fringe with a mean variation of approximately 0.05 fringe. An error of ±0.1 fringe for a total shift of 5 fringes would give ±2 percent deviation, and for a shift of a single fringe the deviation would be ±10 percent. Better absolute accuracy could be made by using a microscope and mechanical stage arrangement to correct for projection distortion. Kendall[2] describes an interferometer fringe pattern analyzer used for routine measurements which has an accuracy of at least 0.1 fringe. Werner[3] devised a means to measure fringe shift with indicated accuracy of better than 1/500th of a fringe separation.

B. Ambient Condition Errors

As shown in the preceding equations, relation of fringe shift data to temperature measurement requires knowledge of the ambient pressure

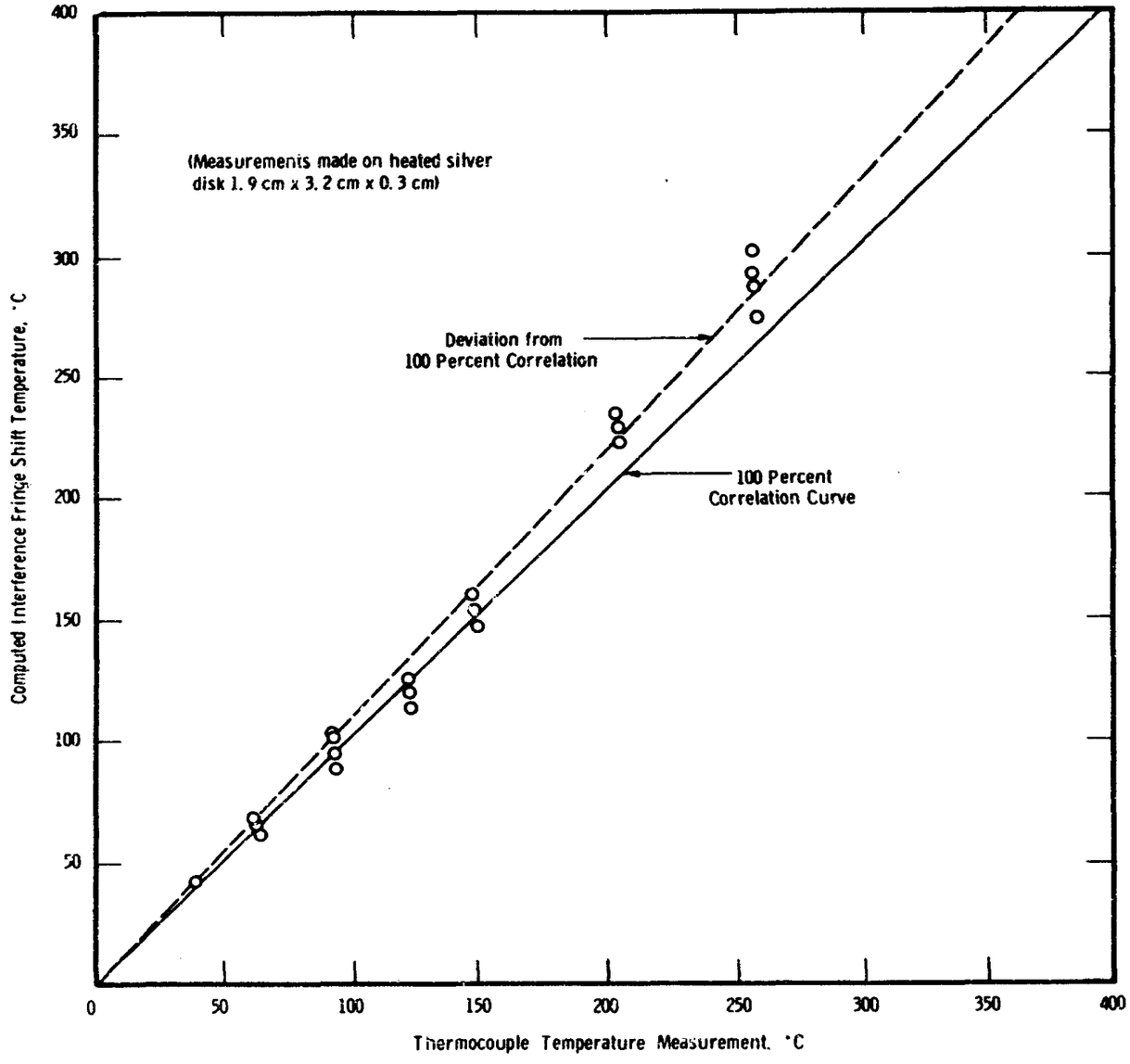

Figure B-4. Correlation of Predicted Interference Fringe Shift Temperature with Thermocouple Measured Temperature (3.2 cm Plate Length)

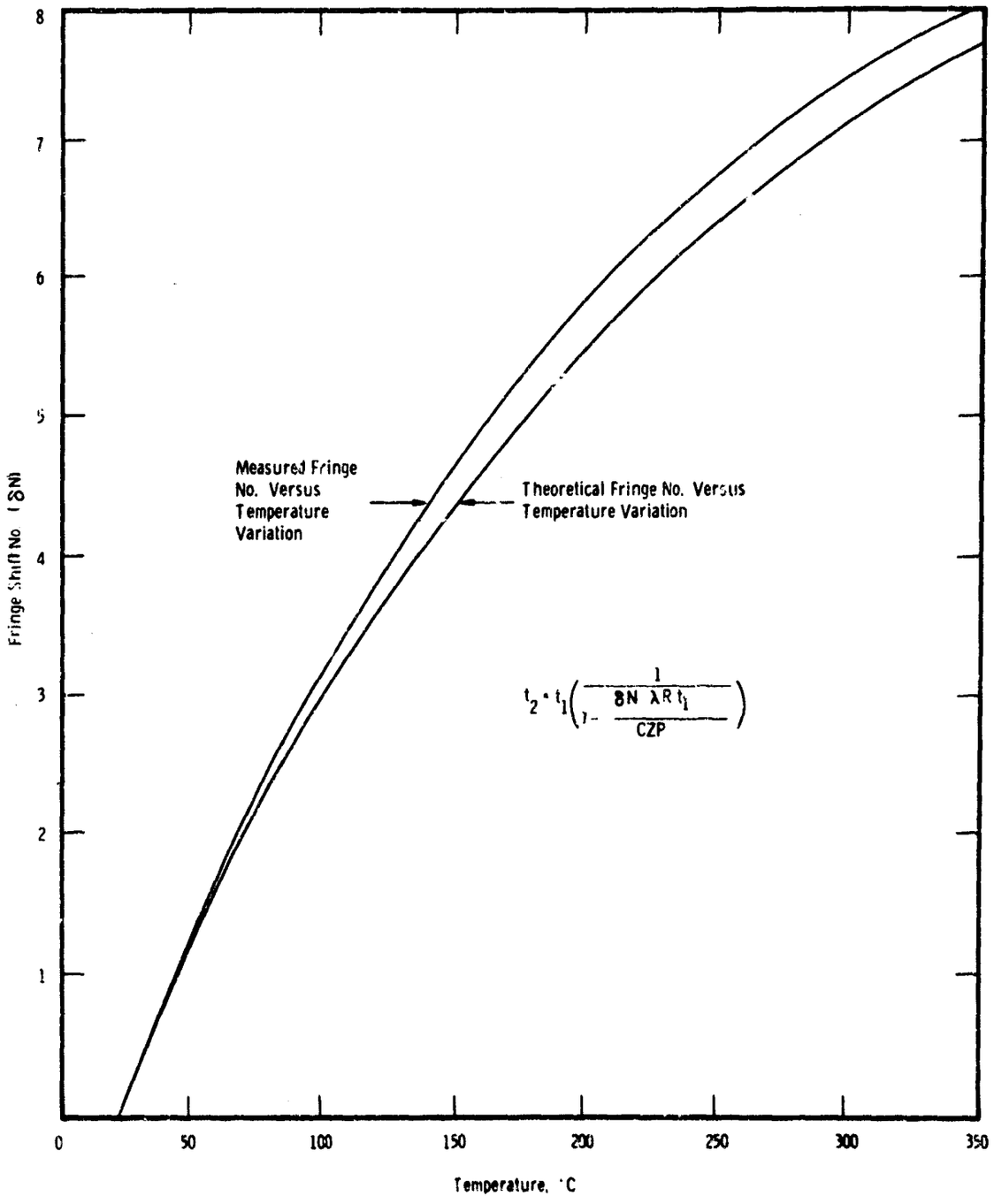

Figure B-5. Variation of Fringe Shift Number with Temperature, Measured and Theoretical (3.2 cm Plate Length)

and temperature. The effects of variations of each for a given plate width (3.18 cm), are shown in Figures B-6 and B-7.

C. Refraction Effect Errors

Light passing through the thermal boundary field near a heated object is bent away from the surface toward the undisturbed region of greater density. Since the path deviates through layers of increasing density, the average density through which the beam passes is higher than it would be if refraction did not occur. Fringe shift count would be less since the difference in density between the undisturbed region and the averaging density is less.

In aerodynamic studies refraction errors were considered by Gooderum, et. al.,[4] Blue,[5] Ladenburg and Bershader,[6] and Howes and Buchele,[7] among others. Gooderum defines the problem quite well and for his study of turbulent mixing of a free supersonic jet found, from developed expressions, that the effects of refraction were negligible. Blue suggests that a wind-tunnel width dimension for a particular boundary layer study be such as to make the sum of refraction error directly proportional to the square of tunnel span. Ladenburg and Howes and their associates present very elegant expressions to correct for refraction effects applicable to wind tunnel conditions.

In heat transfer studies Kennard[8] did not mention refraction errors or may not have been aware of them. Eckert and Carlson[9] in early laminar-free convection studies did not consider the refraction errors, but in a later report Eckert and Soehngen[10] derived a correction for light ray refraction in determining heat transfer coefficients around cylinders in cross flow. The temperature correction was given as

$$\delta t = \frac{CZ^2}{12\,\eta_1} \quad \frac{P}{R\,t_1^2} \left(\frac{dt}{dx}\right)^2 ,$$

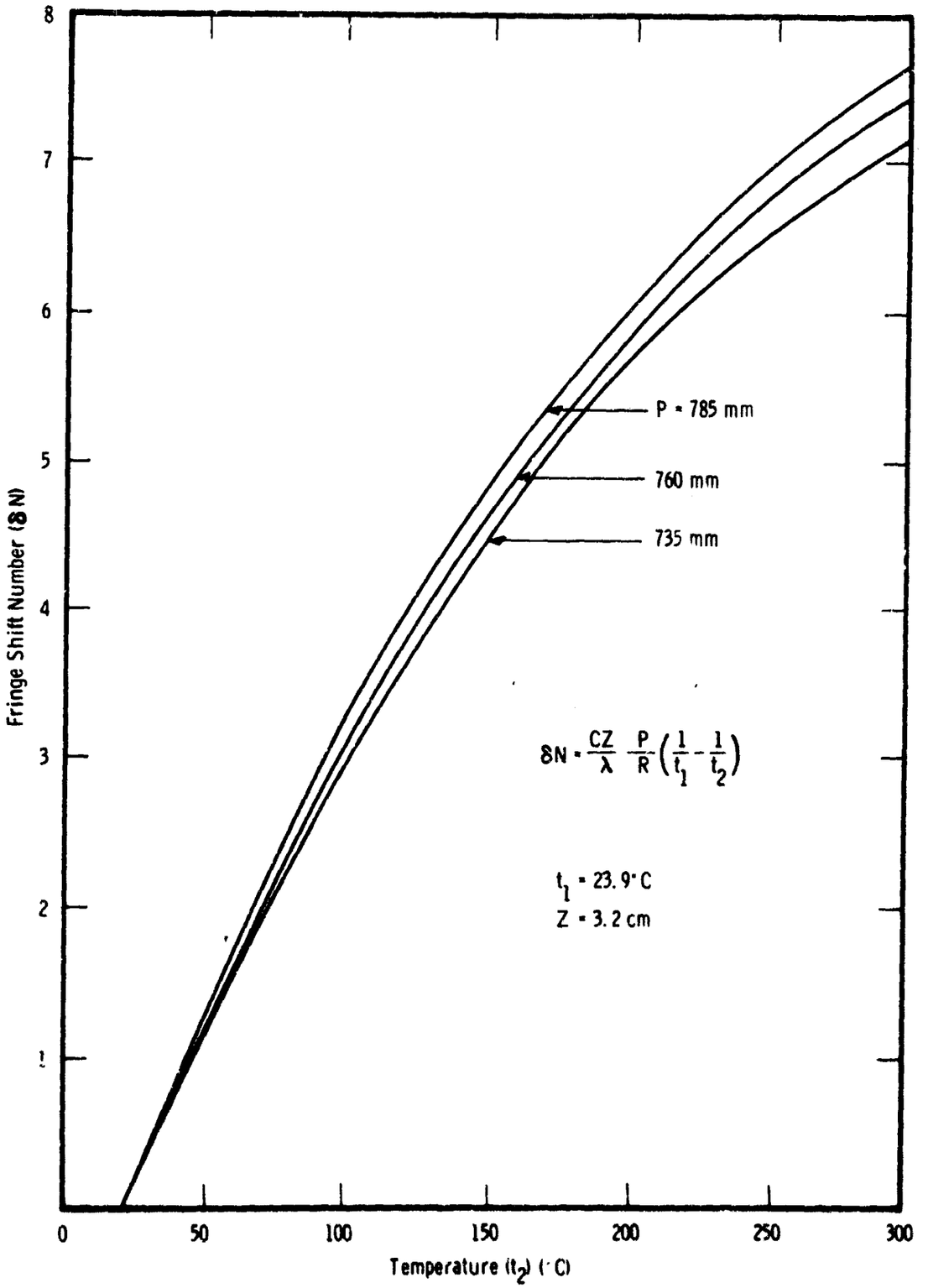

Figure B-6. Variation of Fringe Shift Number with Temperature for Changes in Ambient Pressure

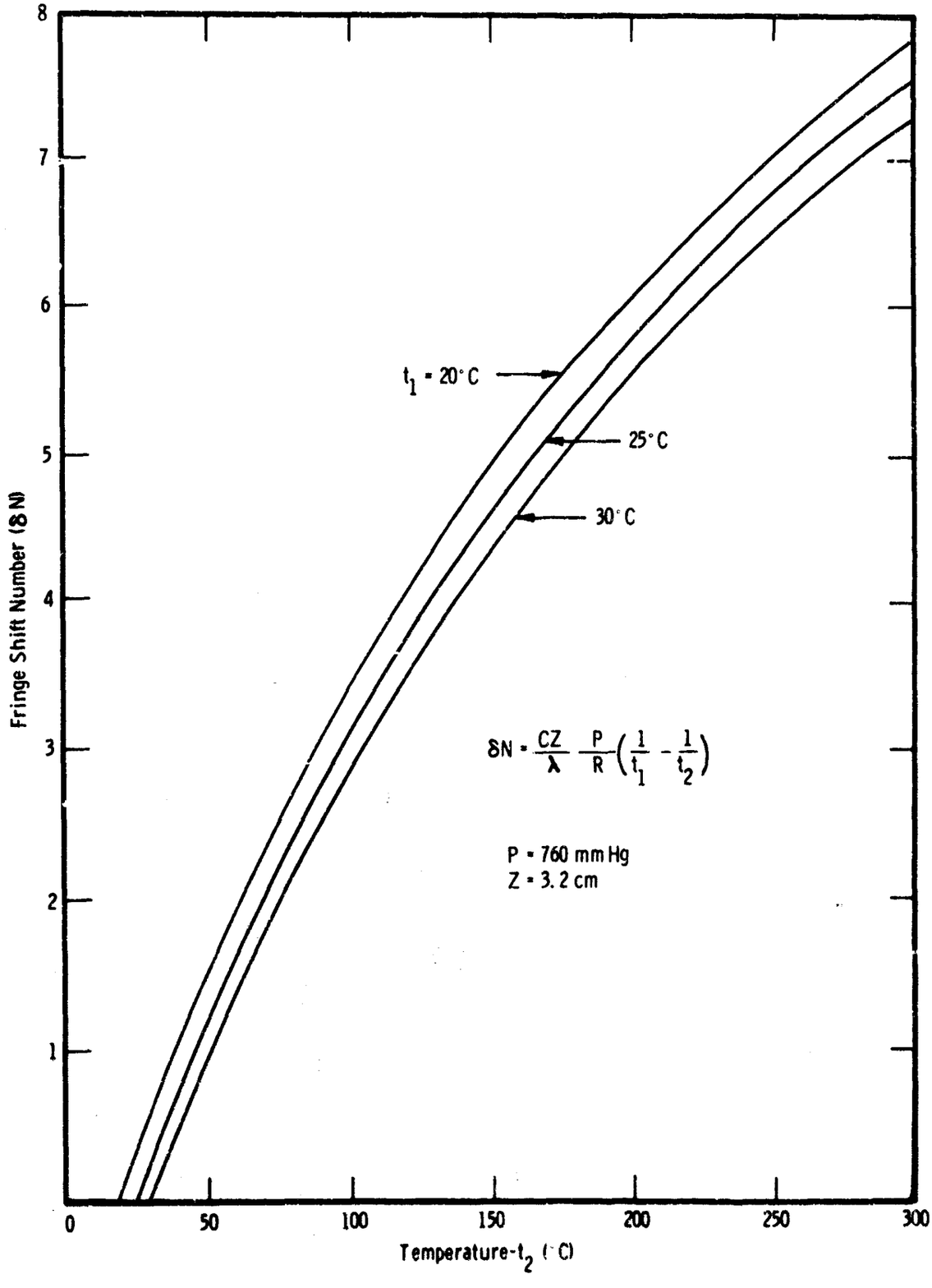

Figure B-7. Variation of Fringe Shift Number with Temperature for Changes in Ambient Temperature

where C is the Gladstone-Dale constant, Z the object length, P reference pressure, R gas constant, and t_1 reference temperature. The temperature gradient $\left(\frac{dt}{dx}\right)$ is determined from the temperature boundary profile as shown in Figure B-8.

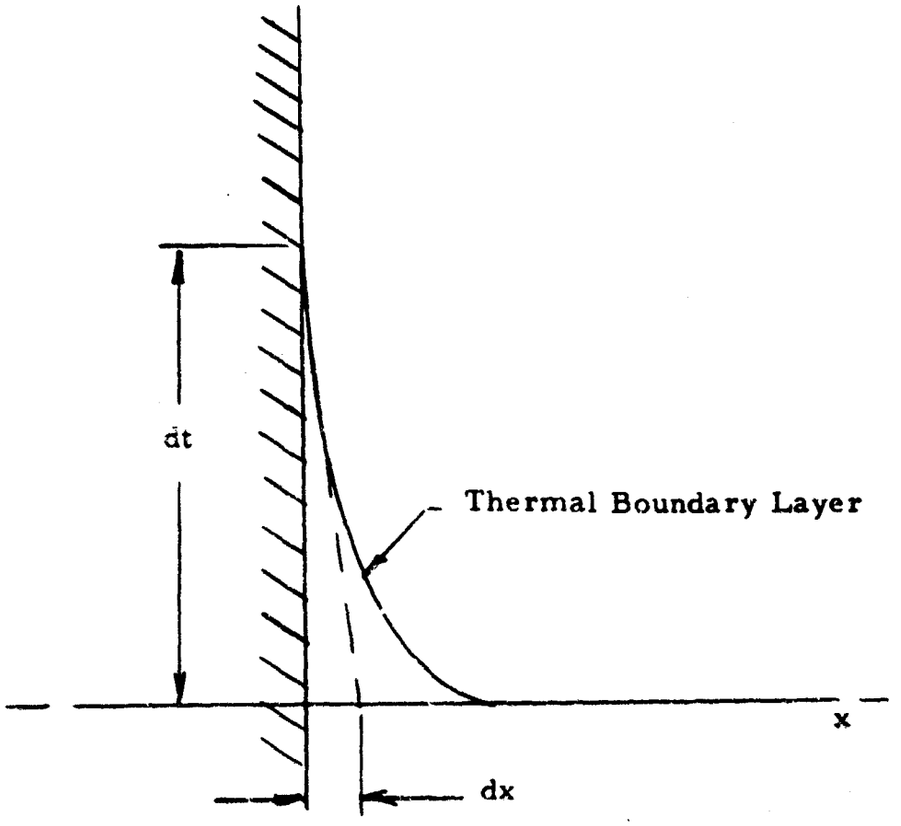

Figure B-8. Temperature Gradient at Wall

Goldstein and Eckert[11] used the derivation developed by Eckert and Soehngen[10] and found that the refractive error was less than 1/2 percent in his free convective boundary layer measurements on a uniformly heated vertical plate. The length dimension of his plate was approximately 10 cm. Carlson[12] applied the same correction

equation, and for a temperature difference of 71 C across an air gap between two 30 cm-wide plates, calculated a negative 2 percent error. Our calculations for refraction errors, using the above relationship, show that for even large temperature gradients, refraction error is very small. The refraction errors may be significant if Z is very large, δt is very large, and a very thin boundary layer exists (forced convection flow).

D. End Effect Errors

The most significant error in fringe shift prediction of temperature for our investigations is the effect of increased path length due to heated air extending beyond the ends of the specimen. The effect of length on fringe shift count for a given temperature is shown in Figure B-9. Compared with variation in ambient temperature or ambient pressure, Figures B-7 and B-6, the length characteristic is considerably more significant.

Before an end correction can be appropriately applied, some consideration of the boundary layer at the ends of a heated specimen must be made. The interferograms in Figures B-10 and B-11, show isotherms about a heated disc. It can be imagined that the boundary layer at the ends would be somewhat similar to that showing at the bottom of the disc. The boundary layer would increase in thickness with vertical height as the convective flow rises and the correction would be different from the bottom to the top of the disc (see Figure B-12).

In our measurements the indicated fringe shift temperature was indeed higher along the vertical axes with fringe count increasing 0.1 to 0.3 fringes from the bottom quarter to the middle of the disc. From the middle to the top of the disc the increase was less (0.1 fringe). An effort was made to determine whether any temperature variations existed along the plate by providing a differential thermocouple circuit

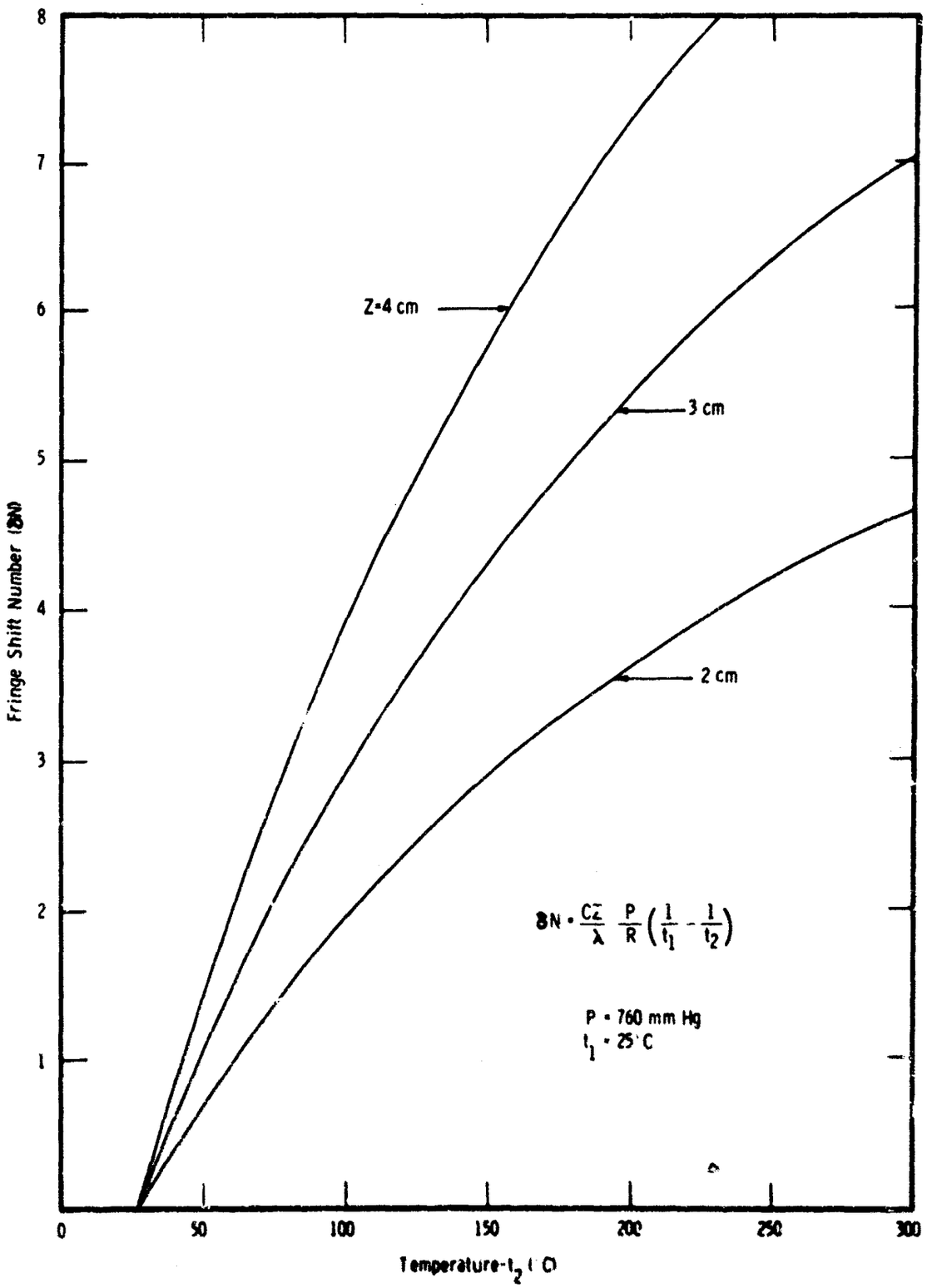

Figure B-9. Variation of Fringe Shift Number with Temperature for Various Specimen Lengths

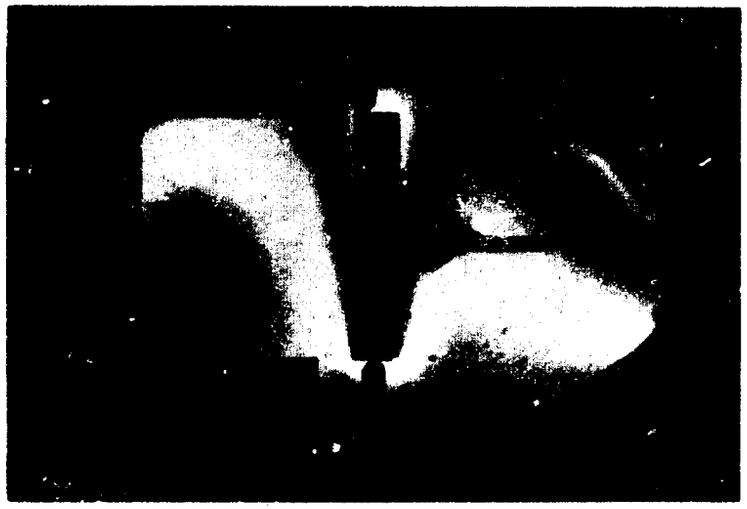

a. 38°C

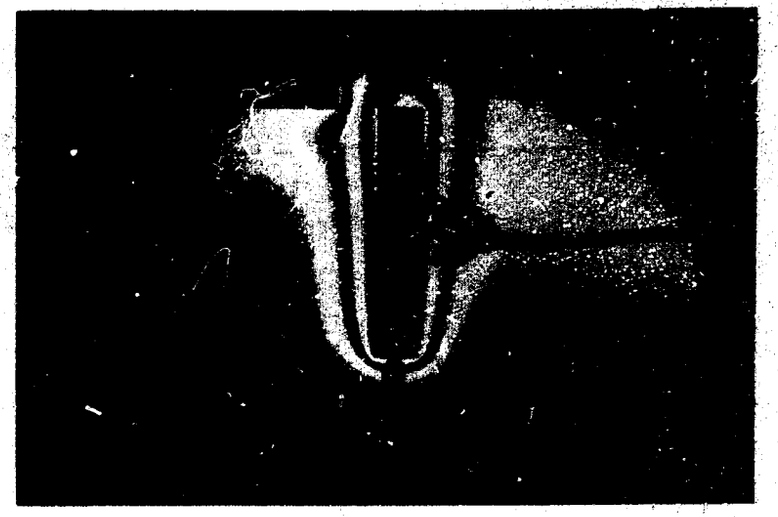

b. 65°C

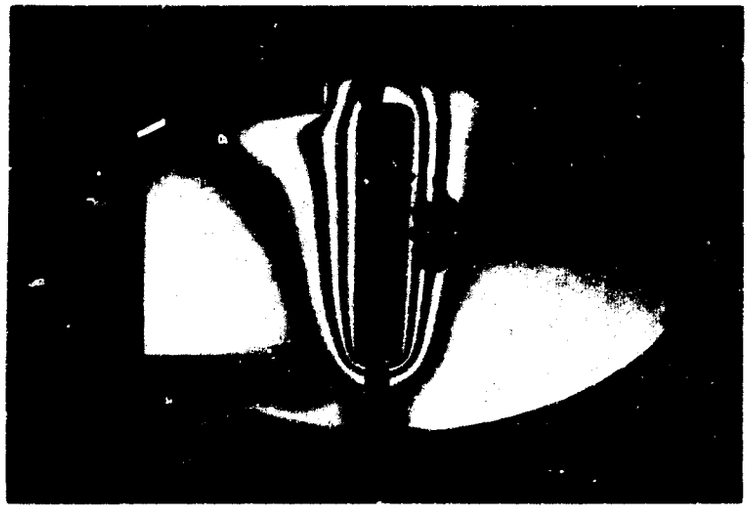

c. 99°C

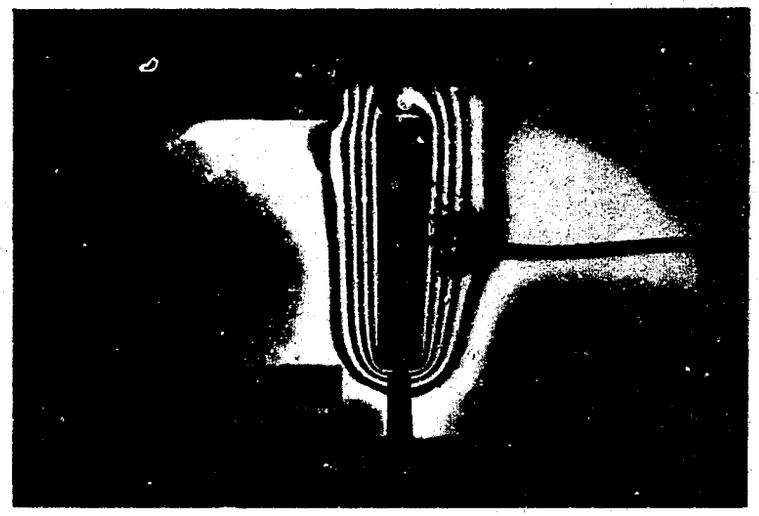

d. 120°C

Figure B-10. Constant Temperature Contours for Vertically Heated Plate

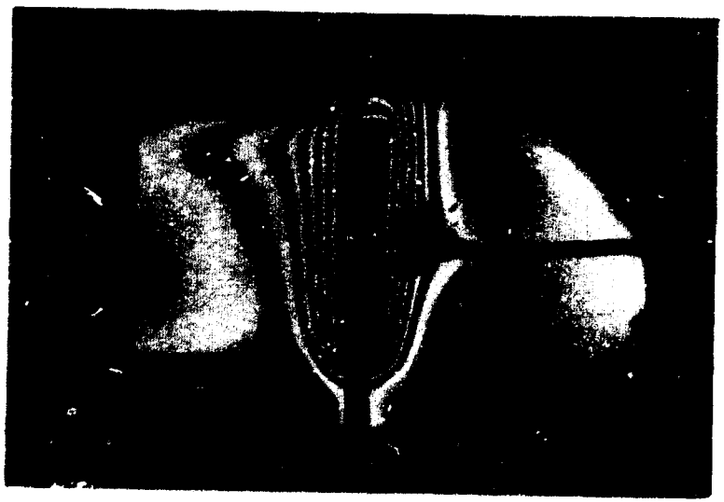

a. 150°C

b. 150°C, Turbulence Caused by Light Blowing

Figure B-11. Constant Temperature Contours for Vertically Heated Plate at 150 C

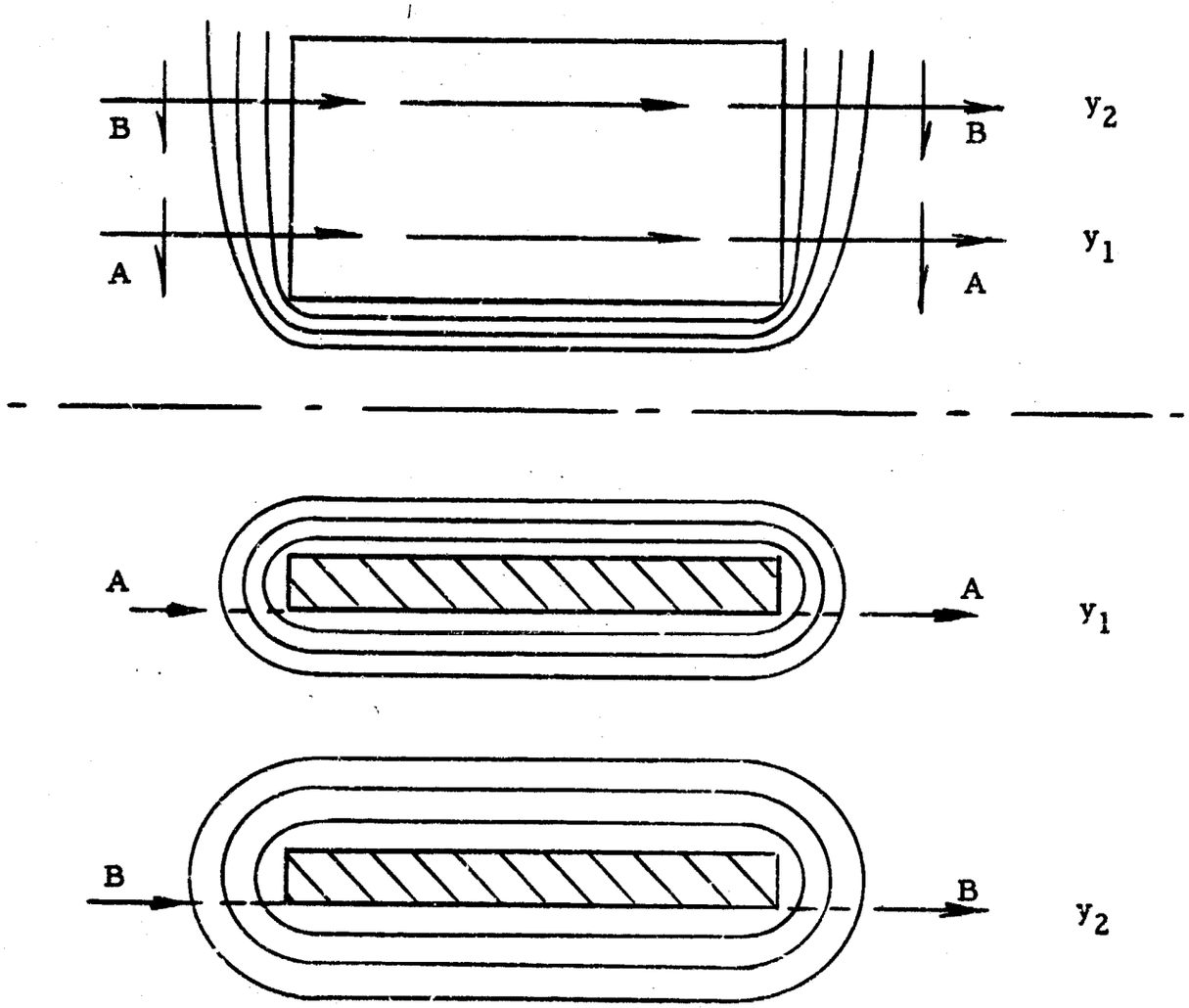

Figure B-12. Views of Heated Plate Showing Isotherms and Boundary Layers as a Function of Vertical Height

to measure temperature difference from center to edge of the disc. Although the tests were inconclusive, indications were that gradients, if existing, were extremely small because of the high thermal diffusivity of silver. More significant gradients might be encountered with fabrics or materials of low conductivity.

With increased temperature, or with time, the boundary layer thickness and end corrections would not remain the same at any path position. This time-temperature effect would certainly be true for transient heating experiments, and probably not as time-dependent when measurements are made during free convective cooling. Under forced convection conditions the entire boundary layer could be radically changed.

Kennard[8] made several assumptions regarding the end corrections. Without allowance for end effects he found that the interference temperature indication was approximately 5 percent higher than the temperature in the plate itself. His correction as one assumption amounted to simply ascribing a 5 percent increase in length. Eckert and Carlson[9] made a reasonable approximation of the end effects by the method of conformal mapping. Goldstein and Eckert[11] and Carlson[12] all considered end effects by the method proposed by Eckert and found, for their conditions of long interference path (10 cm to 30 cm) and thin plate, that end corrections were small and tended to cancel refraction errors of opposite magnitude. Bevans[13] failed to arrive at any quantitative correction for end effects in his experiments of vertical free convection from an isothermal surface. All of the above corrections were made for steady-state or near steady-state conditions.

Experimental and theoretical investigations of the free convection boundary layer growth with time on semi-infinite vertical flat plates under different conditions of heat input are described in the review by Goldstein.[14] We have yet to correlate our experimentally produced boundary profiles with prediction by others. The variations with time, temperature, and vertical location for a given heat input

function describe the difficulty in assuming an end correction based on the boundary layer or thermal boundary condition at the end of the plate.

E. Other Errors

Other errors are inherent in the system. For example, alignment of the test specimen must be perfect with respect to the collimated light beam, or surface fringe shift measurements cannot be made (alignment can be made perfect only if the source is infinitely small and the collimating lens perfectly corrected for the wavelength of light). Also, reference temperature in the undisturbed region must be correctly known or readily determined. Changes of the refractive index due to foreign gases have been mentioned as error possibilities. Heat flux uniformity through the flux redistributor is not optimum and non-adherence to two-dimensionality causes averaging errors. Heated air within the distributor may generate convection flow irregularities. Aberrations in the interferometer optics or lens can distort fringe patterns significantly. Enlargement of interference pictures may give distortion errors.

There are other possible errors but, with due precaution, these and the above sources of error can be reduced or made negligible.

IV. INTERFEROMETER LIGHT SOURCE AND PHOTOGRAPHIC REQUIREMENTS

In optimizing performance characteristics of the interferometer various undisturbed fields or no flow tests were carried out using different light sources and optical filters. Unfortunately the requirements of monochromatic light for optimum fringe patterns and high intensity light for short duration exposures tend to be conflicting thus simultaneous optimization is extremely difficult.

A Pek Model 200-watt high pressure mercury light source met the necessary light intensity and spectral requirements and subsequent interference studies were made with this source. This lamp is capable only of continuous operation and has an effective source size of 0.25 cm x 0.18 cm.

In conjunction with the mercury source, nearly monochromatic light was obtained by using a Baird Atomic Corporation 5641 A type bl interference filter. With the interference filter 90% of the light intensity was lost either in the basic filtering process or in filter absorption or reflection in its bandpass range. Other factors reduce the lightintensity further, such as losses in the interferometer optics (one beam splitter discards 50% of the light in each beam), the small effective source size required and the magnification of image desired. The effective source size (pinhole diameter) was varied and fringe quality found to improve by decreasing the hole diameter. Smaller pinhole sizes than 0.1 centimeters did not appreciably improve the fringe rendition.

The light intensity at the image plane was measured with a light dependent resistor having a negative coefficient of resistance linear over an extremely wide range of light intensities. The light intensity-resistance values for different films were determined and relationships for image magnification, pinhole size and shutter speed expressed.

V. TEMPERATURE CALIBRATION OF INTERFEROMETER

Tests were conducted to calibrate and verify experimentally the ability of the Mach-Zehnder interferometer to indicate temperature directly. The investigation of a free convection boundary layer on a heated plate is a convenient way to check the validity of data. A calorimeter with front and/or rear surface mounted thermocouple was positioned at the flux redistributor exit. These discs were made of silver and had widths corresponding to the actual fabric test pieces (3.2 centimeters, 3.8 centimeter wide). Interferograms were taken of the arc heated disc at different temperatures and fringe shift calculations of surface temperatures were compared with thermocouple measurements.

For interference fringe shift measurement of temperature the undisturbed field behind the calorimeter was taken as an ambient reference temperature. The field between the top and the bottom redistributor plates was found to seek a higher temperature level after each exposure and was not used as ambient reference. Representative interferograms, Figure B-13, show silver discs at different temperatures. Figure B-14 shows a comparison of fringe shift temperature prediction of 3.8 centimeter disc with the thermocouple measurements for temperatures to 150° C. Figure B-15 shows a correlation comparison for a 3.2 centimeter disc up to 350°C in terms of fringe shift number.

Figure B-13a. Interferogram of Thin Heated Plate (275 C)

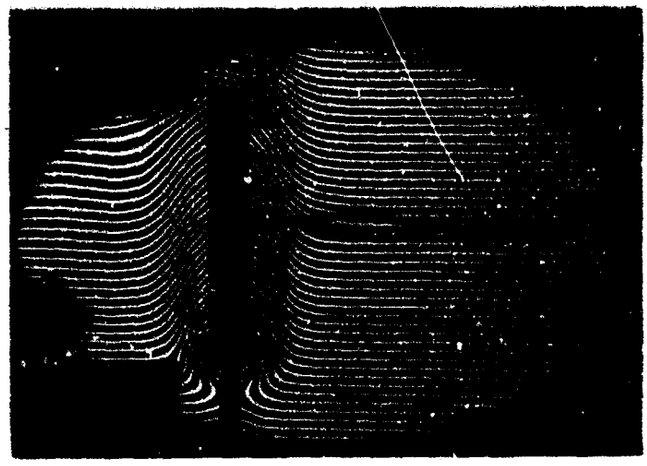

Figure B-13b. Interferogram of Thick Heated Plate (350 C)

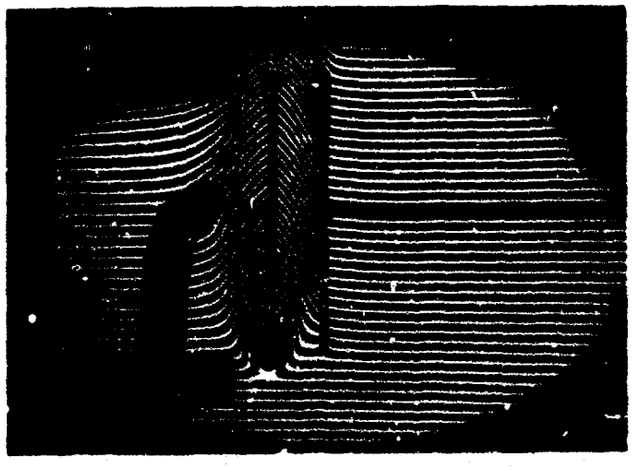

Figure B-13c. Interferogram of Two Thin Heated Plates (Front Plate 375 C)

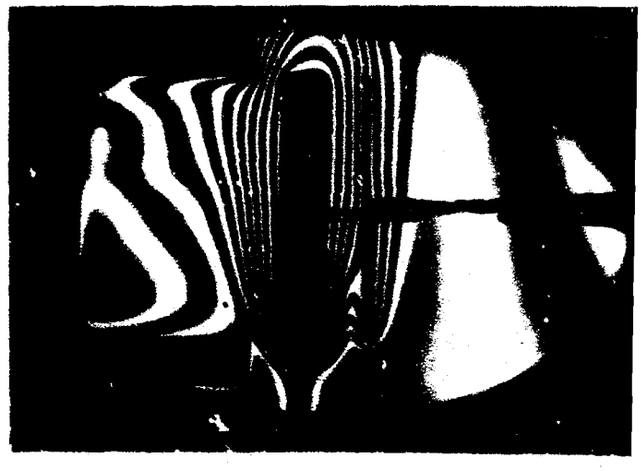

Figure B-13d. Interferogram of Thick and Thin Heated Plates, Infinite Fringe (Front Plate 325 C)

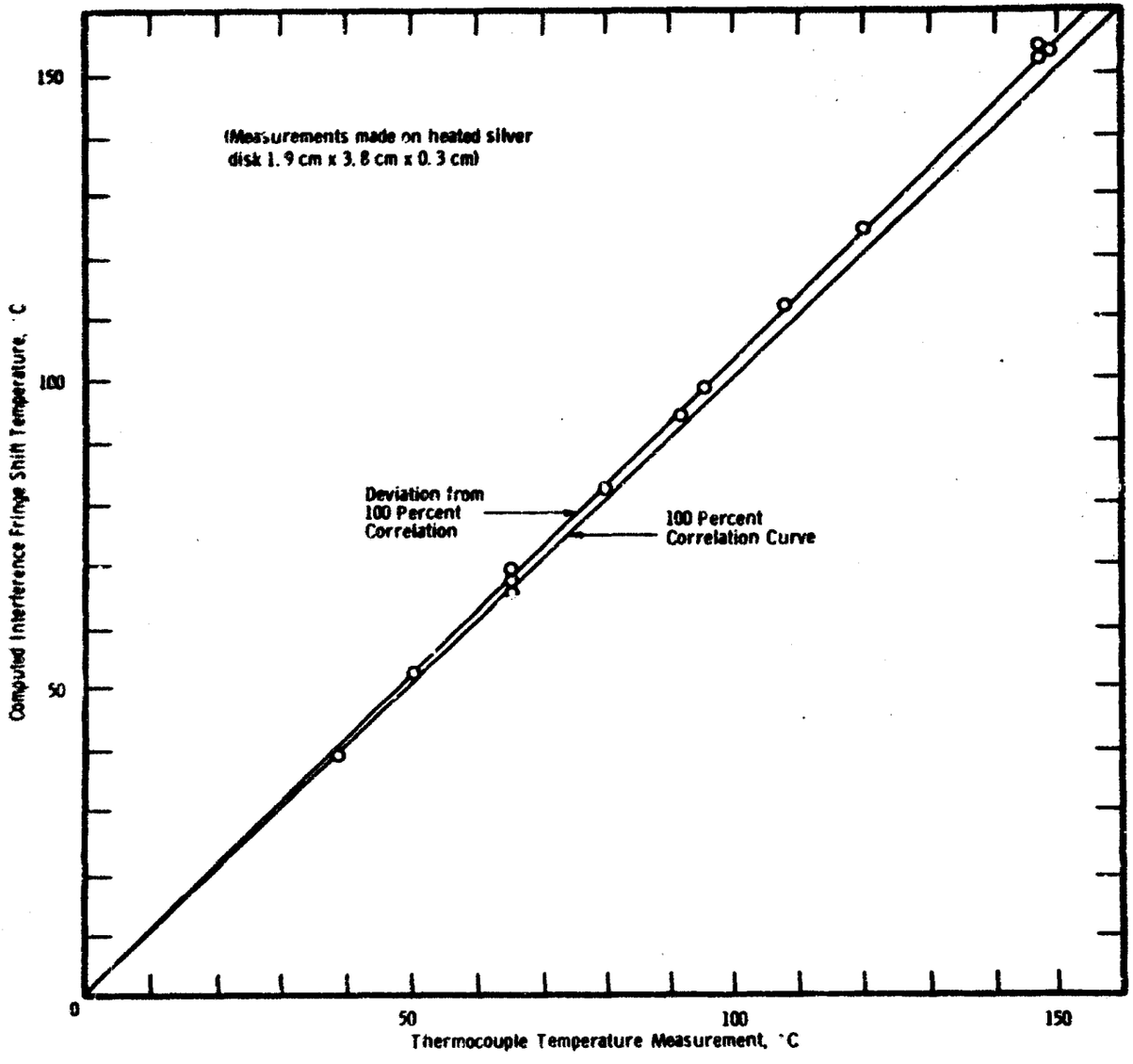

Figure B-14. Correlation of Predicted Interference Fringe Shift Temperature with Thermocouple Measured Temperature

NOMENCLATURE

Symbol	
b	fringe width
C	Gladstone-Dale constant
N	number of wavelengths
δN	wavelength difference or fringe shift count
$(\delta N)_c$	fringe shift referenced to compensated optical path
η	refractive index
P	ambient pressure
δQ	optical path difference
R	gas constant
t	temperature
x, y, z	rectangular coordinates
Y	fringe shift
Z	length of heated body
Z_{TC}	length of test chamber
ρ	density
λ	wavelength of light in vacuum

Subscript	
$1, 2$	location
r	reference

VI. REFERENCES

1) Litton Systems, Inc. Applied Science Division. Report no. 2598. Second annual progress report on thermal-physical parameters of materials, by R. E. Larson, et al. Contract DA-19-129-QM-1998 (OI 6082) (August 5, 1964).

2) U. S. Naval Ordnance Laboratory. Report No. 1596. The NOL interferometer fringe pattern analyzer, by J. M. Kendall (1952).

3) Werner, F. D. and B. M. Leadon. Very accurate measurement of fringe shifts in an optical interferometer study of gas flow. Rev. Sci. Instr. 24: 121-24 (1953).

4) National Advisory Committee for Aeronautics. Technical Note 1857. Investigation with an interferometer of the turbulent mixing of a free supersonic jet, by P. B. Gooderum, G. P. Wood, and M. J. Brevoort (1949).

5) ----. Technical Note 2110. Interferometer corrections and measurements of laminar boundary layer in supersonic stream, by R. E. Blue (1950).

6) Landenburg, R. W. and D. Bershader. Interferometry. In physical measurements in gas dynamics and combustion. Princeton, N. J. Princeton University Press, 1954. pp. 47-78.

7) National Advisory Committee for Aeronautics. Technical Note 2693. A theory and method for applying interferometry to the measurement of certain two-dimensional gaseous density fields, by W. L. Howes and D. R. Buchele (1952).

8) Kennard, R. B. An optical method for measuring temperature distribution and convective heat transfer. J. Res. Nat. Bur. Std. 8: 787-805 (1932).

9) Eckert, E. R. G. and W. D. Carlson. Natural convection in an air layer enclosed between two vertical plates with different temperatures. Intern. J. Heat Mass Transfer 2: 106-20 (1961).

10) Eckert, E. R. G. and E. Soehngen. Distribution of heat-transfer coefficients around circular cylinders in crossflow at Reynolds Numbers from 20 to 5000. Trans. ASME 74: 343-47 (1952).

11) Goldstein, R. J. and E. R. G. Eckert. The steady state and transient free convection boundary layer on a uniformly heated vertical plate. Intern. J. Heat Mass Transfer 1: 208-18 (1960).

12) Carlson, W. D. Interferometric studies of convective flow phenomena in vertical, plane enclosed air layers. Ph.D. Thesis, University of Minnesota (1956).

13) Bevans, J. T. Vertical free convection from an isothermal surface. Ind. Eng. Chem. 49: 114-19 (1957).

14) Goldstein, R. J. Interferometric study of the steady state and transient free convective thermal boundary layers in air and in water about a uniformly heated vertical flat plate. Ph.D. Thesis, University of Minnesota (March 1959).

APPENDIX C

INTERFEROMETRIC DETECTION OF DEGRADATION PRODUCTS

I. GENERAL

Quantitative evaluation of fringe shift data yields an accurate indication of temperature provided additional information is available during release of degradation gases. Among various constants and physical parameters that enter into the equations the gas constant and variation of index of refraction with density must be known.

As fabric absorbs high intensity thermal-radiation a condition is soon reached during which degradation processes start. Changes are evidenced by release of various degradation products accompanied by both exothermic and endothermic heat exchanges. These reactions are sensitive not only to temperature level but to temperature change rates as well. Knowledge of the various gas concentrations in the free convective boundary layers adjacent to the heated fabric is required to allow the assignment of effective gas properties to be used in the temperature evaluation equations.

From preliminary motion picture sequences it was observed that gaseous products were emitted from the fabric at various instances, particularly during the final heating phase. These gases showed as light or dark areas in the interference pattern which would develop initially at the fabric surface and subsequently move out into the boundary layer surrounding the fabric. Although no sharp discontinuities were displayed in the interference fringe patterns, it was recognized that the actual fabric temperature or temperatures in the thermal boundary layer differed from the indicated values due to the presence of gas having an index of refraction different from that of air. It was also recognized that if the reactions occurring have any resemblance to chemical temperature effects of known constituents, the interferometer technique would be ideal for indicating composition.

Two interferometer techniques were considered to determine the extent to which interference fringe shifts temperature data varied from actual values. A two or more wavelength technique and a multi-

environmental experimental technique were considered, the latter extensively utilized in this present program.

II. MULTI-WAVELENGTH INTERFEROMETER TECHNIQUE

A. General

Olsen[1] applied this interferometric method to measure chemical composition and temperature of a multi-component gas mixture. This can be accomplished even when chemical changes occur in the gas mixture. As Olsen points out, the application of this method to combustion processes is complex because of the many gas components present and because of the high temperatures and temperature gradients encountered. No information was found as to how the refractive index for different gases varies with temperatures. In his study of steady-state combustion occurring in Bunsen flames, Olsen first worked out a derivation to apply to a binary gas mixture. His analysis was limited to a two-dimensional air-oxygen jet, but indications show that a more complex mixture can be studied.

Ross, El-Wakil and C. Jaeck[2,3] used the two wavelength interferometric technique for the study of vaporization and combustion of fuels and indicated the usefulness of this method for heat and/or mass transfer investigations.

In our studies such a technique appeared very useful. Initially, a water-saturated fabric was heated with an arc furnace in which release of water vapor associated with the heats of vaporization could be studied. It was conceived that the water would be evaporated from the fabric surface at or somewhat above 100°C. A period of constant temperature exists during vaporization and until the water is fully released, as evidenced by the temperature plateaus in the temperature-time recordings. The indicated fabric surface temperature during vaporization was approximately 150 to 175°C.

To evaluate the two or more wavelength technique a more rigorous investigation of refractive variances associated with the release of water vapor or other foreign gases was conducted.

B. General Temperature Relationship

The relationship expressing temperature changes in air surrounding a heated fabric in terms of fringe distortion has been worked out for our particular studies.[4] The expression is given as

$$\frac{t_2}{t_1} = \frac{1}{1 - \frac{\delta N \lambda}{CZ\rho_1}} \qquad \text{(C-1)}$$

The reference density ρ_1 is determined from the perfect gas relationship

$$\rho_1 = \frac{p}{Rt_1} \qquad \text{(C-2)}$$

where pressure p and temperature t_1 are easily measured in the undisturbed field.

C. Constant of Proportionality

The basic expression relating the index of refraction to gas density for a given wavelength of light includes a constant of proportionality C that would be different for the different wavelengths of light used in the multi-wavelength technique.

Since this number is important it can be considered in some detail.

The proportionality constant is arrived at through the general dispersion expression developed by Lorentz (1936):

$$\frac{\eta^2 - 1}{\eta^2 + 2} = \sum \frac{4}{3} \pi V_o^2 N \frac{e^2}{m} \frac{1}{\frac{1}{\lambda_o^2} - \frac{1}{\lambda^2}} \qquad \text{(C-3)}$$

where N is the number of molecules per unit volume of the gas and, therefore, is proportional to density. The remainder of terms in the summation of the right-hand side of the expression is equal to a constant K, relating density and the index of refraction, and includes the terms e and m, electron charge and mass; V_o, velocity of light in vacuum; λ_o, wavelength of light in vacuum; and λ, the variable wavelength in the summation of dispersion values. For one wavelength of light and for one medium (air), a linear approximation of the Lorentz-Lorenz equation, based on the fact that the index of air is nearly equal to 1, yields the proportionality constant C:

$$C = \frac{\eta - 1}{\rho} \tag{C-4}$$

where C is simply 3/2 K.

This equation (Gladstone-Dale expression 1858, 1863) was experimentally verified and actually preceded the Lorentz-Lorenz relationship, which corrected deviations resulting when a liquid passes to a gaseous state. The constancy of C or K for the Lorentz-Lorenz expression is markedly superior over that of the Gladstone-Dale approximation when the pressure or density of gas increases greatly. However, in the present study the linear expression for density and refractive index provides a constant of proportionality unchanged for the range of conditions encountered.

The exactness in the measure of C is dependent on how accurately ρ_1 can be measured and how precisely η is known for the particular wavelength of light. For our tests, C was calculated from tabulated index values predicted and measured by Edlen[5,6] for standard conditions. Edlen's index of refraction expression is given as

$$(\eta_s - 1)\, 10^8 = 6432.8 + \frac{2949810}{146 - \frac{1}{\lambda^2}} + \frac{25540}{41 - \frac{1}{\lambda^2}} \tag{C-5}$$

where η_s is the refractive index for standard air, and wavelength λ is measured in mi

D. Presence of CO_2 in Air

Standard air, as considered in the above expression, is dry air containing 0.03% CO_2 by volume at normal pressure of 760 mm Hg and having an air temperature of 15°C. Earlier measurements generally neglected the small quantity of CO_2 in air.

Laboratory air may contain considerably greater concentrations of CO_2 than normal air designated as standard. The index of refraction of CO_2 at 20°C and for $\lambda = 0.5461\,\mu$ is 1.00045060 and for air at the same wavelength and temperature is 1.00027310. A concentration change of CO_2 in air from 0.03 to 0.3% would increase the air index value to 1.00027364. Thus, for exact measurements the amount of CO_2 present and its increase in confined areas where refractive studies are being made should be considered.

E. Moist Air Conditions

The above discussion pertains to a dry-air condition which is not generally manifest in laboratory experiments. Lorenz determined a correction, general for all wavelengths of visible light, and applied it to the refractive index of dry air η_s to obtain the index for moist air η_m:

$$\eta_m = \eta_s - 0.556 \times 10^{-6} (p_{wv}) \quad . \qquad (C\text{-}6)$$

The vapor pressure p_{wv} is given in mm of Hg. From the table below it can be seen that the influence of water vapor even at saturated conditions is only felt at higher temperatures when the vapor pressure becomes a substantial portion of the total pressure. Presumably if the relationship holds throughout the temperature range imposed, at 100°C, when the water vapor constitutes the entire gaseous phase, the difference in refractive index is the difference between the indices of water vapor and air.

Table C-1. Change in Index of Air for Saturated Water Vapor Conditions

$\eta_s = 1.00027773$

Temperature °C	Saturated Vapor Pressure mm Hg*	Change in Index at Air due to Water Vapor $\Delta\eta$(at given temperature)
0	4.579	0.000000255
15	12.788	0.000000711
50	92.51	0.000005140
100	760.00**	0.000052250

*values obtained from steam tables

**100 percent water vapor

E. Effects of Water Vapor

For a wetted fabric the surface temperature history after initiation of the radiant pulse shows a temperature plateau near 100°C where the release of water vapor and the vaporization heat exchange occurs. If we consider that saturated water vapor exists near the surface of the fabric, the change in indices is as follows:

	$\frac{\eta_s - \eta_{100}}{\eta_{100}^{-1}} \times 100$	$\frac{\eta_{100} - \eta_{wv}}{\eta_{wv}^{-1}} \times 100$
η (15°C Dry Air) - 1.0002777 η (100°C Dry Air) - 1.0002145	22.8%	
η (100°C Water Vapor) - 1.00017222		19.6%

Calculating an interferometric-indicated temperature under these conditions, the actual temperature should be lower by as much as 70°C.

G. Dispersion Values of Water Vapor

The Lorenz correction earlier stated applies uniformly over the visible spectrum and is based on the consideration that the dispersion

of water vapor is the same as air. In reality the indices of refraction vary from one wavelength to another for different gases. Cuthbertson[7] and Barrell and Sears[8] developed expressions governing the dispersion of water vapor in air-vapor mixtures. Barrell and Sears' expression (not included here) was derived for moist air conditions at approximately 30°C and relative humidity of 80%; it is intended for use at normal atmospheric conditions where vapor pressures of 10 mm is average and rarely exceeds 20 mm. As with the Lorenz correction, the presence of water vapor at standard conditions changes the index value of air only slightly. Whether these expressions hold for the possible higher concentrations of water vapor associated with higher temperatures is not indicated.

H. Measurement of Vapor Concentrations for Dispersion Values

The possibility of measuring the dispersion of water vapor and air-vapor mixtures to arrive at concentration profiles of the water vapor at higher temperatures can be postulated. The change of refractive index from pure water vapor at 100°C to vapor-free air at the same temperature and wavelength is quite substantial as indicated earlier. However, the dispersions of gases at different wavelengths are small. If the interference events are recorded at different wavelengths simultaneously, the indicated temperatures for each interferogram would be different, since the dispersions from λ_1 to λ_2 are not equal:

$$\left(\eta_{\lambda_1} - \eta_{\lambda_2}\right)_A \neq \left(\eta_{\lambda_1} - \eta_{\lambda_2}\right)_{wv} \qquad \text{(C-7)}$$

The subscripts A and wv denote air and water vapor, respectively. Using Barrell and Sears' dispersion formulation for air-water-vapor mixtures, and assuming that it applies at 100°C and for higher water vapor concentrations, one can ascribe different concentration percentages of water vapor in the air-vapor mixture until the simultaneously recorded

interferograms at the different wavelengths yield the same temperature. At that point, the ascribed concentrations percentage would apply. Since the concentrations and temperatures would be different at every location in the thermal or diffusion boundary layers, a series of nomographs relating vapor-air concentrations (for the two wavelengths) with temperature and fringe shift number would eliminate the necessity of solving simultaneous expressions for every location.

I. Accuracy in Predicted Concentrations

In Table C-2 the dispersion correction coefficients by Barrell and Sears are listed (k values) for various wavelengths. The indices of dry air at 15°C and 100°C, and the computed vapor indices $\left[\eta_{wv} = \eta_A - k(p_{wv})\right]$ for pure water vapor (100% saturation of water vapor in air at 100°C) are listed. As an example, if we record simultaneous interference fringe fields using the Hg lines at 0.5461μ and 0.4358μ, we can note that the dispersion for air at 100°C is

$$1.0002146 - 1.0002170 = 0.0000034$$

and for water vapor at the same wavelengths

$$1.0001754 - 1.0001720 = 0.0000024 .$$

The difference between these dispersion values in terms of an equivalent change in air temperature is approximately 1.5°C. This means that if we had 100% water vapor at the fabric surface but assumed a dry air index relationship, the indicated temperatures from both interferograms would differ by only 1.5°C. The indicated temperature, however, would be higher by 70°C since indices of air rather than of water vapor were used. For example, a measure of temperature to 0.1°C from each interferogram would still result in an approximate 6.7% error in the determination of concentration or in temperature difference between

Table C-2. Refractive Index Values for Air at 15°C and 100°C, and for Water Vapor at 100°C at Various Wavelengths

Light Source	Wavelength λ (microns)	Indices of Dry Air η at 15°C	Indices of Dry Air at 100°C	$\eta_m = \eta_s - R(p_{wv})$ $R^* \times 10^{-6}$	Indices of Water Vapor at 100°C
Cadmium	0.6438	1.0002763	1.0002133	0.0567	1.0001702
Helium	0.5876	1.0002771	1.0002140	0.0563	1.0001712
Mercury	0.5461	1.0002779	1.0002146	0.0560	1.0001720
Cadmium	0.5086	1.0002787	1.0002152	0.0557	1.0001729
Cadmium	0.4800	1.0002795	1.0002158	0.0553	1.0001738
Cadmium	0.4678	1.0002799	1.0002161	0.0553	1.0001741
Helium	0.4471	1.0002806	1.0002167	0.0550	1.0001749
Mercury	0.4358	1.0002810	1.0002170	0.0548	1.0001754

*References 8 and 6

indicated and actual values. Therefore, the accuracy of measuring fringe shift differences between interferograms reflects considerably not only on the accuracy of predicted concentration but on the actual temperature as well.

J. Expressions Governing the Two or More Wavelength Interferometric Techniques

From the elastic solid and electromagnetic theories relationships of the index of refraction for a nonabsorbing medium to density and gas constituents has evolved (see earlier discussion).

$$\frac{\eta^2 - 1}{\eta^2 + 2} = \sum_i \frac{\rho_i}{M_i} P_i \qquad \text{(C-8)}$$

where ρ_i/M_i are the concentrations (moles/cm^3) assumed for the constituents and P_i is the molecular refractivity of each constituent given.

$$P_i = \frac{4\pi}{3} N \alpha_i \qquad \text{(C-9)}$$

where N is the Avogadro number and α_i (cm^3) is a frequency-dependent "polarizability" factor (electromagnetic theory of light) which gives significance to the individual atoms and molecules in relating induced dipole moment and the effective electric field. The molar refractivity P is uneffected by a change of state and is independent of density.

Utilizing the Gladstone-Dale approximation and expressing Equation (C-8) in terms of the mol fraction (ρ_i/M_i) of each constituent

$$(\eta - 1) = \frac{3}{2} \frac{p}{Rt} \sum_i x_i P_i \qquad \text{(C-10)}$$

where x_i is the mol fraction (moles/gm) for the i component and P_i is the refractivity of that component.

The relationship between fringe count and change in indices (from the undisturbed interference field to the surface of heated specimen) is given for the one wavelength interference event as

$$\delta N \approx \frac{Z}{\lambda} (\eta_1 - \eta_2) \tag{C-11}$$

where Z is the path length through which refraction of light occurs (width of fabric) and λ is the wavelength of light. The index value for the undisturbed condition is given as

$$(\eta_1 - 1) = \frac{3}{2} \frac{p}{Rt_1} \sum_i \left(x_i P_i\right)_1 \tag{C-12}$$

and for the changed or disturbed condition as

$$(\eta_2 - 1) = \frac{3}{2} \frac{p}{Rt_2} \sum_i \left(x_i P_i\right)_2 \tag{C-13}$$

If these expressions for η_1 and η_2 are substituted into Equation (C-11) the fringe shift equation for the one wavelength then becomes

$$\delta N = \frac{3}{2} \frac{Z}{\lambda} \frac{p}{R} \left[\frac{\sum_i \left(x_i P_i\right)_1}{t_1} - \frac{\sum_i \left(x_i P_i\right)_2}{t_2} \right] \tag{C-14}$$

where fringe shift count δN is now a function of gas constituents and temperature. This equation would predict gas composition or concentration in an isothermal environment, or alternatively temperature, if the gas concentrations did not change.

Since the molar refractivity P_i of a constituent is wavelength-dependent and has dispersion values that differ from other constituents, it can be seen that to measure temperature which varies and gas

concentrations which also vary it is necessary to take as many simultaneous interferograms at different wavelengths as there are gas components. Expressions similar to Equation (C-14) for each fringe count determination are all solved simultaneously to arrive at the concentrations and temperature information.

For gas mixtures of more than two constituents the expressions become quite imposing. As earlier indicated, using two simultaneous wavelength interference recordings to accurately measure concentrations or temperature for air-water-vapor mixture requires extremely precise fringe shift measurements. The method becomes tenuous where dispersion values for the gases are unknown,* where the dispersions themselves are very similar, or where many gases are present at one instant. Gas analysis can be more assuredly accomplished by improving the measure of refractive variances or using variations in the analysis for whatever conditions exist.

If gases are individually released as a function of heat loading and time, the technique reduces to the two-wavelength interferometric approach where the concentration of gas in air (or in any background gaseous field) is more readily measurable.

The interferometric arrangement used to record simultaneous interference fringe fields at two wavelengths is shown in Figure C-1. White light division and recombination of wave amplitude is accomplished in the normal manner using the Mach-Zehnder interferometric model. The light, however, is again divided by an equal path-splitting prism in which each beam is filtered for the appropriate wavelength desired. For an increased number of gas components, the divided beams could conceivably be divided again in similar fashion to provide additional wavelength interference fields.

---

*The International Critical Tables (1933) has dispersion formulae for various gases. Seemingly little information has been published since 1933, especially for refractivities of gases and their dispersions at higher temperatures.

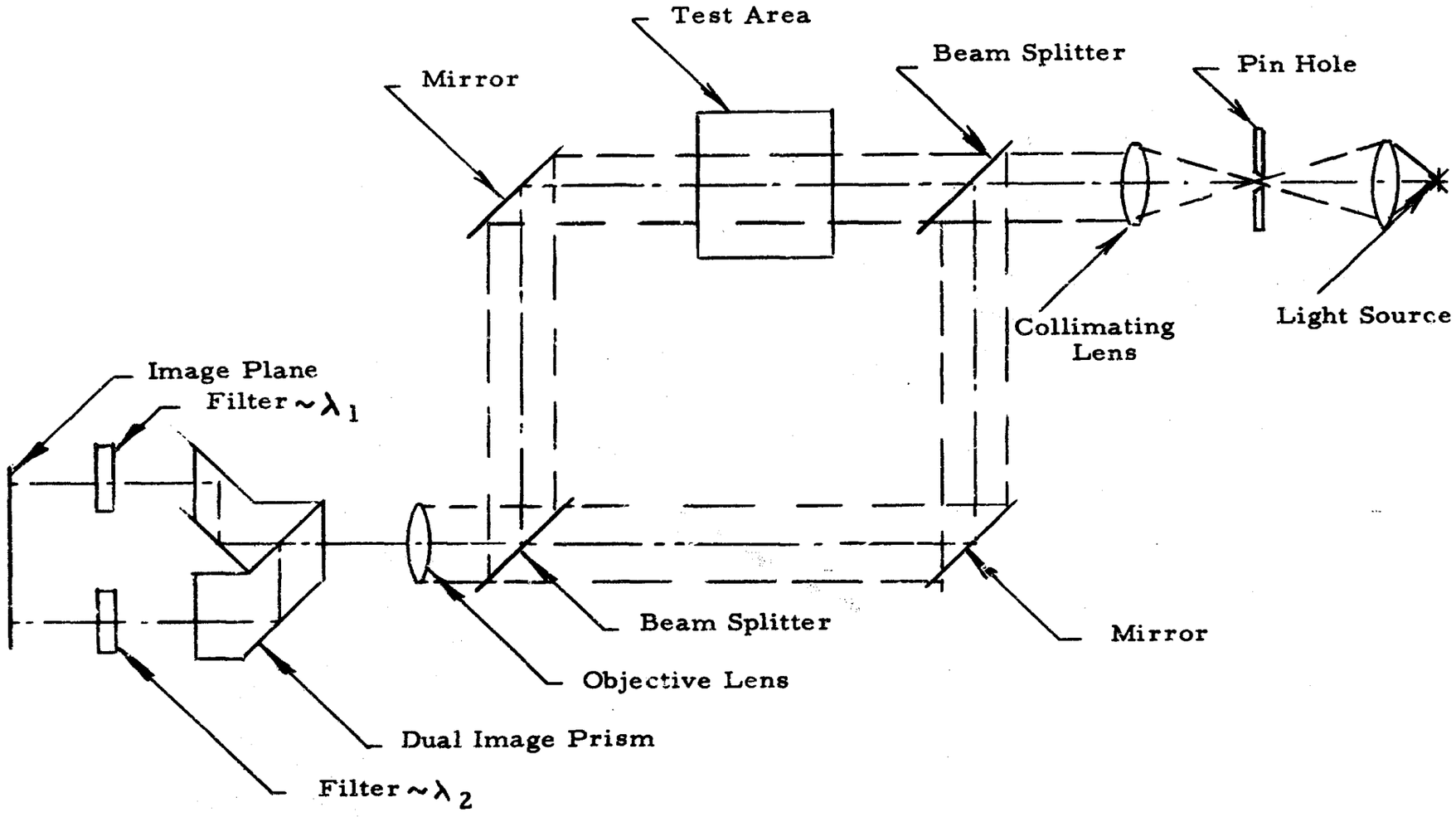

Figure C-1. Schematic of Mach-Zehnder Two-Wavelength Interferometer

K. Means of Improving Fringe Count Accuracy

Gas analysis using this method requires stringent measurement accuracies as indicated in the foregoing discussion. Fringe-count accuracy can be improved greatly by using refined techniques in measuring small fractions of fringe separation itself and by increasing the length through which the light is refracted. The gas environment in which tests are conducted can be varied to provide the greatest dispersive powers for identifying and quantifying emitted gases. The wavelengths of light used in a two-wavelength interferometric study can be separated widely in the visible spectrum also to permit as great a dispersion difference as possible.

Our present fringe count accuracy is approximately 0.1 of a fringe separation which can readily be improved to 0.01 fringe by methods indicated in the literature. Werner and Leadon[9] suggested a method to obtain fringe measurement accuracy to 1/500 fringe spacing. Since variations in fringe spacing occur from the undisturbed to the displaced fringe fields, this accuracy for their particular measurements has been questioned by Winkler.[10]

Peters and Stroke[11] proposed a means of electronic location and measurement of fringes with a capability of discerning a displacement of 1/400 of a fringe. With irregularities in peripheral servo equipment to restore zero position, an accuracy of 1/100 fringe was possible.

More recently a photoelectric scanning device described by Dew[12] evaluated interferograms to 1/100 fringe or better. The same accuracy was claimed by Dipon[13] for a device used to measure fringe displacement from streak photographs.

In Figure C-2 it can be noted that fringe count accuracy is improved considerably by increasing the path length through which refraction occurs. The curves can be read in terms of absolute fringe count δN or as a measure of changes in fringe count $\Delta\delta N$ since a linear relationship exists. The corresponding temperature difference associated with change in

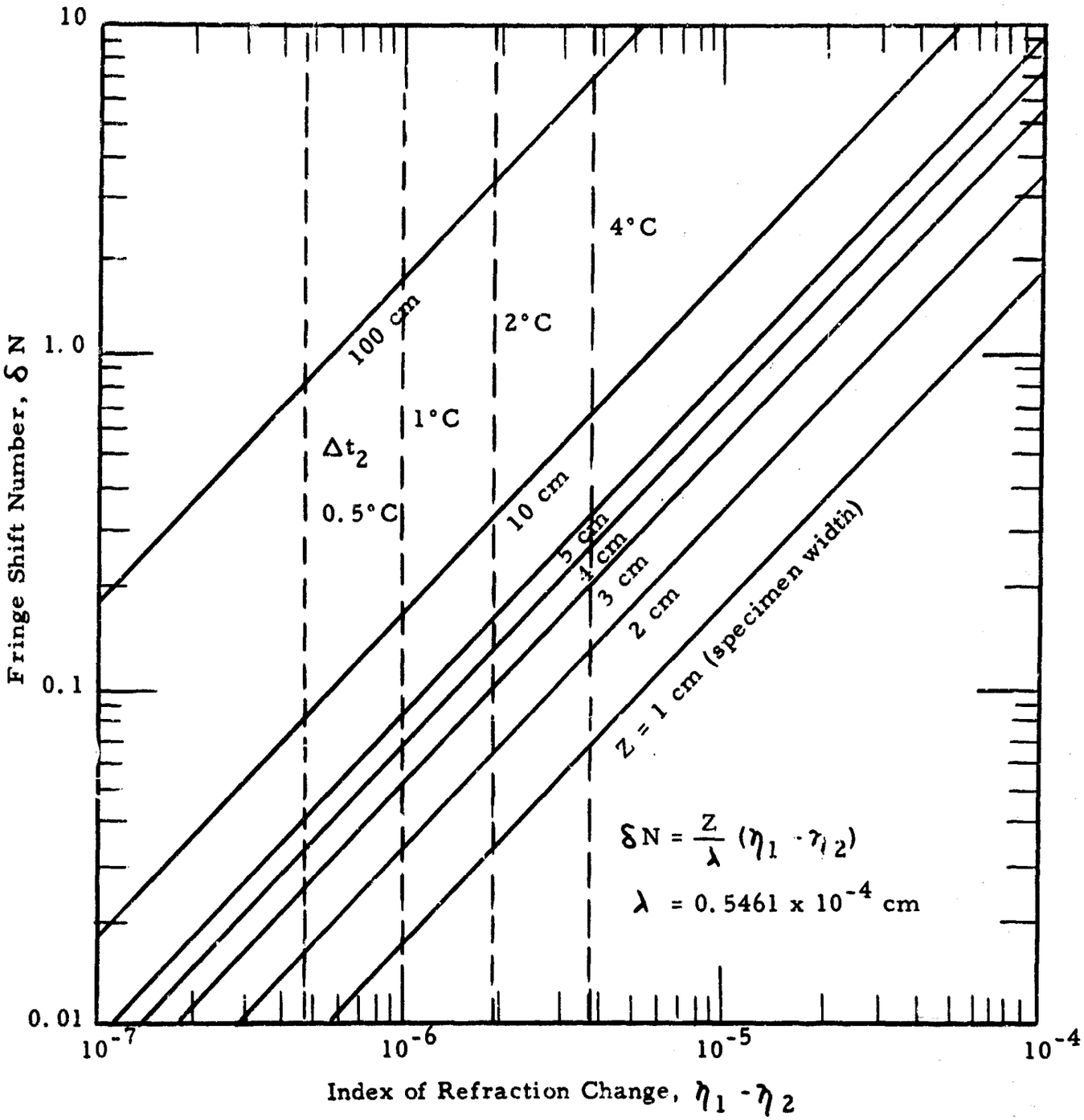

Figure C-2. Variation of Fringe Shift Number with Change in Indices for Different Specimen Widths

index of refraction and fringe shift number (constant pressure) is also shown. From this plot it is seen that for our presently obtained fringe count accuracy (0.1 fringe) and for our path length (fabric width) of approximately 3 cm, our temperature measurement accuracy is somewhat less than 2°C. If fringe count accuracy can be improved to 0.01 fringe and an accuracy of 0.1°C or better is required, a path length of approximately 10 cm must be used.

Although the multi-wavelength technique does not appear to lend itself to precise measurements of water vapor in an air environment (since the dispersion values of water vapor are not considerably different from that of air), the technique would be sensitive in detecting gases having high dispersion characteristics. If the temperature was measured by other means the interferometer would predict concentration levels accurately. This, of course, would involve only one wavelength of light, and it would not be necessary to consider separation of light into two or more wavelengths except for correlation measurements.

It can be recognized that if the wavelengths of light used in the multi-wavelength technique are at extremes in the visible spectrum or, if possible extended well into the infrared at one extreme and into the ultra violet at the other, maximum consideration of the gas dispersion characteristics is possible. However, operational limitation of the Mach-Zehnder interferometer prevent wide separation of wavelengths in utilizing the two or more wavelength technique. Usually, optimum interference fringes are obtained from one wavelength of light, and for the second wavelength an effective "out of focus" condition exists. This results in part because of the finite size of the interferometer aperture and because of the non-monochromacity of the light source. The optical path adjustment elements are generally set in the compensated leg of the interferometer and any scheme to compensate optical path length for more than one wavelength is difficult.

Several methods were devised to permit compensation of two or more wavelengths. Since modification of our Mach-Zehnder interferometer would be necessary, the multi-wavelength technique was not used in this phase our program.

III. MULTI-ENVIRONMENTAL INTERFEROMETER TECHNIQUE

A. General

Separate but identical fabric heating tests in different environments provides the basis for this technique. The unknown variables are separated by solving simultaneously the fringe shift expressions for the tests in the various environmental gases.

B. Expressions Governing the Two or More Environmental Interferometer Technique

For a single environment the basic equation of the Mach-Zehnder interferometer has been previously worked out[2]. The expression is given as

$$\delta N = \frac{CZ}{\lambda} (\rho_1 - \rho_2) \qquad \text{(C-15)}$$

where δN is the observed fringe shift, C the Gladstone-Dale constant for the particular environmental gas, ρ_1 the gas density in the undisturbed portion of the interference field, ρ_2 the gas density at the point under investigation, Z the length of the heated fabric, and λ the wavelength in vacuum of the light used. From the ideal gas law we can express the density as

$$\rho = pM/R't \qquad \text{(C-16)}$$

where p is the pressure, t the temperature, M the molecular weight of the gas, and R' the universal gas constant. Equation (C-15) then becomes

$$\delta N = \frac{CZ}{\lambda} \left(\frac{P_1 M_1}{R t_1} - \frac{P_2 M_2}{R t_2}\right) \qquad \text{(C-17)}$$

In a single gas environment

$$M_1 = M_2$$

and for a constant pressure condition

$$P_1 = P_2$$

When a foreign gas is introduced a universal Gladstone-Dale constant cannot be used and Equation (C-17) thus becomes

$$\delta N = \frac{ZP}{\lambda R'} \left[\frac{(CM)_1}{t_1} - \frac{(CM)_2}{t_2} \right] \qquad \text{(C-18)}$$

where the quantity CM is defined as the molecular refractivity of a gas.

If we assume that a gas at any point consists of a mixture of the environmental gas and of the foreign gases then

$$(CM)_2 = \sum_i \chi_i (CM)_i \qquad \text{(C-19)}$$

where χ_i is the percentage concentration of gas component i. With only one species of foreign gas present, for example, the expression may be written

$$\delta N = \frac{ZP}{\lambda R'} \left[\frac{(CM)_1}{t_1} - \frac{\chi(CM)_1 + (1-\chi)(CM)_2}{t_2} \right] \qquad \text{(C-20)}$$

The three unknowns in the above expression, molecular refractivity $(CM)_2$, temperature (t_2), and gas concentration (χ), can be determined by solving simultaneously the fringe shift values (as a function of these variables) obtained from tests in three different environmental gases.

Nitrogen, having essentially the same molecular weight and refractivity as air, was used in our tests principally to determine fabric degradation characteristics that may be different from oxidation or combustion in air. Argon and helium, readily obtainable inert gases,

were chosen to represent molecular weights above and below that of air or nitrogen. As shown below, air and argon have quite similar molecular refractivities despite the fact that each has relatively large differences in molecular weight.

Table C-3. Molecular Weight and Refractivity Values for Various Gases

Environment Gas	Index of Refraction η^*	Gladstone-Dale Constant C	Molecular Weight M	Molecular Refractivity CM
Air	1.0002936	0.2262	29	6.56
Nitrogen	1.0002998	0.2397	28	6.71
Argon	1.000281	0.1583	39.9	6.32
Helium	1.000036	0.1958	4	0.783
Water Vapor	1.00025	0.3143	18	5.66
Carbon Dioxide	1.00045	0.2280	44	10.03

*Standard Conditions: 0°C, 760 mm Hg, λ = 5461 A.

C. Theoretical Fringe Shift Variations

Theoretical predictions of fringe shift values versus temperature for various gases are shown in Figure C-3. These curves display the marked effect different gases have on fringe count. If temperature measurement sensitivity is required, a gas environment with a high molecular refractivity may be chosen with light interference occurring over a long optical path (Figure C-3 b).

If a foreign gas is introduced across the interference light path, either a positive or a negative fringe count can occur, depending on the molecular refractivity of both foreign and environmental gas.

Environment	C	M
Helium	0.1958	4.003
Water Vapor	0.3143	18
Argon	0.1583	39.94

Environment	C	M
Air	0.2262	29
Nitrogen	0.2397	28.016
Carbon Dioxide	0.2280	44

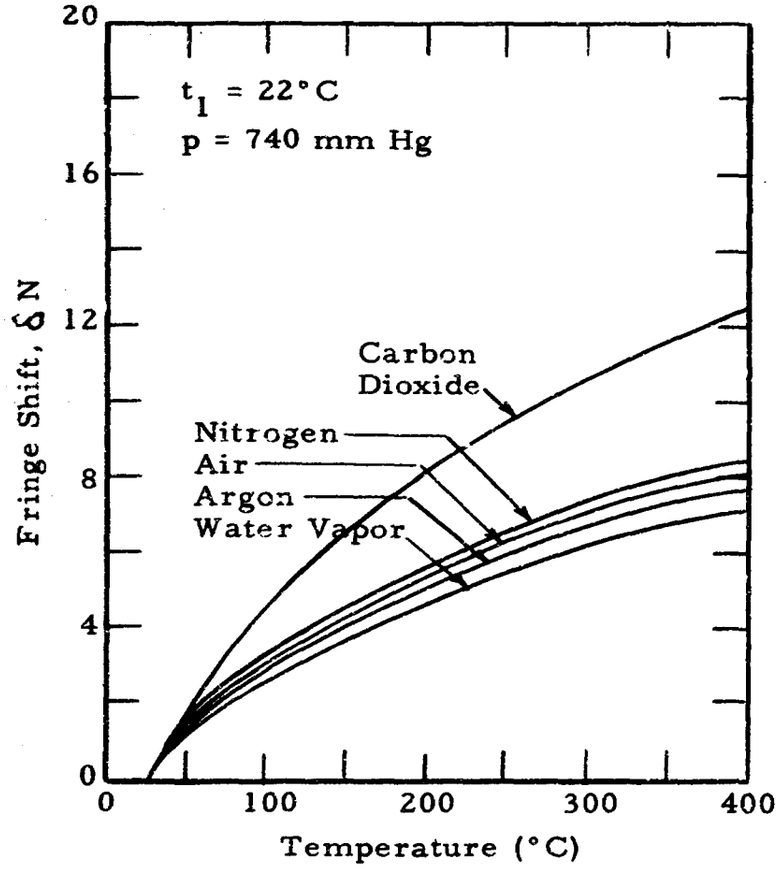

a) Z = 3.0 cm

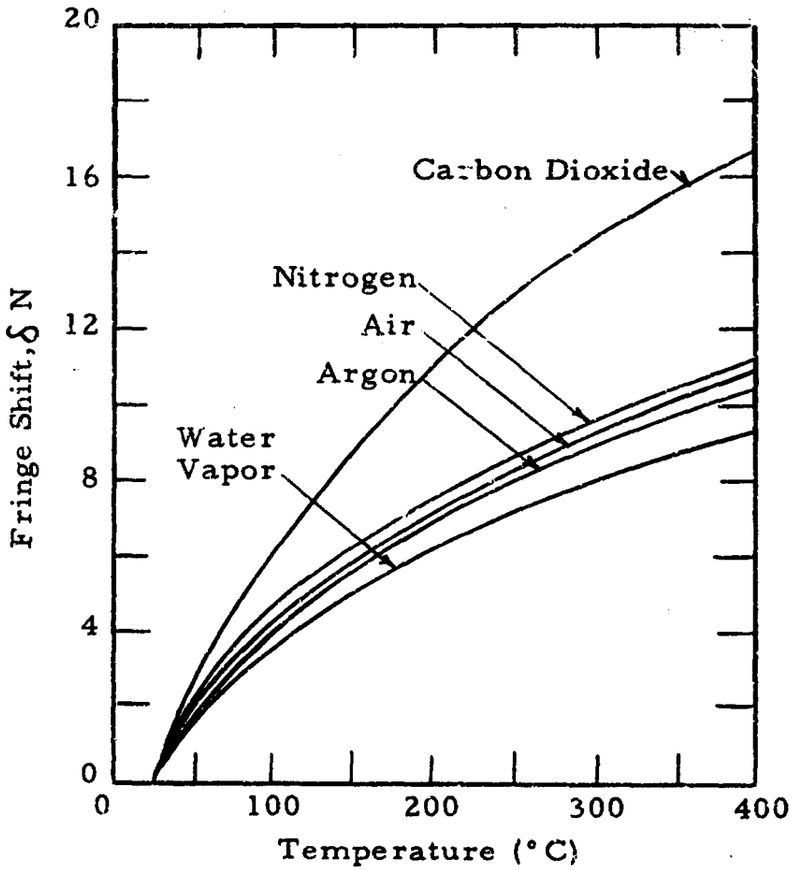

b) Z = 4.0 cm

Figure C-3. Theoretical Predicted Fringe Shift Values versus Temperature in Various Environments

The sensitivity of this multi-gas interferometric technique for detecting water vapor, its concentration, and the temperature of a heated specimen, can be considered from the fringe number associated with the several environmental gases. In a background of carbon dioxide, for example, the introduction of water vapor would increase fringe count, whereas in an environment of helium the fringe count becomes negative. If fringe count measurements are made to a small fraction of a fringe separation, then the two equations expressing the fringe values for tests in both gases would normally permit considerable accuracy in temperature and in vapor concentration determinations. If the identity of the foreign gas is not known, three or more tests and at least three equations are required.

A computerized program with readout similar to that shown in Figure C-4 may be utilized to rapidly determine molecular weight, concentration and temperature from measured fringe shift values in the different environments. This may be plotted as a series of graphs for more rapid determination of degradation gases in the multi-environmental test technique. This method has several pronounced limitations. It would be inconceivable that exactly identical tests could be conducted since variances exist in the test procedures; inhomogeneties exist in the arc furnace heating rates, in the fabric specimens and in the environmental conditions. Thus, for rapidly changing events interference fringe shift correspondence for separate tests in different environments is not possible and analysis therefore limited to quasi-steady state conditions. A further limitation of this test technique occurs since the fabric thermal boundary layer profiles are different for tests in each environment, and thus the free

SATURATION OF OUTGAS...PARTS PER 100= 30

TEMP CENT.=	200	225	250	275	300	325	350
UDEG= 10							
HEL=	.898	1.323	1.707	2.056	2.375	2.667	2.935
NIT=	32.526	34.181	35.678	37.038	38.279	39.417	40.463
AIR=	33.822	35.528	37.070	38.471	39.751	40.923	42.001
ARG=	48.237	50.593	52.552	54.414	56.114	57.672	59.105
UDEG= 15							
HEL=	-1.288	-.754	-.271	.169	.570	.937	1.275
NIT=	30.339	32.104	33.700	35.150	36.474	37.687	38.803
AIR=	31.635	33.450	35.092	36.584	37.945	39.193	40.341
ARG=	46.050	48.425	50.574	52.597	54.309	55.942	57.444
UDEG= 20							
HEL=	-3.475	-2.831	-2.249	-1.719	-1.236	-.793	-.386
NIT=	28.152	30.027	31.722	33.263	34.669	35.957	37.143
AIR=	29.448	31.373	33.114	34.696	36.140	37.463	38.680
ARG=	43.863	46.348	48.596	50.639	52.504	54.213	55.784
UDEG= 25							
HEL=	-5.662	-4.908	-4.226	-3.607	-3.041	-2.523	-2.046
NIT=	25.965	27.950	29.744	31.375	32.864	34.228	35.482
AIR=	27.261	29.296	31.136	32.809	34.335	35.734	37.020
ARG=	41.676	44.271	46.618	48.752	50.699	52.483	54.124
UDEG= 30							
HEL=	-7.849	-6.985	-6.204	-5.494	-4.846	-4.252	-3.706
NIT=	23.778	25.872	27.766	29.487	31.058	32.498	33.822
AIR=	25.074	27.219	29.158	30.921	32.530	34.004	35.360
ARG=	39.489	42.194	44.641	46.864	48.893	50.753	52.463
UDEG= 35							
HEL=	-10.036	-9.063	-8.182	-7.382	-6.652	-5.982	-5.367
NIT=	21.591	23.795	25.788	27.600	29.253	30.768	32.161
AIR=	22.887	25.142	27.181	29.033	30.724	32.274	33.699
ARG=	37.302	40.117	42.663	44.976	47.088	49.023	50.803
UDEG= 40							
HEL=	-12.223	-11.140	-10.160	-9.270	-8.457	-7.712	-7.027
NIT=	19.405	21.718	23.811	25.712	27.448	29.038	30.501
AIR=	20.701	23.065	25.203	27.146	28.919	30.544	32.039
ARG=	35.115	38.040	40.685	43.089	45.283	47.293	49.143
UDEG= 45							
HEL=	-14.410	-13.217	-12.138	-11.157	-10.262	-9.442	-8.687
NIT=	17.218	19.641	21.833	23.895	25.642	27.388	28.841
AIR=	18.514	20.987	23.225	25.258	27.114	28.814	30.379
ARG=	32.928	35.963	38.707	41.201	43.477	45.563	47.482
UDEG= 50							
HEL=	-16.597	-15.294	-14.116	-13.045	-12.067	-11.172	-10.348
NIT=	15.031	17.564	19.855	21.937	23.837	25.579	27.180
AIR=	16.327	18.910	21.247	23.370	25.309	27.085	28.718
ARG=	30.741	33.885	36.729	39.313	41.672	43.814	45.822

Figure C-4. Example of Programmed Data Expressing Fringe Shift Values in the Various Gases in Terms of Molecular Weight, Concentration and Temperature.

convective heat transfer characteristics are also different. It is expected that the mass diffusion processes differ for the separate environments such that measurements are only possible at the gas-fabric interfaces where zero velocity is postulated. This condition is not altogether true, and since the convective heat transfer coefficients would vary for each test as a function of time and heat loading the actual temperature of the fabric and possible the water vapor concentration would be somewhat different one test to another.

Another question arises as to what degradation gases are present in the different heating tests. The surrounding environment would influence to some extent the type and degree of fabric degradation that would occur. It is anticipated, however, that the behavior of a heated fabric would be somewhat similar for tests in inert environments. Our subsequent tests were made in helium, nitrogen, argon and CO_2.

Although the above restrictions are quite imposing, several important findings are possible. For a water saturated fabric a temperature plateau exists at or near 100°C until vaporization is complete. Thereafter fabric surface temperatures increase with time until more complete degradation or combustion occurs. During the vaporization period a quasi-steady state condition exists permitting ready analysis of concentrations. The fringe shift values in the different environments are quite different and an extremely sensitive measure of temperature and vapor concentration from separate environmental tests is possible.

Although the vapor concentrations and temperature indications would be somewhat different in the combinational evaluation of separate environment tests, a consistent variance would be recognized from repeated experiments and comparisons between these different environmental combinations (i.e., comparison of nitrogen-helium with nitrogen-CO_2) would be possible. An averaging procedure based on the contributing effects of the molecular weights and refractive index constants of

environment and foreign (water vapor) gases could be conceived. Comparisons were made from our tests on water-saturated fabrics; however, no averaging procedure was devised.

Extensive heating tests were made in different environments on a single wool type and on two different cotton fabrics under both dry and wet fabric conditions. For the water-saturated tests, concentrations of water vapor at the fabric surfaces were determined for a single heating load (approximately 6 cal/cm^2-sec). To facilitate determinations of molecular weight, concentration, and temperature for tests of the various gases, the equations expressing interference fringe shift values as a function of above variables were programmed for solution on a Control Data 1604 digital computer.

NOMENCLATURE

Symbol	
b	fringe width
C	Gladstone-Dale constant
N	number of wavelengths or number of molecules per unit volume
δN	wavelength difference or fringe shift count
$(\delta N)_c$	fringe shift referenced to compensated optical path
η	refractive index
P	ambient pressure or molar refractivity
Q	optical path difference
R	gas constant
t	temperature
x, y, z	rectangular coordinates
Y	fringe shift
Z	length of heated body
Z_{TC}	length of test chamber
ρ	density
λ	wavelength of light in vacuum
M	molecular weight
MC	molecular refractivity
χ, x	concentration percentage, mol fraction
R'	universal gas constant
α	polarizability factor
V_o	velocity of light in vacuum
e	electron charge
m	electron mass
p	partial pressure
K, k	constants

Subscript

1, 2	location or condition
r	reference
s	standard condition (dry air)
m	moist air
wv	water vapor
v	referenced to vacuum
i	component

IV. REFERENCES

1) Olsen, H. L. An interferometric method of gas analysis. Third Symposium on combustion. Flame and Explosion Phenomena. Baltimore, Williams and Wilkins, 1949. pp. 663-67.

2) Ross, P. A. and M. M. El-Wakil. A two-wavelength interferometric technique for the study of vaporization and combustion of fuels. In Progress in astronautics and rocketry, Vol. 2. N. Y., Academic, 1960. pp. 265-98.

3) El-Wakil, M. M. and C. L. Jaeck. A two-wavelength interferometer for the study of heat and mass transfer. Trans. ASME, Ser. C 86: 464-66 (1964).

4) General Mills, Inc. Electronics Division. Report no. 2409. Thermal-physical parameters of materials, by S. Steinberg, R. E. Larson and A. R. Kydd. Contract DA-19-129-QM-1998 (OI 6082) (June 30, 1963).

5) Edlen, B. The dispersion of standard air. J. Opt. Soc. Am. 43: 339-44 (1953).

6) Penndorf, R. Tables of the refractive index for standard air and the Rayleigh scattering coefficient for the spectral region between 0.2 and 20.0 microns and their application to atmospheric optics. J. Opt. Soc. Am. 47: 176-82 (1957).

7) Cuthbertson, C. and M. Proc. Roy Soc. (London) Ser. A 97: 152- (1920).

8) Barrell, H. and J. E. Sears. The refraction and dispersion of air for the visible spectrum. Phil. Trans. Roy. Soc. London, Ser. A 238: 1-64 (1939).

9) Werner, F. D. and B. M. Leadon. Very accurate measurement of fringe shifts in an optical interferometer study of gas flow. Rev. Sci. Instr. 24: 121-24 (1953).

10) Winkler, E. H. Very accurate measurement of fringe shifts in an optical interferometer study of gas flow. Rev. Sci. Instr. 24: 1067-68 (1953).

11) Peters, J. and G. Stroke. Electronic location of interference fringes. J. Opt. Soc. Am. 43: 668-72 (1953).

12) Dew, G. D. A method for the precise evaluation of interferograms. J. Sci. Instr. 41: 160-62 (1964).

13) Dipon, J. The rapid measurement of photographic records of interference fringes. Appl. Optics 2: 487-90 (1963).

Unclassified
Security Classification

DOCUMENT CONTROL DATA - R&D
(Security classification of title, body of abstract and indexing annotation must be entered when the overall report is classified)

1. ORIGINATING ACTIVITY (Corporate author) Applied Science Division Litton Systems, Inc. St. Paul Minnesota 55113	2a. REPORT SECURITY CLASSIFICATION Unclassified 2b. GROUP

3. REPORT TITLE

THERMAL-PHYSICAL PARAMETERS OF MATERIALS

4. DESCRIPTIVE NOTES (Type of report and inclusive dates)
Final Report for period 21 May 1962 through 20 May 1965

5. AUTHOR(S) (Last name, first name, initial)
Larson, R. E. and Kydd, A. R.

6. REPORT DATE	7a. TOTAL NO. OF PAGES	7b. NO. OF REFS
January 1966	223	70

8a. CONTRACT OR GRANT NO. DA-19-129-QM-1998(OI 6082) b. PROJECT NO. 1KO-24401-A113 c. d.	9a. ORIGINATOR'S REPORT NUMBER(S) 9b. OTHER REPORT NO(S) (Any other numbers that may be assigned this report) 66-3 QM C&OM-16

10. AVAILABILITY/LIMITATION NOTICES
Distribution of this document is unlimited.
Release to CHFSTI is authorized.

11. SUPPLEMENTARY NOTES	12. SPONSORING MILITARY ACTIVITY
	Materials Research Branch Clothing and Organic Materials Division U.S. Army Natick Labs., Natick, Mass.

13. ABSTRACT

This is the final report of a three-year program of research on the thermal-physical parameters of materials necessary for protection against intense thermal radiation. It briefly summarizes the theoretical and experimental studies of the first two years, and includes a more comprehensive discussion of the work performed during the final year of the contract.

In the theoretical studies, a simplified model of the fabric-skin system was chosen and the heat flow equations were solved using an explicit finite difference calculation procedure programmed for solution on a Control Data G-15D digital computer. Several sample calculations were compared with results existing in the literature and a limited parameter study was performed with variation of the fabric surface heat transfer coefficients.

Fabric test samples were irradiated in an arc-image furnace test facility and the heating and degradation processes were qualitatively and quantitatively studied with a Mach-Zehnder interferometer. This instrument provided fabric surface temperature data, heat transfer coefficient information, and a better insight into the chemical processes taking place

DD FORM 1 JAN 64 1473

Unclassified
Security Classification

14. KEY WORDS	LINK A		LINK B		LINK C	
	ROLE	WT	ROLE	WT	ROLE	WT
Parameters	8					
Thermal properties	8					
Physical properties	8					
Materials	9					
Protection	4					
Thermal radiation	4					
Measurement			8			
Heat transfer			9			
Fabrics			9			
Arc-image furnaces			10			
Irradiation			10			
Interferometers			10			
Coefficient of variation			10			

INSTRUCTIONS

1. ORIGINATING ACTIVITY: Enter the name and address of the contractor, subcontractor, grantee, Department of Defense activity or other organization *(corporate author)* issuing the report.

2a. REPORT SECURITY CLASSIFICATION: Enter the overall security classification of the report. Indicate whether "Restricted Data" is included. Marking is to be in accordance with appropriate security regulations.

2b. GROUP: Automatic downgrading is specified in DoD Directive 5200.10 and Armed Forces Industrial Manual. Enter the group number. Also, when applicable, show that optional markings have been used for Group 3 and Group 4 as authorized.

3. REPORT TITLE: Enter the complete report title in all capital letters. Titles in all cases should be unclassified. If a meaningful title cannot be selected without classification, show title classification in all capitals in parenthesis immediately following the title.

4. DESCRIPTIVE NOTES: If appropriate, enter the type of report, e.g., interim, progress, summary, annual, or final. Give the inclusive dates when a specific reporting period is covered.

5. AUTHOR(S): Enter the name(s) of author(s) as shown on or in the report. Enter last name, first name, middle initial. If military, show rank and branch of service. The name of the principal author is an absolute minimum requirement.

6. REPORT DATE: Enter the date of the report as day, month, year; or month, year. If more than one date appears on the report, use date of publication.

7a. TOTAL NUMBER OF PAGES: The total page count should follow normal pagination procedures, i.e., enter the number of pages containing information.

7b. NUMBER OF REFERENCES: Enter the total number of references cited in the report.

8a. CONTRACT OR GRANT NUMBER: If appropriate, enter the applicable number of the contract or grant under which the report was written.

8b, 8c, & 8d. PROJECT NUMBER: Enter the appropriate military department identification, such as project number, subproject number, system numbers, task number, etc.

9a. ORIGINATOR'S REPORT NUMBER(S): Enter the official report number by which the document will be identified and controlled by the originating activity. This number must be unique to this report.

9b. OTHER REPORT NUMBER(S): If the report has been assigned any other report numbers *(either by the originator or by the sponsor)*, also enter this number(s).

10. AVAILABILITY/LIMITATION NOTICES: Enter any limitations on further dissemination of the report, other than those imposed by security classification, using standard statements such as:

(1) "Qualified requesters may obtain copies of this report from DDC."

(2) "Foreign announcement and dissemination of this report by DDC is not authorized."

(3) "U. S. Government agencies may obtain copies of this report directly from DDC. Other qualified DDC users shall request through _____."

(4) "U. S. military agencies may obtain copies of this report directly from DDC. Other qualified users shall request through _____."

(5) "All distribution of this report is controlled. Qualified DDC users shall request through _____."

If the report has been furnished to the Office of Technical Services, Department of Commerce, for sale to the public, indicate this fact and enter the price, if known.

11. SUPPLEMENTARY NOTES: Use for additional explanatory notes.

12. SPONSORING MILITARY ACTIVITY: Enter the name of the departmental project office or laboratory sponsoring *(paying for)* the research and development. Include address.

13. ABSTRACT: Enter an abstract giving a brief and factual summary of the document indicative of the report, even though it may also appear elsewhere in the body of the technical report. If additional space is required, a continuation sheet shall be attached.

It is highly desirable that the abstract of classified reports be unclassified. Each paragraph of the abstract shall end with an indication of the military security classification of the information in the paragraph, represented as *(TS), (S), (C), or (U)*.

There is no limitation on the length of the abstract. However, the suggested length is from 150 to 225 words.

14. KEY WORDS: Key words are technically meaningful terms or short phrases that characterize a report and may be used as index entries for cataloging the report. Key words must be selected so that no security classification is required. Identifiers, such as equipment model designation, trade name, military project code name, geographic location, may be used as key words but will be followed by an indication of technical context. The assignment of links, rules, and weights is optional.